UMTA-CO-06-0009-83-1

STEADY STATE CURVING AND WHEEL/RAIL WEAR PROPERTIES OF A TRANSIT VEHICLE ON THE TIGHT TURN LOOP

PREPARED FOR

U.S. DEPARTMENT OF TRANSPORTATION

URBAN MASS TRANSPORTATION ADMINISTRATION
Office of Technical Assistance
WASHINGTON, D.C. 20590

NOTICE

This document describes testing conducted at the Transportation Test Center, Pueblo, Colorado, under the sponsorship of the Urban Mass Transportation Administration, U.S. Department of Transportation. It was prepared under the auspices of Boeing Services International, Inc. at the Transportation Test Center in the interest of information exchange. The Transportation Test Center does not endorse products or manufacturers. Trade or manufacturers' names appear herein solely because they are considered essential to the object of this report.

Technical Report Documentation Page

1. Report No.	2. Government Accession No.	3. Recipient's Catalog No.
UMTA-CO-06-0009-83-1		

4. Title and Subtitle	5. Report Date
Steady State Curving and Wheel/Rail Wear Properties of a Transit Vehicle on the Tight Turn Loop	December, 1982
	6. Performing Organization Code
7. Author(s) Elkins, John A.* and John Peters, Gerry Arnold and Britto Rajkumar	8. Performing Organization Report No.
9. Performing Organization Name and Address Transportation Test Center P.O. Box 11008 Pueblo, Colorado 81001	10. Work Unit No. (TRAIS) 11. Contract or Grant No.
12. Sponsoring Agency Name and Address U.S. Department of Transportation Urban Mass Transportation Administration	13. Type of Report and Period Covered Interim Report July - September, 1982 14. Sponsoring Agency Code

15. Supplementary Notes Boeing Services International, Inc., Operations and Maintenance Contractor, Federal Railroad Administration, Transportation Test Center, Pueblo, CO. Contract No. DOT-FR-67001. *Consultants: The Analytic Sciences Corporation (TASC).

16. Abstract This report describes the results of a test series carried out on the Tight Turn Loop at the Transportation Test Center to assess the curving and wheel/rail wear performance of a transit vehicle negotiating a very tight turn. Tests were performed on unlubricated rail to ensure constant coefficients of friction. Wheel/rail forces and angles-of-attack were recorded using onboard and wayside instrumentation. Wear rates were systematically recorded.

The report details the test setup and results, stressing the correlation between experimental data and computer model predictions.

The report concludes with recommendations for improved experimental techniques, suggesting developments to the computer model and a proposal for further testing on the Tight Turn Loop.

17. Key Words	18. Distribution Statement
	Document may be purchased from the National Technical Information Service, 5285 Port Royal Road, Springfield, Virginia 22161

19. Security Classif. (of this report)	20. Security Classif. (of this page)	21. No. of Pages	22. Price
Unclassified	Unclassified	160	

ACKNOWLEDGEMENTS

The Transportation Test Center wishes to acknowledge the contributions of Boeing Services International, Inc. and The Analytic Sciences Corporation in the management and data analysis of the Steady State Curving Tests.

TABLE OF CONTENTS

		Page
List of Figures		iii
List of Tables		v
Acronyms and Abbreviations		vi
Executive Summary		vi
1.0	INTRODUCTON	1
1.1	General	1
1.2	Two Point Contact on the Leading Wheels	1
1.3	Advantages of the Tight Turn Loop for Controlled Experiments	2
1.4	Outline of Experimental Tests	3
1.5	Computer Model and Experimental Comparisons	4
1.6	Conclusions and Recommendations	4
2.0	DESCRIPTION OF TEST FACILITIES AND EQUIPMENT	5
2.1	Track	5
2.2	Description of the State-of-the-Art-Car (SOAC)	5
2.2.1	General	5
2.2.2	Truck and Suspension	9
2.2.3	Instrumentation	9
3.0	EXPERIMENTAL RESULTS	17
3.1	Track Survey	17
3.2	Wheel and Rail Wear	26
3.2.1	General	26
3.2.2	Test Schedule	29
3.2.3	Data Analysis	32
3.2.4	Wheel and Rail Wear Rates	32
3.2.5	Discussion	42
3.3	Angle-of-Attack	44
3.3.1	Static Calibration	44
3.3.2	Measurement of Dynamic Angle-of-Attack	46
3.4	Wayside Rail Force Measurement	51
3.4.1	General	51
3.4.2	Calibraton	51
3.4.3	Data Reduction	55
3.4.4	Results	56
3.4.5	Discussion	56
3.5	Tractive Resistance	59
3.5.1	Tractive Resistance on Tangent Track	59
3.5.2	Tractive Resistance on Tight Turn Loop Without Restraining Rail	70
3.5.3	Tractive Resistance on Tight Turn Loop With Restraining Rail	70

TABLE OF CONTENTS (CONTINUED)

		Page
3.6	Static Suspension Characteristics	76
3.6.1	General	76
3.6.2	Methods of Obtaining Data	77
3.6.3	Discussion	85
3.7	Suspension Forces	87
3.7.1	General	87
3.7.2	Discussion	89
3.8	Acoustic Characteristics	91
3.8.1	General	91
3.8.2	Wheel Impact Test	92
3.8.3	Tests Without Restraining Rail	92
3.8.4	Tests With Restraining Rail	97
3.8.5	Discussion	97
4.0	COMPARISON OF CURVING PERFORMANCE WITH MATHEMATICAL MODEL PREDICTIONS	103
4.1	Mathematical Model	103
4.2	Vehicle and Track Parameters Used in the Curving Model	107
4.2.1	General	107
4.2.2	Vehicle Parameters	107
4.2.3	Track Geometry	109
4.3	Test Results Without Restraining Rail and Comparison with Theoretical Predictions	109
4.4	Test Results With Restraining Rail and Comparison with Theoretical Predictions	117
5.0	COMPARISON OF WEAR DATA WITH WEAR INDEX PREDICTIONS FROM MATHEMATICAL MODEL	127
5.1	Background	127
5.2	Wheel Wear Test Results and Comparison with Theoretical Wear Index	127
5.3	Rail Wear Test Results and Comparison with Theoretical Wear Index	131
6.0	CONCLUSIONS	135
7.0	RECOMMENDATIONS	137
7.1	Mathematical Model	137
7.2	Experimental Technique and Future Testing	137
References		139
Appendices		

LIST OF FIGURES

		Page
Figure 2.1	Track Layout at the Transportation Test Center	6
Figure 2.2	Tight Turn Loop Track Construction	7
Figure 2.3	Tight Turn Loop Marking and Instrumentation Locations	8
Figure 2.4	SOAC Performance and Design Characteristics	10
Figure 2.5	SOAC Truck Assembly	11
Figure 2.6	Rail Vertical Force Strain Gage Placement	14
Figure 2.7	Rail Lateral Force Strain Gage Placement	15
Figure 3.1	Pre-Test Radius of Curvature	19
Figure 3.2	Post-Test Radius of Curvature	20
Figure 3.3	Pre- and Post-Test Radius of Curvature	21
Figure 3.4	Pre-Test Superelevation	22
Figure 3.5	Post-Test Superelevation	23
Figure 3.6	Pre- and Post-Test Superelevation	24
Figure 3.7	Post-Test Gage	25
Figure 3.8	Restraining Rail Clearance	27
Figure 3.9	Restraining Rail Height	28
Figure 3.10	Typical Wheel Profile Overlay--Tread Wear	33
Figure 3.11	Typical Wheel Profile Overlay--Flange Wear	34
Figure 3.12	Typical Wheel Profile Overlay--Flange Back	35
Figure 3.13	Wheel Wear Versus Number of Laps, Wheelsets 1 and 5 Without Restraining Rail	37
Figure 3.14	Rail Wear Versus Number of Laps, Without Restraining Rail	38
Figure 3.15	Flange Back Wear Versus Number of Laps	40
Figure 3.16	Wheel Wear Versus Number of Laps, Outside Lead Wheelset With Restraining Rail	41
Figure 3.17	Tread Wear Versus Number of Laps, Inside Lead Wheelset Without Restraining Rail	43
Figure 3.18	Angle-of-Attack--Static Calibration Bar	45
Figure 3.19	Angle-of-Attack--Static Calibration by Sight Lines	47
Figure 3.20	Angle-of-Attack Calibration--Measurement of Axle End Offset to Sight Lines	48
Figure 3.21	Angle-of-Attack Versus Speed, Without Restraining Rail	49
Figure 3.22	Angle-of-Attack Versus Speed, With Restraining Rail	50
Figure 3.23	Typical LVDT Output Versus Track Location	52
Figure 3.24	Typical String Pot Output Versus Track Location	53
Figure 3.25	Hydraulic Calibration of Rails	54
Figure 3.26	Tractive Resistance, Tangent Track--May 11th, Forward	60
Figure 3.27	Tractive Resistance, Tangent--May 11th, Reverse	61
Figure 3.28	Tractive Resistance, Tangent Track--May 28th, Forward	63
Figure 3.29	Tractive Resistance, Tangent Track--May 28th, Forward	64
Figure 3.30	Two LVDT Outputs (Longitudinal), Lead Axle During Drift Test of Normal Tractive Resistance	65
Figure 3.31	Two LVDT Outputs (Longitudinal), Lead Axle During Drift Test of Abnormally High Tractive Resistance	66
Figure 3.32	Two LVDT Outputs (Longitudinal) for Trailing Axle During Drift Test of Abnormally High Resistance	67
Figure 3.33	Two LVDT Outputs for Lead and Trail Axles--One Side of Truck During Drift Test of Abnormally High Resistance	68

LIST OF FIGURES (CONTINUED)

		Page
Figure 3.34	Effective Conicity Plots, New and Worn Wheels--SOAC on Tangent Track	69
Figure 3.35	Tractive Resistance Characteristic, From Station 119000 Without Restraining Rail	71
Figure 3.36	Tractive Resistance Characteristic, From Station 118700 Without Restraining Rail	72
Figure 3.37	Tractive Resistance Characteristic, From Station 118700 Without Restraining Rail	73
Figure 3.38	Typical Tractive Resistance Characteristic--Forward, With Restraining Rail.	74
Figure 3.39	Typical Tractive Resistance Characteristic--Reverse, With Restraining Rail.	75
Figure 3.40	Primary Vertical Chevron Characteristic	79
Figure 3.41	Primary Longitudinal Characteristic from LVDT Readings.	81
Figure 3.42	Primary Longitudinal Chevron Characteristic from Dial Gage Readings.	82
Figure 3.43	Primary Lateral Chevron Characteristic from Measurements at the Chevrons.	83
Figure 3.44	Primary Lateral Chevron Characteristic from Measurements at the Point of Load Application	84
Figure 3.45	Radius Rod Resilient Mounting Characteristic.	86
Figure 3.46	1/3 Octave Spectrum of Hammer Blow to SOAC Wheel when Lifted Off Track	93
Figure 3.47	1/3 Octave Band Spectrum--On-board at 15 mi/h Clockwise Without Restraining Rail.	94
Figure 3.48	1/3 Octave Band Spectrum--Center of Loop at 15 mi/h Clockwise Without Restraining Rail.	95
Figure 3.49	5 kHz and 600 Hz Band Time Histories--15 mi/h Clockwise at Center of Loop	96
Figure 3.50	1/3 Octave Band Spectrum--On-board at 15 mi/h Clockwise With Restraining Rail	98
Figure 3.51	1/3 Octave Band Spectrum--Center of Loop at 15 mi/h Clockwise With Restraining Rail	99
Figure 3.52	20 kHz and 6.3 kHz Band Time Histories--10 ft from Track With Restraining Rail	100
Figure 3.53	20 Hz and 6.3 kHz Band Time Histories--Pass-by Data 10 ft from Track.	101
Figure 4.1	End View of Wheel and Rail with Second Contact Point on Flange Front	105
Figure 4.2	Forces and Torques Acting about Wheelset Bearing Axis with Second Point of Contact on Flange Front	105
Figure 4.3	End View of Wheel and Rail with Second Contact Point on Flange Back.	106
Figure 4.4	Forces and Torques Acting about Wheelset Bearing Axis with Second Contact Point on Flange Back	106
Figure 4.5	Cant Deficiency ~ Speed (1.5 inch Superelevation)	110
Figure 4.6	Lead Axle High and Low Rail Lateral Force ~ Speed (Without Restraining Rail).	111

LIST OF FIGURES (CONTINUED)

Page

Figure 4.7 Trail Axle High and Low Rail Lateral Force ~ Speed (Without Restraining Rail). 113
Figure 4.8 Lead and Trail Axle Yaw Moment ~ Speed (Without Restraining Rail). 114
Figure 4.9 Lead and Trail Axle Angle-of-Attack ~ Speed (Without Restraining Rail). 115
Figure 4.10 Truck Tractive Resistnce Due to Creep Forces ~ Speed (Without Restraining Rail). 116
Figure 4.11 Lead Axle Low Rail and Restraining Rail Vertical Force ~ Speed (With Restraining Rail) 118
Figure 4.12 Lead Axle High and Low Rail Lateral Force ~ Speed (With Restraining Rail) 120
Figure 4.13 Lead Axle Restraining Rail Lateral Force ~ Speed (With Restraining Rail) 121
Figure 4.14 Trail Axle High and Low Rail Lateral Force ~ Speed (With Restraining Rail) 122
Figure 4.15 Lead and Trail Axle Yaw Moment ~ Speed (With Restraining Rail) 123
Figure 4.16 Lead and Trail Axle Angle-of-Attack ~ Speed (With Restraining Rail) 124
Figure 4.17 Truck Tractive Resistance Due to Creep Forces ~ Speed (With Restraining Rail) 126
Figure 5.1 Laboratory Wear Rate/Wear Index Relationship. 128
Figure 6.2 Measured Wheel Wear Rate ~ Work Done Wear Index 130
Figure 6.3 Measured Rail Wear Rate ~ Work Done Wear Index. 133

LIST OF TABLES

Table 3.1 Profile Identification. 30
Table 3.2a Wheel and Rail Wear Rates 36
Table 3.2b Rail Wear 36
Table 3.2c Wheel Wear. 39
Table 3.3 Rail Force Data--Overall Average Values (With Restraining Rail) 57
Table 3.4 Rail Force Data--Overall Average Values (Without Restraining Rail). 58
Table 3.5 Suspension Characterization 77
Table 3.6 Summary of Suspension Forces Without Restraining Rail 89
Table 3.7 Summary of Suspension Forces With Restraining Rail. 90
Table 4.1 Average Vertical Wheel Loads at Balance Speed 107
Table 4.2 Vehicle Parameters Used in Curving Model. 108
Table 5.1 Theoretical Wheel Wear Index Values 131
Table 5.2 Theoretical Wear Indices for Head and Gage Face 132

ACRONYMS

ALD	Automatic Location Detector
BSI	Boeing Services International, Inc.
CW	clockwise
CCW	counterclockwise
FM	Frequency Modulation
L/V	Lateral/Vertical
LVDT	Linear Variable Displacement Transducer
RMS	Root-Mean-Square
SOAC	State-of-the-Art Car
TASC	The Analystic Sciences Corporation
TTC	Transportation Test Center
TTL	Tight Turn Loop
TTT	Transit Test Track
UMTA	Urban Mass Transportation Administration
URB	Urban Rail Building
URRVS	Urban Rapid Rail Vehicles and Systems Program
VHF	Very high frequency
WMATA	Washington Metropolitan Area Transit Authority

ABBREVIATIONS AND METRIC CONVERSIONS

ft,'	=	foot feet	=	0.305 meters
in,"	=	inch, inches	=	2.54 centimeters
ips	=	inches per second		
Hz	=	Hertz		
kHz	=	kilohertz		
lbs	=	pounds	=	0.454 kilograms
mrad	=	milliradian		
psig	=	pounds per square inch, gage		

EXECUTIVE SUMMARY

This report describes the results of a test series carried out on the Tight Turn Loop at the Transportation Test Center (TTC), Pueblo, Colorado, in order to assess the curving and wheel/rail wear performance of a transit vehicle when negotiating a very tight turn. Tests were performed with and without a restraining rail, and were limited to dry rail to ensure constant coefficient of friction. Wheel/rail forces and wheelset angles-of-attack were measured using both onboard and wayside instrumentation. In addition, rates of wheel and rail wear were measured using special profilometers available at the TTC.

This report details the experimental results and makes comparisons between the experimental data and the computer model predictions, which in this case showed exceptionally good correlation. A relationship between theoretical wear index and wheel wear is shown, but the corresponding relationship for rail wear was undetermined because of the lack of adequate rail wear.

The report concludes with recommendations for improved experimental techniques, suggested developments to the computer model, and a proposal for further testing on the Tight Turn Loop.

This work was performed by the Transportation Test Center and TASC (The Analytical Sciences Corporation) under the sponsorship of UMTA (Urban Mass Transportation Administration), Department of Transportation.

1.0 INTRODUCTION

1.1 GENERAL

The problem of calculating the forces that guide a railroad axle has been the subject of much study over the last century. There has been particular interest in the prediction of forces that occur during the negotiation of sharp curves because of the large forces that can be generated. In particular, there is special concern regarding the high rates of wheel and rail wear which sometime occur and the large expenditures on maintenance and renewal which can result from this situation.

The ability to predict the forces at the wheel/rail interface and the consequent rates of wheel and rail wear is important to the understanding and possible alleviation of these problems. Separate approaches for modeling the wheel/rail interaction have been used by different investigators for predicting the wheel/rail forces that occur during curve negotiation and for estimating the likely rates of wheel and rail wear. Insufficient experimental data has existed for complete verification of the predictions of these various models. Tests conducted by British Rail, which were reported by Elkins and Gostling in 1977[1], showed excellent agreement with predictions using a single point contact representation of the actual wheel and rail profiles. However, an attempt to apply the same analysis directly to evaluating the influence of wheel profile changes on the curving performance of transit trucks[2] failed to yield agreement with the experimental observations.

1.2 TWO POINT CONTACT ON THE LEADING WHEELS

Accordingly, a review of the modeling approaches in current use was conducted to find the reasons for this discrepancy. The review showed that the single point of contact assumption was a gross mathematical approximation for the new wheel and rail profiles in current use on U.S. railroads and transit properties. For these wheel profiles, the curving behavior is dominated by wheel/rail contact at two points on the leading axle wheel at the high rail. This proposal has now been modeled by one of the authors and has been shown to give much better agreement with the experimental observations[3].

In this work, the two point contact model is used to examine the curving behavior of a transit vehicle on a very tight curve (150 ft radius).

The creepages that occur between wheel and rail on curves and the resulting forces can cause high rates of wear of both wheels and rails. In particular, wheel flange wear and high rail gage

face wear has been a problem that has been experienced by a number of transit properties. This situation tends to be worse on tighter curves. For this reason, some transit properties have used restraining rails on the sharper curves, the purpose of the restraining rail being to prevent the contact between lead axle outer wheel and the gage face of the high rail which causes the wear problems. However, contact occurs instead between the flange back of the lead axle low rail wheel and the restraining rail and high rates of wear may be experienced as a result of this contact.

The forces that are generated between wheel and rail at the various points of contact with the restraining rail present are investigated and compared with those obtained without a restraining rail. Predictions are compared with measurements made during a test program performed by Boeing Services International (BSI) for the Urban Mass Transportation Administration (UMTA) on the Tight Turn Loop at the Transportation Test Center, Pueblo, Colorado.

There are many factors that might affect the rates of wear that could occur in a particular circumstance. Among these factors are the metallurgy of the wheel and rail, the degree of surface contamination and the stresses in the material due to the forces and creepages which occur at the interface.

There has been much work carried out in this field, although most of the literature has resulted from laboratory experiments. Relatively little field work has been carried out, partly because of the high cost associated with this type of testing, but also because of the difficulty of achieving a controlled wear environment. For instance, when studying wheel wear data in service, the results can be very difficult to analyze because of changes in the environmental conditions, varying rail metallurgies and the fact that vehicles in service typically encounter a wide range of track curvatures. Similarly, rail wear data in service is difficult to analyze because of the wide variety of vehicles that might pass over the test site and variations in environmental conditions.

1.3 ADVANTAGES OF THE TIGHT TURN LOOP FOR CONTROLLED EXPERIMENTS

Use of the Tight Turn Loop for wear testing permits the elimination of most of these problems. The vehicle is running continuously on track of nominally constant curvature, and, because of the high degree of curvature, measurable wear rates can be determined after relatively short periods of running. Also, because of the relatively dry climate at the test site, it is possible to complete such a test under almost constant environmental conditions. For these reasons, the Tight Turn Loop is nearly an ideal site for performing carefully controlled full scale wear tests. A disadvantage might be that the curve is tighter than the majority of service curves and, therefore, it might be difficult to relate the wear data to typical service conditions.

These tests were performed on this curve, with and without the restraining rail, in order to provide some basic wear data, which could be compared with a theoretical wear index provided by the mathematical curving model. Given that a relatively simple relationship could be established between the measured wear rates and this wear index, the mathematical model could then be used to predict wear rates for other more typical circumstances.

1.4 OUTLINE OF EXPERIMENTAL TESTS

The experimental test results are detailed in Section 3.0 of this report. The tests are summarized as follows:

SUB-SECTION	TEST	NOTES
3.1	Track Survey	The major track parameters both before and after the tests.
3.2	Wheel and Rail Wear	Establishes the rates of wear for wheels and rails.
3.3	Angle-of-Attack	Includes static calibration methods and dynamic measurements.
3.4	Wayside Rail Force Measurement	Details calibration methods, correction techniques, and values.
3.5	Tractive Resistance	Presents the 'drift' method to obtain values of resistance versus speed. Details resistance on tangent track and the Tight Turn Loop.
3.6	Static Suspension Characteristics	Details the methods and results of tests to obtain the major suspension characteristics.
3.7	Suspension Forces	Details the estimation of suspension forces on the Tight Turn Loop.
3.8	Acoustic Characteristics	Details results of a series of acoustic measurements.

1.5 COMPUTER MODEL AND EXPERIMENTAL COMPARISONS

Section 4 of this report details the mathematical model and makes comparisons between mathematical predictions and the experimental data of the curving properties of the SOAC. The comparisons of the model wear index and the measured rates of wear of wheels and rails is detailed in Section 5.

1.6 CONCLUSIONS AND RECOMMENDATIONS

Section 6 of this report discusses the conclusions of the test series and Section 7 makes the recommendations for future work.

2.0 DESCRIPTION OF TEST FACILITIES AND EQUIPMENT

2.1 TRACK

The Tight Turn Loop (TTL) forms part of Urban Rail Transit test facilities at the Transportation Test Center (TTC), Pueblo, Colorado. It is situated off the southeast curve of the Transit Test Track (TTT), identified in Figure 2.1. The TTL track construction, shown in Figure 2.2, consists of a continuous welded 119 lb/yd rail on wood ties with a 90 lb/yd inner guard rail or restraining rail. The nominal radius of the TTL is 150 ft, installed as a full circle. It is connected to the main TTT by means of a 488 ft long 326 ft radius track. The main purpose of the TTL installation is to provide a facility for the detailed investigation of wheel noise, truck curving behavior, and vehicle stability.

Track location is determined from marks painted on the outside rail at approximately 100 ft intervals in a clockwise direction, beginning with station 1183 + 00 just past the switch and ending with station 1192 + 00 just short of the switch.

As part of the test, the Tight Turn Loop was surveyed for mid-chord-offset, gage, and superelevation based on a 20 ft nominal chord on the outside rail. The chord was applied at the 1183 + 00 point and the first measurement taken at 1183 + 10 ft (designated measurement location #1).

The relationship between the 100 ft station markers, the chord measurement numbers, angle-of-attack calibration site, rail wear measurement sites, and rail force measurement sites is shown in Figure 2.3.

Reflective boards were used to give event marks for the on-board instrumentation. These were located at the 100 ft station marks and also at the angle-of-attack calibration site and the rail force measurement sites.

2.2 DESCRIPTION OF THE STATE-OF-THE-ART-CAR (SOAC)

2.2.1 General

The vehicle used for this test was SOAC number 1, one of the two State-of-the-Art-Cars, which were designed and constructed as part of the Urban Rapid Rail Vehicle and Systems Program (URRVS). Both SOAC cars are presently stationed at the TTC.

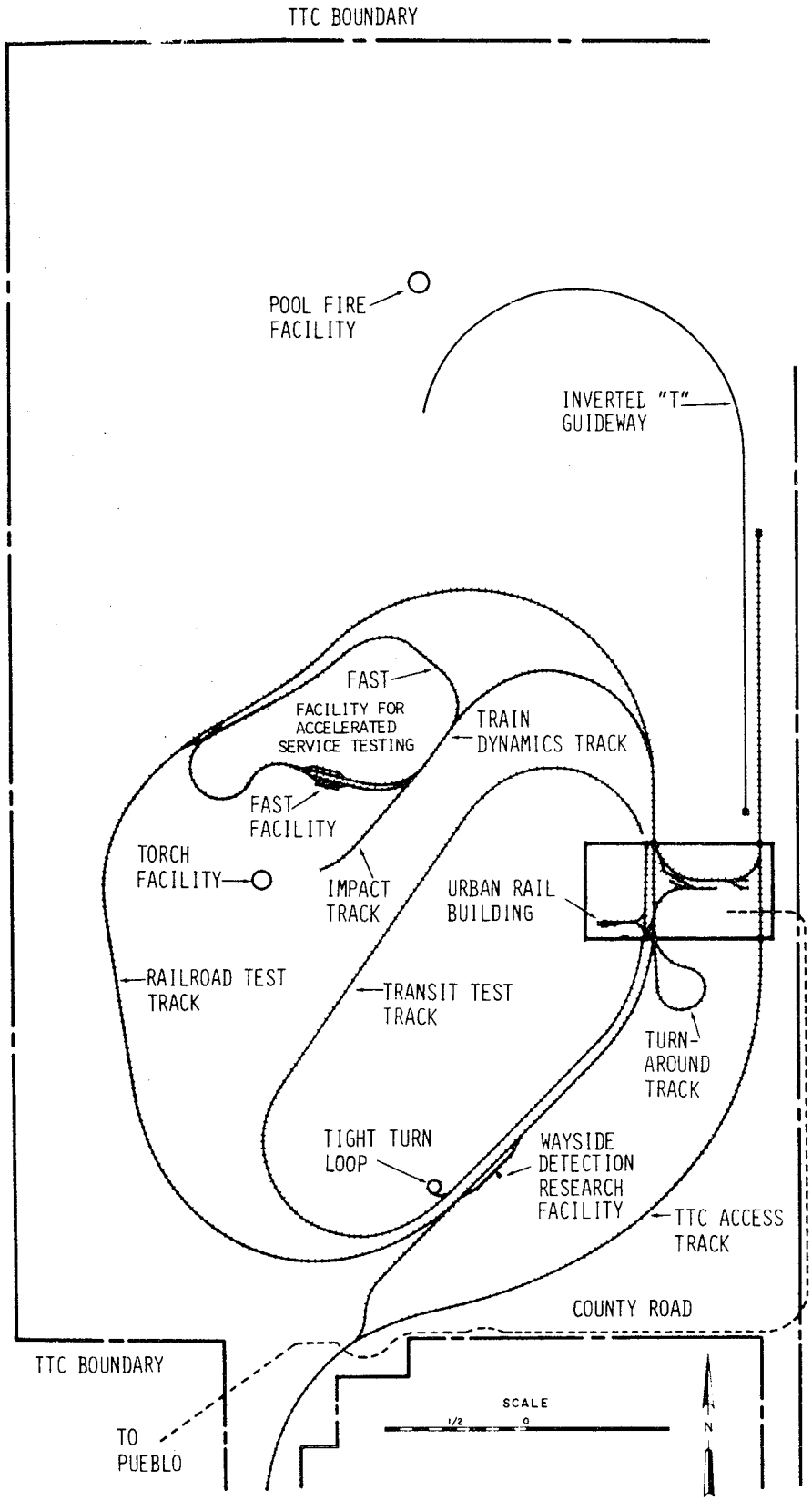

FIGURE 2.1. TRACK LAYOUT AT THE TRANSPORTATION TEST CENTER.

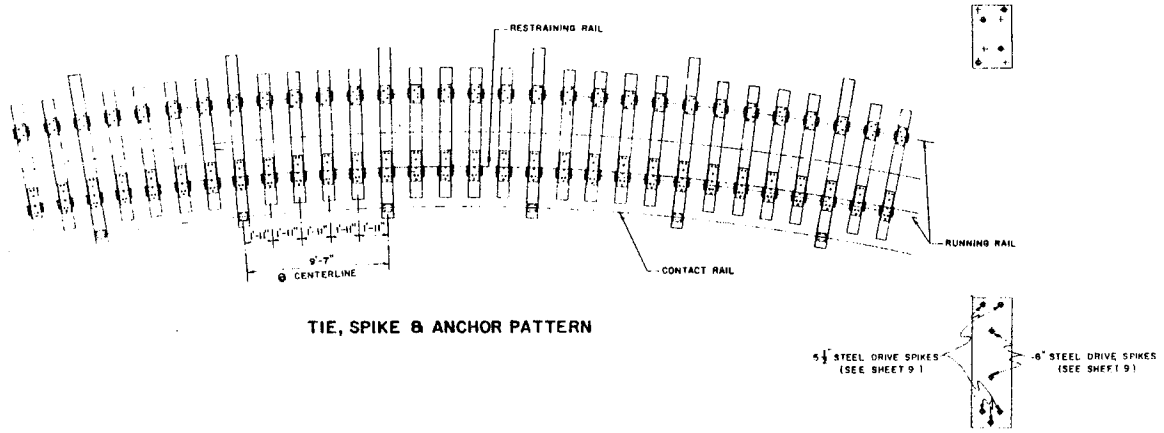

TIE, SPIKE & ANCHOR PATTERN

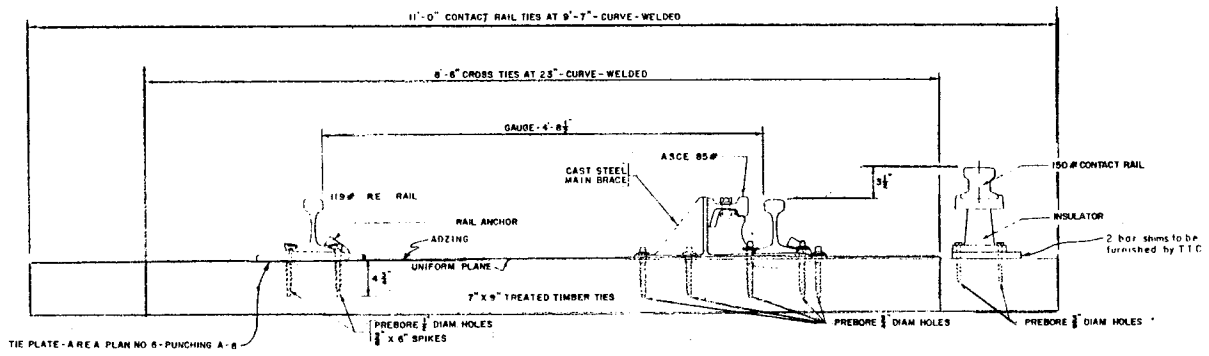

CROSS SECTION OF TRACK ASSEMBLY

FIGURE 2.2. TIGHT TURN LOOP TRACK CONSTRUCTION.

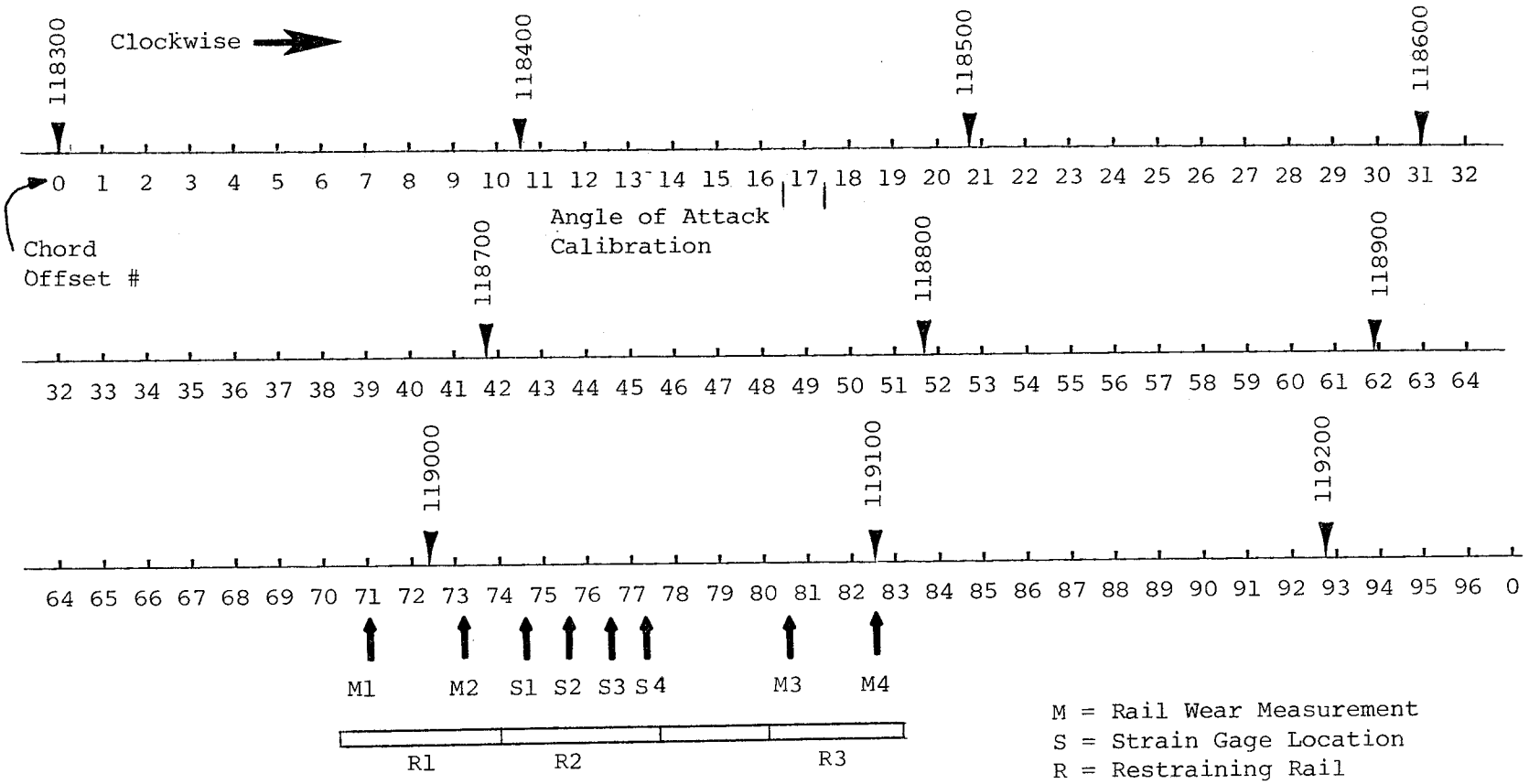

FIGURE 2.3. TIGHT TURN LOOP MARKING AND INSTRUMENTATION LOCATIONS.

Figure 2.4 shows the main dimensions and performance characteristics. Of interest in the tight turn tests was the truck centerline spacing of 54 ft and the axle spacing of 7 ft 6 inches. The vehicle is permitted to operate on a minimum track curve radius of 145 ft with the floor at 3'10½" and 295 ft radius with the floor at 3'5½".

The lateral semi-spacing between side bearers is 46.0 inches; nominal wheel diameter 30.0 inches. Vehicle weight for the tests was 97,020 lbs; 49,220 lbs A-end and 47,800 lbs B-end.

2.2.2 Truck and Suspension

The SOAC body is suspended by two self-leveling air springs per truck which transfer the vehicle weight into the bolster, (see Figure 2.5). The body is constrained longitudinally to the bolster by two links with rubber mounts, but is free to move laterally with respect to the bolster up to the limit imposed by rubber bump stops. Vertical and lateral damping of the carbody to the bolster motion is provided by rotary hydraulic shock absorbers. The vehicle weight is transferred from the bolster by the side bearers into a lightweight cast steel 'H' truck frame which rotates relative to the bolster about a center pin. The primary suspension consists of Chevron rubber springs, two for each journal. The traction motors (two motors per truck) are supported by links to the truck frame and by a gear box unit hung on each axle.

2.2.3 Instrumentation

Instrumentation for the tests consisted of two independent systems--on-board and wayside.

a. On-Board

The following transducers were used.

MEASUREMENT	TRANSDUCER	QUANTITY
Truck Longitudinal & Lateral Primary Displacements	Trans-Tek ±.5" LVDT's	6
Truck Yaw Angles	Celesco ±5" String Pots	2
Automatic Location Detector (ALD)	Modulated IR Light Source w/Reflective Tape	1

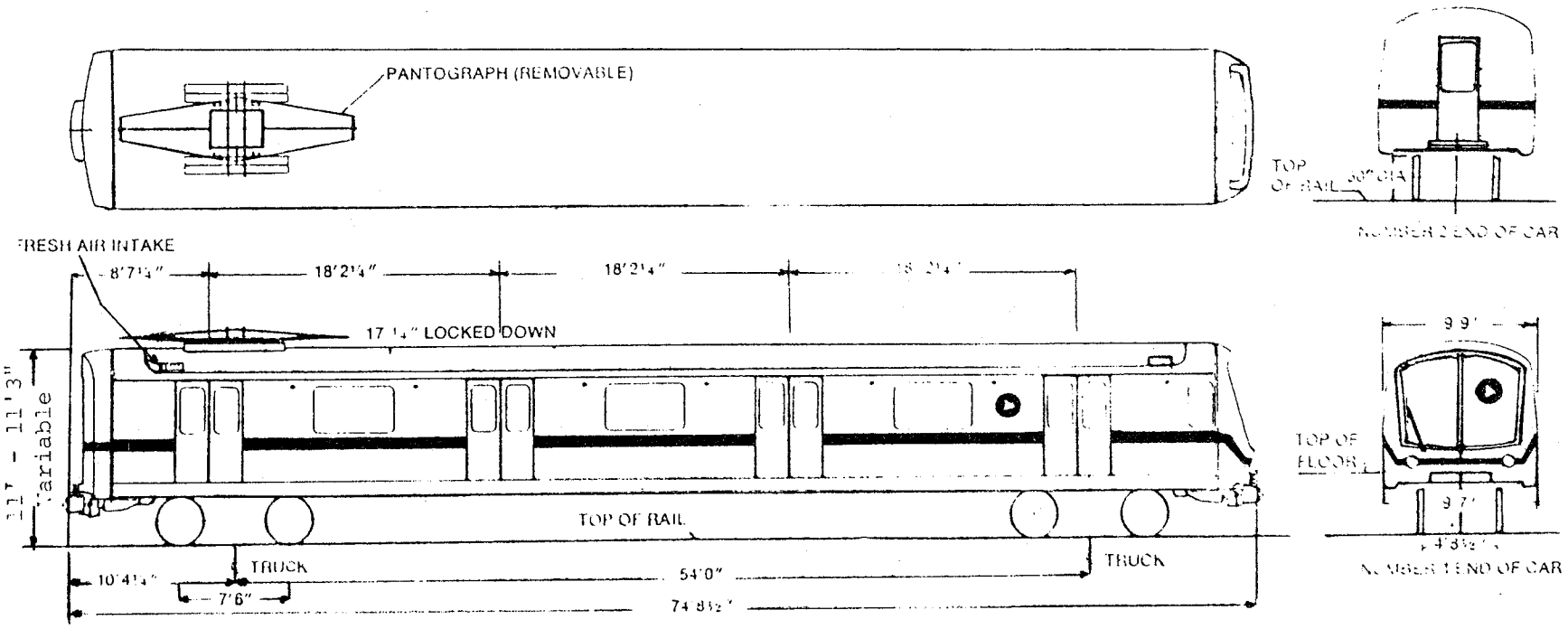

Length	75 Feet
Width	9.75 Feet
Minimum Track Curve Radius	145 Feet
Speed	80 MI/H
Acceleration, initial	3.0 MI/H/Sec.
Jerk Rate	2.5 MI/H/Sec^2
Power	600 VDC Nominal
Noise Level, interior	spec 75 dBA @ 50 MI/H actual 63 dBA @ 50 MI/H
Noise Level, 50 ft wayside	78 dBA @ 50 MI/H actual 73 dBA @ 50 MI/H

Passenger Capacity (No. 1 car)

Seated	62
Nominal	100
Maximum	220

Passenger Capacity (No. 2 car)

Seated	72
Nominal	100
Maximum	300

FIGURE 2.4. SOAC PERFORMANCE AND DESIGN CHARACTERISTICS.

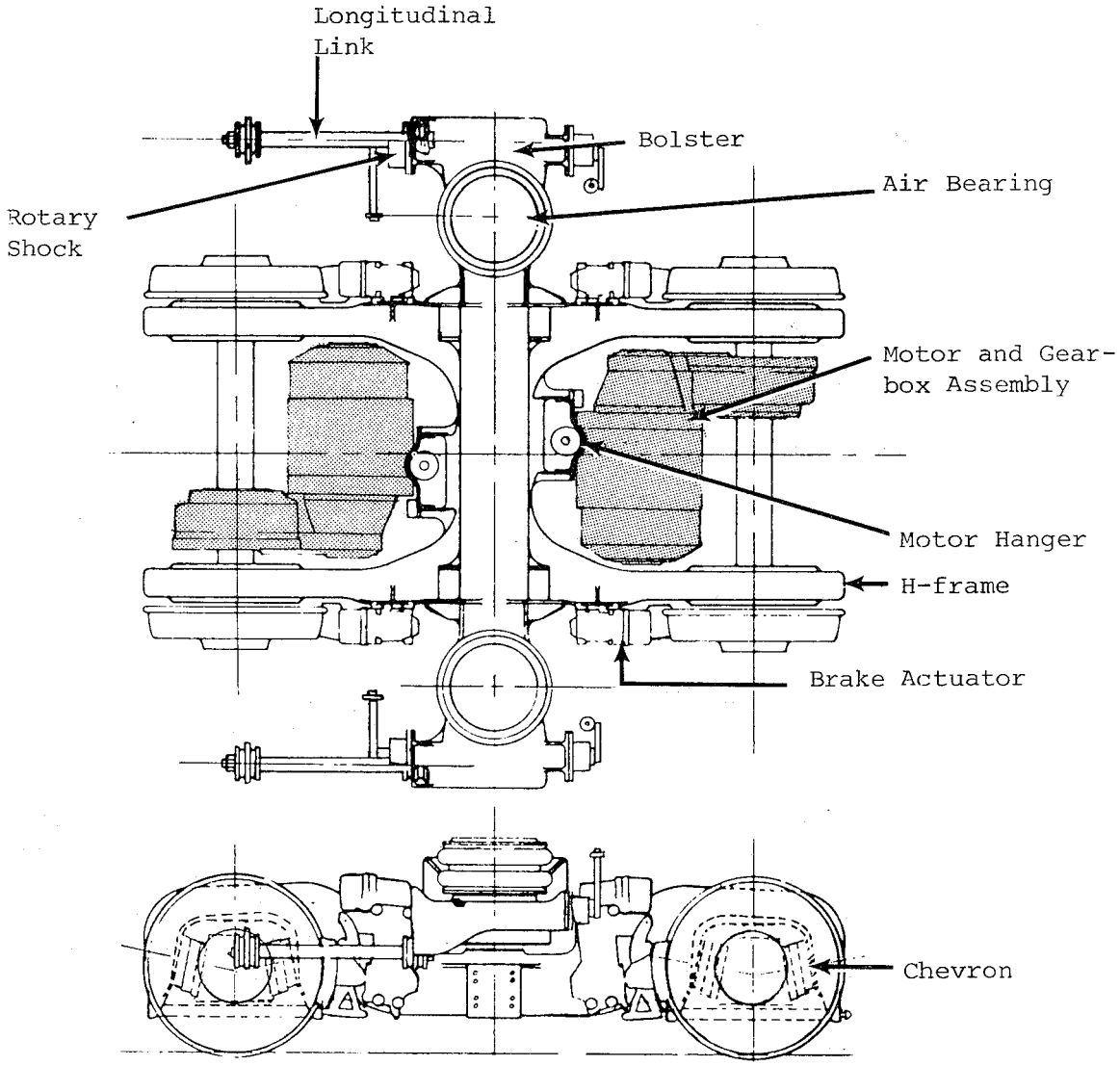

FIGURE 2.5. SOAC TRUCK ASSEMBLY.

Truck Air Bag Pressures	BLH 250 psig	2
Line Voltage	Divider (Monitor Panel)	1
Line Current	(Monitor Panel)	1
Speed	(Monitor Panel)	1
Time	Time Code Generator	1
	TOTAL NO. OF CHANNELS	15

The signal conditioning was by a 15-channel Endevco package which provided amplification, buffering, calibration and balancing of data channels. Filtering was provided by 15 channels of Ithaco low-pass selectable filters. Recording was performed on:

- Strip Chart: Two Brush Model 481 8-channel analog recorders.
- Analog Tape: One 14-track Bell & Howell Model 4010B tape recorder.

In addition, a data logger was used to monitor selected propulsion temperatures because of the sustained low speed running.

The two string pots used to measure truck rotation were set in such a way that the string was normal to a line through the center pin at the point of attachment when the truck was in position on the Tight Turn Loop. The string pots were disconnected when the car was run off the loop because the resultant string extension would exceed the string pot range.

b. Wayside

Wayside data collection used 24 channels of rail force data, 1 channel for timing. Rail force measurements were made at each of four center-of-crib locations and provided the following information:

- Outside Rail--Vertical Force
  --Lateral Force
- Inside Rail--Vertical Force
  --Lateral Force
- Restraining Rail--Vertical Force
  --Lateral Force

Strain gages used for rail force circuits were:

- Running Rail Vertical Forces: Hitec Shear 90° Dual Element Type No. HBWS-350-125-6-10GP
- Running Rail Lateral Forces: Hitec Individual Element Type No. HBS-350-125-6-10GP
- Restraining (Guard) Rail Vertical Forces: Hitec Individual Element Type No. HBW-350-125-6-10GP
- Restraining (Guard) Rail Lateral Forces: Hitec Shear 90° Dual Element Type No. HBWS-350-125-6-10GP

A timing signal was acquired via a FM-VHF timing receiver tuned to TTC Standard timing. The receiver output was then fed to a Datum 9300 time code generator which generated an IRIG-B signal for recording on analog tape.

The signal conditioning system used was a 30-channel Dynamics package. The Dynamics conditioners provided amplification, filtering, buffering, calibration, and balancing for the strain gage circuits and ALD channel.

The recording devices used were:

- Strip Chart: One Brush Model 481 8-channel analog recorder.
- Analog Tape: One Honeywell 101 28-track FM Intermediate-band magnetic tape recorder running at a tape speed of 1-7/8 ips. The data bandwidth for the rail force data channels was 625 Hz.

Figures 2.6 and 2.7 show the strain gage layout for vertical and lateral forces.

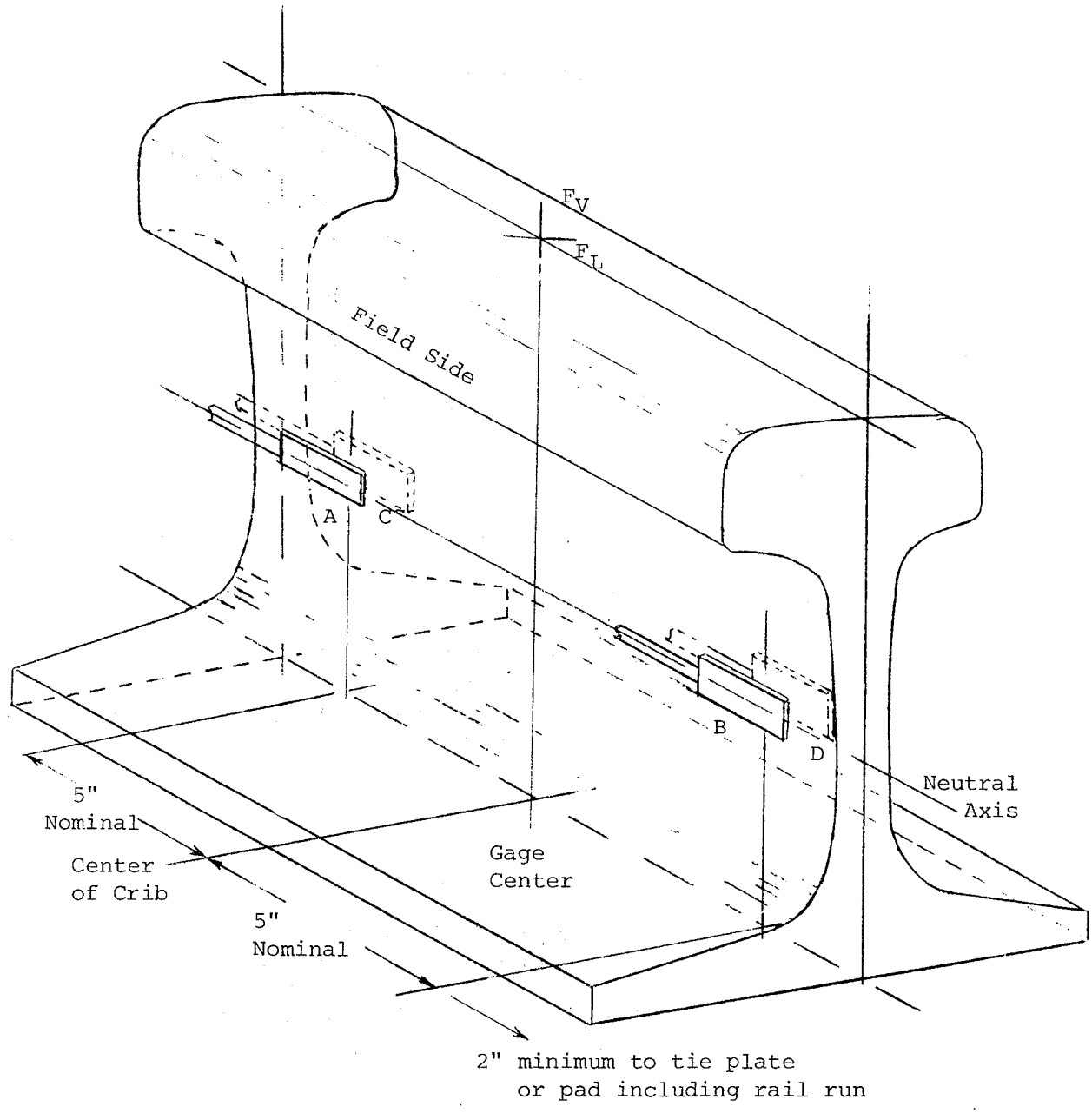

FIGURE 2.6. RAIL VERTICAL FORCE STRAIN GAGE PLACEMENT.

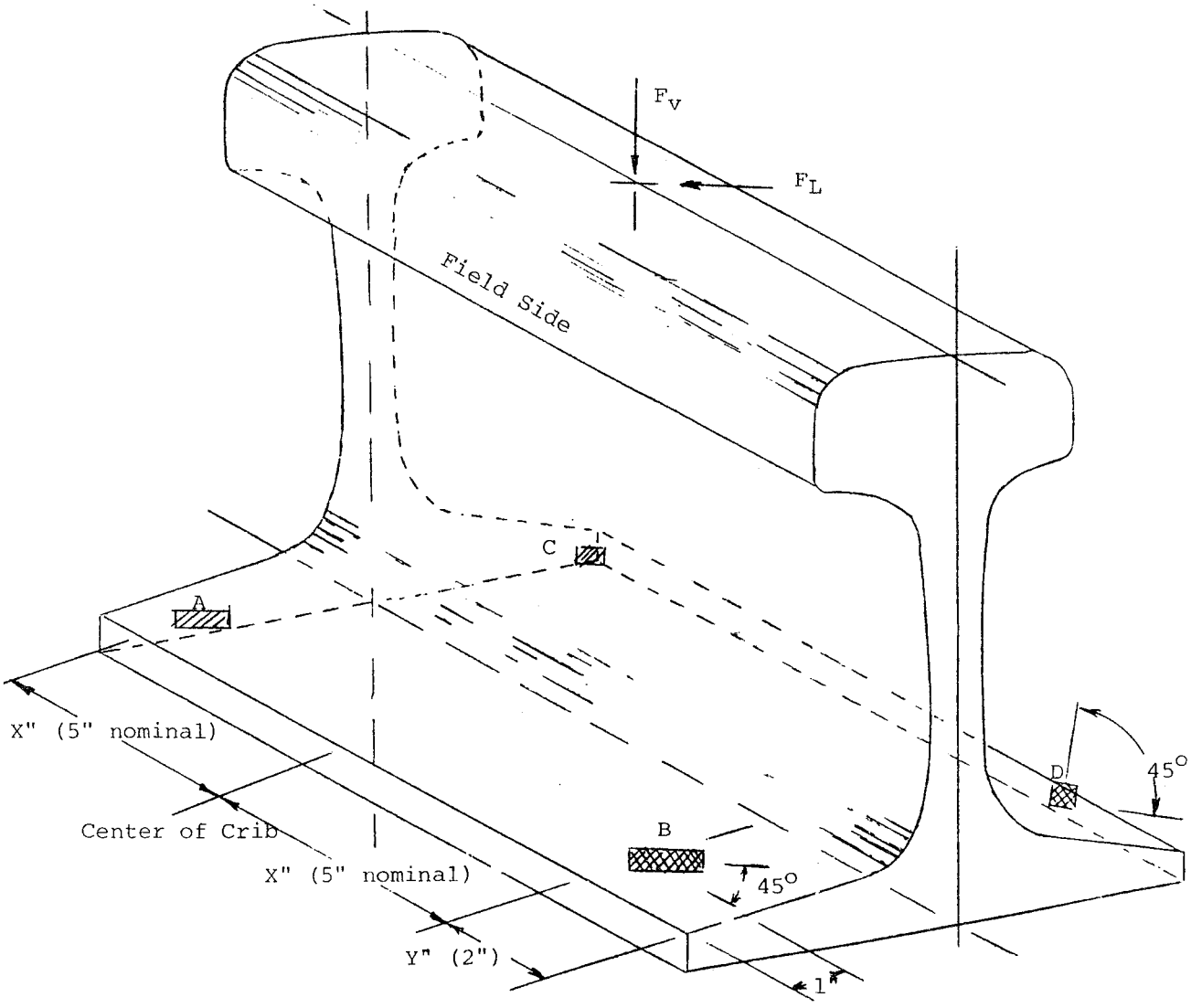

GAGE PLACEMENT

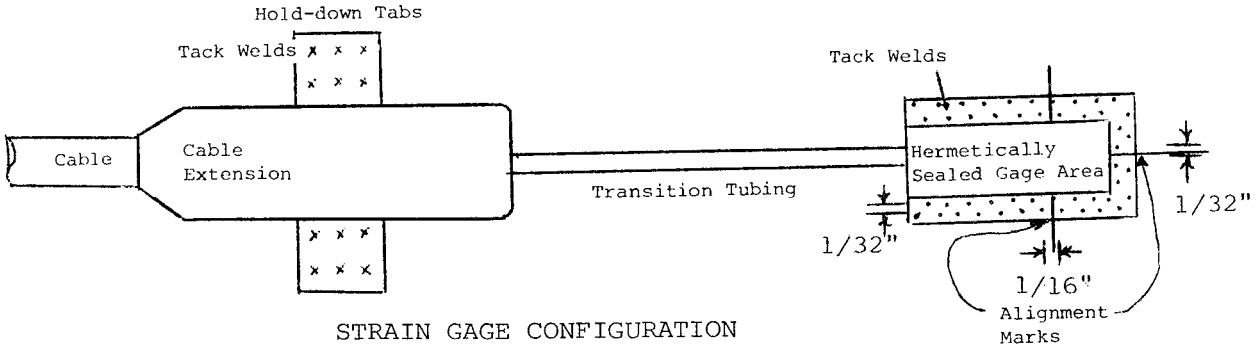

STRAIN GAGE CONFIGURATION

FIGURE 2.7. RAIL LATERAL FORCE STRAIN GAGE PLACEMENT.

3.0 EXPERIMENTAL RESULTS

The experimental results are detailed as follows:

3.1 TRACK SURVEY

As part of the test the Tight Turn Loop was surveyed for the following parameters:

- o True Center of Track
- o Alignment (mid-chord offset)
- o Crosslevel
- o Gage
- o Restraining Rail Clearance
- o Restraining Rail Height

The survey was performed in order to relate any apparent irregularities in measured data with track conditions. The alignment, crosslevel, track gage, restraining rail clearance, and restraining rail height were all taken at the same 10 ft intervals.

a. True Center of Track

In order to provide an accurate datum for the angle of attack measurement, it was required that the true center of the Tight Turn Loop be located in order to set up sight lines at the angle-of-attack calibration site. This was accomplished by the use of an HP electronic laser surveyor. The laser surveyor was set up at the nominal center of the track circle, a reflective prism was placed at intervals around the loop on the inside rail, and the distance from surveyor to the prism and corresponding swept angle were measured. The values were then converted into XY coordinate form, and an area minimization program run to find the effective center of the curve.

The effective center of the curve was found to have coordinates of:

X = -0.019 foot
Y = +0.006 foot

from the location of the survey. For all practical purposes the marked curve center was at the effective center of the track.

b. Alignment (Mid-Chord Offset)

The mid-ordinate-to-chord method (string lining) was used to assess the curve alignment. The common chord length of 62 ft (in which the mid-ordinate-to-chord measurement in inches is equal to the curvature of the track in degrees) was not used

because of the tightness of the curve. A nominal 20 ft chord was chosen which gave convenient mid-ordinate-to-chord measurements of the order of 4 inches, and the measurements were taken on the outside rail. The readings presented are in tabular form in appendix A.

The effective track radius of curvature for each mid-ordinate-to-chord value was calculated. Figure 3.1 shows the 'pre-test' data plotted versus track location and Figure 3.2 the 'post-test' data. The two figures are shown overlayed in Figure 3.3.

The data shows that the poorest alignment is located in the region between 118300 and 118400 and between 118900 and 119100. The angle of attack calibration site is in a region of good alignment, but the strain gage and measurement sites are in a poor region.

The overlay, Figure 3.3, shows that the alignment was substantially consistent during the test. Most of the track has an effective radius between 140 ft and 160 ft.

c. Crosslevel

The readings are presented in tabular form in appendix A.

The 'pre-test' data plotted versus track location is shown in Figure 3.4 and the 'post-test' data in Figure 3.5. The two figures are shown overlayed in Figure 3.6.

The data shows the track to be in two sections. Between 118300 and 118700 the nominal superelevation is 0.75 inch, between 118800 and 119100 superelevation is 1.5 inch. Two peaks are of note, one is located at 118500 which is in the vicinity of the angle-of-attack calibration site, and the other at 118970 is near the rail force measurement site. The data shows that the wavelengths and the crosslevel variations are of the same order as the truck center spacing of the SOAC (at 54 ft). It is probable that the vehicle would be highly sensitive to these irregularities.

The overlay of data in Figure 3.6 indicates that the crosslevel was consistent for the duration of the test.

d. Gage

The readings are presented in tabular form in appendix A.

The 'post-test' data plotted versus track location is shown in Figure 3.7. The data shows that between station 118300 to 118900 the gage lies in the region 56.8 inches. Between station 118900 to 119100 the gage is slightly wider at 57.05 inches. This region of wider gage corresponds to the region of 1½" superelevation.

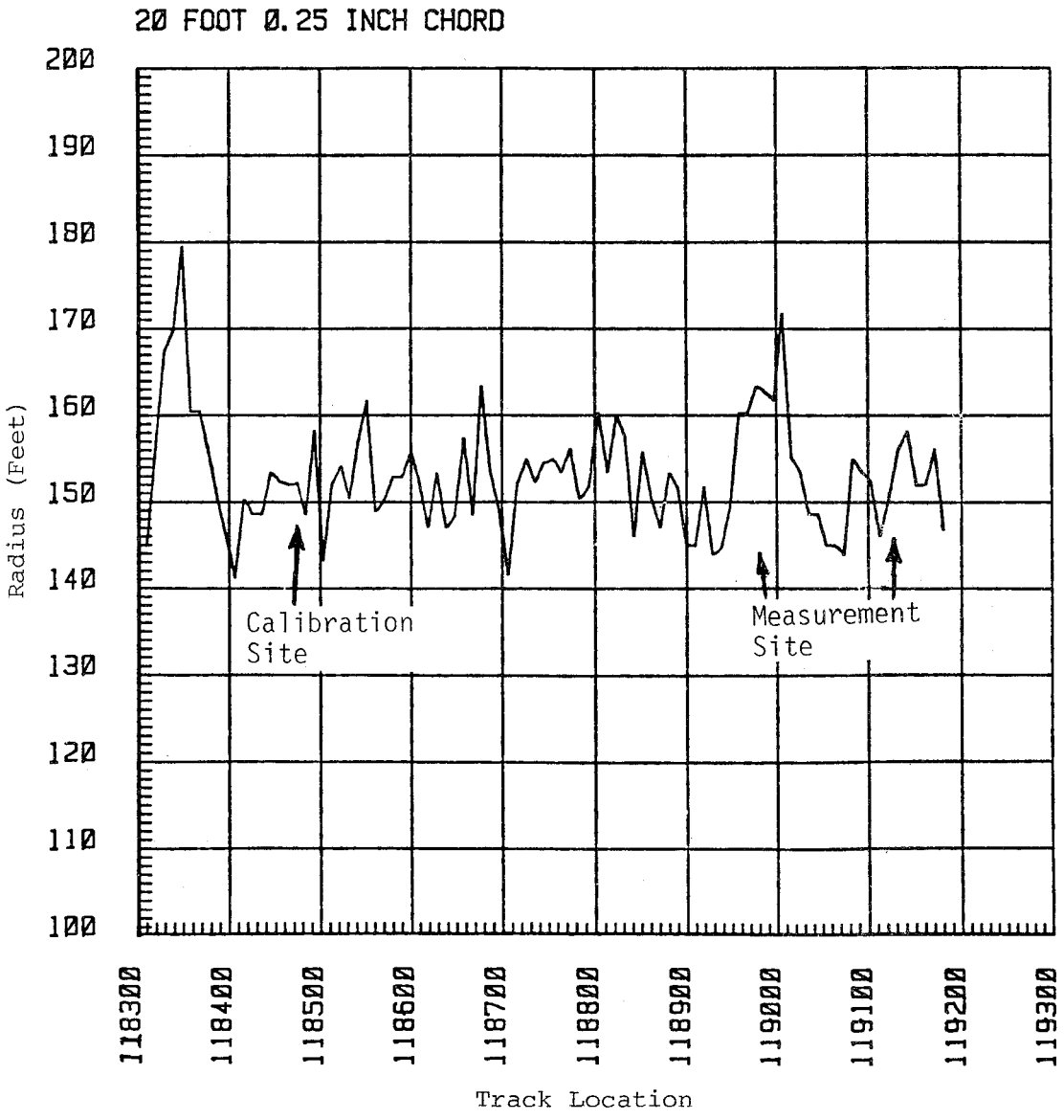

FIGURE 3.1. PRE-TEST RADIUS OF CURVATURE.

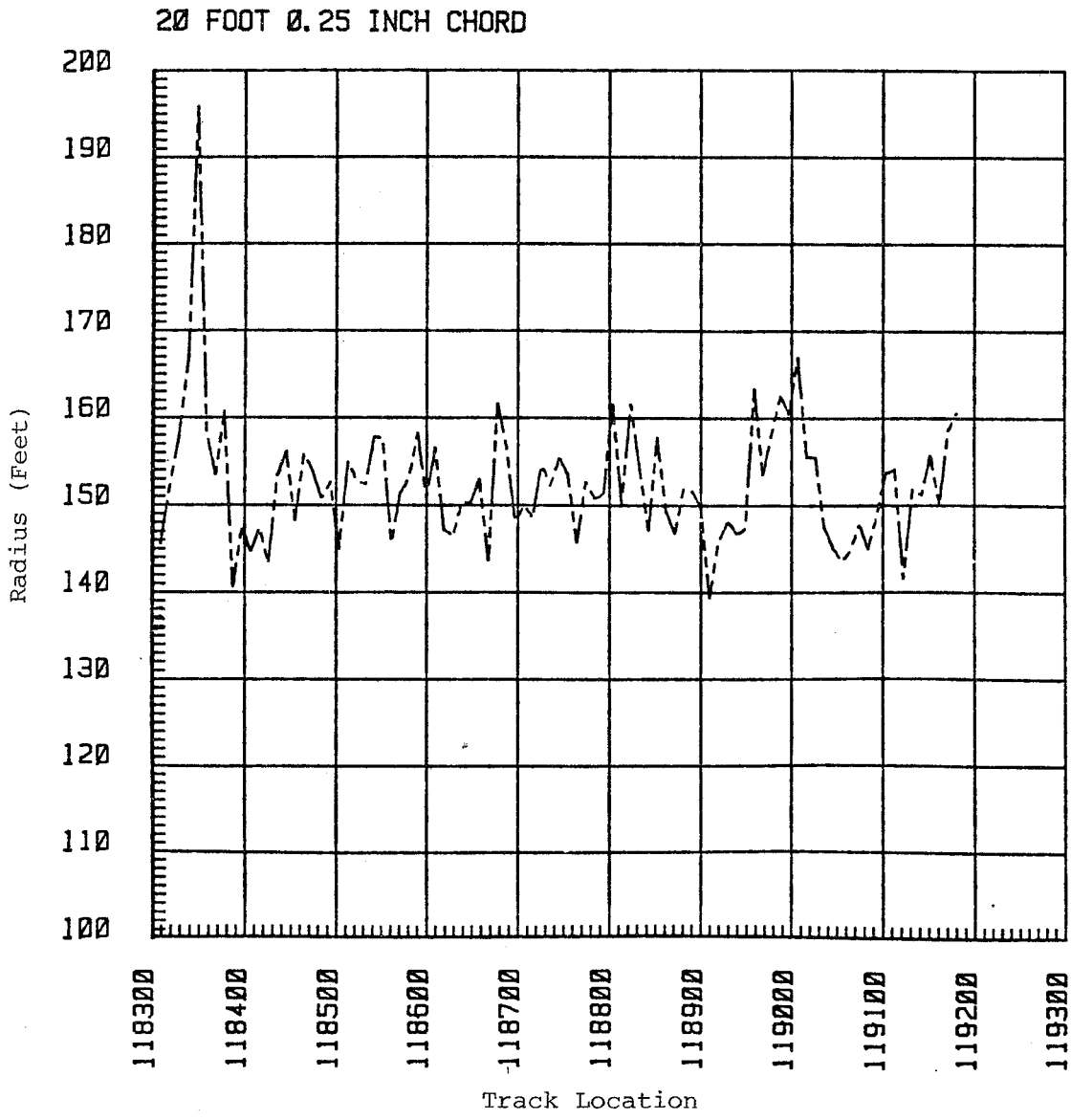

FIGURE 3.2. POST-TEST RADIUS OF CURVATURE.

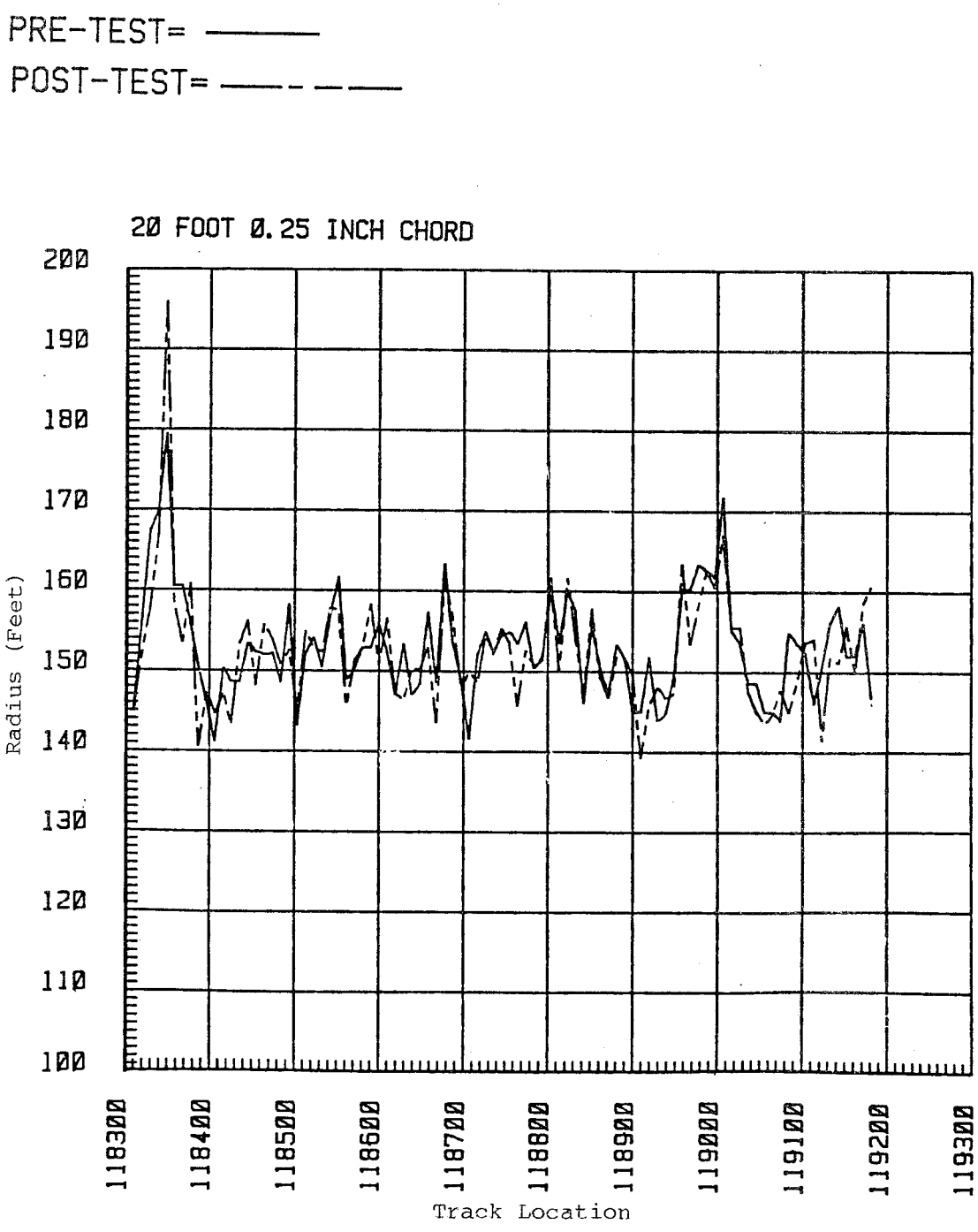

FIGURE 3.3. PRE- AND POST-TEST RADIUS OF CURVATURE.

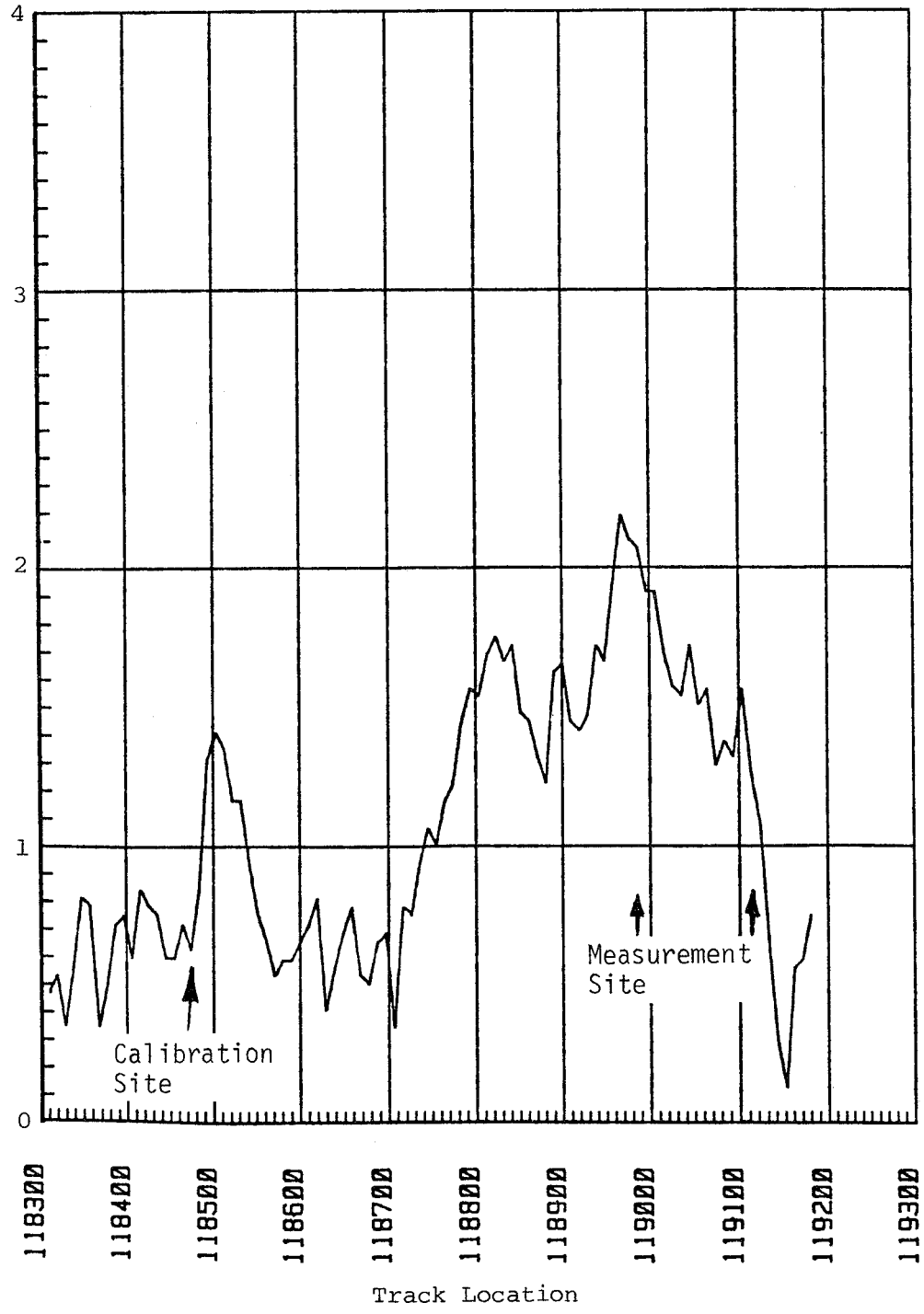

FIGURE 3.4. PRE-TEST SUPERELEVATION.

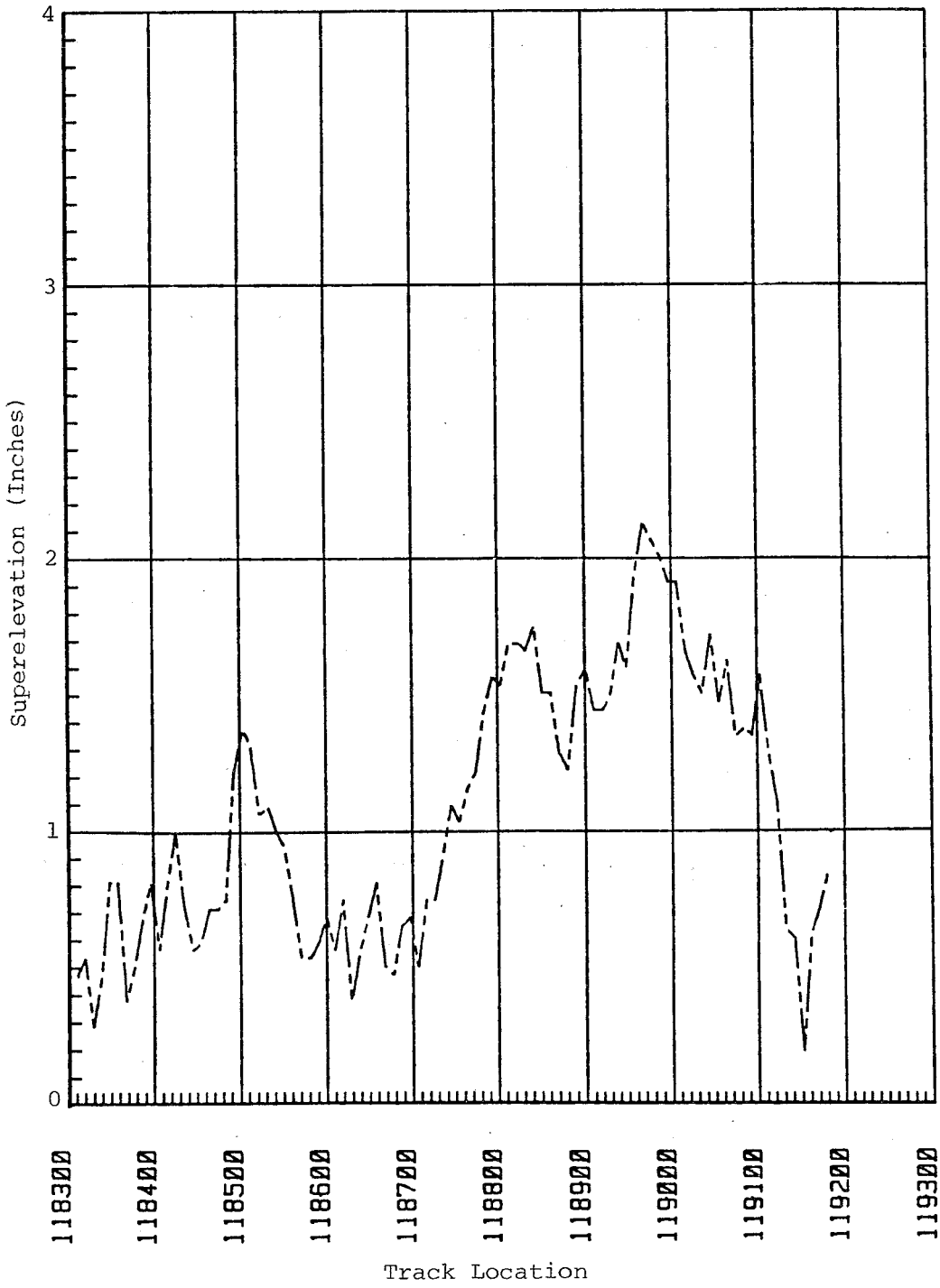

FIGURE 3.5. POST-TEST SUPERELEVATION.

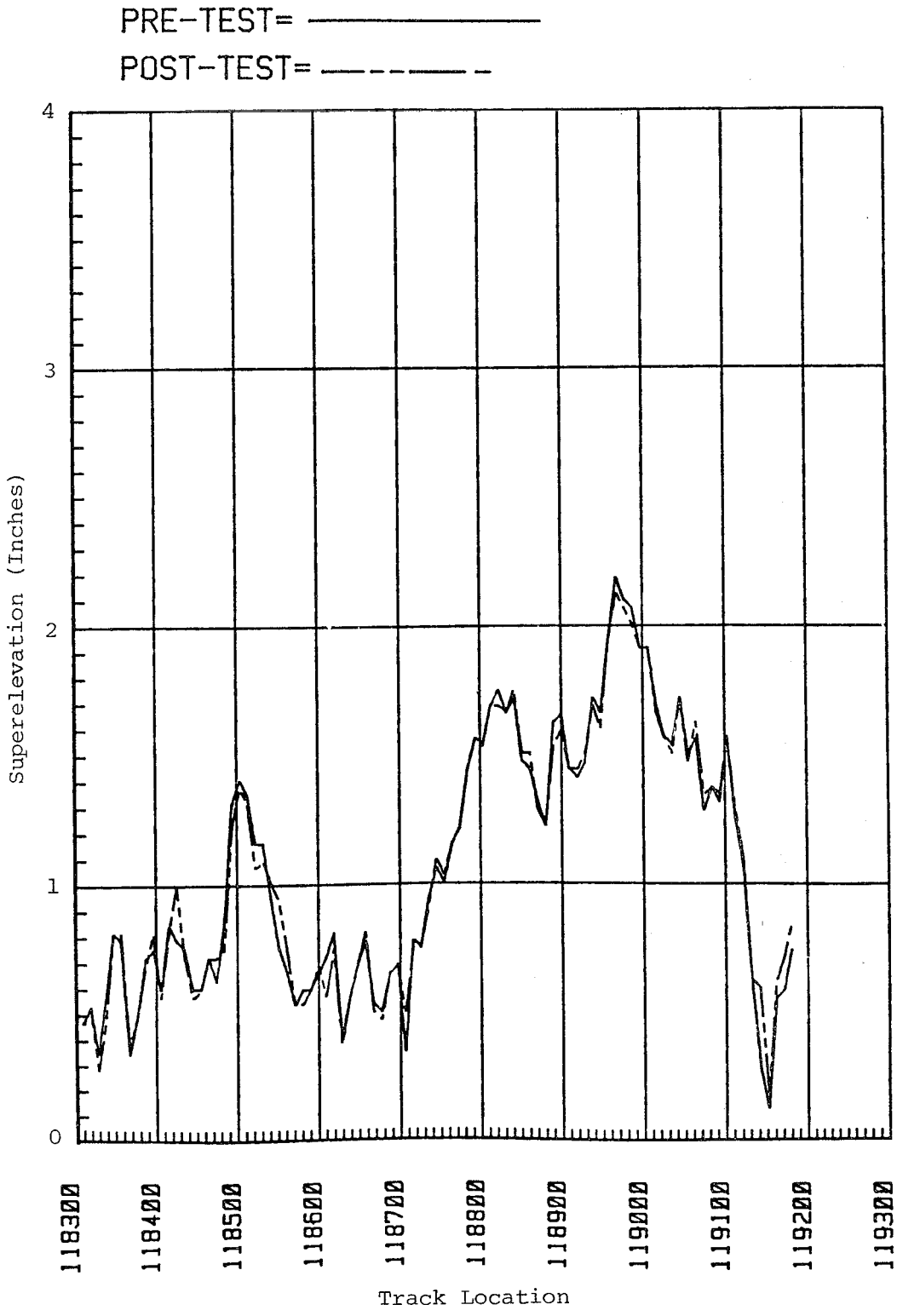

FIGURE 3.6. PRE- AND POST-TEST SUPERELEVATION.

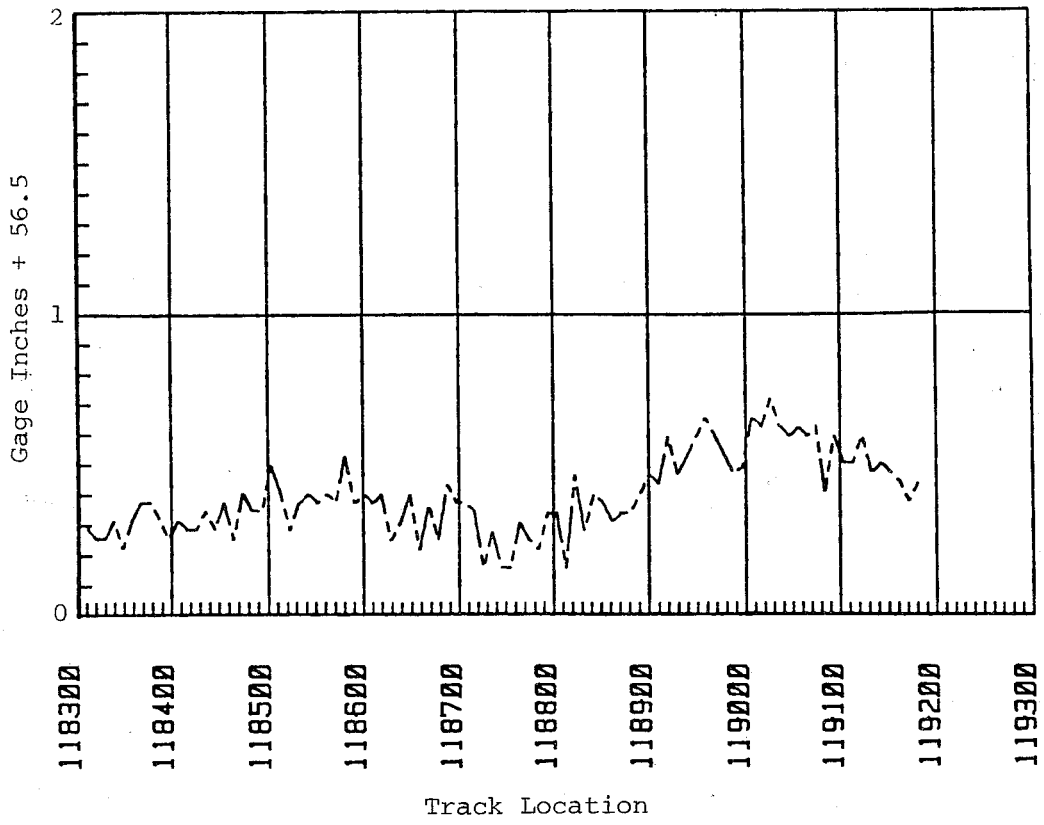

FIGURE 3.7. POST-TEST GAGE.

e. Restraining Rail Clearance

The readings are presented in tabular form in appendix B.

The readings were taken with inside calipers and the minimum clearance between the two rails noted. The caliper dimension was transferred to vernier outside calipers for reading.

The 'post-test' data plotted versus track location is shown in Figure 3.8. The data shows no trend with track location, the average value is at 2.0" with a range of ± 0.1 inch.

f. Restraining Rail Height

The readings are presented in tabular form in appendix B.

The 'post-test' readings were taken with a crosslevel gage as a reference and a depth gage. Figure 3.9 shows the data plotted versus track location. The data shows no trend with track location, with an average value of $0.6"^{+0.1}_{-0.3}$.

3.2 WHEEL AND RAIL WEAR

3.2.1 General

Rail wear measurements were made at 4 sites, close to, but not at, the strain gaged locations (see Figure 2.3). For convenience, two measurement locations were selected on either side of the strain gage sites. At each location (designated #1, #2, #3, #4 in clockwise direction) both running rails and restraining rail profiles were measured to detect loss of material or deformation.

Initially, wheel profiles were measured only on the lead truck of SOAC. As the test progressed measurements were extended to include the rear truck.

During the planning stage, it was predicted that the rail wear rates would be substantially lower than the corresponding wheel wear rates because a given point on a wheel experiences 30 times the contact per lap as does an equivalent point on the rail. This is based on the relationship of the number of axles on the SOAC car and the ratio of diameters of the SOAC wheel and Tight Turn Loop. The simplistic assumption was made that the wheel and rail materials were similar in wear properties.

All standard wheel and rail profiles were taken using British Rail profilometers. During the tests with restraining rail, which caused flange back wear, a special flange back profilometer was used. However, this device proved to be difficult to use and

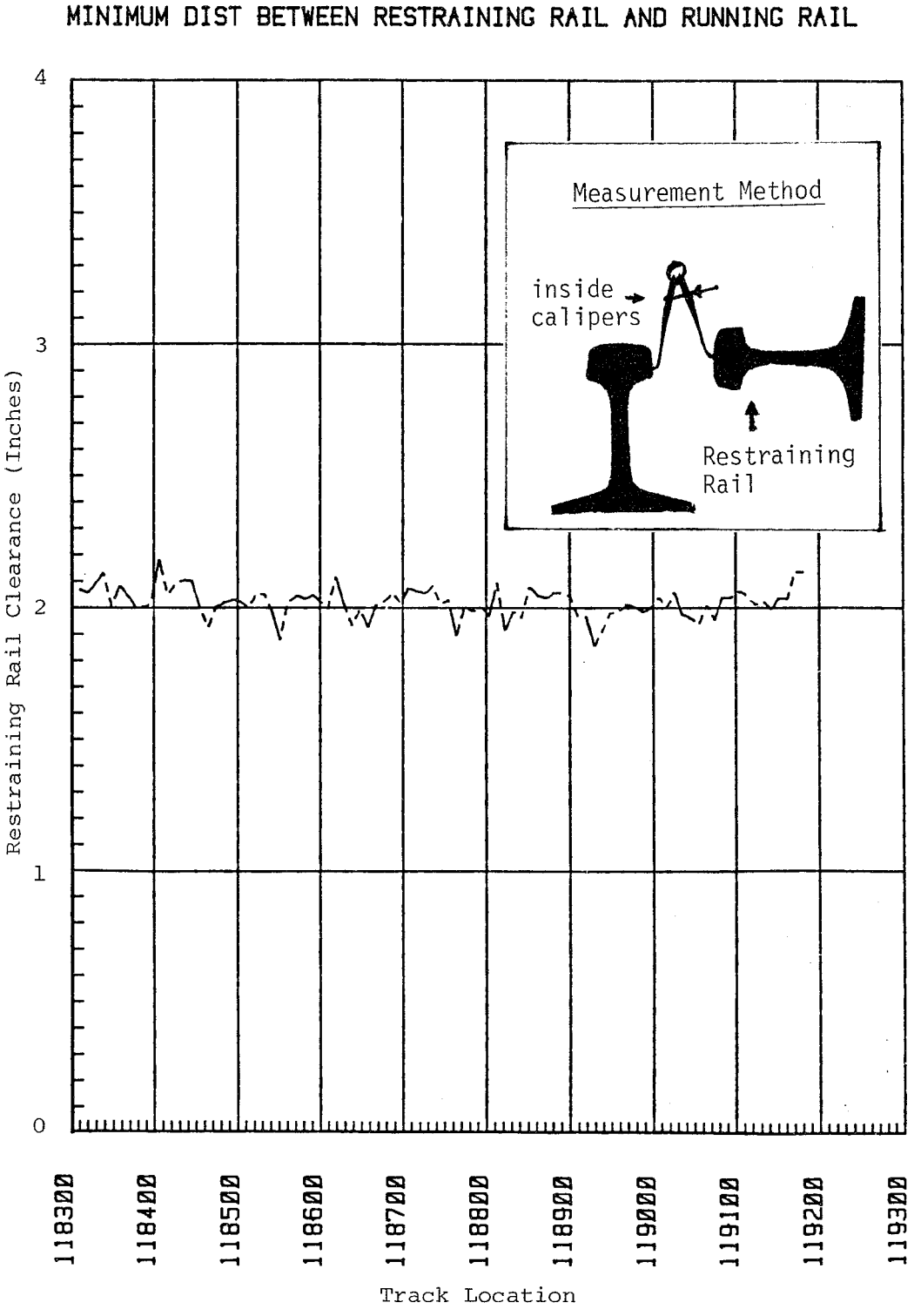

FIGURE 3.8. RESTRAINING RAIL CLEARANCE.

HEIGHT FROM THE CROWN OF THE

LOW RUNNING RAIL TO THE

TOP SURFACE OF THE RESTRAINING RAIL

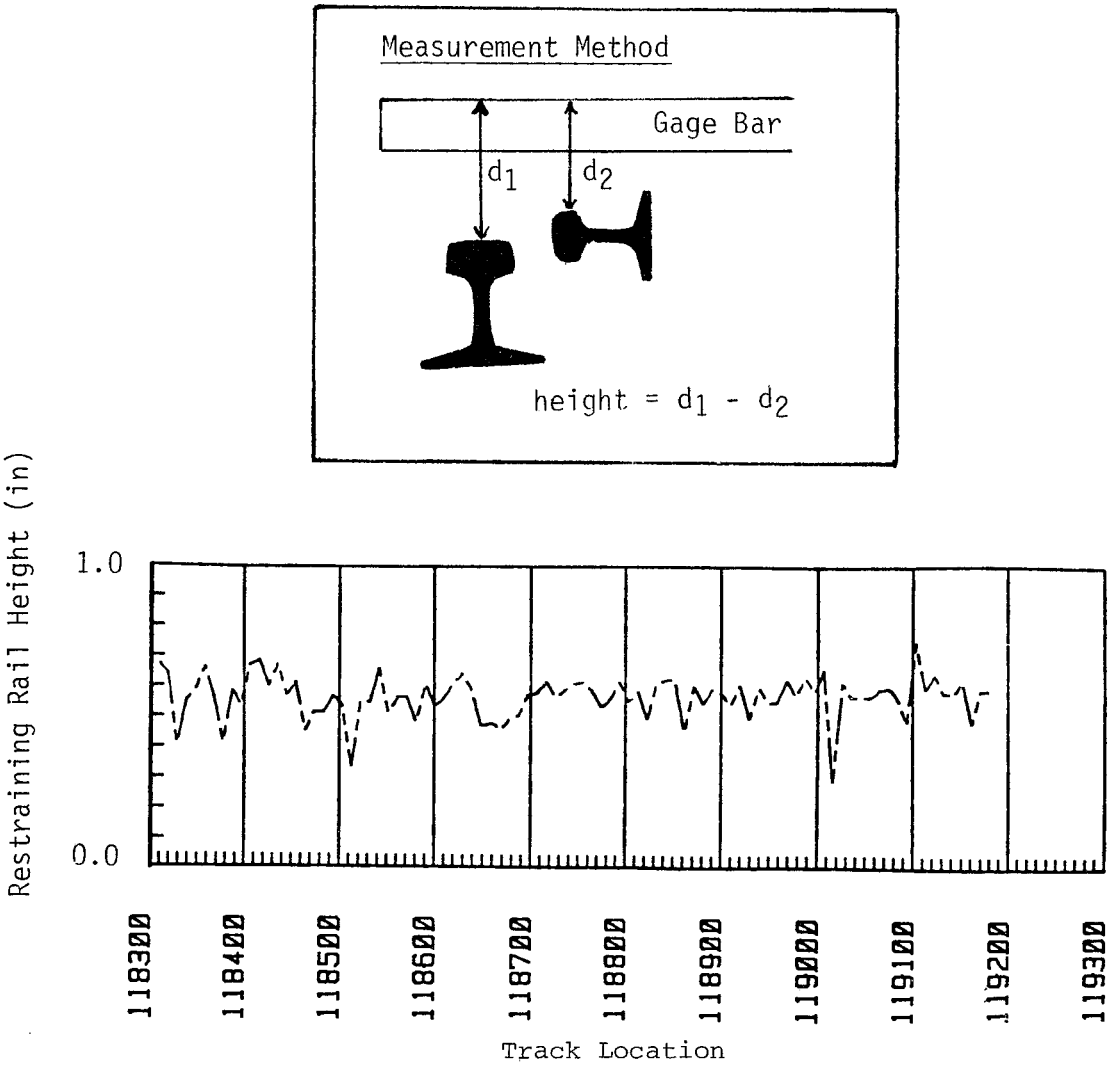

FIGURE 3.9. RESTRAINING RAIL HEIGHT.

repeatability was poor. A redesign for future work of this type is essential to significantly improve the data collected.

Standard wheel and rail profiles were entered into the Honeywell data bank using 'WHRL1 and WHRL2' programs. After testing without the restraining rail was completed, the wheel profiles were expanded to include 42 data points, the extra two points were designed to better define the flange area. The Honeywell software was modified accordingly with alternative versions for 40 and 42 point profiles being available. All profiles were quality controlled at the data entry stage with any 'bad' points being corrected. All flange back profiles were hand plotted.

Standard profile wear rates (both wheel and rail) were determined using the profile overlay program WHRL9 by which the profile area loss is directly calculated. The flange back area loss was determined by measurement from an expanded (20X) plot of the flange back.

3.2.2 Test Schedule

The objective of the test was to obtain a number of wear/mileage data points for both the wheels and rails, limited to the clockwise direction and to axles 1 and 2 only. However, as the test developed, the test sequence became quite complicated, including reverse running of the vehicle. Although at the end of the test, the data was able to produce the required information.

For both wheels and rails, each profile was assigned a unique name which included a 'sequence' letter for the wheels and a sequence number for the rails to identify the type of running, etc. The following tables describe the sequence letter/number and remarks.

TABLE 3.1. PROFILE IDENTIFICATION.

a. Wheel Profiles.

Sequence Letter	Date	# Laps from Last Profile	Restraining Rail	Remarks
A	3/31/82	0	No	Initial profiles prior to Force, Angle-of-Attack, and Drift Tests
B	5/12/82	40 Forward 40 Reverse	No	Start of Wear Tests. Only wheelsets #1 and #2 were measured during this phase of testing
C	5/17/82	120	No	
D	5/18/82	120	No	
E	5/21/82	140	No	End of Test without restraining rail
F	6/3/82	20 Test + 20 Filming	Yes	Force, Angle-of-Attack, and Drift Tests
G	6/4/82	120	Yes	Wear Test with cab leading
H	6/7/82	20	Yes	Wear Test with cab trailing
I	6/9/82	72	Yes	End of Wear Test

b. Flange Back Profiles (with restraining rail only).

Wheels	Date	# Laps (from start of test phase)	Remarks
2 & 4	6/7/82	0	Initial profiles used for both phases of Wear Test with restraining rail
2 & 4	6/8/82	20	
	6/8/82	40	Intermediate profile
	6/8/82	60	
2 & 4	6/17/82	92	
1 & 3	6/17/82	160	Data from initial runs with restraining rail

c. Rail Profiles.

Sequence #	Date	# Laps Since previous profile	Restraining Rail?	Remarks
1	3/18/82	0	No	All reference profiles
2	5/13/82	40 Forward 40 Reverse	No	Not used for wear data
3	5/17/82	120	No	1st wear data point
4	5/19/82	120	No	2nd wear data point
5	5/21/82	140	No	3rd wear data point and reference for re-straining rail test
Initial Restraining Rail				
6	6/9/82	252	Yes	Only wear data point with restraining rail

a. Wheel Profiles

The profiles are stored on the Honeywell computer as follows.

SOACTL/Wheelset #/Sequence letter (A thru G)

For example SOACTL1B refers to the second profile taken on the #1 wheelset. The left and right wheels were identified as the normal hand convention when standing in the rear of vehicle looking towards the cab. The axles were numbered sequentially from the cab end of the vehicle. This convention was retained even when the car ran in the reverse direction during the final stage of the test; consequently, according to the identification convention, the right wheel ran on the left rail during this test phase.

When the 42 point wheel profile was adopted, the names of the profiles were modified to reflect this change as follows.

S42CTL/Wheelset #/Sequence letter (F thru I)

For example S42CTL2H refers to the 8th profile taken on the #2 wheelset, the data set having 42 points.

b. Rail Profiles

The rail profiles were also named in accordance with data base standards. Here the name was assigned to reflect the track, the type of rail (running or restraining), the location, and sequence number. Thus the typical name is comprised of

TTL/Rail Type (R - restraining, N - running)/Location (1 thru 4)/Sequence # (1 thru 6)

For example TTLR0103 was the third profile taken on the restraining rail at station 1.

For the running rails the left rail was assigned as the left hand rail when facing the clockwise direction of travel on the TTL. In order that restraining rail data formats comply with the data base requirements, the single rail measurements for each location were assigned to both rails in the data base.

3.2.3 Data Analysis

A typical wheel profile overlay which shows tread wear is shown in Figure 3.10 and one which shows flange wear is shown in Figure 3.11. WHRL9 program computes the wear in mm^2. A typical flange back overlay, hand plotted in expanded form is shown in Figure 3.12. The area loss was found by planimeter.

3.2.4 Wheel and Rail Wear Rates

The results are presented as follows:

Wheels - Flange & Tread, Rails - Outside & Inside } Without Restraining Rail

Wheels - Flange back, Flange & Tread, Rails - Outside, Inside & Restraining Rail } With Restraining Rail

a. Wheels - Flange and Tread, without restraining rail

The data tabulated below is from the lead truck only and for clockwise running only.

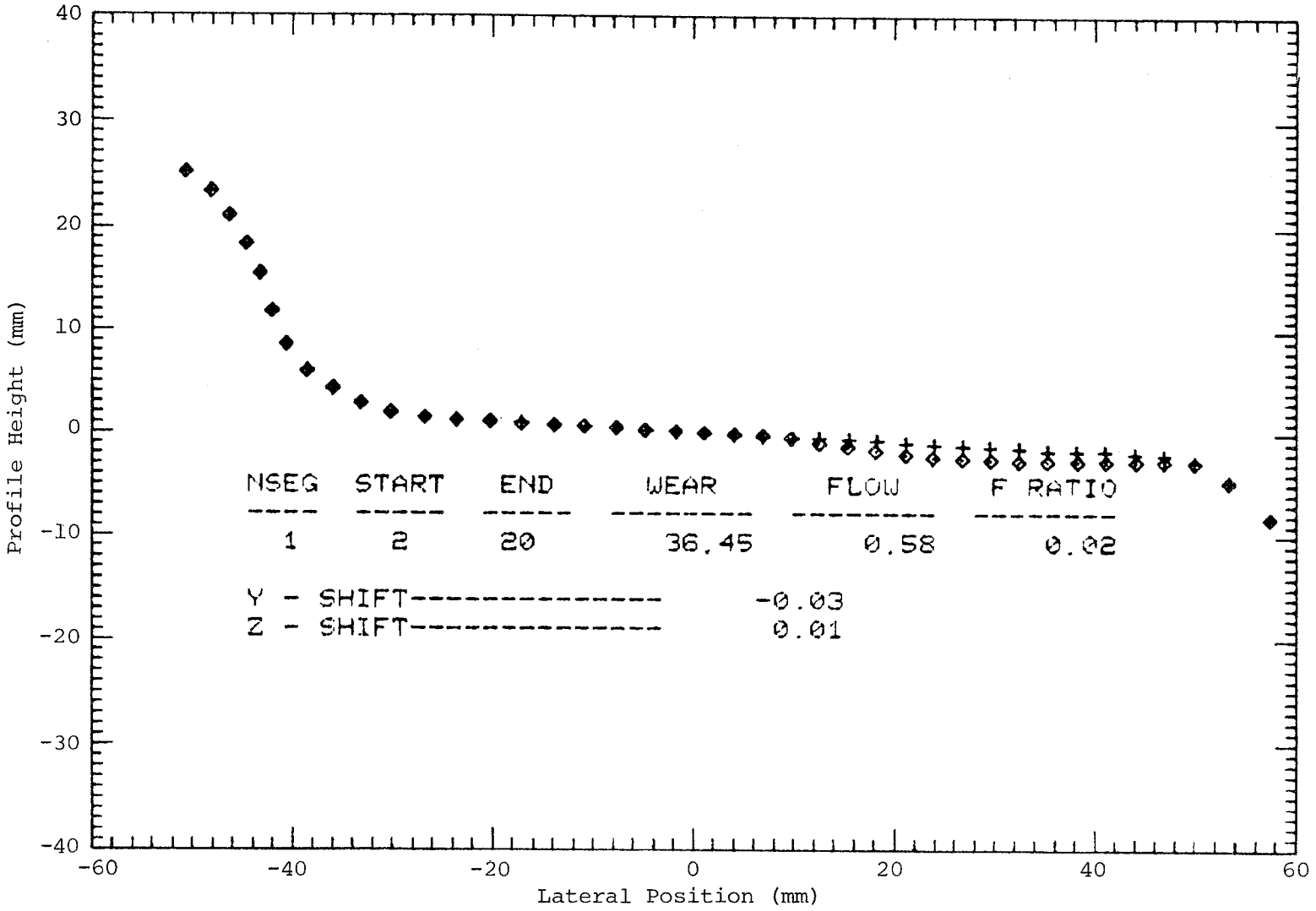

FIGURE 3.10. TYPICAL WHEEL PROFILE OVERLAY--TREAD WEAR.

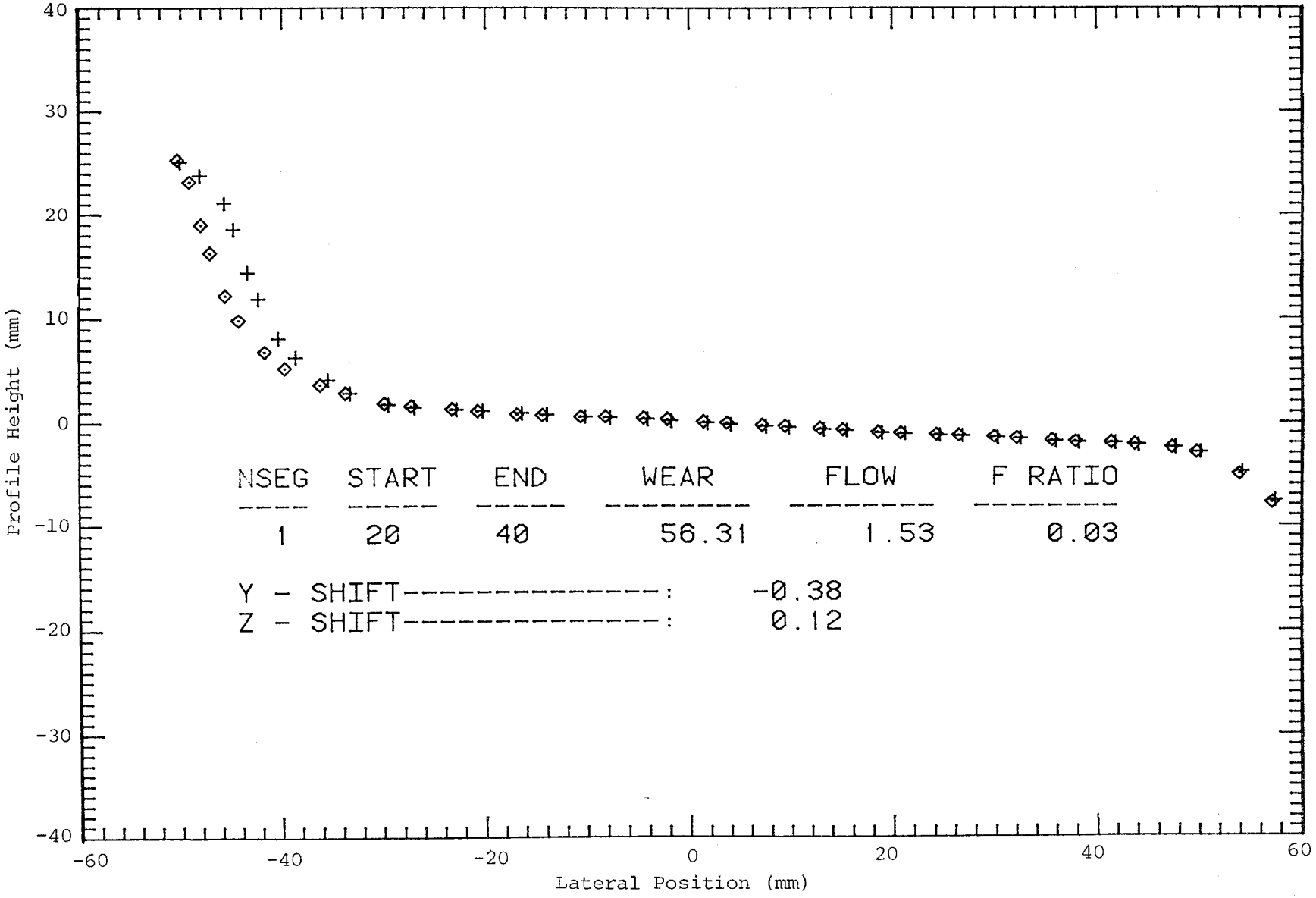

FIGURE 3.11. TYPICAL WHEEL PROFILE OVERLAY--FLANGE WEAR.

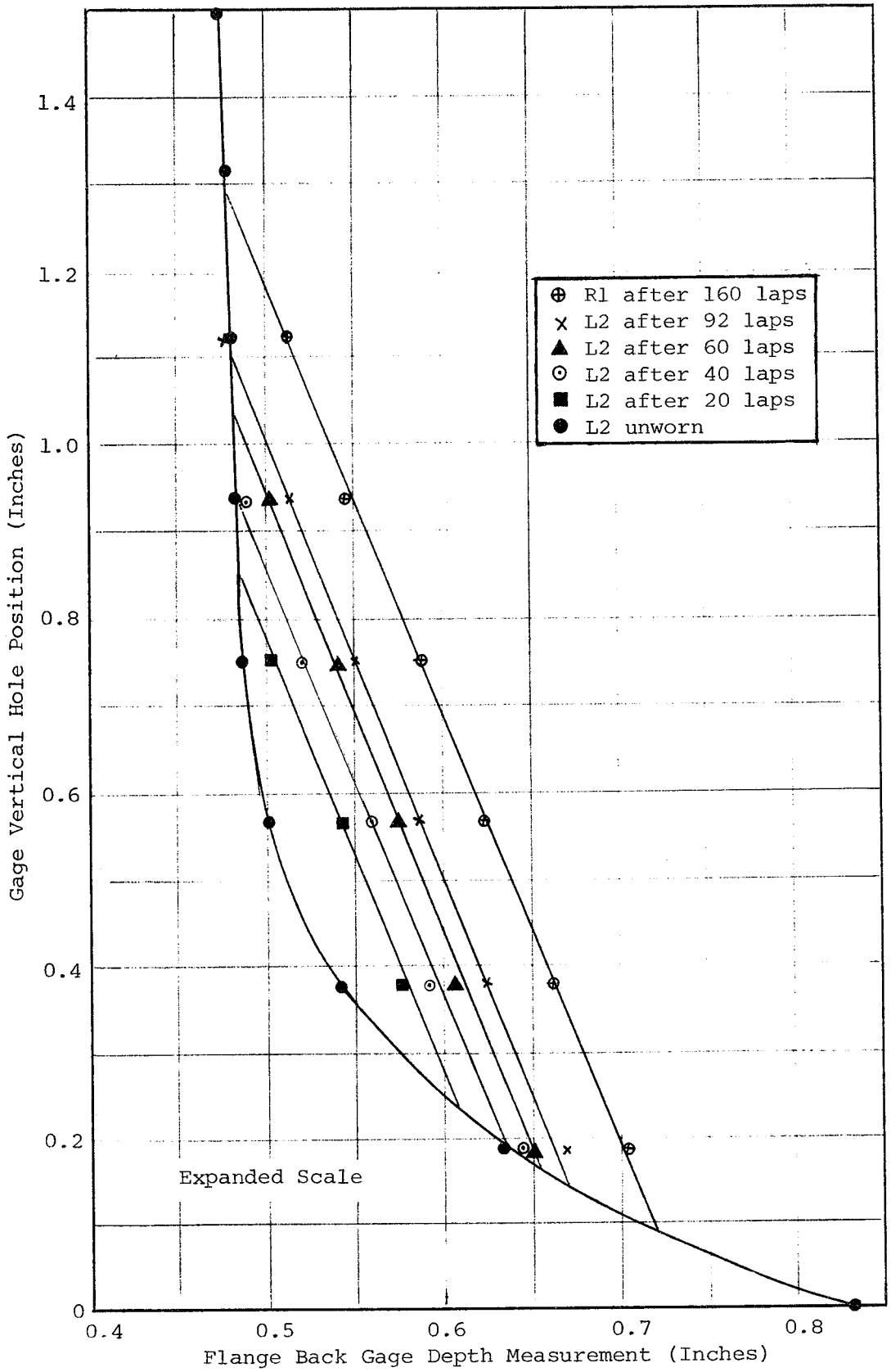

FIGURE 3.12. TYPICAL WHEEL PROFILE OVERLAY--FLANGE BACK.

TABLE 3.2a. WHEEL AND RAIL WEAR RATES.

			Type of Wear	Wear Rate mm^2/lap
Wheelset #1	L1	(Outside)	Flange	0.15
	R1	(Inside)	Tread	0.1
Wheelset #2	L2	(Outside)	Tread	0.01
	R2	(Inside)	Flange	0.03

The wear rates are taken from Figure 3.13, wheel wear area loss versus number of laps (1 lap = 943 feet = 0.18 mile). Although the data is limited to a small number of data points, it shows good consistency and linearity. As expected, the heaviest wear occurs on the outside lead wheel.

b. Rails - Outside and Inside, without restraining rail

The data in the following table was produced by clockwise running of the vehicle.

TABLE 3.2b. RAIL WEAR.

	Type of Wear	Wear Rate mm^2/vehicle pass
Outside Rail	On gage corner of rail	0.0125
Inside Rail	On rail head	0.005

Note that the wear rate is given per vehicle pass, 4 wheelsets, both lead and trail trucks. As expected the material loss is much lower, being an order of magnitude lower than the corresponding wheel wear. The data has been derived from Figure 3.14.

c. Wheels - Flange back, Flange and Tread, with restraining rail

The data in the following table was produced by clockwise running on the track but included running with the vehicle in both the cab leading and cab trailing direction.

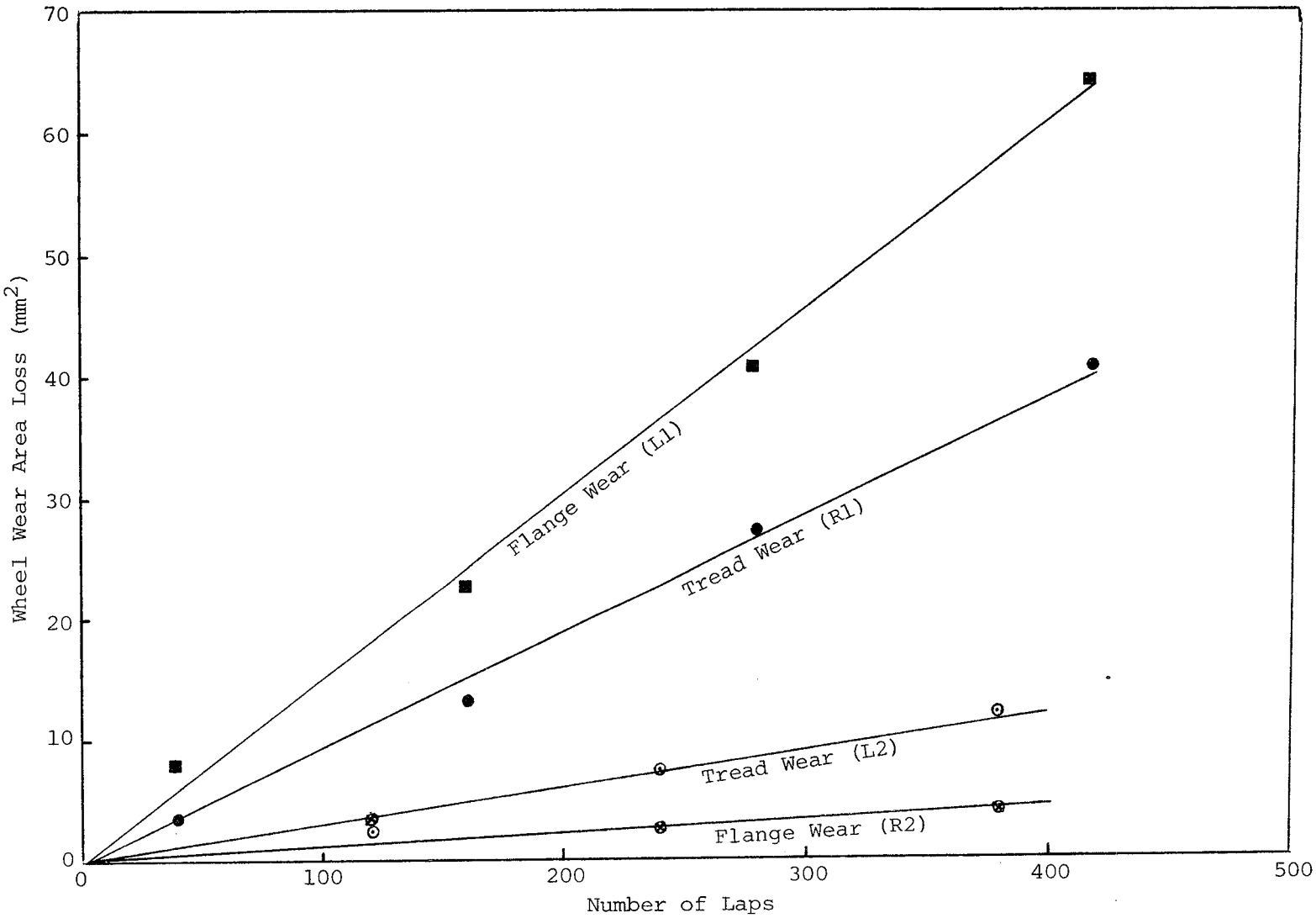

FIGURE 3.13. WHEEL WEAR VERSUS NUMBER OF LAPS, WHEELSETS 1 AND 5 WITHOUT RESTRAINING RAIL.

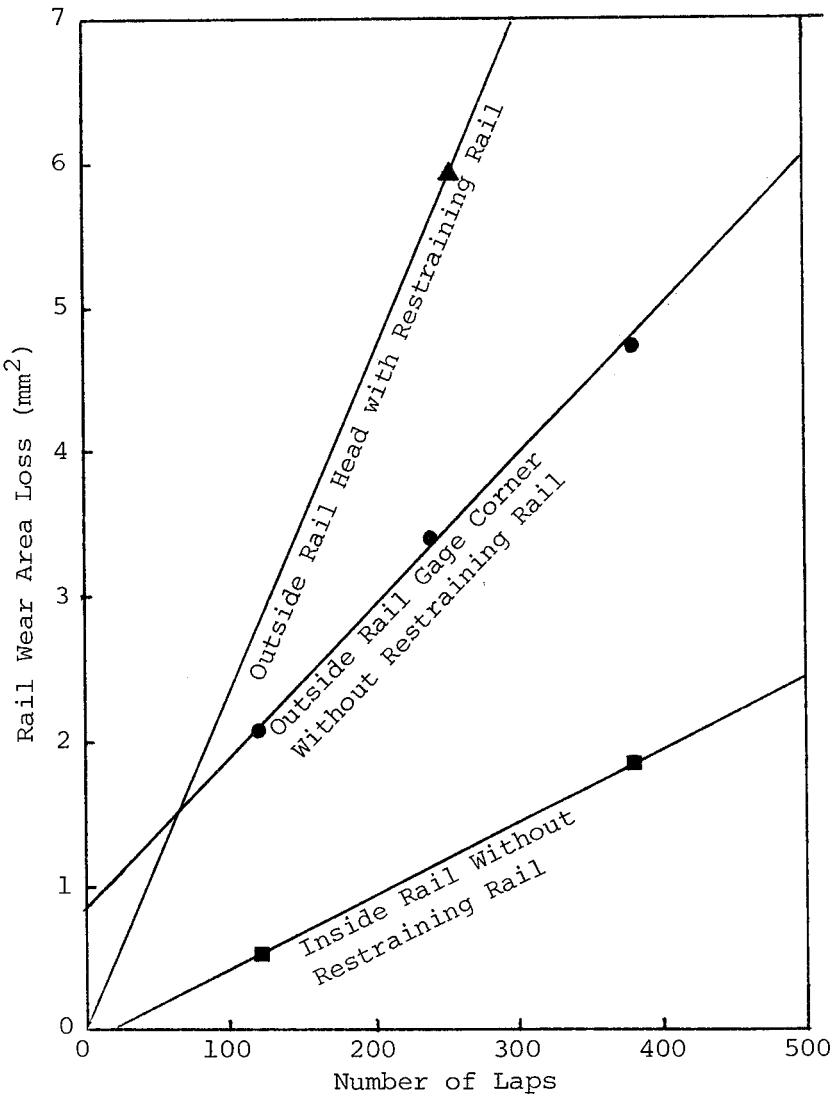

FIGURE 3.14. RAIL WEAR VERSUS NUMBER OF LAPS, WITHOUT RESTRAINING RAIL.

TABLE 3.2c. WHEEL WEAR.

	Type of Wear	Wear Rate mm^2/lap
R1 L2 R3 L4	Flange back	0.4
L1 R2 L3 R4	Combination of tread and flange	0.26

The data was collected in two parts. First, the car was operated with the cab leading in a clockwise direction of travel. In this mode the angle-of-attack and rail force measurements were made, followed by a 120 lap wear test phase. For cab leading operation, wheels R1, R2, R3 and R4 were adjacent to the restraining rail and wheels R1 and R3 experienced flange back wear. It was during this first phase that the limitations of the flange back gage were determined. Consequently, reliable data for one flange back data point per wheel was acquired during this phase of testing.

In addition, it was found that as the flange back wear progressed the wheelset moved toward the outside of the curve so that intermittent contact between the outside flanges and outside rail gage face was established. Once intermittent contact (detected by polishing of the outside rail gage face) reached 25% this test phase was terminated. It was decided that further useful data could be had by running the vehicle in the same track direction but with the cab trailing and taking flange back wear data from second wheelsets on the trucks.

In this mode the wheels adjacent to the restraining rail were L4, L3, L2 and L1, with L4 and L2 experiencing flange back wear. In this instance a total of 92 laps were made before outside rail gage face to flange contact occurred. The number of laps which could be accumulated with restraining rail before unacceptable high rail flange contact occurred depended on the effective flangeway clearance developed by the flange wear during the test without restraining rail. The normally leading wheelsets, #1 and #3, developed greater flangeway clearance than the normally trailing wheelsets, #2 and #4. Therefore, when the orientation of the car was reversed during the restraining rail test, and the #2 and #4 wheelsets were in the lead position, fewer wear data laps were available.

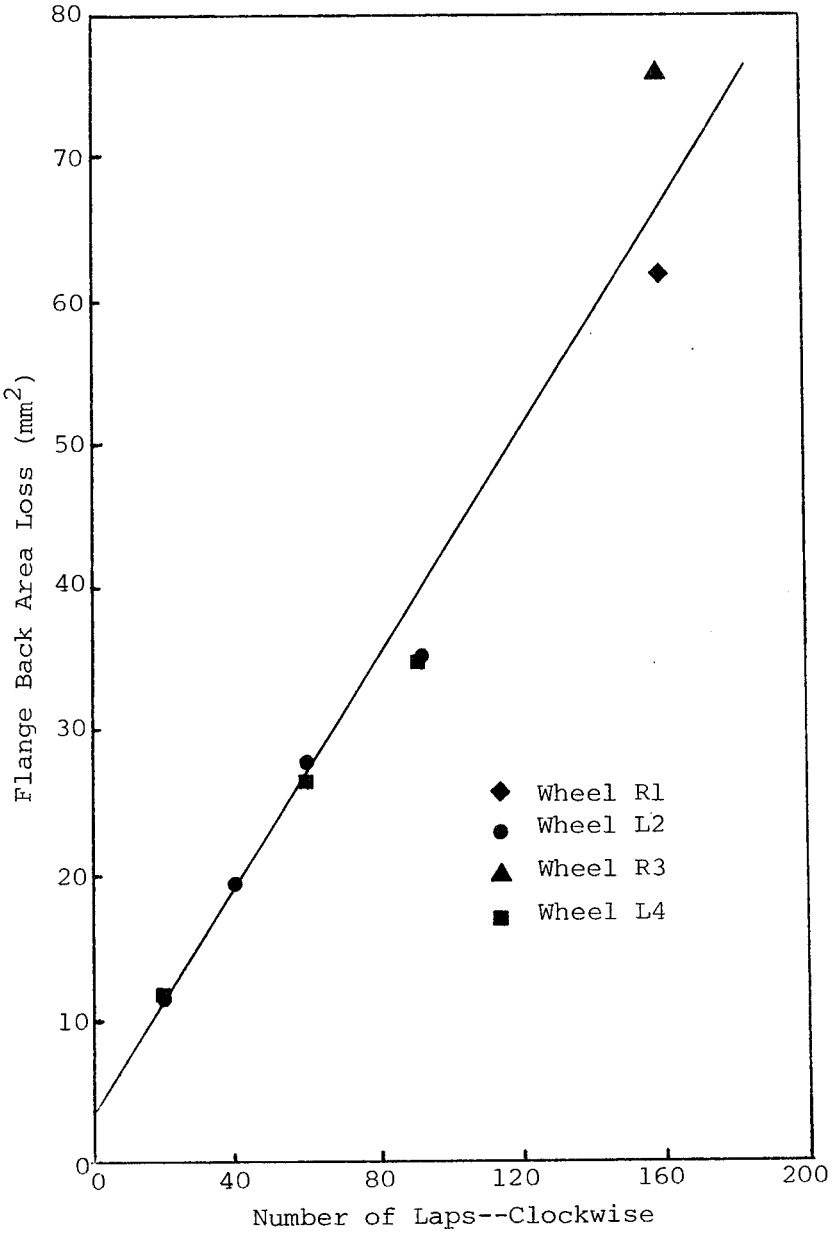

FIGURE 3.15. FLANGE BACK WEAR VERSUS NUMBER OF LAPS.

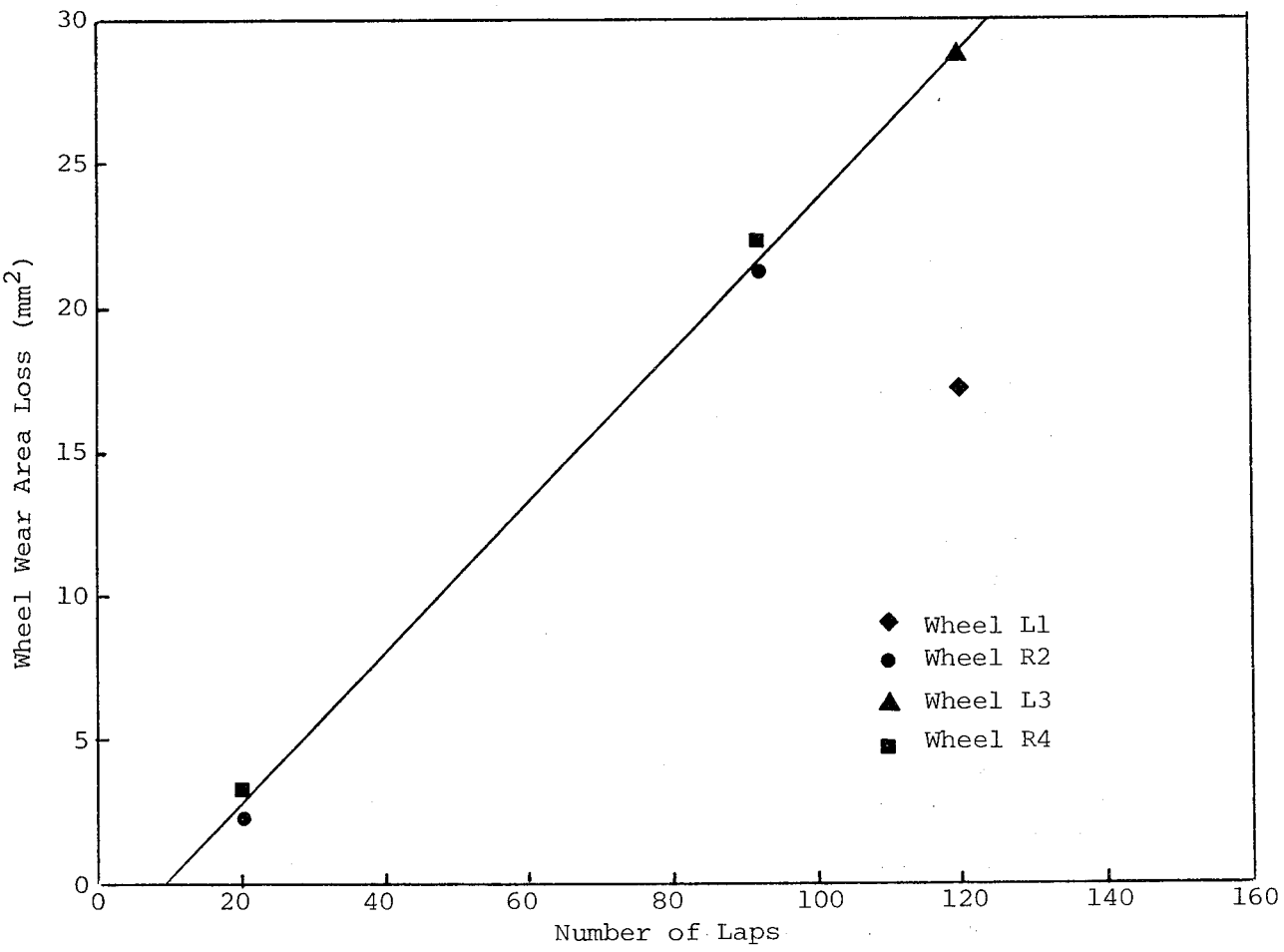

FIGURE 3.16. WHEEL WEAR VERSUS NUMBER OF LAPS, OUTSIDE LEAD WHEELSET WITH RESTRAINING RAIL.

Figure 3.15 shows the flange back data from which the wear rate shown in Table 3.2c was derived. The figure is a composite of wheels R1, L2, R3 and L4 for the two modes of operation. During the last 20 laps of the second phase, observation of the gage face of the outside rail showed an intermittent flange contact over approximately 50% of the loop. This may account for the apparent low value of wear at the 92 lap mark. No measurable corresponding flange wear was observed however, presumably because the wear index on that wheel had not reached a high enough value.

Figure 3.16 shows the data from which the tread and flange wear rate in Table 3.2c was derived from wheels L1, R2, L3 and R4. The profile overlays were limited because fewer full wheel profiles could be taken, unlike the flange back gage which could be used in situ on the TTL. The overlays did show, however, a 'migration' of wear towards the flange. The wear rate shown in the table is a combination of tread and flange.

The final presentation in Figure 3.17 is for wear of the tread on the flange back contacting wheel (inside lead). The wear was barely measurable, therefore interpretation of this data is somewhat suspect. It would appear that the tread wear starts off at a low rate, but as the outer wheel develops flange contact the rate of tread wear on the inner wheel increases and tends towards the value achieved on that wheel without restraining rail. However, since the data on this graph is taken from a number of different wheelsets with different flangeway clearances, definite conditions on the wear trends are not possible. Thus, Figure 3.17 is only used to support the theory of the gradual development of outside wheel flange contact during this test and not for absolute wear data.

3.2.5 Discussion

Despite difficulties with the flange back gage and by such occurrences as the '4' point contact, the wear rate data was consistent with expectations, although the analysis was more complicated than expected.

A number of improvements in the measurement techniques should be made for future work, since a number of critical reference profiles showed slight errors which are not normally important but become significant when such small wear rates are to be determined.

- The profile should be measured at precisely the same locations after the wheel or rail surface has been thoroughly cleaned.

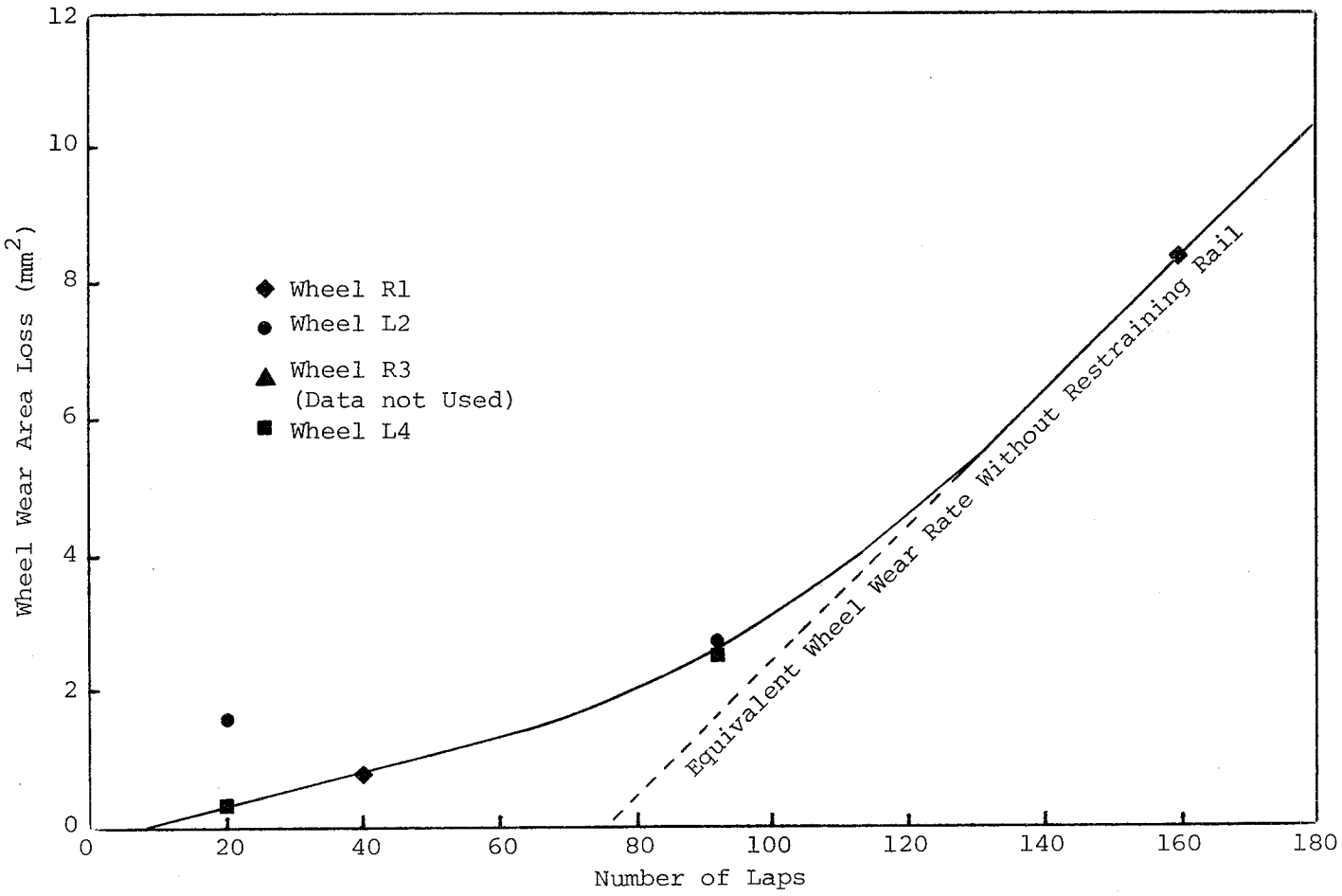

FIGURE 3.17. TREAD WEAR VERSUS NUMBER OF LAPS, INSIDE LEAD WHEELSET WITHOUT RESTRAINING RAIL.

- o Profiles should be taken at two locations per wheel, or alternatively be taken twice at the same location to ensure that repeatability errors are minimized.

- o As previously stated, a new flange back gage should be manufactured.

- o All future wheel profiles measured with the BR profilometer should have 42 points in the data set.

Considering the shortfalls already identified, and the fact that this is the first time such a precise full scale test has been conducted on this facility, the data shows remarkable consistency.

3.3 ANGLE-OF-ATTACK

For this test a new method of obtaining dynamic angle-of-attack was used. The method consisted of a static angle-of-attack measurement of the axles with respect to the track by direct measurement. LVDT's (linear voltage displacement transducer) and string potentiometers were then used to monitor all truck and axle movement relative to the carbody when the vehicle was in motion. This method was chosen because the Tight Turn Loop is a closed loop of constant radius of curvature on which the wheelsets tend to develop and maintain large angles-of-attack.

3.3.1 Static Calibration

Two methods were used, a calibration bar and a plum-bob to calibration lines. The second method was developed as an improvement on the first.

a. Calibration Bar

A 4 ft long calibration bar was clamped to the inside of the wheel and depth gage measurements made to the rail head. See Figure 3.18. The gage was found to give repeatable and accurate values for local angle-of-attack. It was decided that the method would not be used because it did not give an average angle-of-attack with reference to the track as a whole, and it was the average value which was required for the modeling exercise.

b. Static Calibration with Reference to the Effective Center of the Tight Turn Loop

The second caibration method consisted of measuring the wheel angle-of-attack, not with reference to local track geometry, but with reference to sight lines which were set to pass through the effective center of the track.

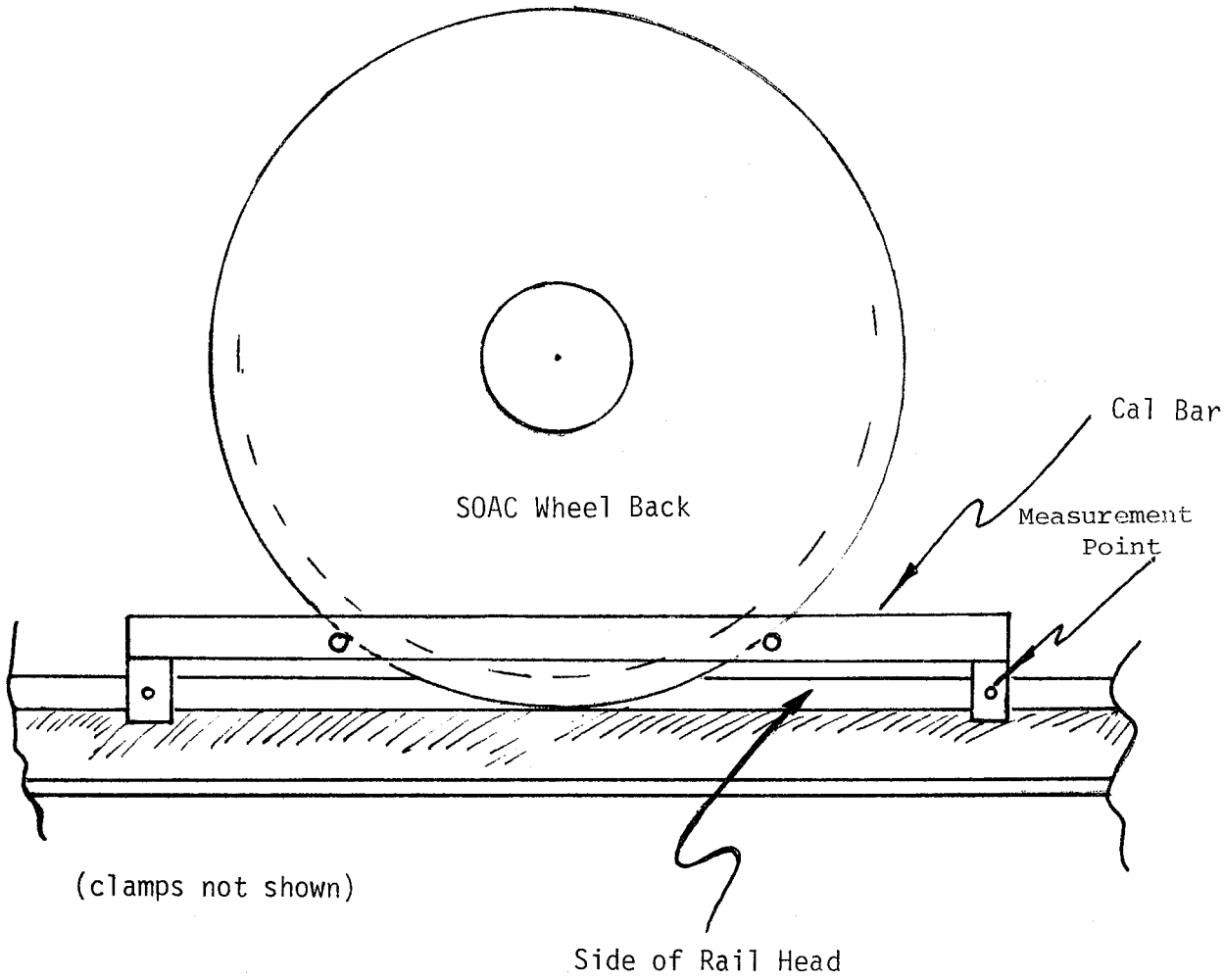

FIGURE 3.18. ANGLE-OF-ATTACK--STATIC CALIBRATION BAR.

Figure 3.19 shows the layout. Two sight lines were laid by the HP laser surveyor and scribed on boards at either side of the track. The two sight lines were spaced at 2°52'6" apart which corresponds to 7'6-1/32" at the center of track, the measured axle spacing.

To find the angle-of-attack with reference to the sight lines, a plum-bob was dropped from each axle end in turn down to the scribed line on a plate mounted on the cross ties and the offset measured by 6" steel rule, (see Figure 3.20). Simple geometry gave the axle angle-of-attack at that point with reference to the center of the Tight Turn Loop. At this point the outputs of the truck LVDT's were noted, and the two string potentiometer outputs between truck and body set to zero. All angular movements were now referenced to this datum position for subsequent runs.

3.3.2 Measurement of Dynamic Angle-of-Attack

The major assumption of the method is that the carbody remains normal to the center of the track so that the body can be used as a datum. The angle of the axles relative to the body are then monitored.

The string potentiometers were placed so that the string was normal to a line through the truck center pin when the truck was on the Tight Turn Loop. They were also located so that the sum of their outputs gave truck rotation. Any output due to truck lateral translation between bump stops was equal and opposite and cancelled out. The expression for angle of attack was:

Dynamic Angle-of-Attack = Calibration Angle

+ truck rotation with respect to vehicle body (derived from string pots)

+ axle rotation with respect to truck (derived from longitudinal LVDT's)

Care was taken during data analysis to ensure that the polarity of the string pot and LVDT signals were consistent.

The outputs of the LVDT's and string pots were plotted in the form of time histories for one complete loop of the Tight Turn Loop. An average value of the output was manually extracted. The final data is shown in the two Figures, 3.21 and 3.22, for without restraining rail and with restraining rail. The figures show that angle-of-attack changed little with speed from the original value

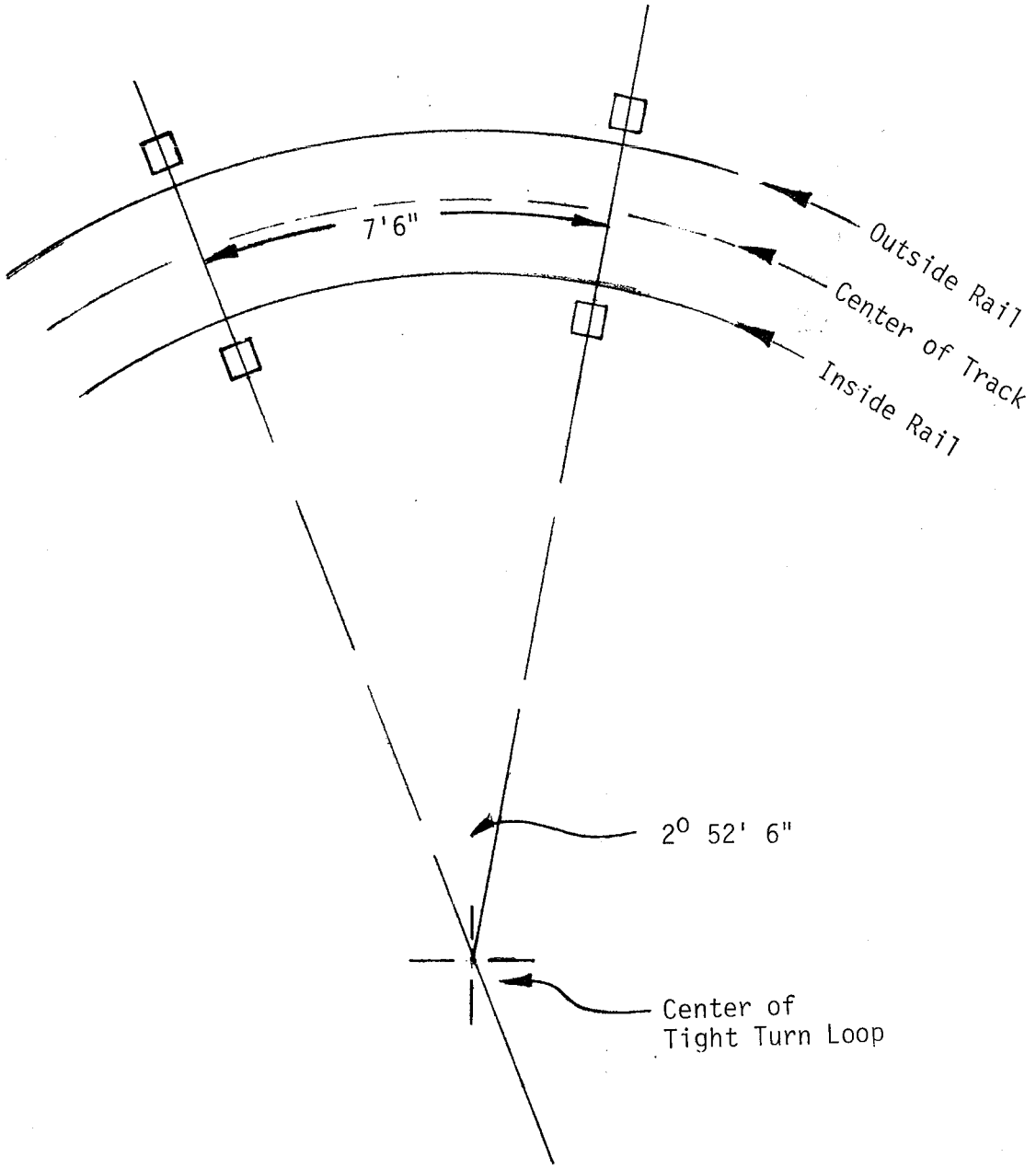

FIGURE 3.19. ANGLE-OF-ATTACK--STATIC CALIBRATION BY SIGHT LINES.

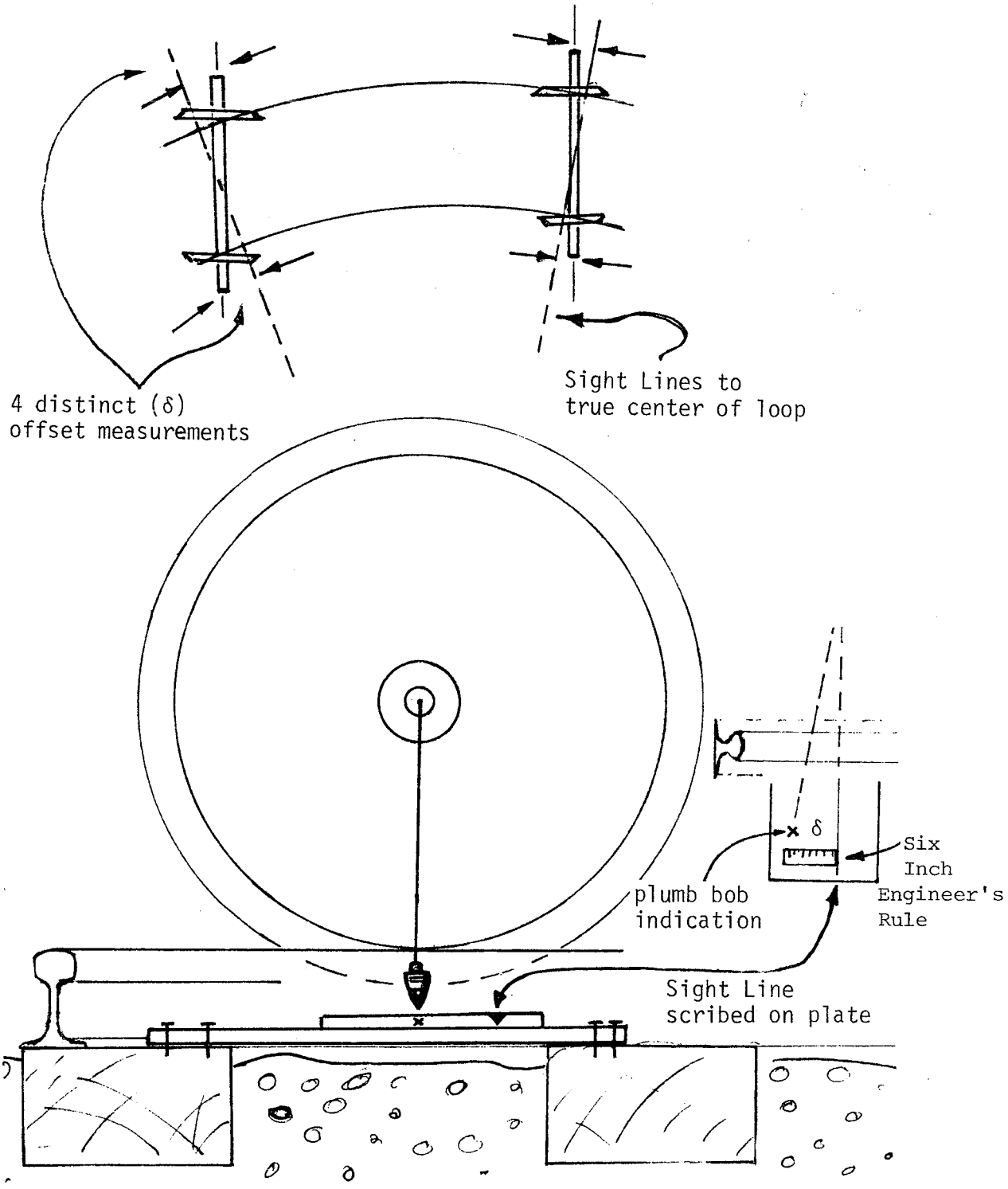

FIGURE 3.20. ANGLE-OF-ATTACK CALIBRATION--MEASUREMENT OF AXLE END OFFSET TO SIGHT LINES.

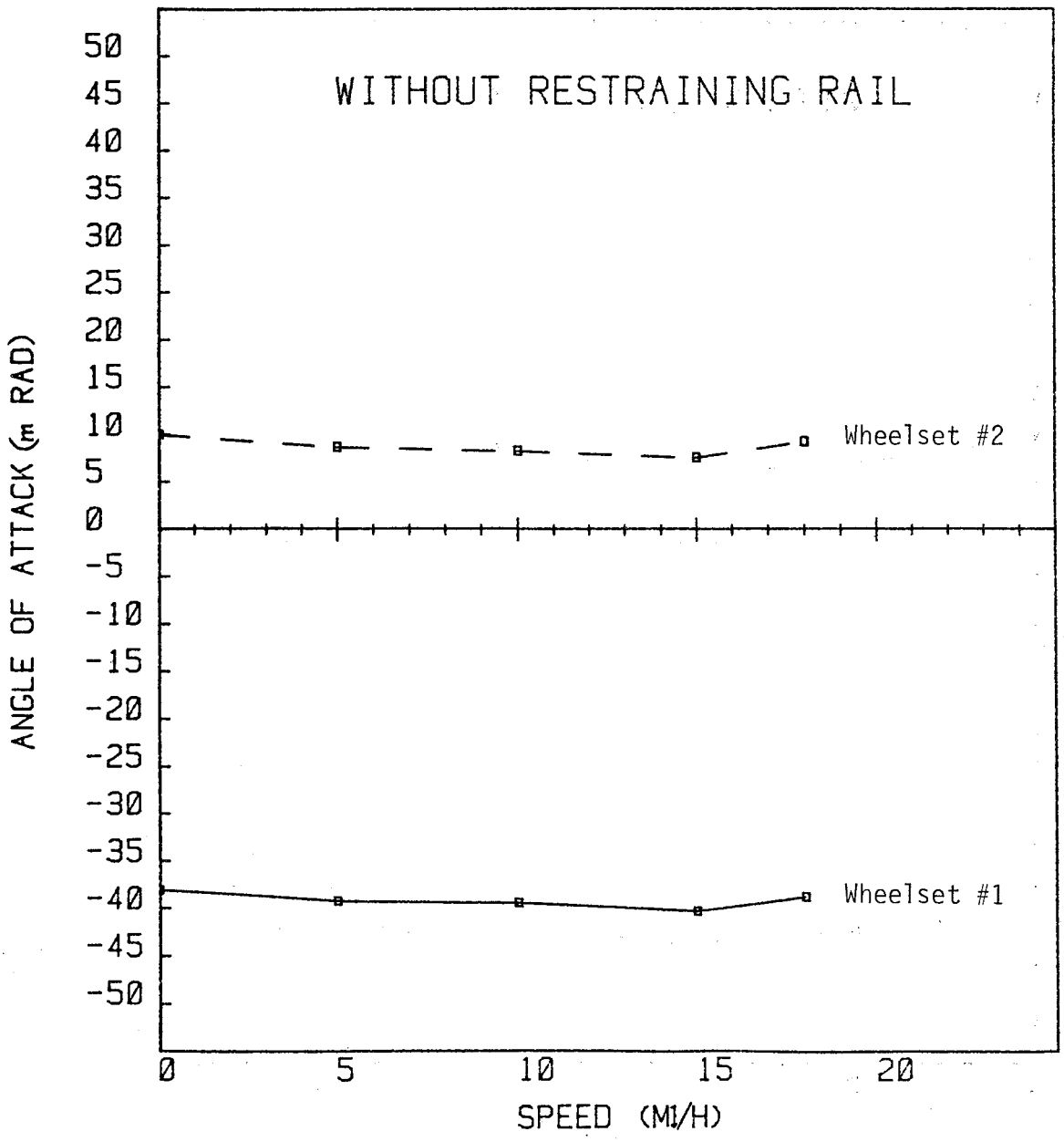

FIGURE 3.21. ANGLE-OF-ATTACK VERSUS SPEED, WITHOUT RESTRAINING RAIL.

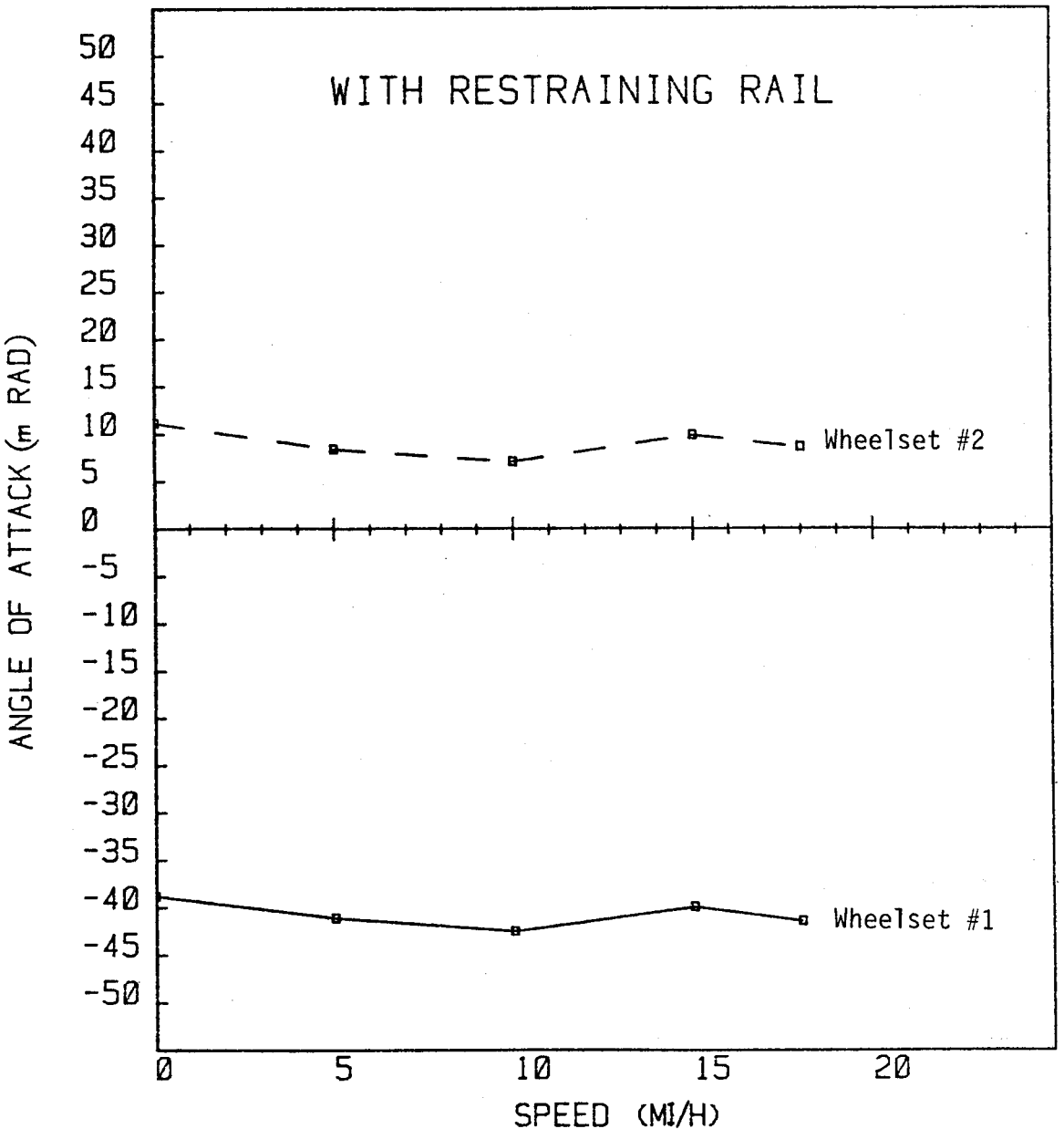

FIGURE 3.22. ANGLE-OF-ATTACK VERSUS SPEED, WITH RESTRAINING RAIL.

at the calibration spot and also shows that the restraining rail did not change the angle significantly either.

Of interest in the LVDT outputs is the way they closely followed track irregularities. This is shown in Figure 3.23, where the output from a typical channel is shown at 5 and 10 mi/h. Clearly the wheel is tightly restrained to follow the track with little freedom of movement. The string pots also showed behavior relating to crack characterization, as shown in Figure 3.24.

3.4 WAYSIDE RAIL FORCE MEASUREMENT

3.4.1 General

Rail force measurements were carried out at four sites spaced approximately 8 feet apart, (see Figure 2.3). At each site, both the running rails and restraining rails were strain gaged, (see Section 2.2.3, Figures 2.6 and 2.7). The four sites had been prepared as part of a previous TTL test.

3.4.2 Calibration

Prior to the test, a pre-test calibration was performed at all 4 sites. The sensitivities produced were used for the monitoring of L/V values during the test. It was found that unexpectedly high L/V ratios were produced suggesting that the pre-test sensitivities could be subject to a number of errors. Since the pre-test data showed good agreement among sites (if not accurate values), it was assumed that all 4 sites had approximately the same characteristics and an in-depth post-calibration was performed to investigate the effects of crosstalk and load application at site #4.

A hydraulic rig capable of applying both vertical and lateral loads was used in the calibration, (see Figure 3.25).

The major difference between the post-test calibration and the pre-test calibration was in the method of application of the lateral loads. In the case of the running rails, the pre-test calibration loads were applied to a 'shoe' which distributed the load over a 4" length. For post-test, a pin was inserted between shoe and rail to apply the load at a point. In the case of the restraining rail, the pre-test calibration loads were applied to a 'clamp system' which distributed the load over a 6" length. For post-test, again a pin was inserted, and the clamp system slackened so that the load was applied at a point.

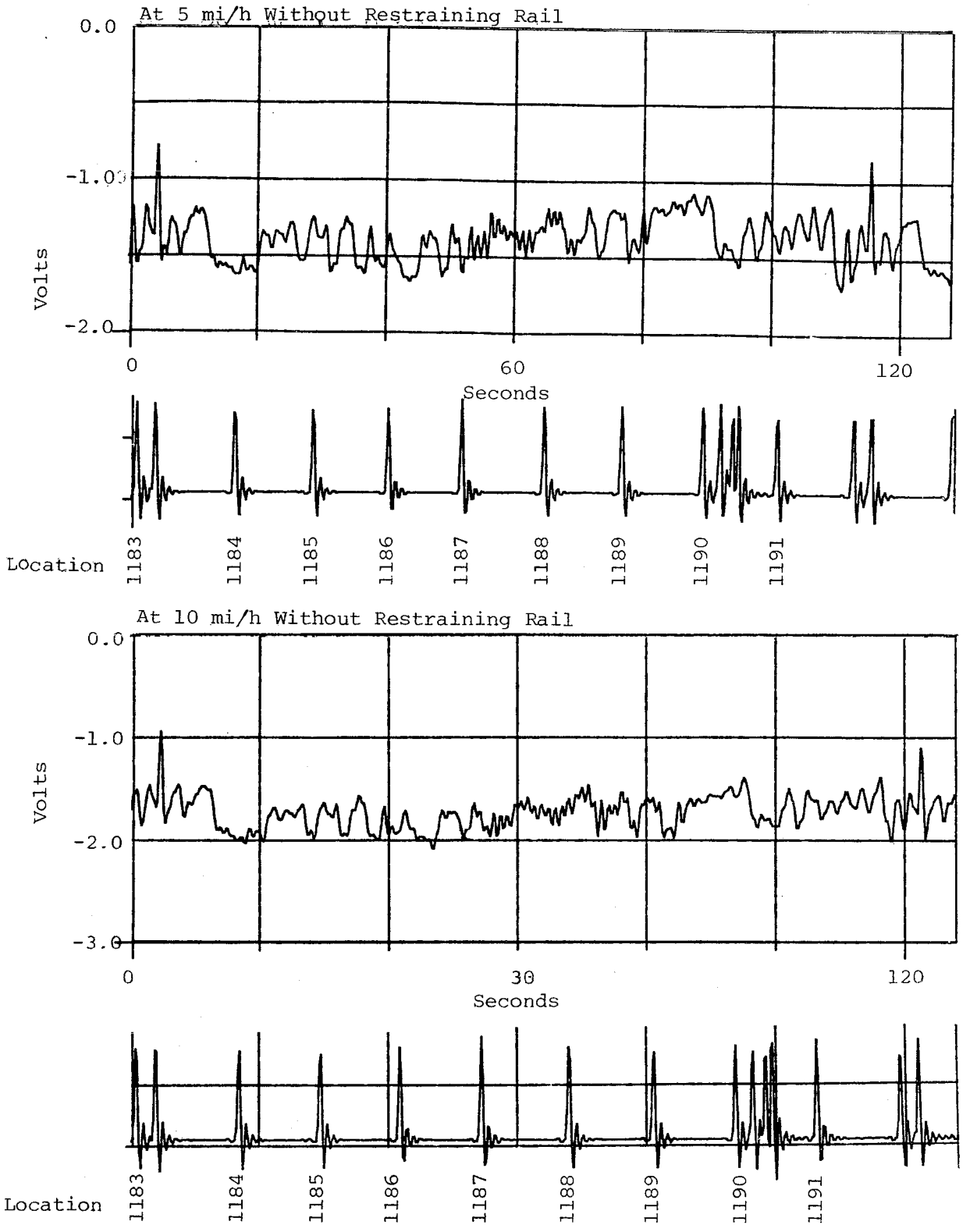

FIGURE 3.23. TYPICAL LVDT OUTPUT VERSUS TRACK LOCATION.

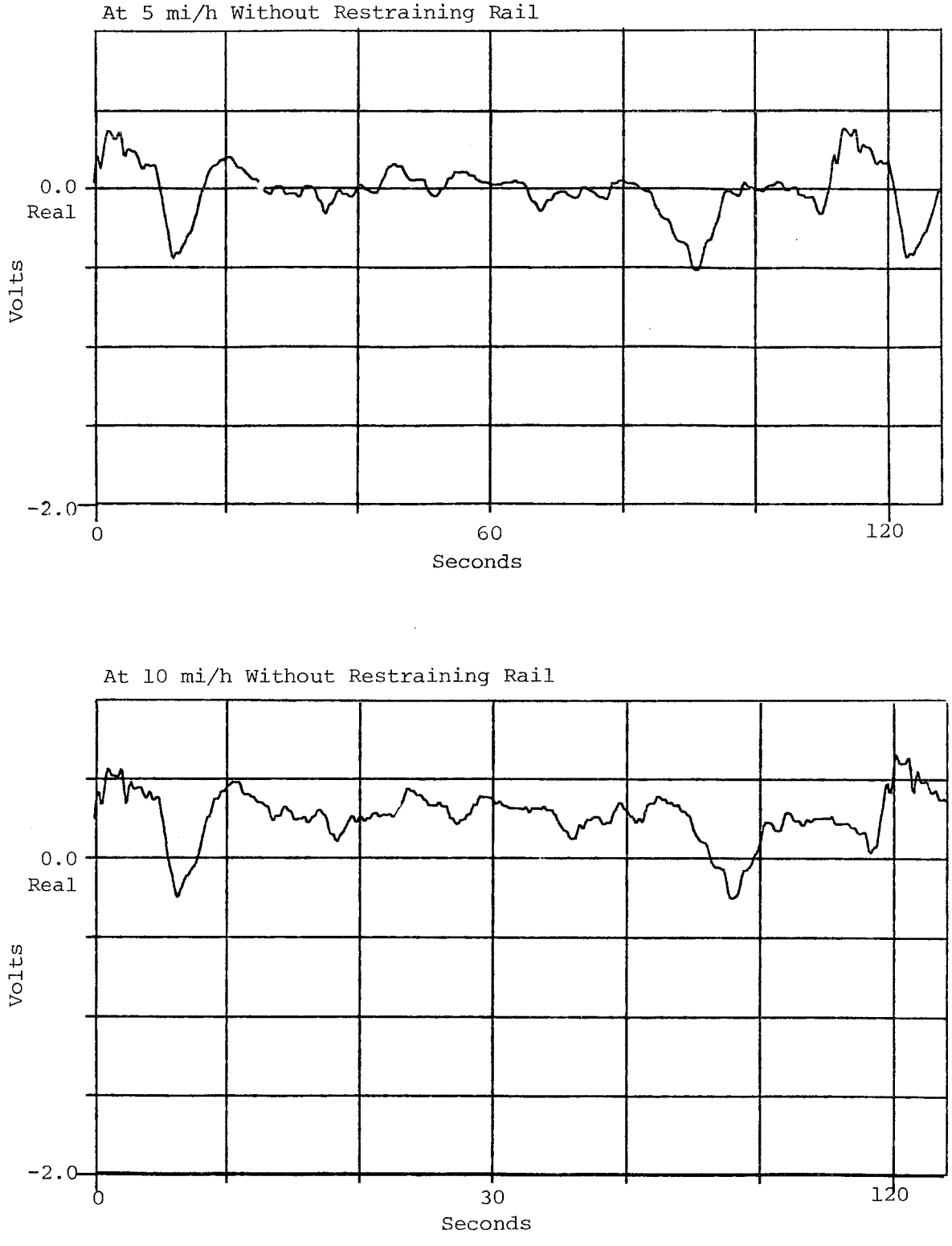

FIGURE 3.24. TYPICAL STRING POT OUTPUT VERSUS TRACK LOCATION.

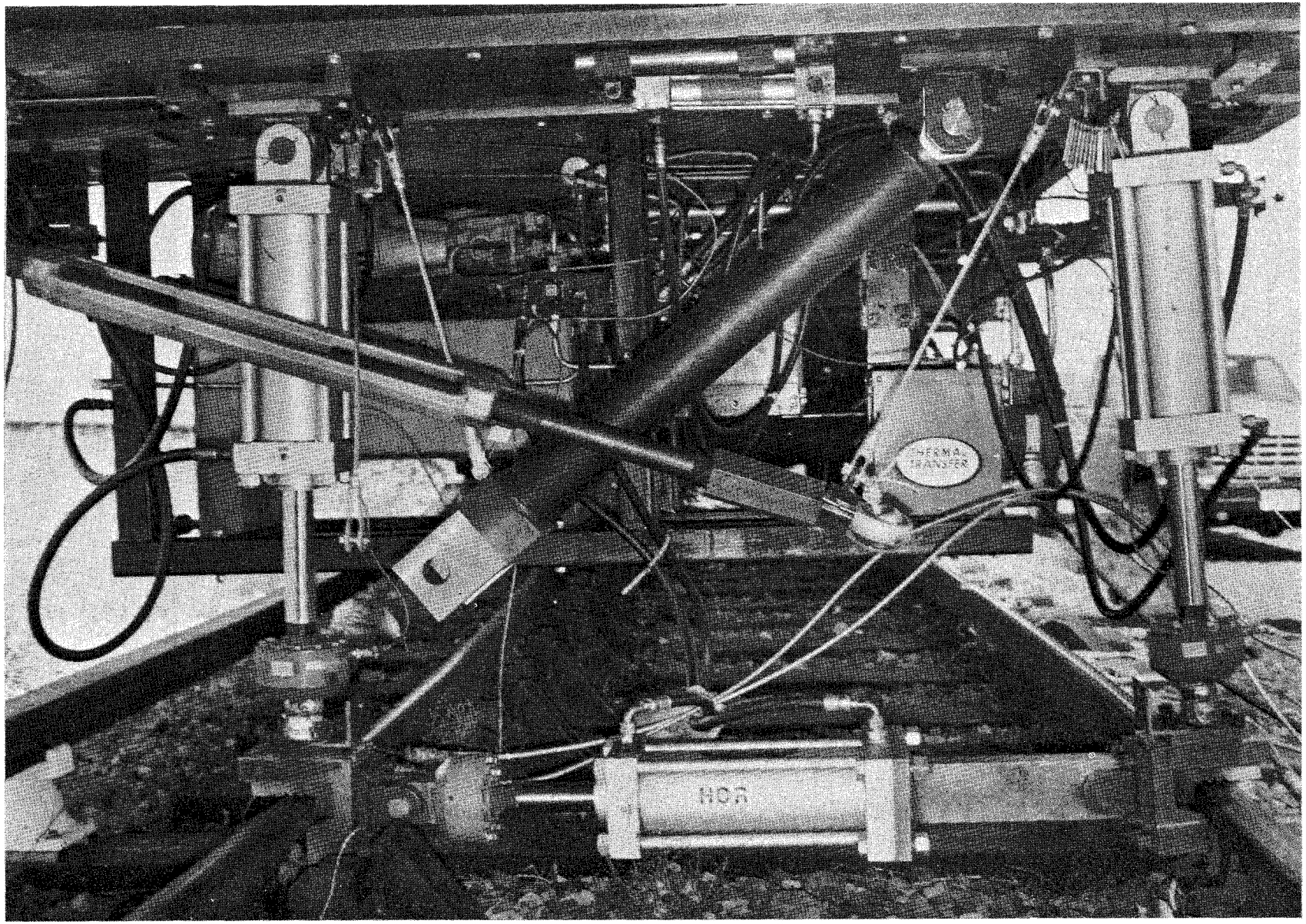

FIGURE 3.25. HYDRAULIC CALIBRATION OF RAILS.

It was found that, as expected, the point loads gave greater sensitivity values, which modified the high L/V values measured during testing to levels of more realistic values.

A study of cross-sensitivity was also undertaken at the post-test calibration. It was found that the cross-sensitivity relationships were not easy to establish. The lateral force on the running rails had little (less than 2% typically) effect on the indicated vertical force. The vertical forces have more effect on the individual lateral forces, but because of relative magnitudes, have little effect on the overall results. The most significant effect is on the restraining rail measurements where, because the restraining rail is effectively rotated through 90 degrees with respect to the running rail, the high lateral force has a large effect on the indicated vertical force.

To complicate matters further, it was discovered that the vertical crosstalk onto the lateral gages was very sensitive to the lateral portion of the point of contact. However, wheel/rail geometry plots were produced which showed that the rolling line was located near the axis of least cross-sensitivity and was remarkably consistent regardless of wheelset position until flange contact occurred. At flange contact, where no cross-sensitivity data was available, the lateral forces were high enough to completely dominate any cross-sensitivity correction. It was decided during the computer prediction comparison phase of the program that due to the uncertainty in the cross-sensitivity data and the low magnitude of the correction on the running rails that cross-sensitivity corrections would only be applied to the restraining rail data only.

During the cross-sensitivity investigation, it was discovered that the outer running rail does not sit squarely on the tie plates. Thus, the rail cannot be considered to be inclined at 1 in 40 gradient with respect to the tie. The actual gradient varies from 1 in 40 maximum, to a minimum of -1 in 40. The most likely cause of the tilted rail is the conflict between the pure lateral prebending of the rail and the actual installation, where the rail is superelevated and inclined. The conventional spikes are not able to hold the resultant torque on the rail, and thus allow it to twist. The inner rail with the restraining rail bolted-type tie plate is much more stable.

3.4.3 Data Reduction

The procedure for reduction of the rail force data was as follows.

1. Strip charts were examined and the maximum strain gage output noted as each wheel of the lead truck passed the site.

2. Readings were converted into force data by multiplication of calibration sensitivity factors.

3. For a given site and a given speed repeat runs were averaged.

4. All sites were then averaged to give 4 data sets: clockwise with and without restraining rail, and counterclockwise with and without restraining rail.

5. Cross-sensitivity correction factors were then applied (these were later discarded for all but the restraining rail).

An accuracy assessment of the rail force measurement, taking into account the strip chart accuracy, calibration accuracy, and the cross-sensitivity corrections, would seem to indicate that the method is, at best, 10% accurate. This should be borne in mind when comparing the results to the theoretical predictions.

3.4.4 Results

The results of the reduction of the rail force data are presented in Tables 3.3 and 3.4.

3.4.5 Discussion

In some cases the rail is exposed to high vertical and low lateral forces, thus the resolution of the lateral forces to good accuracy requires very careful calibration with good attention given to cross-sensitivity, point load, and the exact point of application of the load. During calibration, loads in the range expected should be applied so that the rail is sitting down in the tie plate.

For this test the sum of the vertical loads measured relates well to the known weight of the car. However, large differences were found among the individual wheels on a truck, much greater differences than could be explained by variations in suspension parameters. Furthermore, a definite pattern of load variations was noted in which the lead outside wheel and trailing inside wheel experienced higher than average loads and the remaining two wheels correspondingly lower than average loads. When the direction of travel of the car was reversed, the load variations also reversed to comply with the original pattern. At first crosstalk between lateral force and vertical strain gage output was considered to be the probable cause but was discarded after the post-test calibrations were completed. Attention was then focused on the traction motor drive train reaction forces and their load paths within the truck frame/wheelset/track structure. Preliminary engineering analysis indicates that the mechanism for load transfer is present

TABLE 3.3. RAIL FORCE DATA--OVERALL AVERAGE VALUES (WITH RESTRAINING RAIL) (CROSS-SENSITIVITY CORRECTIONS APPLIED TO RESTRAINING RAIL VERTICAL ONLY).

FORCE IN KIPS

WHEELSET #1

VERTICAL			LATERAL			
OUT	IN	RES	OUT	IN	RES	SP (mi/h)
*	*	*	*	*	*	2
12.2	6.3	6.6	-5.7	-3.0	12.3	5
13.0	5.1	6.7	-6.6	-2.8	13.4	10
13.4	3.2	6.9	-7.1	-1.7	13.8	15
14.0	2.0	6.9	-7.5	-0.9	14.0	18

WHEELSET #2

VERTICAL			LATERAL			
OUT	IN	RES	OUT	IN	RES	SP (mi/h)
*	*	*	*	*	*	2
10.5	14.5	0.0	.9	-5.5	0.0	5
11.4	13.6	0.0	1.4	-5.1	0.0	10
12.3	11.6	0.0	3.0	-4.7	0.0	15
13.7	10.6	0.0	4.7	-4.2	0.0	18

WHEELSET #3

VERTICAL			LATERAL			
OUT	IN	RES	OUT	IN	RES	SP (mi/h)
*	*	*	*	*	*	2
12.7	6.7	6.2	-6.3	-3.3	12.0	5
13.0	5.5	6.5	-6.9	-3.3	12.9	10
13.1	4.4	6.6	-7.1	-2.6	13.8	15
14.6	3.7	7.0	-7.7	-2.1	14.2	18

WHEELSET #4

VERTICAL			LATERAL			
OUT	IN	RES	OUT	IN	RES	SP (mi/h)
*	*	*	*	*	*	2
10.0	15.5	0.0	.9	-4.4	0.0	5
10.5	14.8	0.0	1.1	-4.0	0.0	10
10.7	13.2	0.0	1.7	-2.7	0.0	15
11.4	11.9	0.0	2.4	-2.2	0.0	18

* - No Data

TABLE 3.4. RAIL FORCE DATA--OVERALL AVERAGE VALUES (WITHOUT RESTRAINING RAIL).

FORCE IN KIPS

WHEELSET #1

VERTICAL			LATERAL			
OUT	IN	RES	OUT	IN	RES	SP (mi/h)
13.0	11.4	0.0	8.6	-6.3	0.0	2
13.5	11.3	0.0	9.3	-6.8	0.0	5
14.4	10.3	0.0	9.6	-6.2	0.0	10
15.7	8.6	0.0	10.2	-5.1	0.0	15
16.1	6.7	0.0	10.2	-4.0	0.0	18

WHEELSET #2

VERTICAL			LATERAL			
OUT	IN	RES	OUT	IN	RES	SP (mi/h)
9.8	14.6	0.0	1.2	-5.3	0.0	2
10.2	14.8	0.0	1.1	-5.5	0.0	5
11.2	13.1	0.0	1.0	-4.7	0.0	10
12.8	11.4	0.0	2.5	-4.6	0.0	15
14.1	10.3	0.0	3.8	-4.0	0.0	18

WHEELSET #3

VERTICAL			LATERAL			
OUT	IN	RES	OUT	IN	RES	SP (mi/h)
13.7	11.7	0.0	5.9	-4.8	0.0	2
14.0	11.8	0.0	6.2	-5.4	0.0	5
15.0	10.9	0.0	6.7	-5.2	0.0	10
15.4	8.6	0.0	7.5	-4.5	0.0	15
17.0	8.2	0.0	8.0	-3.3	0.0	18

WHEELSET #4

VERTICAL			LATERAL			
OUT	IN	RES	OUT	IN	RES	SP (mi/h)
9.9	15.4	0.0	1.1	-4.4	0.0	2
9.9	15.6	0.0	.8	-4.1	0.0	5
10.6	14.0	0.0	1.0	-3.1	0.0	10
11.4	12.5	0.0	1.0	-1.9	0.0	15
12.6	11.4	0.0	1.9	-1.4	0.0	18

* - No Data

in the eccentric loading arrangement of the traction motors to contribute to the effect, although magnitudes could not be confirmed. This phenomenon could be investigated further during any future follow-up test program by setting the vehicle on the strain gage locations with the brakes on and looking for any changes in indicated vertical load when partial traction power is applied. Whatever the cause of the vertical load variations, their significance on the flange climbing proneness of the vehicle will be further discussed in Section 4.2.2.

The lateral loads were found to be in the range expected. After detailed analysis of the cross-sensitivity corrections factors these were not used for the final data presentation because of the doubts concerning their validity after comparisons with the theoretical predictions indicated better agreement with uncorrected values. Some further investigation of rail force cross-sensitivity is necessary for future testing of this nature.

3.5 TRACTIVE RESISTANCE

Tractive resistance values for both tangent track and the Tight Turn Loop (with and without restraining rail) were required for comparison with the computer model. They were obtained by allowing the vehicle to coast and equating the tractive resistance at any instance, with the deceleration and total inertia of the car.

The lead axle of SOAC was fitted with a magnetic tachometer which produced a square wave signal of 60 pulses per wheel revolution. This was recorded on the FM tape recorder. On playback an HP 5345A electronic counter, controlled by an HP 85 desk-top computer, produced frequency values, time interval averaged over 1 second. The frequency values were converted to speed values and subtraction of successive speed values provided deceleration data. Tractive resistance values were obtained by the use of the total inertia of the car, taken as the total car weight and an allowance for the rotating parts.

3.5.1 Tractive Resistance on Tangent Track

Tangent track tests were performed on two occasions, May 11th and May 28th. On the May 11th test 4 runs were made, 2 in each direction. The data produced 4 tractive resistance characteristics, two of which are shown in Figures 3.26 and 3.27. The data shows good repeatability and no difference between forward and reverse direction of travel. At 15 mi/h the tractive resistance values were:

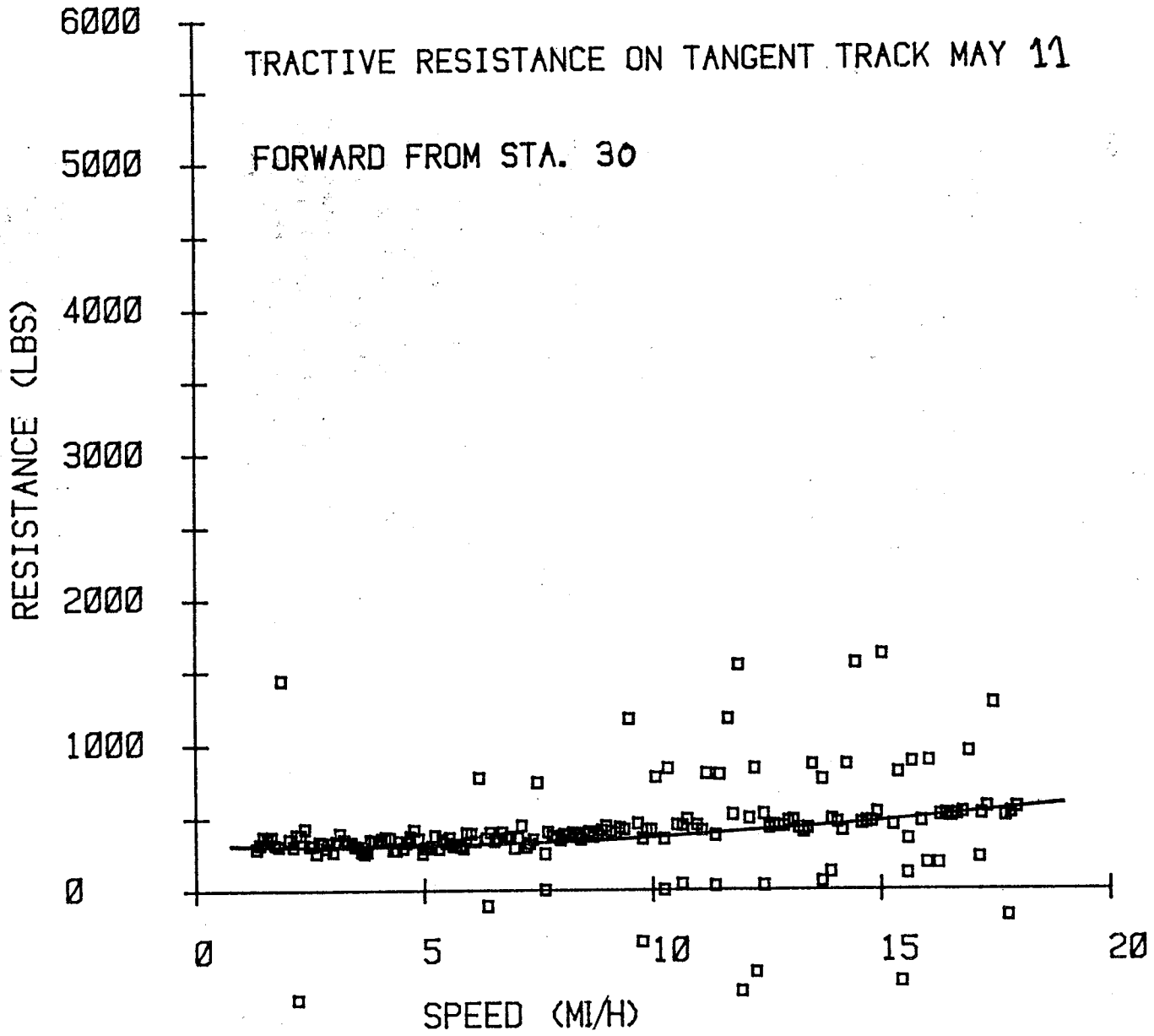

FIGURE 3.26. TRACTIVE RESISTANCE, TANGENT TRACK--MAY 11TH, FORWARD.

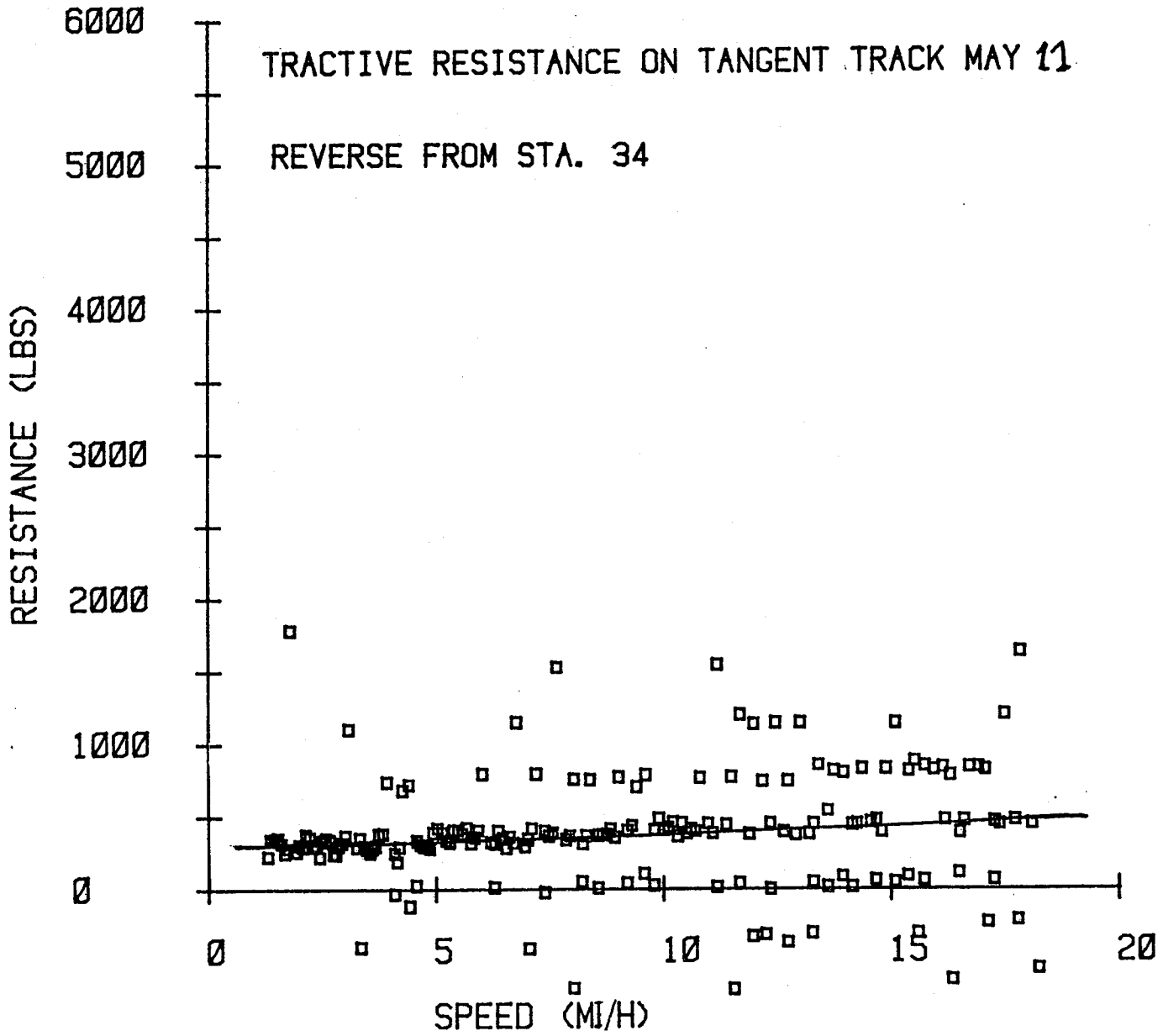

FIGURE 3.27. TRACTIVE RESISTANCE, TANGENT TRACK--MAY 11TH, REVERSE.

Test	#1	Forward	480 lbs
	#2	Reverse	450 lbs
	#3	Forward	450 lbs
	#4	Reverse	470 lbs
		Average	470 lbs

This is in agreement with previous tests on SOAC (by Boeing-Vertol, Ref. UMTA-MA-06-0025-75-1) with a value of 400 lb for a 105,000 pound single car.

On the May 28th tests 2 runs were made, 1 in each direction. The two tractive resistance characteristics produced are shown in Figures 3.28 and 3.29. In this instance, the data shows similar resistance in forward and reverse but has an unexpectedly high resistance. At 15 mi/h the values were:

Forward	1100 lbs
Reverse	1200 lbs

These values are approximately 3 times higher than those of May 11th. At the time of the test the high values could not be explained, but during the subsequent analysis of the primary suspension LVDT data it was decided to look at the outputs during the drift runs in case they gave differences which could indicate brake rubbing, etc.

A series of primary longitudinal time histories was produced for the two sets of tangent drift data. The first set corresponding to the 400 lb car resistance showed there to be little axle longitudinal motion. Figure 3.30 shows a 30 second time history of signal output for the two longitudinal LVDT's on the lead axle (#1). The corresponding time histories for the high resistance 1200 lb case are shown in Figure 3.31. In this instance the outputs are unstable and show a large amplitude 0.75-1.25 Hz frequency motion. The two outputs are clearly in anti-phase indicating wheelset yaw motion. Figure 3.32 shows the LVDT outputs for the trailing axle (#2) and, as with axle #1, instability is evident.

To further clarify the motion, Figure 3.33 shows the two LVDT outputs on one side of the truck. The motion of the wheelsets is in phase with the largest amplitude present in the lead wheelset, indicating that the #1 wheelset was the probable cause of the instability.

Following this discovery, a series of wheel/rail effective conicity plots was produced for the new and worn wheels of wheelset #1. These are shown in Figure 3.34. The effective conicity value for the new wheel was 0.056, as would be expected for a 1 in 20 taper. The worn wheel profile conicity plot yields a value of 0.040 for one-half of the wheelset displacement, and 0.009 for the other half. Reference to the relevant profiles shows that the outer portion of the tread of the right wheel is sufficiently worn to develop a negative conicity on that wheel.

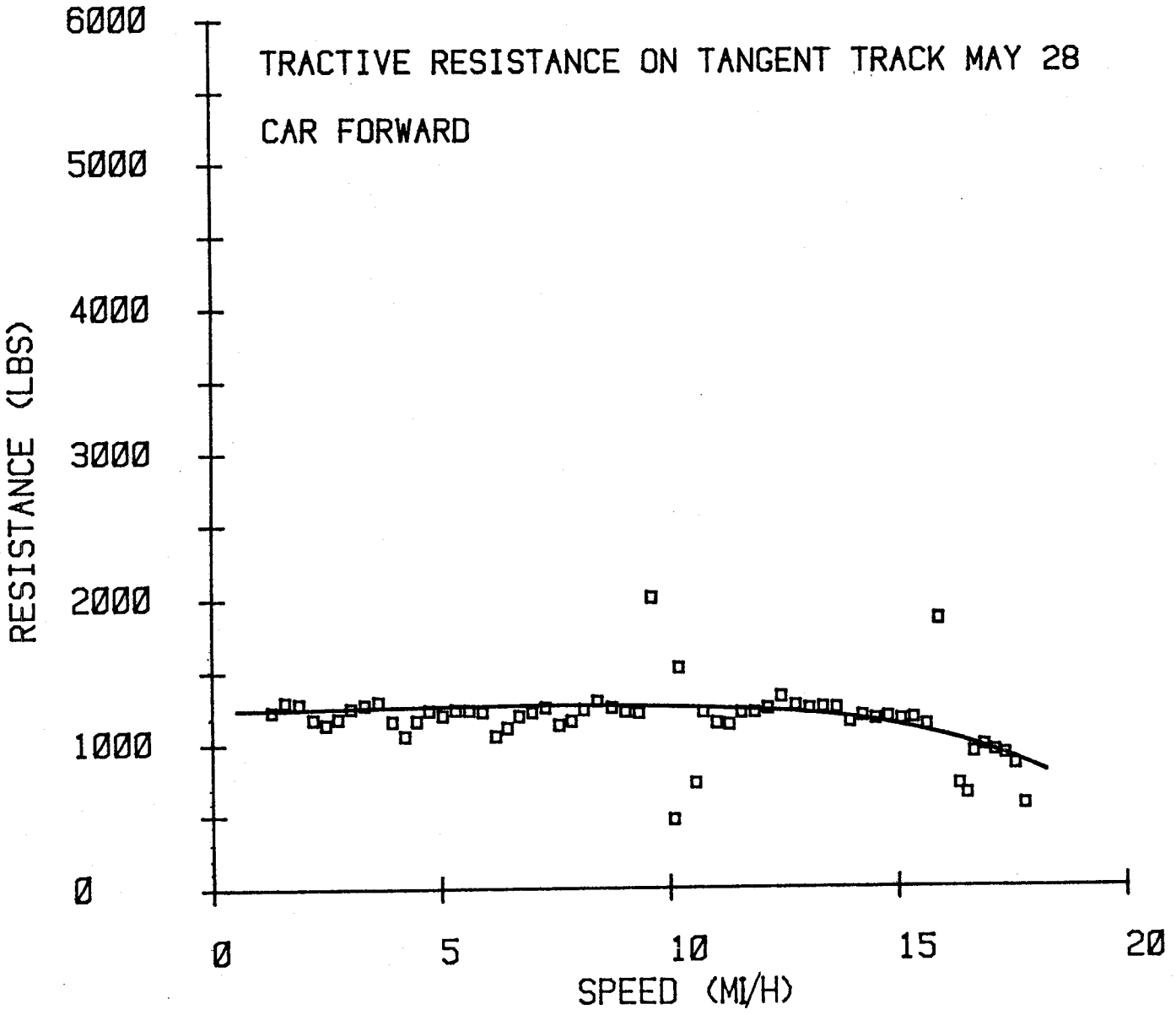

FIGURE 3.28. TRACTIVE RESISTANCE, TANGENT TRACK--MAY 28TH, FORWARD.

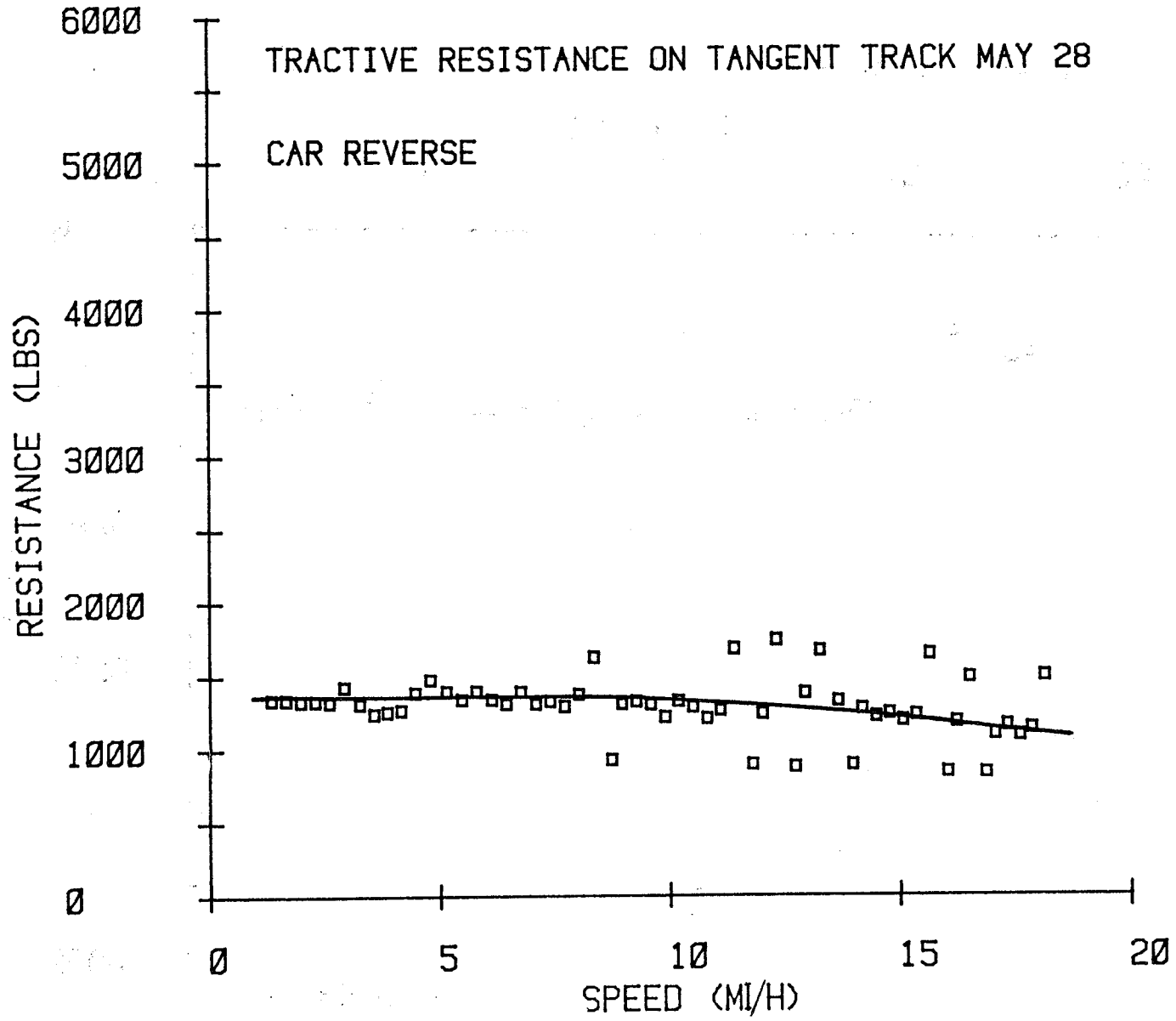

FIGURE 3.29. TRACTIVE RESISTANCE, TANGENT TRACK--MAY 28TH, REVERSE.

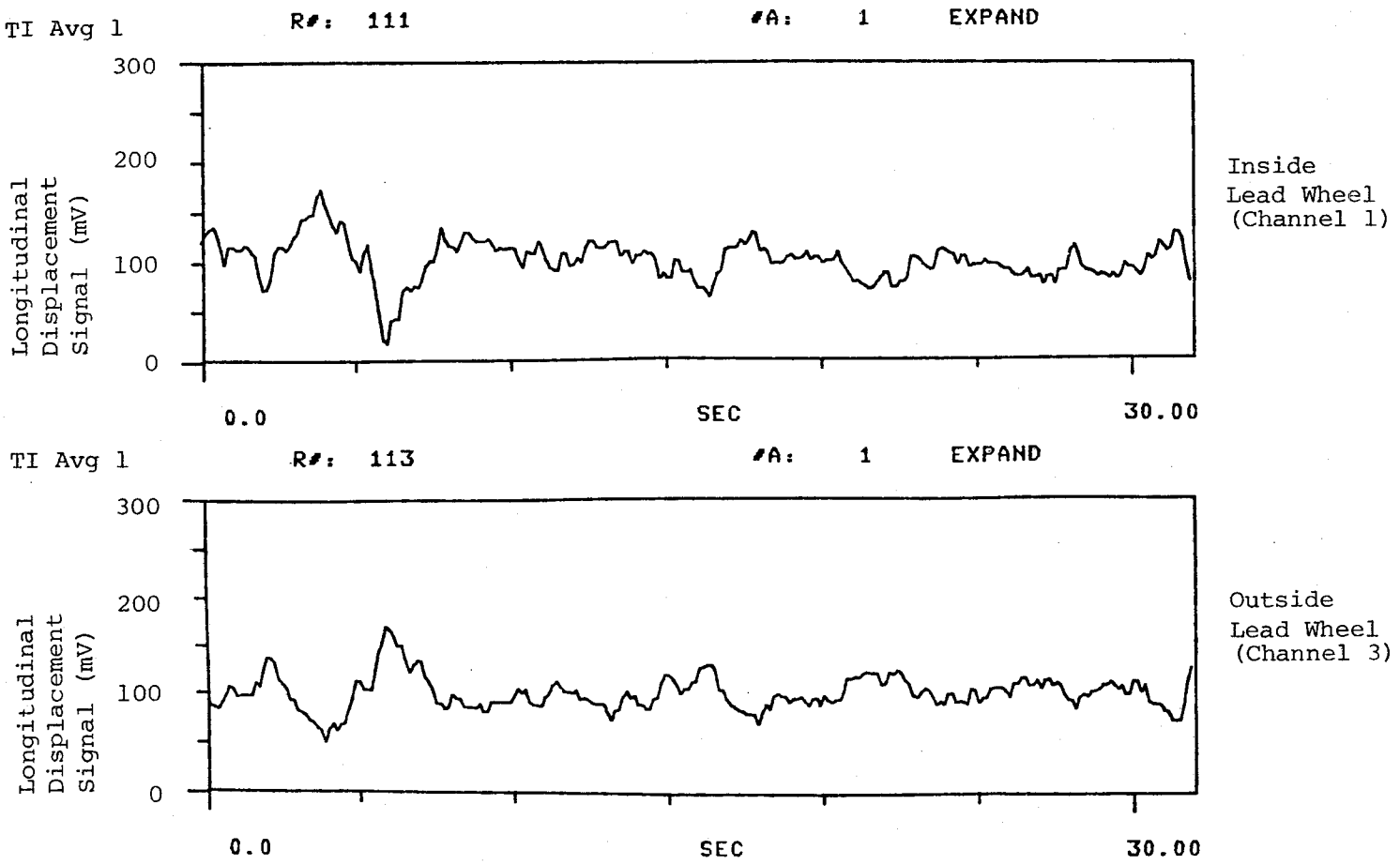

FIGURE 3.30. TWO LVDT OUTPUTS (LONGITUDINAL), LEAD AXLE DURING DRIFT TEST OF NORMAL TRACTIVE RESISTANCE.

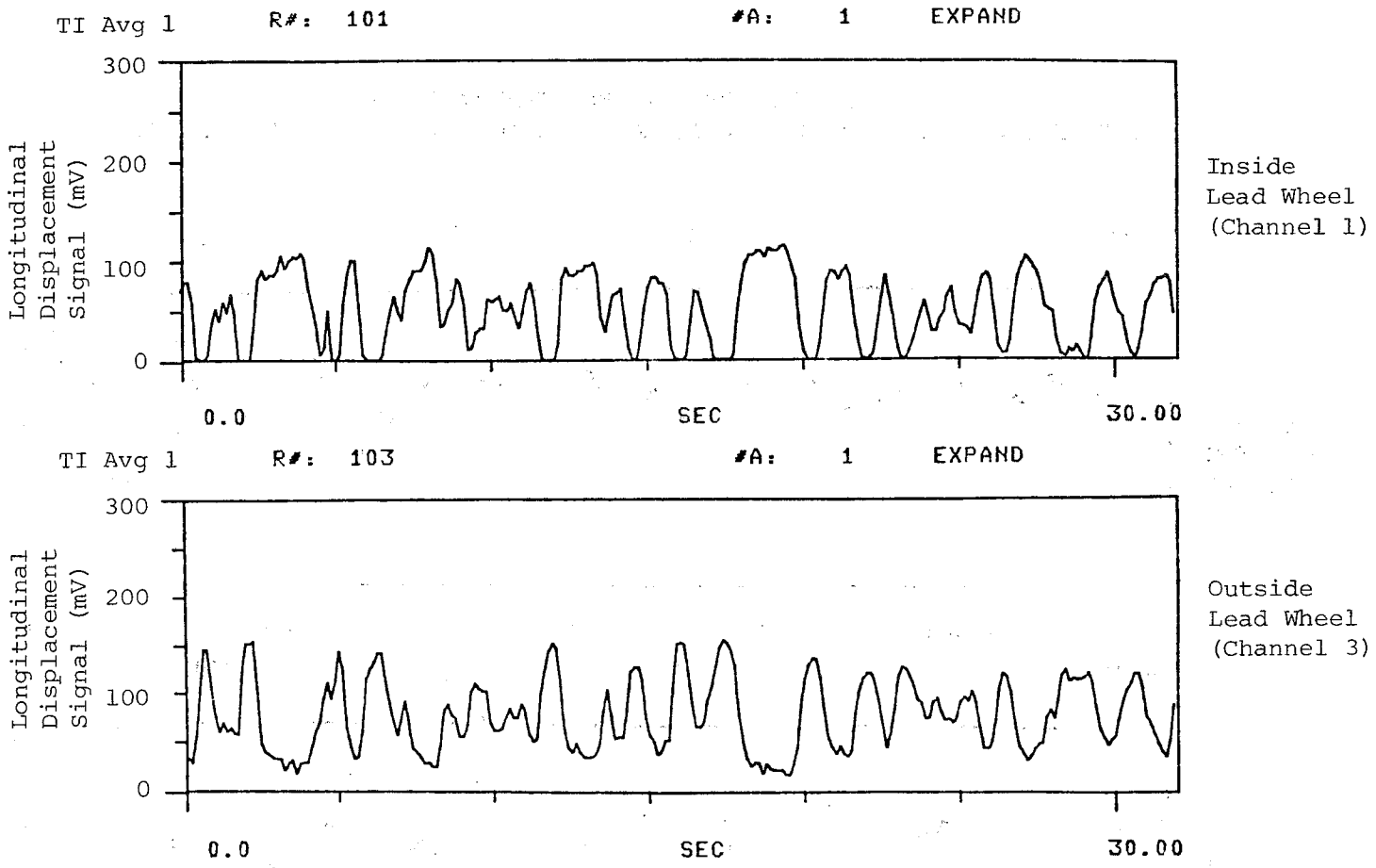

FIGURE 3.31. TWO LVDT OUTPUTS (LONGITUDINAL), LEAD AXLE DURING DRIFT TEST OF ABNORMALLY HIGH TRACTIVE RESISTANCE.

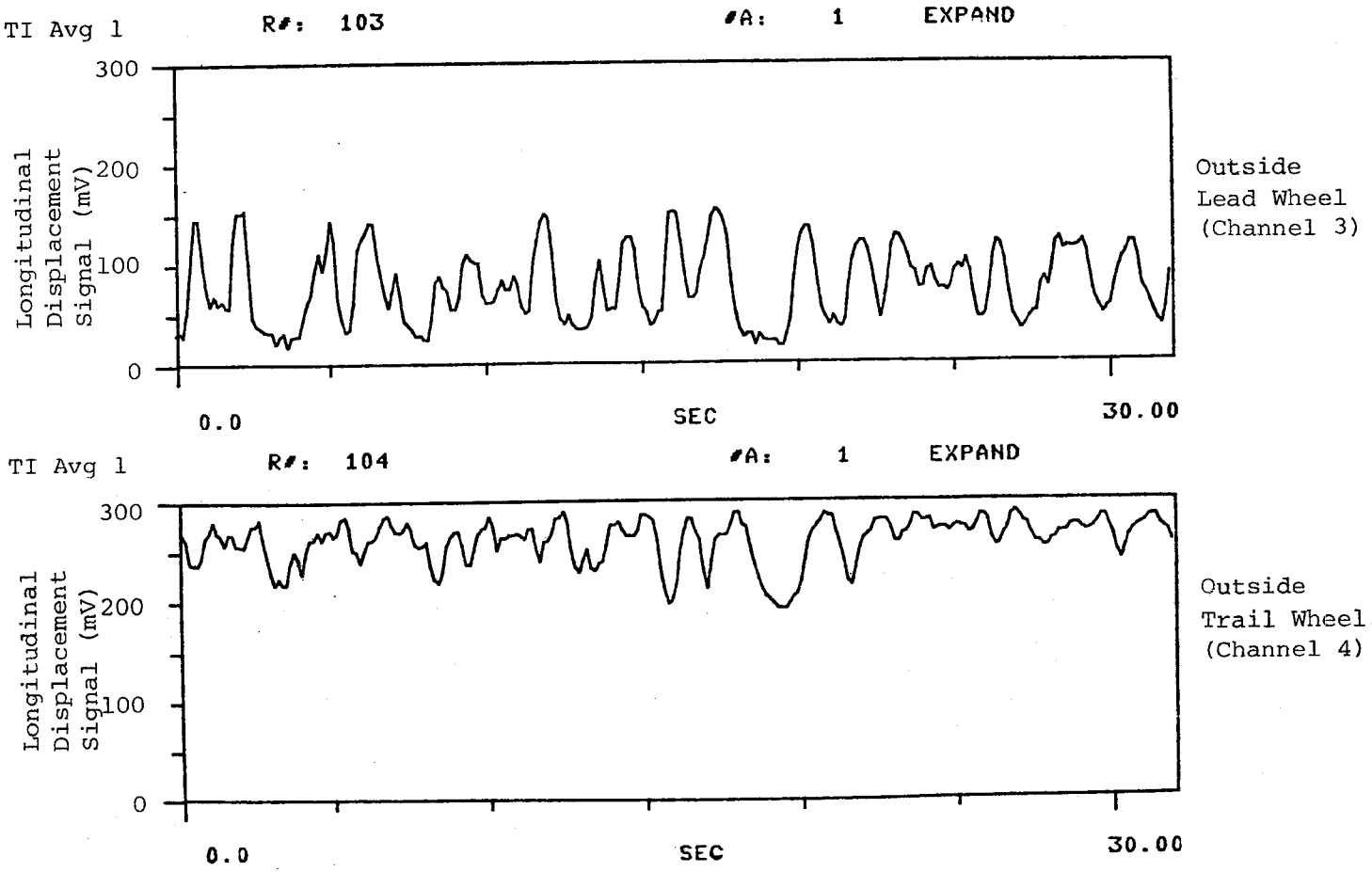

FIGURE 3.32. TWO LVDT OUTPUTS (LONGITUDINAL) FOR TRAILING AXLE DURING DRIFT TEST OF ABNORMALLY HIGH RESISTANCE.

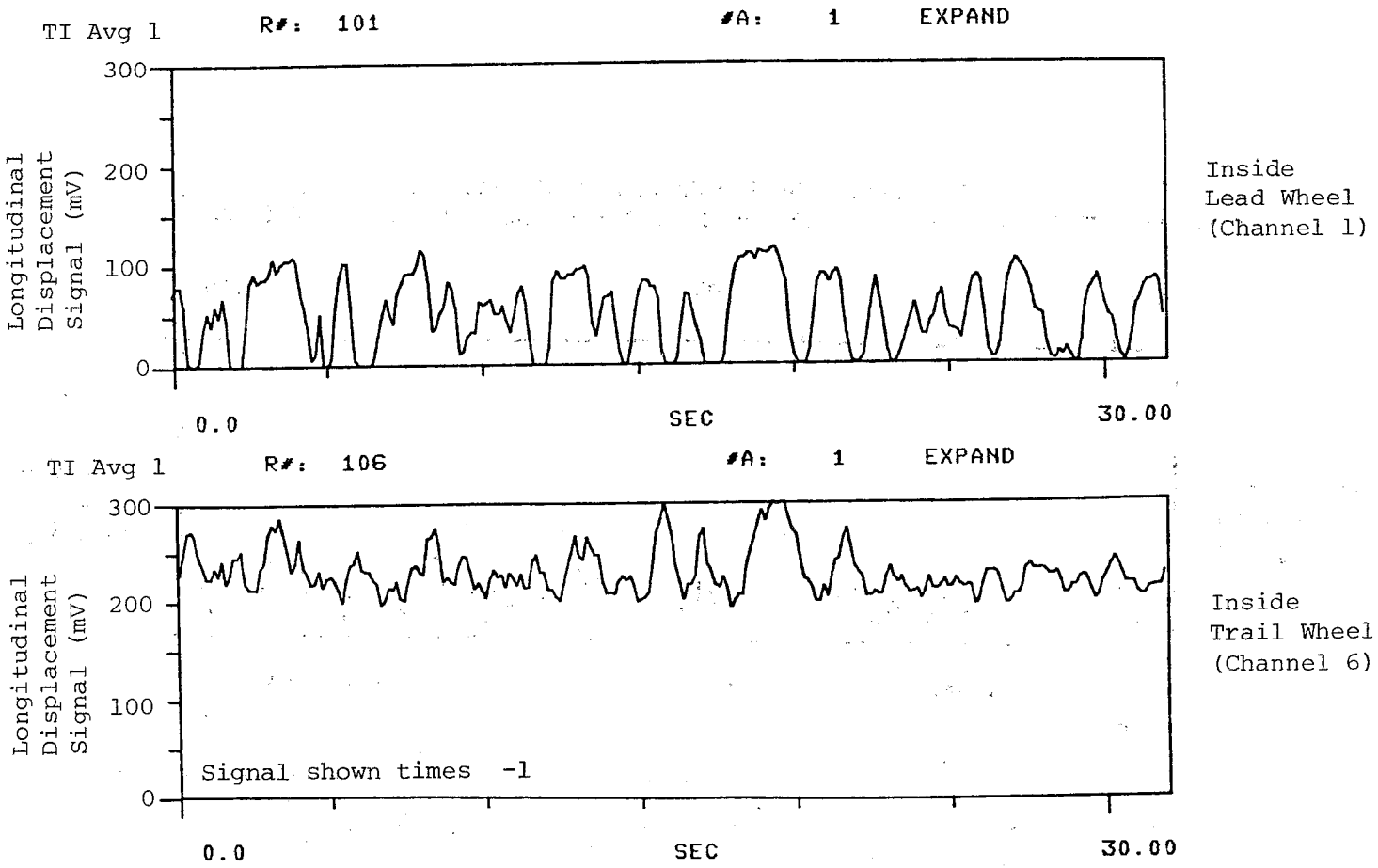

FIGURE 3.33. TWO LVDT OUTPUTS FOR LEAD AND TRAIL AXLES--ONE SIDE OF TRUCK DURING DRIFT TEST OF ABNORMALLY HIGH RESISTANCE.

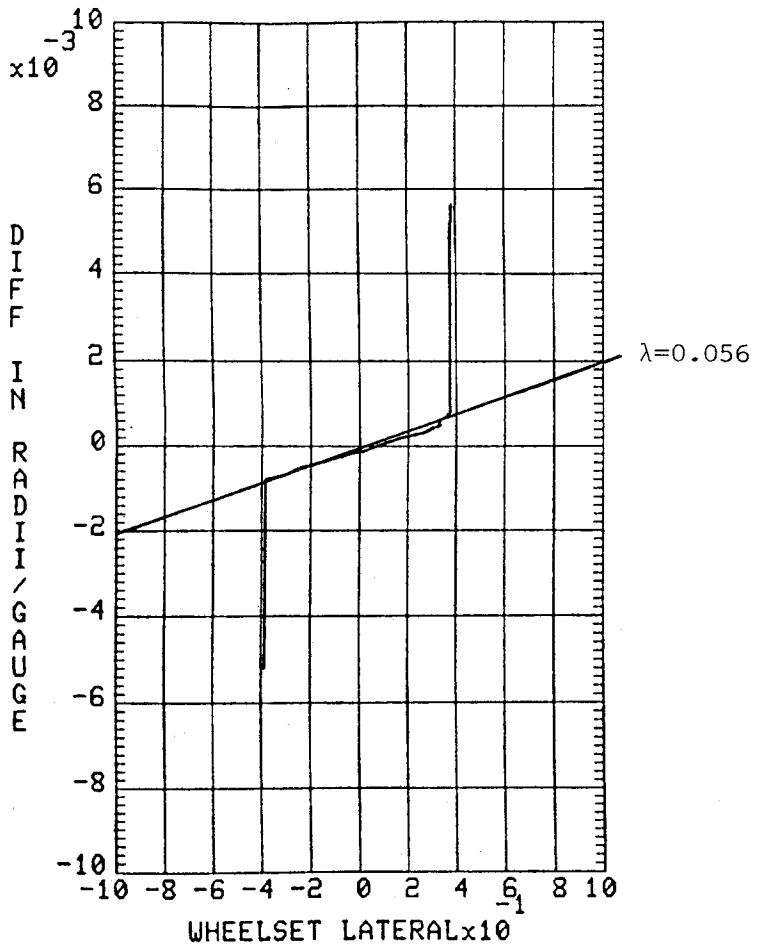

a) New Wheel Profiles (First Drift Test)

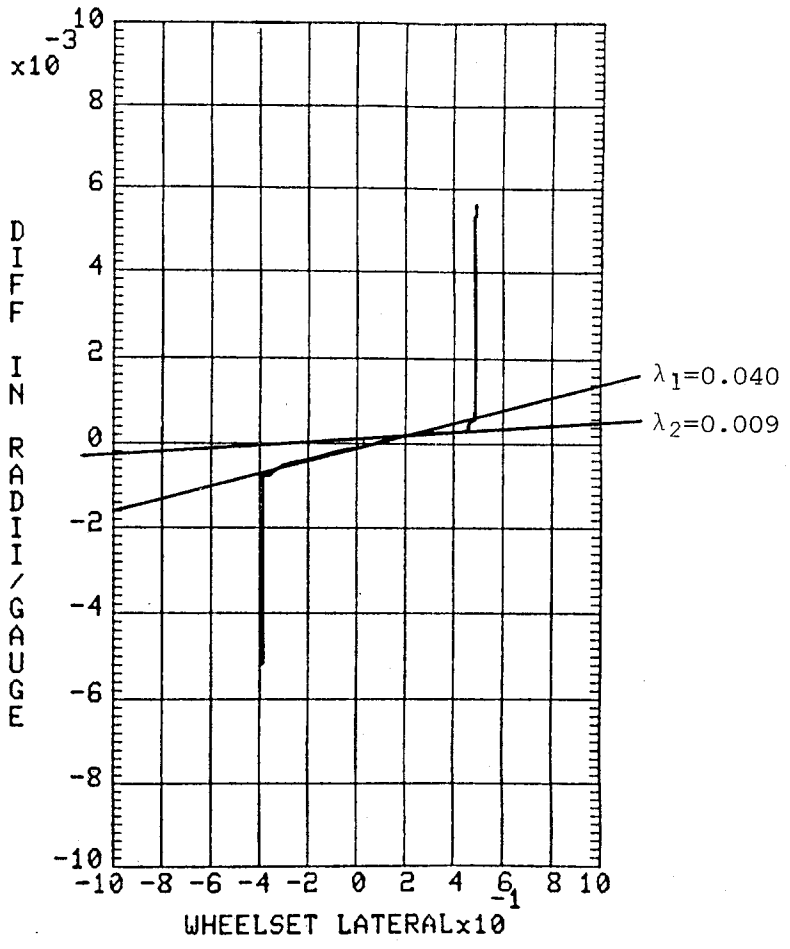

b) Worn Wheel Profiles (Second Drift Test)

FIGURE 3.34. EFFECTIVE CONICITY PLOTS, NEW AND WORN WHEELS-- SOAC ON TANGENT TRACK.

Based on the above, the rolling mechanism would probably be as follows:

> The #1 wheelset rolling line would tend to bias itself towards the outside of the right wheel, due to the negative conicity. However, since the tangent track gage is nominally 0.5 inch less than the TTL, the left wheel would flange before the rolling line equilibrium could be reached. At that point, the wheelset would bounce off the left flange, only to run back onto the flange once more.

While this motion results from the somewhat unique wear pattern, the apparent increase in rolling resistance due to flanging is surprising and has implications in both the transit car and freight car contexts.

The conclusion reached as a result of this study was that the high resistance value occurred because of unique rolling behavior on the tangent track due to the unevenly worn wheel profiles. The tractive resistance data taken on the same day on the Tight Turn Loop (see Section 3.5.3) was not compromised, since rolling behavior on the Tight Turn Loop was of a different nature.

3.5.2 Tractive Resistance on Tight Turn Loop Without Restraining Rail

On May 11th, three runs were made on the Tight Turn Loop in a clockwise direction. One run was made from station 119000 and two from 118700. The data produced three tractive resistance/speed characteristics shown in Figures 3.35, 3.36 and 3.37. At 15 mi/h the data gave the following resistances:

From station 119000	3250 lbs
From station 118700	2400 lbs
From station 118700	2500 lbs
Average	2716 lbs

The two runs from station 118700 show fair repeatability but show lower values than the run from station 119000. This shows that the Tight Turn Loop did not produce consistent resistance with location.

3.5.3 Tractive Resistance on Tight Turn Loop With Restraining Rail

On May 28th, 10 runs were made, 5 in each direction. In order to investigate variation in resistance with track location, runs were made from successive locations spaced at 200 ft intervals. The data produced 10 tractive resistance characteristics, 5 forward and 5 reverse. A typical forward characteristic is shown in Figure 3.38 and a typical reverse characteristic is shown in Figure 3.39. The data produced the following resistance values at 15 mi/h:

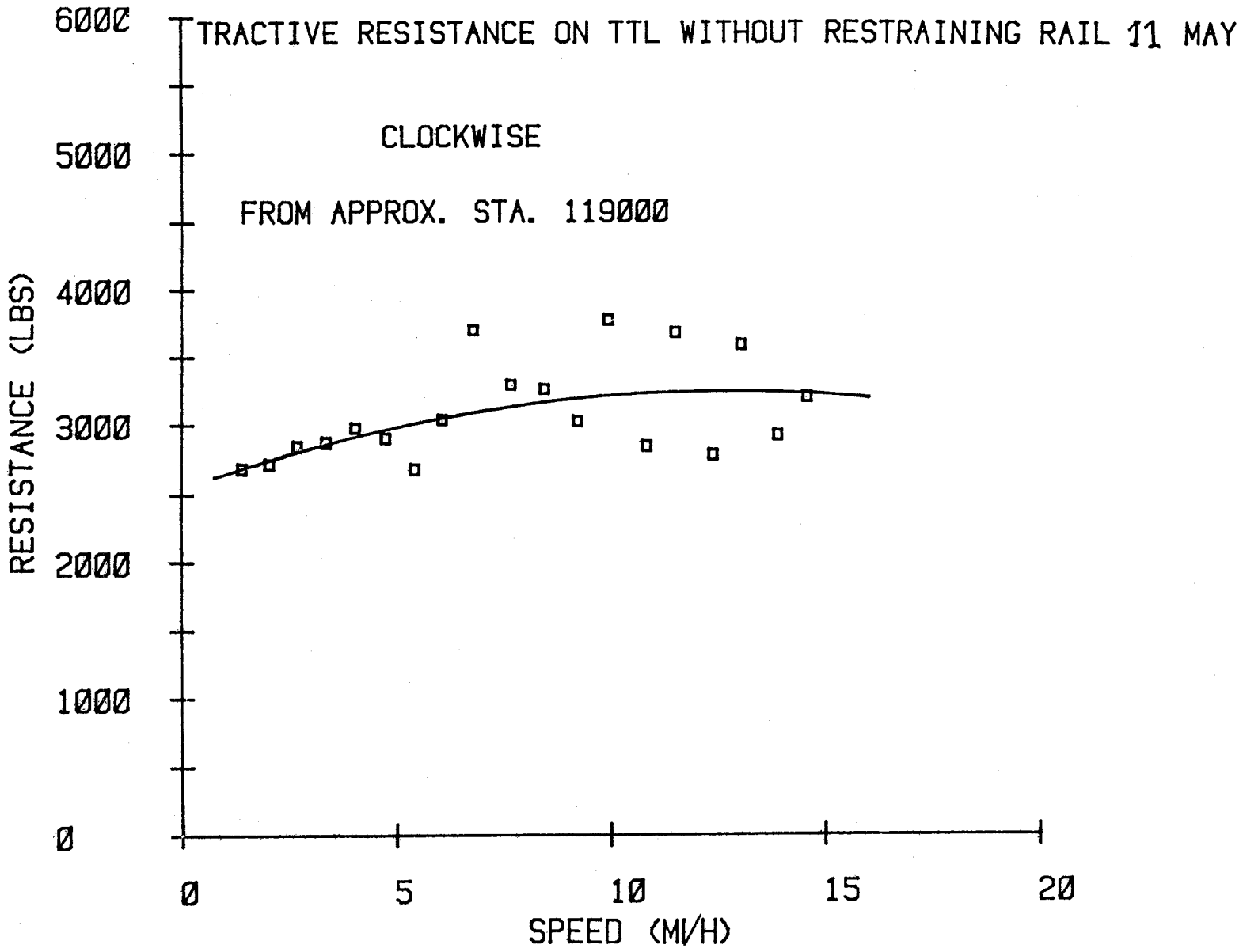

FIGURE 3.35. TRACTIVE RESISTANCE CHARACTERISTIC, FROM STATION 119000 WITHOUT RESTRAINING RAIL.

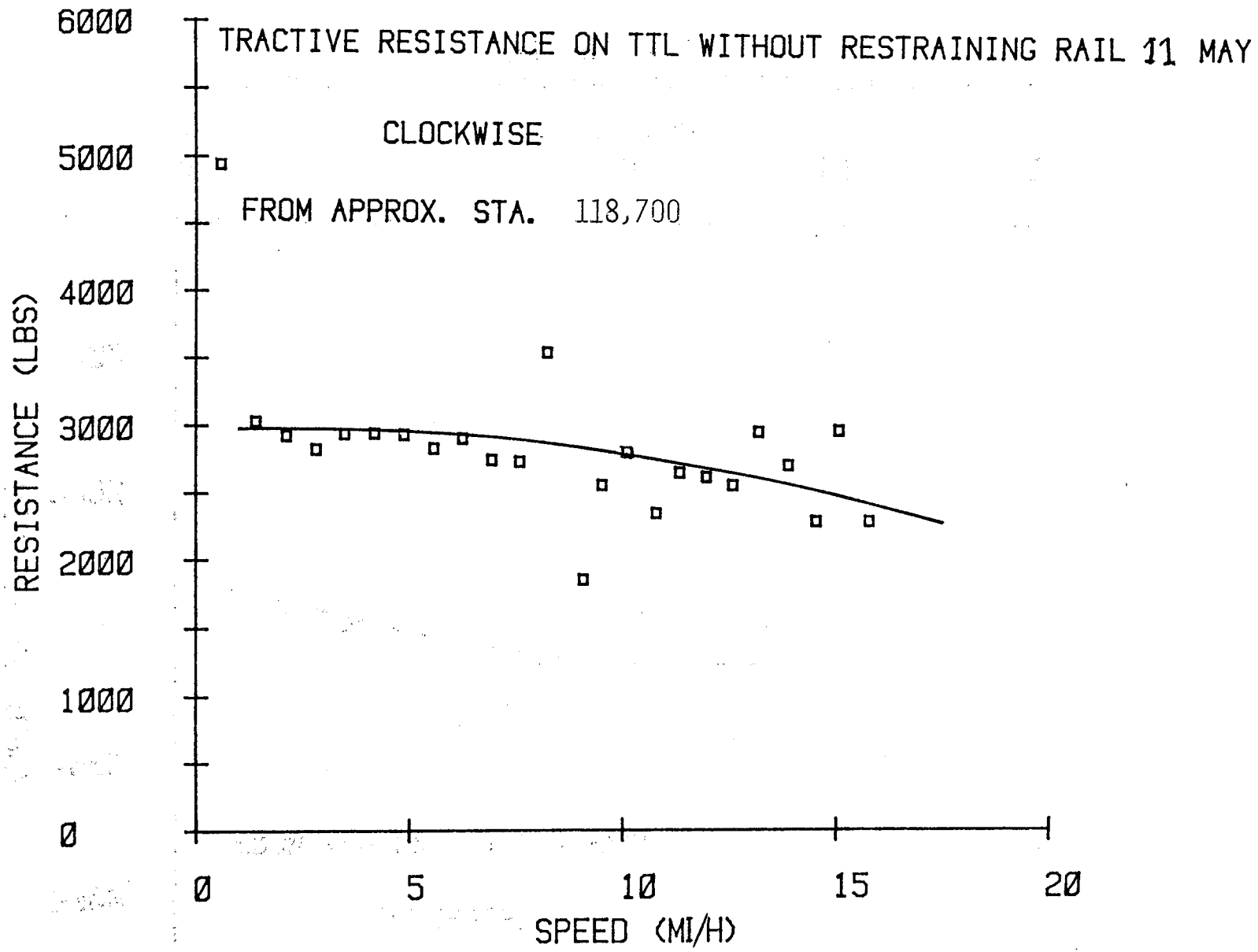

FIGURE 3.36. TRACTIVE RESISTANCE CHARACTERISTIC, FROM STATION 118700 WITHOUT RESTRAINING RAIL.

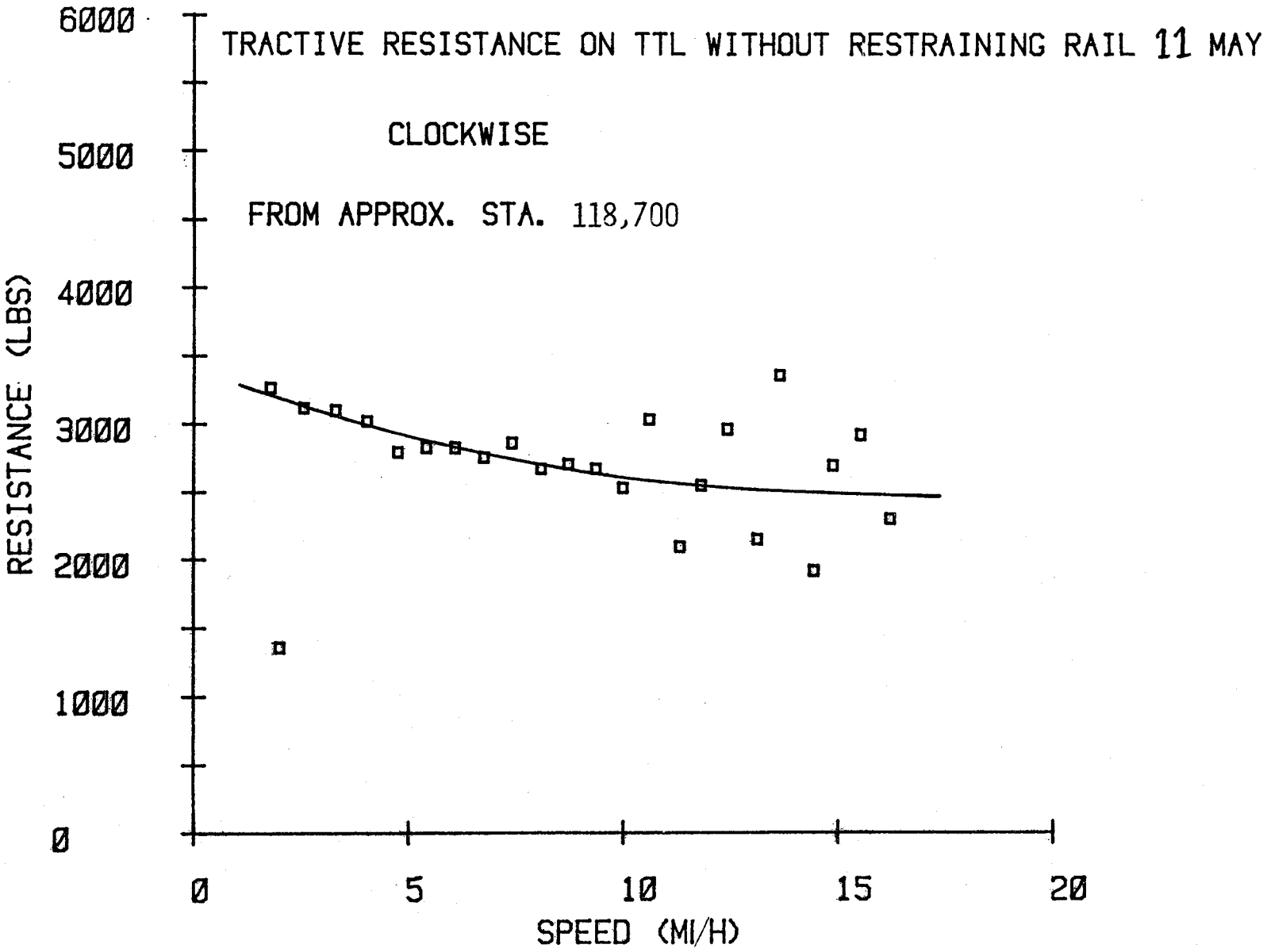

FIGURE 3.37. TRACTIVE RESISTANCE CHARACTERISTIC, FROM STATION 118700 WITHOUT RESTRAINING RAIL.

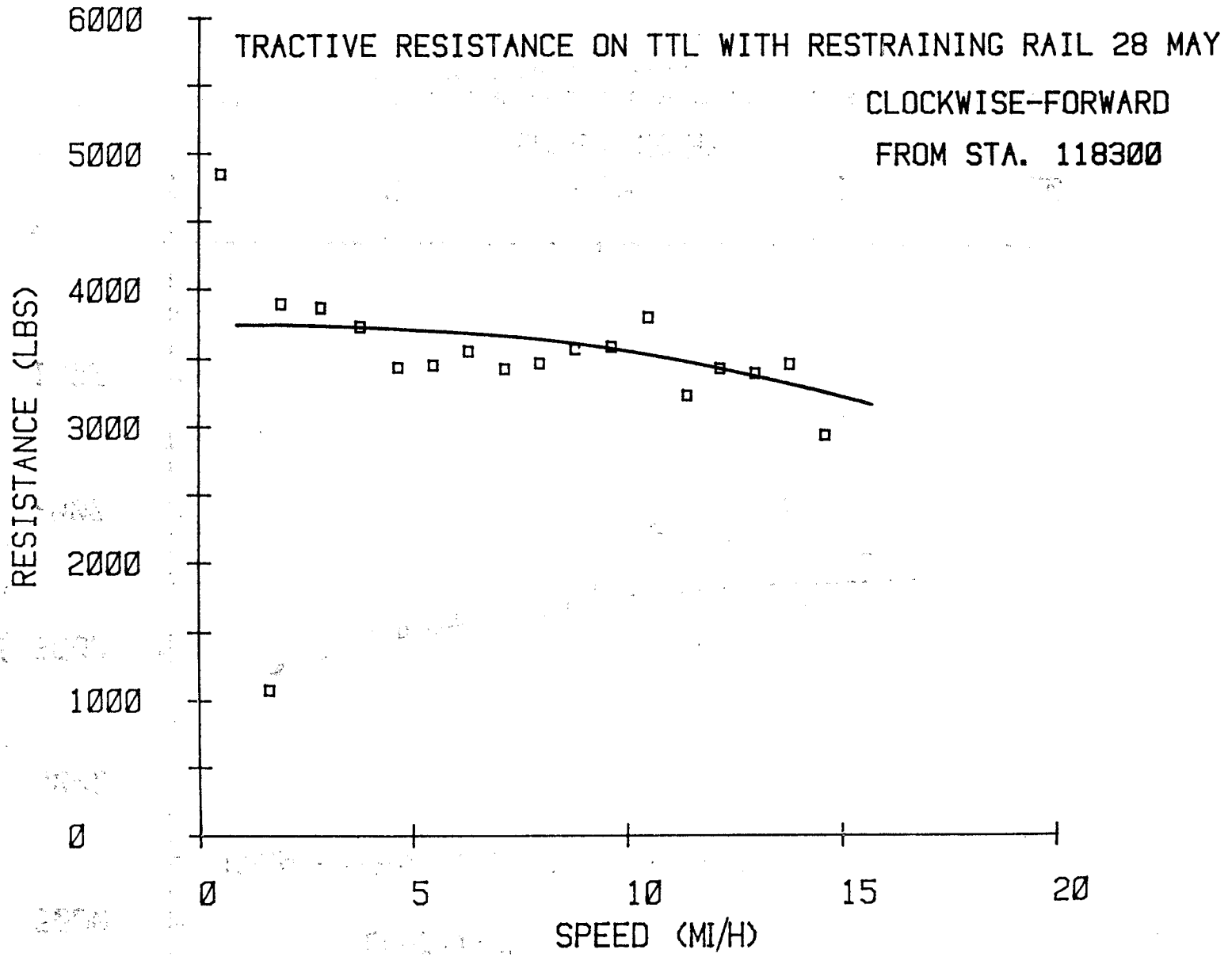

FIGURE 3.38. TYPICAL TRACTIVE RESISTANCE CHARACTERISTIC--FORWARD, WITH RESTRAINING RAIL.

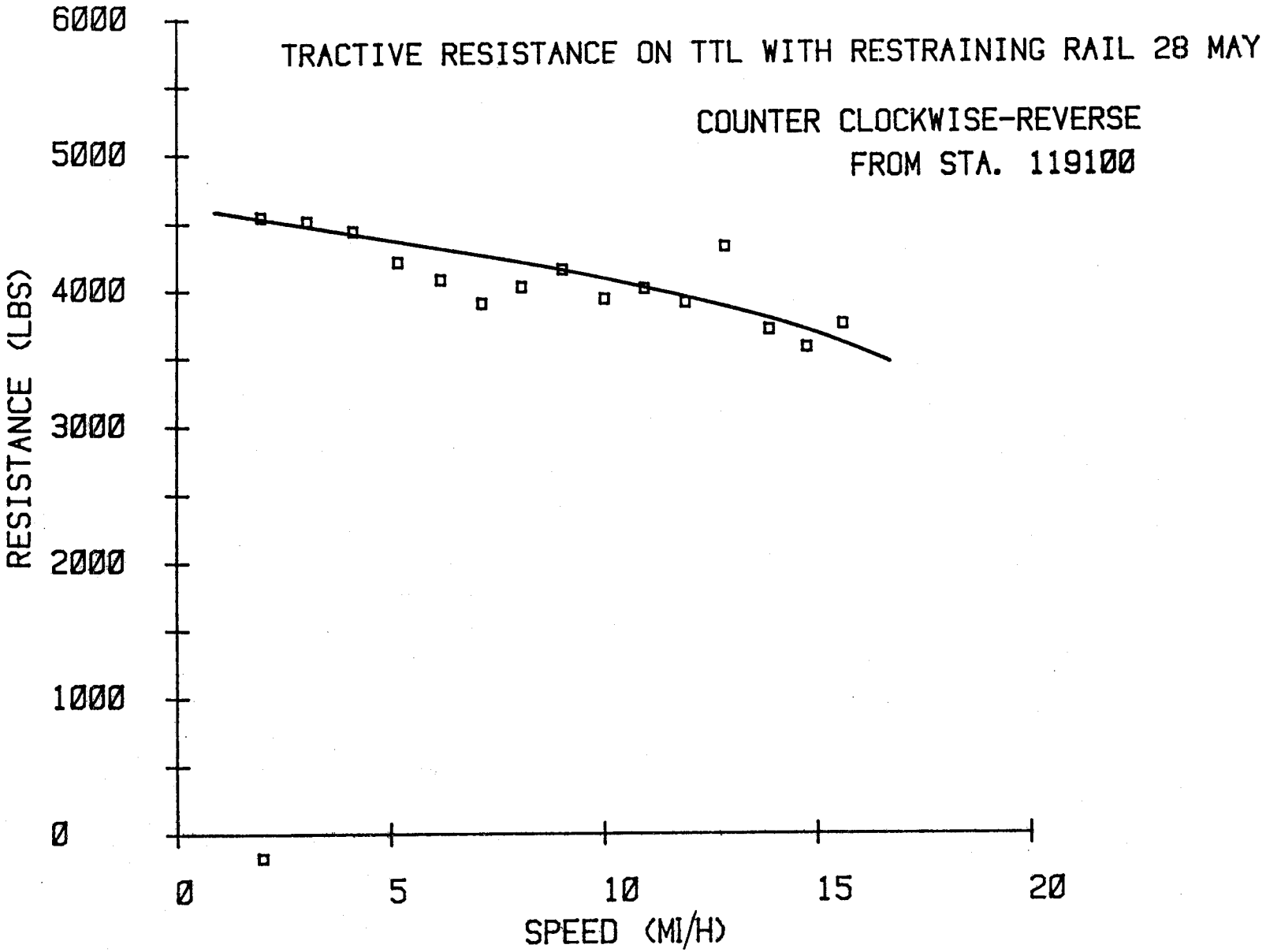

FIGURE 3.39. TYPICAL TRACTIVE RESISTANCE CHARACTERISTIC--REVERSE, WITH RESTRAINING RAIL.

From Station	Clockwise Forward	Counterclockwise Reverse
118300	3200 lbs	3600 lbs
118500	4200 lbs	3400 lbs
118700	4000 lbs	3400 lbs
118900	3900 lbs	3900 lbs
119100	3800 lbs	3700 lbs

The average value of resistance for all runs at 15 mi/h was 3700 lbs. In general, the data shows an upward trend of resistance as speed fell. This trend tends to mask any conclusions that can be drawn as to the variation of resistance by location. However, there is a spread of resistance values at 15 mi/h between 3200 lbs and 4200 lbs, a standard deviation of 300 lbs.

3.6 STATIC SUSPENSION CHARACTERISTICS

3.6.1 General

Static suspension characteristics were evaluated to provide input to the math model and to apply to LVDT deflections to produce estimates of suspension forces. The characteristics were obtained by loading the suspension hydraulically via load cells, and measuring suspension deflections with dial gages. Where appropriate LVDT outputs were also monitored. The following table presents the results:

TABLE 3.5. SUSPENSION CHARACTERIZATION.

	Sensitivity	Notes
Primary Vertical Stiffness	47,200 lbs/inch	Per truck
	11,805 lbs/inch	Per axle box (two chevrons)
Longitudinal Stiffness	166,000 lbs/inch (LVDT)	Per axle box; Based on LVDT output
	135,000 lbs/inch	Per axle box; Based on dial gage readings including axle bending stiffness
	156,000 lbs/inch	Per axle box; Based on dial gage readings with axle bending correction
Lateral Stiffness	57,500 lbs/inch (LVDT)	Per axle box
	36,500 lbs/inch	Overall stiffness per axle including the 'H' frame stiffness
Rotational Stiffness (Break away torque)	8,600 ft lbs	Counterclockwise
	7,840 ft lbs	Clockwise
	8,200 ft lbs	Average
Radius Rod Resilient Mountings	27,900 ft lbs/mrads	Per truck
Axle Alignment	-0.161 mrads	Lead axle, First test
	-1.04 mrads	Trail axle, First test
	-0.293 mrads	Lead axle, Second test
	-0.705 mrads	Trail axle, Second test

3.6.2 Methods of Obtaining Data

The data in the above table was obtained as follows.

a. Primary Vertical Stiffness

A simple but effective method was used in which the load carried by the primary chevron springs was reduced by 10% and the movement measured. The vehicle was positioned as normal resting on the track. A screw jack was placed under the jacking

points on each side of the carbody with a load cell between each jack and the carbody. The air pressure in the secondary suspension air springs was reduced in increments which caused a weight transfer into the jacks via the load cells. As the jacks took vehicle weight, the chevron springs took less weight and the 'H' frame moved vertically. Four dial gages, one at each axle box measured the 'H' frame vertical movement. Because the load cells were not at the truck center pin but at a point inboard of the truck, the ratio 561/648 was applied to the load cell data. The test was performed four times and the data averaged. Figure 3.40 shows the load/deflection characteristic.

The characteristic obtained is the stiffness for the range vertical load -10% and it is assumed that it can be applied to vertical load +10%. The stiffness obtained applies to vertical axle movement in which the two chevrons at the axle box deflect in the same manner (mostly in shear).

Although the data is not as comprehensive as could be found by more complex testing, it satisfied the test objective. The method used was simple to conduct and took only a short time to perform. It could be a useful method to monitor spring rate change throughout a test.

b. Longitudinal Stiffness

The method was to apply a longitudinal force to the lead axle and measure the axle box deflection. The force was applied by the brake actuators at each wheel, and the brake shoes were removed and replaced by load cells. The actual line of action of the applied force was not longitudinal but was considered as such because the angle was small. The force was also applied 7½" from the center of the chevrons. Deflections were measured at each wheel tread by dial gages and the outputs of the LVDT's mounted across the chevrons were monitored. After differences were noted between dial gage and LVDT readings, additional dial gages were mounted in parallel with the LVDT's to confirm their accuracy. The difference between the deflection of axle with respect to the truck frame was identified as the result of axle bending.

The lead axle was 'floated' on an air table and the trail axle elevated on blocks to maintain normal attitude of the truck. The longitudinal stiffness obtained applied to the chevrons under the normal vertical weight of the car. In the longitudinal mode the chevrons do not deflect in the same manner as the vertical case, but in a differential mode. At an axle box, one chevron is compressed and the other decompressed.

The test was performed four times up to a load of approximately 7000 lbs per brake actuator, or 14,000 lbs for the axle. Because there is only one brake actuator per wheel, mounted

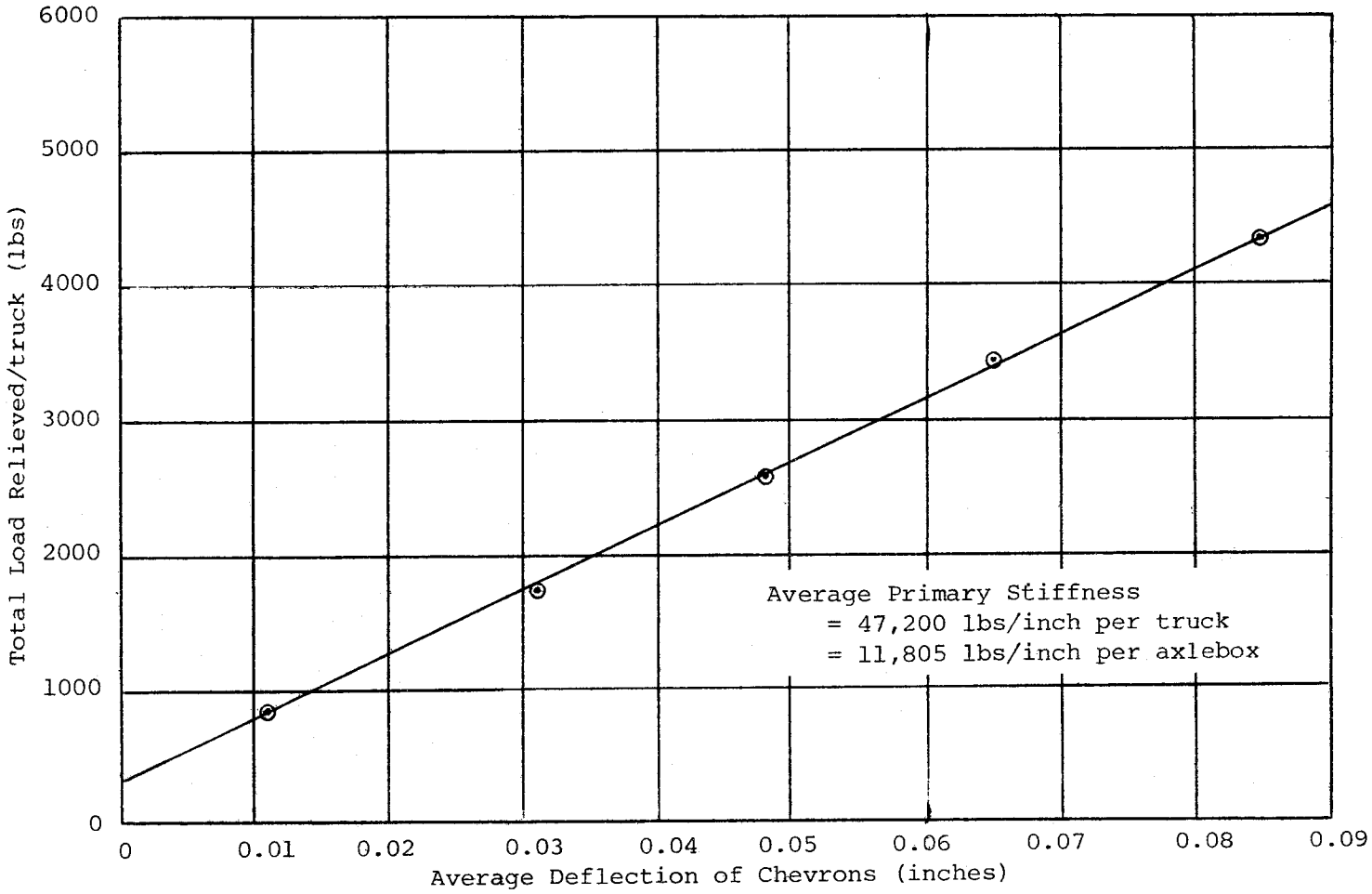

FIGURE 3.40. PRIMARY VERTICAL CHEVRON CHARACTERISTIC.

inboard, the force applied could only be away from the truck center pin. The applied force was applied in increasing and decreasing increments to indicate the hysteresis of the system.

Figure 3.41 shows the force deflection characteristic as measured by the LVDT's. It shows moderate hysteresis with the final data point close to zero. The corresponding characteristic based on the dial gage readings is shown in Figure 3.42. The difference in indicated deflection was shown to result from bending of the axle. This behaved as a spring in series with the chevron suspension.

The system value used when estimating truck suspension forces was the LVDT stiffness of 166,000 lbs/inch. The stiffness used for input to the math model was that based on the dial gage readings with a correction factor applied to allow for the axle bending effect. The axle bending correction changed the dial gage stiffness value from 135,000 lbs/inch to 154,000 lbs/inch, the latter value being very close to the LVDT value of 166,000 lbs/inch.

A cross-check on the axle bending correction factor was derived by application of beam bending theory to the axle of 5½ inch diameter (see Appendix C).

c. Lateral Stiffness

The method of obtaining the stiffness was to apply a load by hydraulic cylinder via a load cell to the 'H' frame at the attachment point of the current collector arm. The vehicle was resting in a normal manner on the track. The loading arrangement was such that the 'H' frame could only be 'pulled' laterally. The deflection of the chevrons was measured with dial gages and the LVDT outputs monitored. The lateral deflection of the truck frame at the load point was also measured. The load was applied as close to the chevron center line as possible.

The stiffness characteristic as measured by the LVDT and dial gages mounted on the chevrons is shown in Figure 3.43. The corresponding stiffness value is 57,500 lbs/inch. The corresponding characteristic for the dial gage deflection measured at the point of load application is shown in Figure 3.44. The data shows that the 'H' frame has a stiffness in the lateral direction of the same order as the chevron springs, giving a combined effective lateral stiffness of 36,500 lbs/inch per axle.

For estimating the lateral suspension forces, the equivalent LVDT stiffness of 57,500 lbs/inch per axle was used. For application to the curving math model the stiffness value of 57,500 lbs/inch per axle was used; for whole vehicle modeling

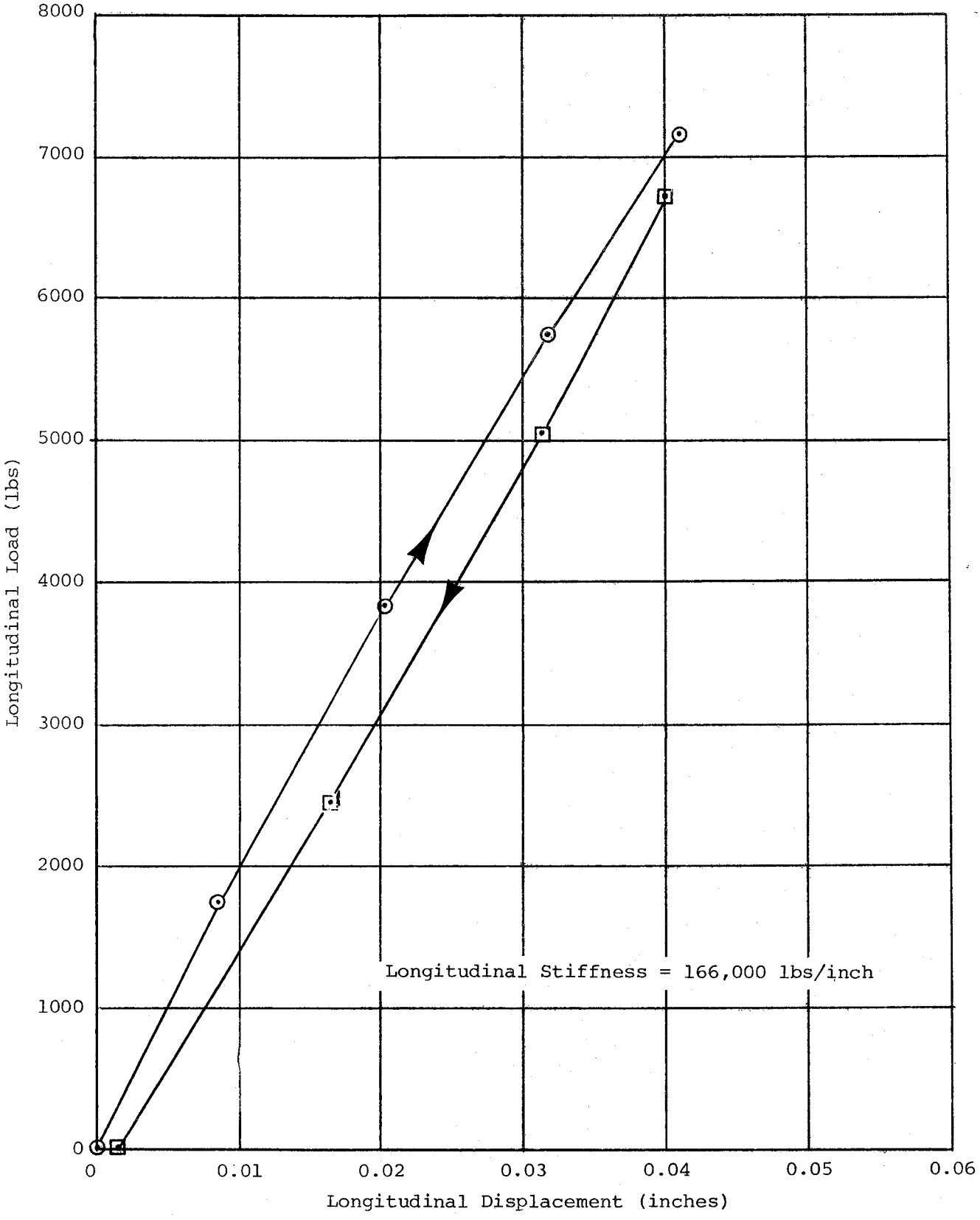

FIGURE 3.41. PRIMARY LONGITUDINAL CHEVRON CHARACTERISTIC FROM LVDT READINGS.

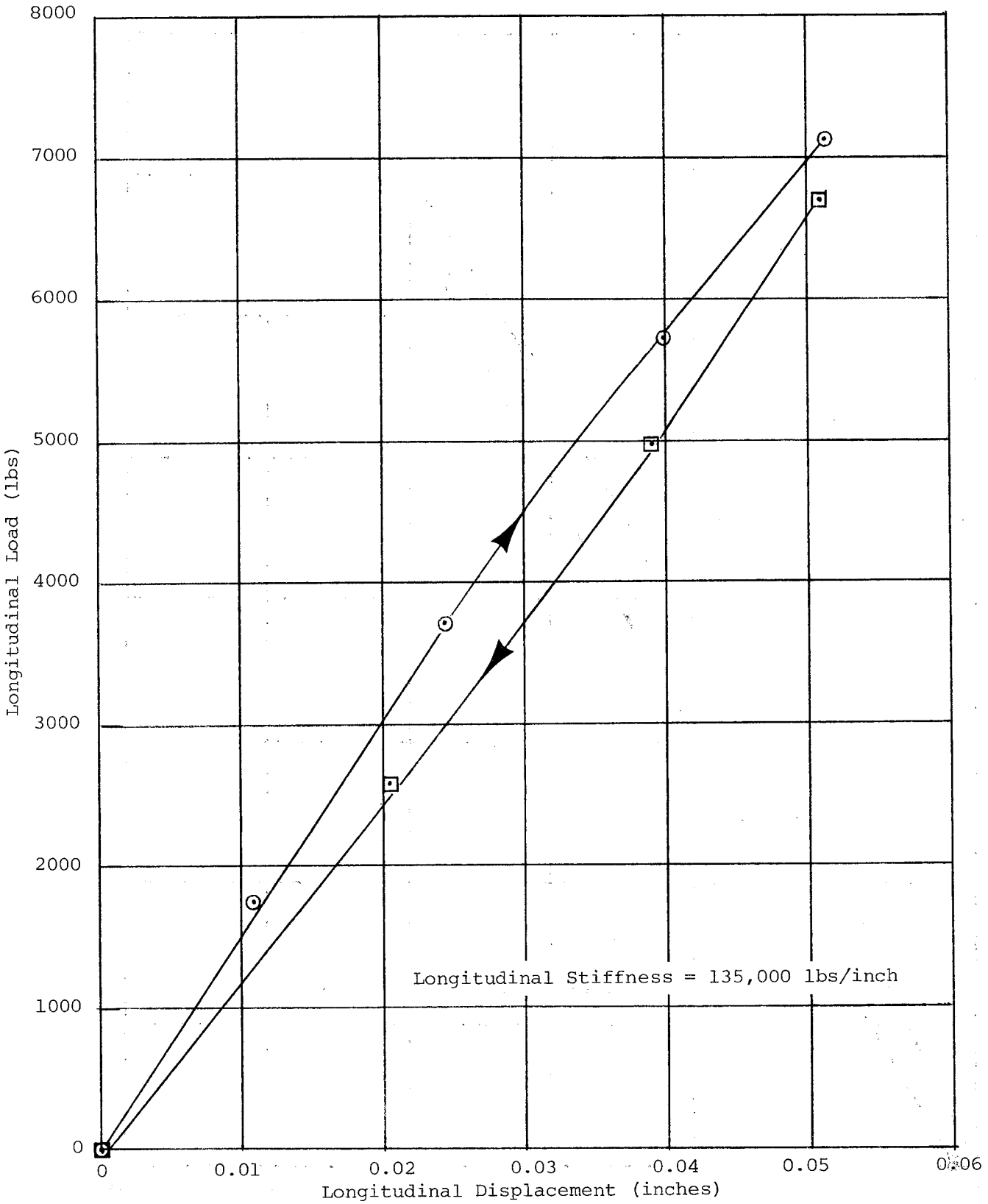

FIGURE 3.42. PRIMARY LONGITUDINAL CHEVRON CHARACTERISTIC FROM DIAL GAGE READINGS.

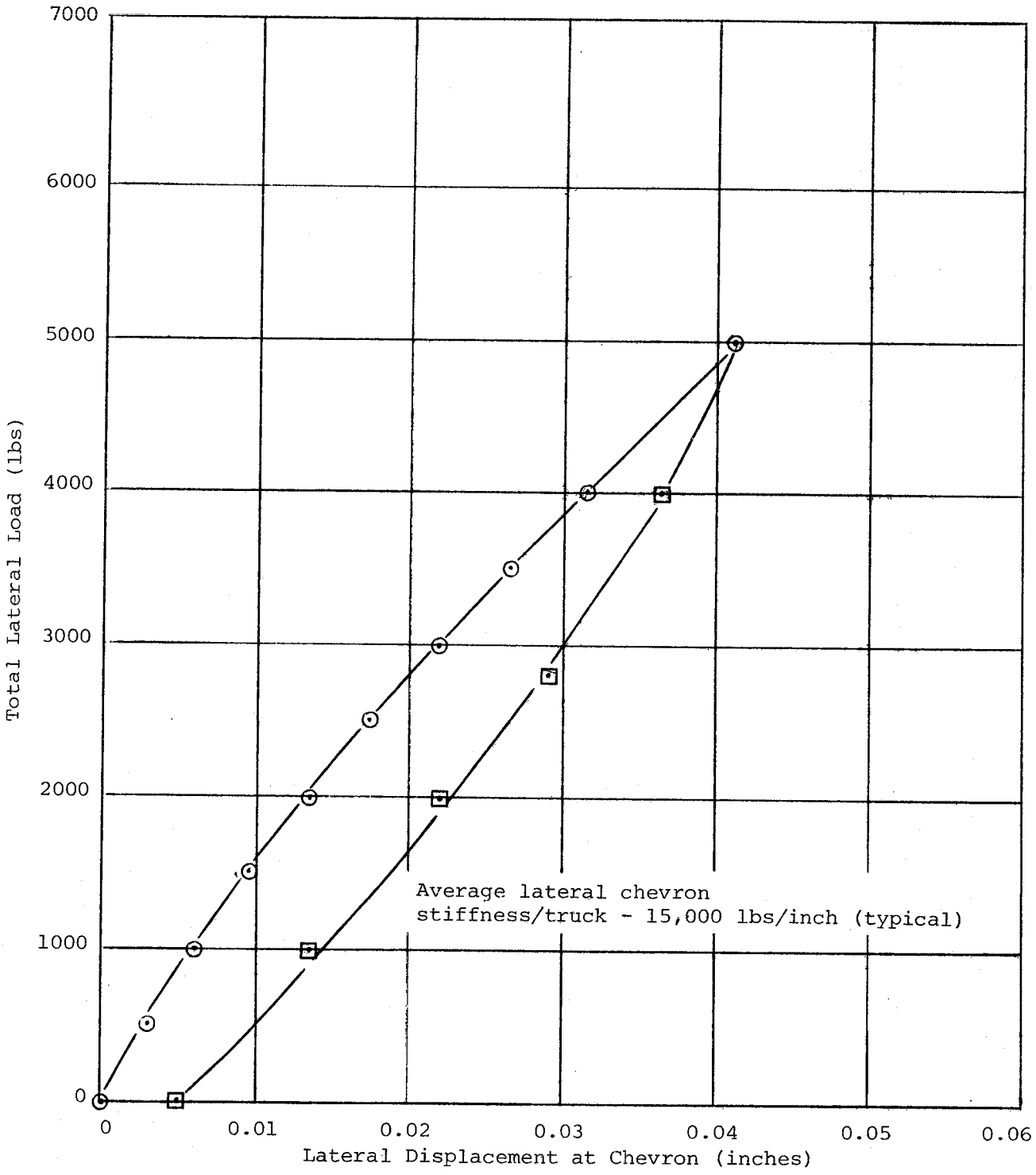

FIGURE 3.43. PRIMARY LATERAL CHEVRON CHARACTERISTIC FROM MEASUREMENTS AT THE CHEVRONS.

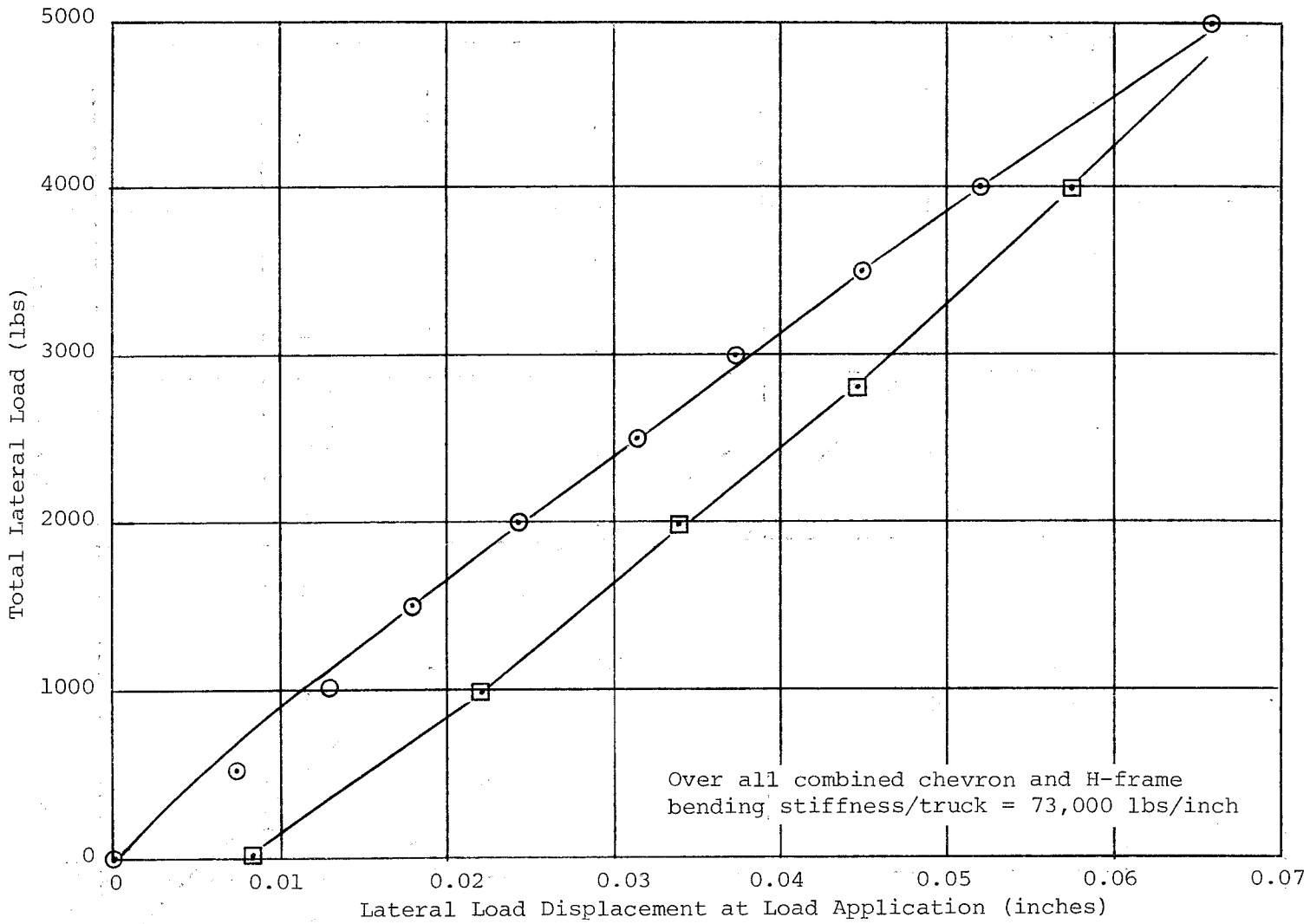

FIGURE 3.44. PRIMARY LATERAL CHEVRON CHARACTERISTIC FROM MEASUREMENTS AT THE POINT OF LOAD APPLICATION.

the combined stiffness of 36,500 lbs/inch per axle would be used. The characteristics show greater hysteresis than was the case with the longitudinal characteristics.

The truck tested had steel cable carrier attachment welded across the 'H' frame sides which restricted the full independent flexure of the side members.

d. Rotational Stiffness

To obtain the 'break-away' rotational stiffness the complete truck was 'floated' on a single air bearing and a torque applied to the air bearing acting about the center pin of the bolster. Rotation of the 'H' frame at the break-away torque was sensed by two string pots mounted between the 'H' frame and carbody. In this mode, the break-away torque of the truck was found for the normal car weight at the time of test.

The torque was applied by hydraulic actuators acting through load cells, attached to two diagonally opposite corners of the air bearing. The test was repeated a number of times for both the clockwise and counterclockwise directions, and an average value calculated.

In addition, a dial gage was mounted across the longitudinal radius rods and resilient mountings on each side of the truck. These were read during the truck break-away tests to obtain the spring rate.

Figure 3.45 shows the torque/rotation (mrads) obtained from one of the tests. These longitudinal restraint rods are designed to accommodate a small amount of truck rotation without motion of the side bearers.

e. Axle Alignment

The axle alignment test was performed by floating the two axles independently on air bearings and then allowing them to gradually settle in an 'unstrained' manner. Measurements were then taken from the wheel side to the sight line of a surveyer set parallel with the carbody. Simple geometry then gave the alignment of the axles relative to the sight line. The data showed that the axles were in good alignment.

3.6.3 Discussion

The static suspension parameter tests were successful in obtaining the required stiffnesses and also the force/LVDT deflection sensitivites for use in suspension force estimation. In general, the truck was found to have very high chevron stiffness,

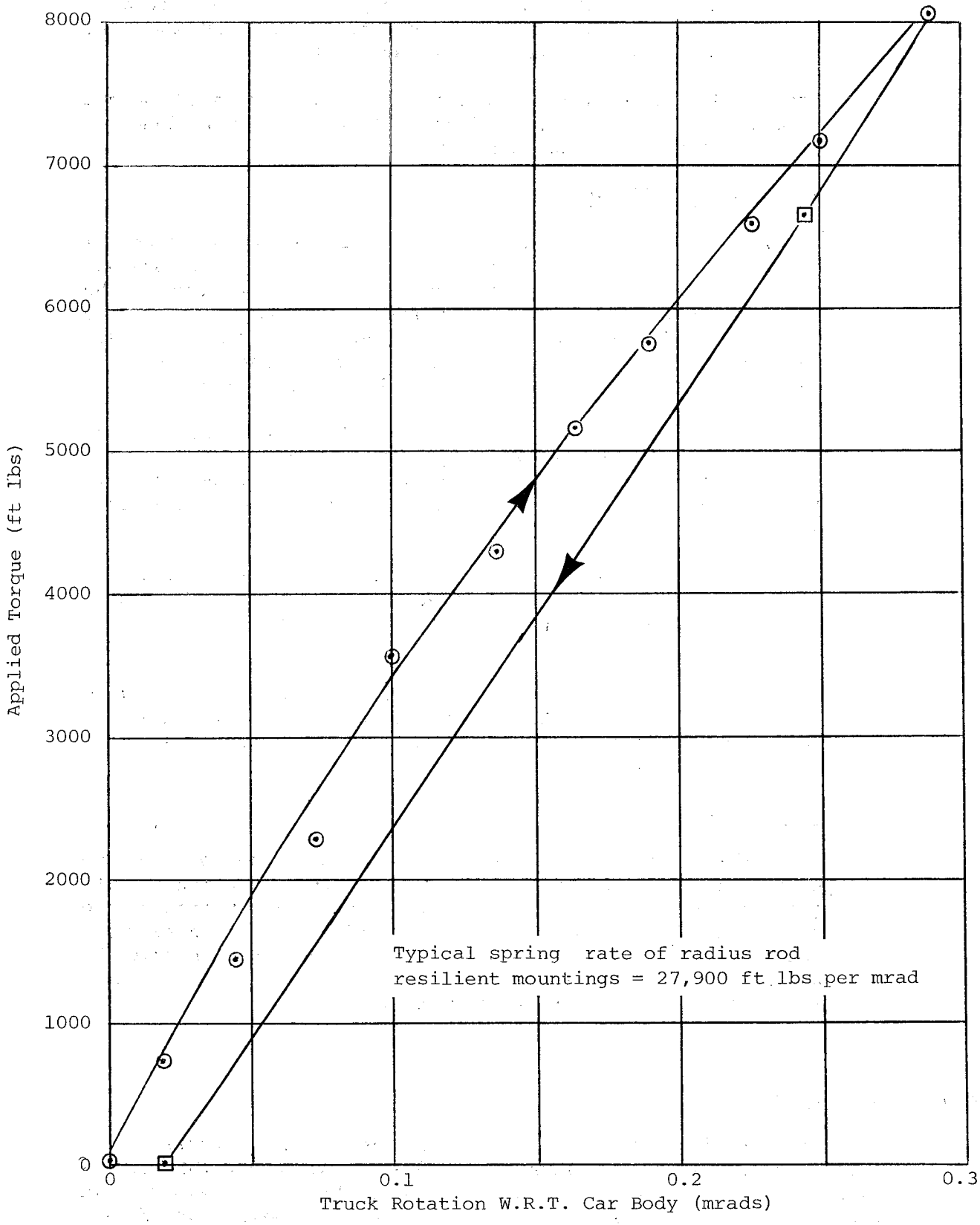

FIGURE 3.45. RADIUS ROD RESILIENT MOUNTING CHARACTERISTIC.

allowing little radial motion of the axles to reduce the angle-of-attack values experienced on the TTL. The relatively low lateral stiffness of the 'H' frame is of interest because it is of the same order as the lateral stiffness of the chevrons and, as such, could be included in a model. Another important finding of this test was that the equivalent axle bending stiffness is sufficiently low to modify the overall longitudinal primary stiffness.

3.7 SUSPENSION FORCES

3.7.1 General

The test objective was to estimate the suspension forces by applying suspension stiffness values to LVDT deflections. The major difficulty of this method was in obtaining and maintaining a datum level. The first approach was to use a datum level obtained by "floating" the truck on air bearings. This was performed twice, at 'pre-test' and at 'post-test'. At the 'pre-test' flotation the LVDT signal conditioning was balanced to zero volts output and the controls locked. Unfortunately the 'pre-test' flotation was invalidated because the two axles of the lead truck were not floated independently. On the post-test 'flotation' the axles were floated independently and the LVDT signal conditioning voltage outputs for the 6 LVDT's noted. These values were modified by applying the tape recorder 'DC offset' characteristic for each channel and the resultant datum voltages applied to the dynamic data recorded on the Tight Turn Loop.

After the suspension forces were calculated the following consistency checks were applied:

a. The net longitudinal force should be zero.

b. The net longitudinal force on the lead axle should be in the opposite direction to the direction of motion.

c. The lead wheelset centerline should be approximately perpendicular to the truck frame (the longitudinal forces at each end should be approximately equal).

d. The trailing wheelset centerline should be significantly skewed with respect to the truck frame (the longitudinal forces at each end should exhibit a large difference).

e. The trend in the truck residual lateral force should be upward, in keeping with the equivalent centripetal force tabulated below:

SPEED (mi/h)	CENTRIPETAL FORCE (kips)
5	0.5
10	2.2
15	4.9
18	7.1

The results were disappointing, and it was concluded that either

- o the mechanical datum had not remained steady,
- o the electrical datum had not remained steady,
- o the method of flotation did not produce a true unrestrained data, or
- o the problem was a combination of the above.

It was decided that a better datum may be available from the signals recorded at the end of the drift test at which the suspension came to rest without the brakes applied on tangent track. This had the advantage of providing a better comparison between Tangent Track and the TTL.

The first drift test performed showed the vehicles to be running on good profiles with low rolling resistance. The voltage levels for the 4 runs performed at the end of each run were:

Channel	CW 1	CCW 1	CW 2	CCW 2	Average
1 (Long.)	0.09	0.12	0.09	0.06	0.09
2 (Lat.)	-0.22	-0.13	-0.22	-0.17	-0.19
3 (Long.)	0.18	0.14	0.11	0.14	0.14
4 (Long.)	0.12	0.12	0.14	0.09	0.12
5 (Lat.)	0.06	0.10	0.03	0.09	0.07
6 (Long.)	0.08	0.05	0.01	0.07	0.05

The average voltage level was applied to the dynamic signal as a datum for the 'without restraining rail' case and the suspension forces calculated by multiplying the displacements from the datum by the equivalent stiffness values obtained from the static stiffness tests (see Section 3.6.1). These values were 166 kips/inch for longitudinal and 57.5 kips/inch for the lateral.

TABLE 3.6. SUMMARY OF SUSPENSION FORCES WITHOUT RESTRAINING RAIL.

Suspension Force (kips)

Direction	CW				CCW
Channel #1 Speed (mi/h):	5	10	15	18	10
1 (Long.)	-0.8	-0.3	-0.2	-0.3	-7.1
2 (Lat.)	7.0	9.0	10.8	11.4	-3.0
3 (Long.)	-2.8	-3.0	-3.5	-3.5	4.6
4 (Long.)	-3.8	-4.0	-3.5	-2.3	2.1
5 (Lat.)	-5.2	-4.4	-2.9	-1.4	6.3
6 (Long.)	7.8	7.5	7.0	6.3	0.5
Residual Lat.	1.8	4.6	7.9	10.0	3.3
Residual Long.	0.4	0.2	-0.2	0.2	0.1
Residual Long. Ax. 1	-3.6	-3.3	-3.7	-3.8	-2.5
Residual Long. Ax. 2	4.0	3.5	3.5	4.0	2.6

Again the consistency criteria were applied and the data was found to be more as expected than that using the 'flotation' datum.

In the case of the 'with restraining rail' datum, the drift datum was found for the second drift test performed at the same time as the 'with restraining rail' running. These voltage levels were:

CHANNEL	ZERO (Second Drift)
1 (Long.)	0.12
2 (Lat.)	0.09
3 (Long.)	0.06
4 (Long.)	0.11
5 (Lat.)	-0.26
6 (Long.)	0.04

In comparison to the first drift test datum levels the two lateral channels (#2 and #3) show a large change. The longitudinal channels were more consistent with the original drift zeros. It was decided to use the second drift test zeros for the lateral channels and the first drift test zeros for the longitudinals, since the longitudinals were more likely to be affected by the off-center rolling of the wheelsets during the second drift test. The following zero voltage levels have been used accordingly:

CHANNEL	ZERO (Applied)
1 (Long.)	0.09
2 (Lat.)	0.09
3 (Long.)	0.14
4 (Long.)	0.12
5 (Lat.)	-0.26
6 (Long.)	0.05

The suspension forces produced when the above datum levels were applied were as follows:

TABLE 3.7. SUMMARY OF SUSPENSION FORCES WITH RESTRAINING RAIL.

Suspension Force (kips)

Channel #1	Direction	CW				CCW
	Speed (mi/h):	5	10	15	18	10
1 (Long.)		-0.5	-0.3	-0.7	-1.0	-8.5
2 (Lat.)		6.2	8.1	10.3	10.5	-2.8
3 (Long.)		-1.8	-2.1	-2.1	-2.3	3.8
4 (Long.)		-3.5	-4.0	-3.3	-2.2	0.8
5 (Lat.)		-4.3	-4.1	-2.0	0.5	6.4
6 (Long.)		5.3	6.5	6.2	5.8	1.0
Residual Lat.		1.9	4.0	8.3	10.0	3.6
Residual Long.		-0.5	0.1	0.1	0.3	-2.5
Residual Long. Ax. 1		-2.3	-2.4	-2.8	-3.3	1.8
Residual Long. Ax. 2		1.8	2.5	2.9	3.6	-4.3

Again the consistency criteria was applied and the data looks quite good with the exception of the 10-mi/h counterclockwise run with restraining rail. Here the residual longitudinal force is substantially less than zero, indicating a large offset on at least one channel. No satisfactory explanation was found for this error.

3.7.2 Discussion

The data produced the required results but the difficulty of establishing zero datum proved substantial. Future testing should explore the possibilities of 'drift' datum levels more thoroughly. The advantage of these levels is that they can be checked on a daily basis rather than before and after the test as was possible with the flotation method.

3.8 ACOUSTIC CHARACTERISTICS

3.8.1 General

The acoustic tests were of a limited nature, with the objective of studying the possibility that acoustic data could provide additional support to the other tests performed on the Tight Turn Loop. It was not intended that the acoustic tests would be a "stand alone" study.

It was noticed, simply by listening, that the squeal of the wheels of the SOAC did not remain constant as it traversed the loop, and the major mode of the analysis was to quantify this feature. The acoustic tests consisted of making recordings of the wheel/rail noise both on the car and at wayside. The wayside tests had two locations, one at the center of the loop and the other 10 ft from the track at one of the strain gage locations. Recordings were made at a number of speeds with the restraining rail both removed and in place.

Recordings were made with a tripod mounted microphone connected to a B&K Type 2209 sound level meter. The signal was passed through a B&K Type 1616 1/3 octave filter set, operating in the 'linear' mode and then onto channel 1 of a Nagra IV-SJ recorder, also in the linear mode. This setup was chosen because the filter set applies a high pass filter with the 3 dB point at 22.5 Hz, which eliminates troublesome infra-sound generated in the moving vehicle. In addition, the B&K Type 2209 has good overload indicators which are lacking in the Nagra IV-SJ.

Calibration of the system was by a B&K 94 dB re 20μ Pa, 1000 Hz calibrator. This type of calibrator is uneffected by atmospheric pressure and made calibration correction for the altitude at TTC unnecessary. However, it can be concluded that the sound power levels generated by the SOAC car would have been higher if the Tight Turn Loop had been operating at sea level.

Analysis of the recordings was made with a General Radio Type 1921 real-time analyzer which had 1/3 octave filters for the standard bands of 11 through 40 covering center frequencies between 12.5 Hz and 10 kHz, and produced RMS levels integrated over selectable time intervals. In addition, the B&K Type 1616 1/3 octave set was used connected to a B&K Type 2306 level recorder. This produced 1/3 octave band level time histories. A set of earphones was also connected to the filter set so that individual 1/3 octave bands could be listened to.

To identify the natural resonant frequencies of the SOAC wheels, an impact test was performed over the pit in the URB.

3.8.2 Wheel Impact Test

With the wheel raised from the rail and struck on the rim with a hammer, a recording was made to identify strong resonant frequencies. The 1/3 octave spectrum up to 10 kHz is shown in Figure 3.46. In the high frequency area the spectrum identifies the 5 kHz band and 2.5 kHz band. In addition, the 500 Hz, 630 Hz, 1.25 kHz and 1.60 kHz bands are evident. The SOAC wheels did not have the damping ring fitted.

3.8.3 Tests Without Restraining Rail

The recording from an on-board clockwise run at 15 mi/h was analyzed into 1/3 octave band levels over a 30 second time interval. Figure 3.47 shows the spectrum with salient bands at 80 Hz, 630 Hz, 5 kHz and 10 kHz. By listening to these bands with earphones the 80 Hz band appeared to be produced by SOAC equipment. The 630 Hz band sounded like a fundamental wheel resonance while the 5 kHz and 10 kHz produced the objectional wheel squeal.

The corresponding spectrum produced from recording, made at the center of the track, identifies the same bands and is shown in Figure 3.48.

The 5 kHz 1/3 octave time history is shown in Figure 3.49. Identified on the trace is the approximate time that the car crossed the switch, taken from the voice track. The time history shows remarkable repeatability. Of interest is the 30 dB drop in squeal which occurred just past the switch, and it is evident that the section of track at the strain gage location produced high squeal levels. The 30 dB drop in level is very significant since a 10 dB drop is subjectively 1/2 as loud.

The corresponding 630 Hz 1/3 octave band time history is also shown in Figure 3.49. Again it shows the remarkable repeatability. Although the time history does not show identical signature to the 5 kHz time history, it shows a high level in the region of the strain gage site and low level just past the switch.

Because the time history signatures show that band level relates to location on the track and contain little random content, it is concluded that band level could be related to track geometry very closely. Unfortunately for this test the cue channel of the Nagra IV-SJ was not cued to track markers so that an exact relationship between band level and track location is not possible.

Comparing the band levels in Figure 3.49 with the track geometry data in Section 4.2, it is hard to produce conclusive correlation. It is possible that the sudden increase of radius of curvature, from 145 ft to 179 ft over distance round the track of 100 ft, could be responsible for the sudden drop of the 5 kHz band in

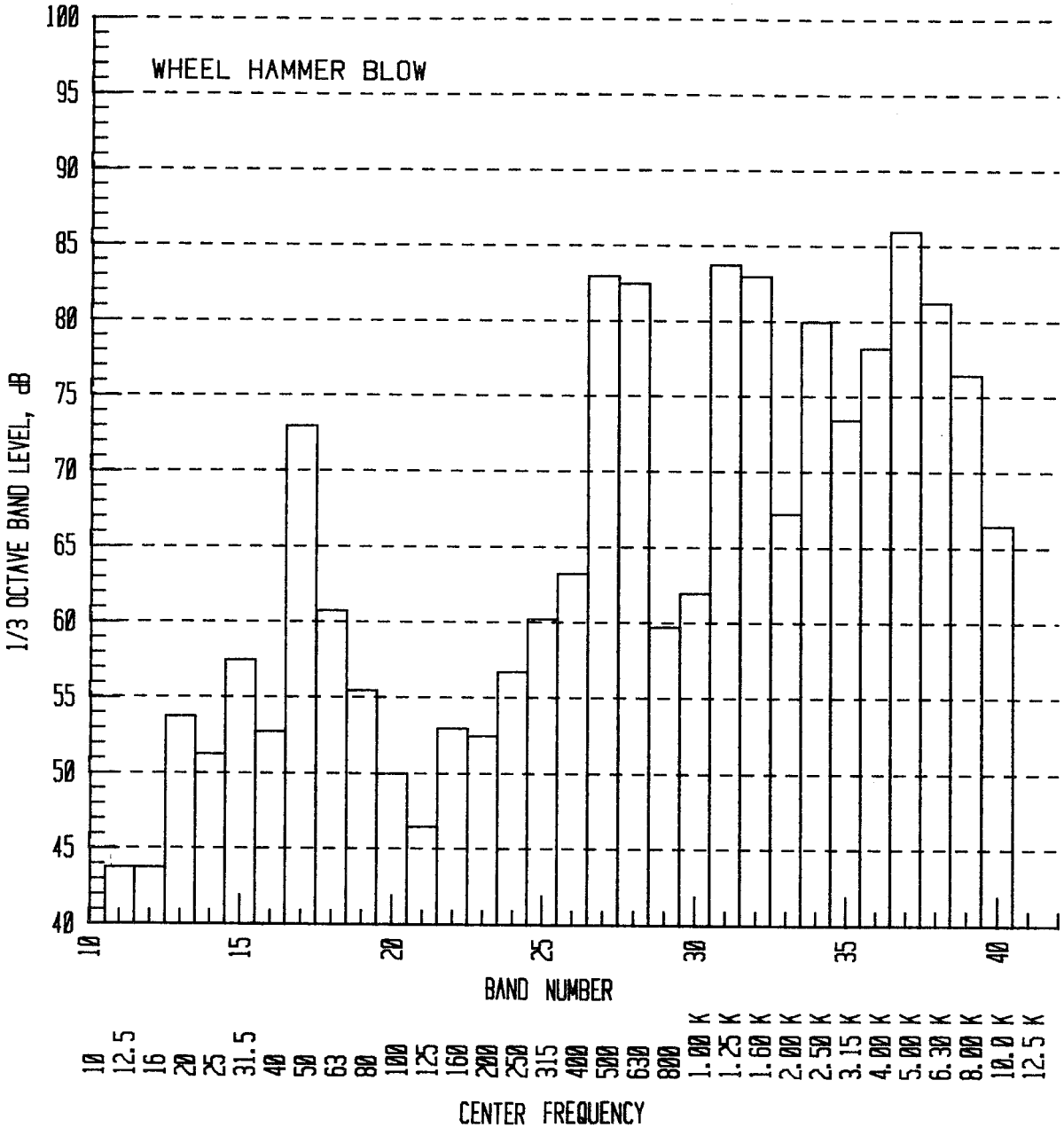

FIGURE 3.46. 1/3 OCTAVE SPECTRUM OF HAMMER BLOW TO SOAC WHEEL WHEN LIFTED OFF TRACK.

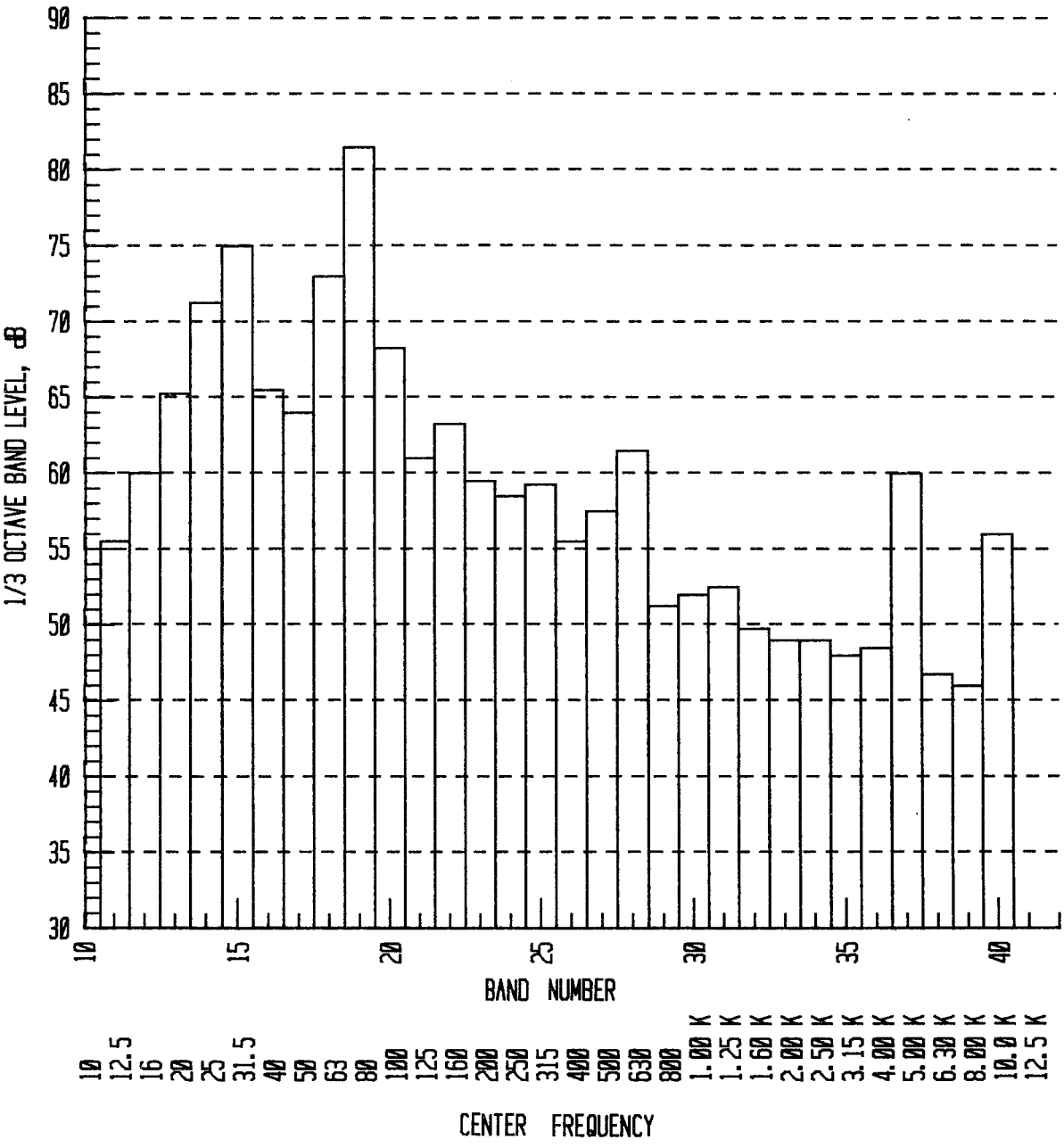

FIGURE 3.47. 1/3 OCTAVE BAND SPECTRUM--ON-BOARD AT 15 MI/H CLOCKWISE WITHOUT RESTRAINING RAIL.

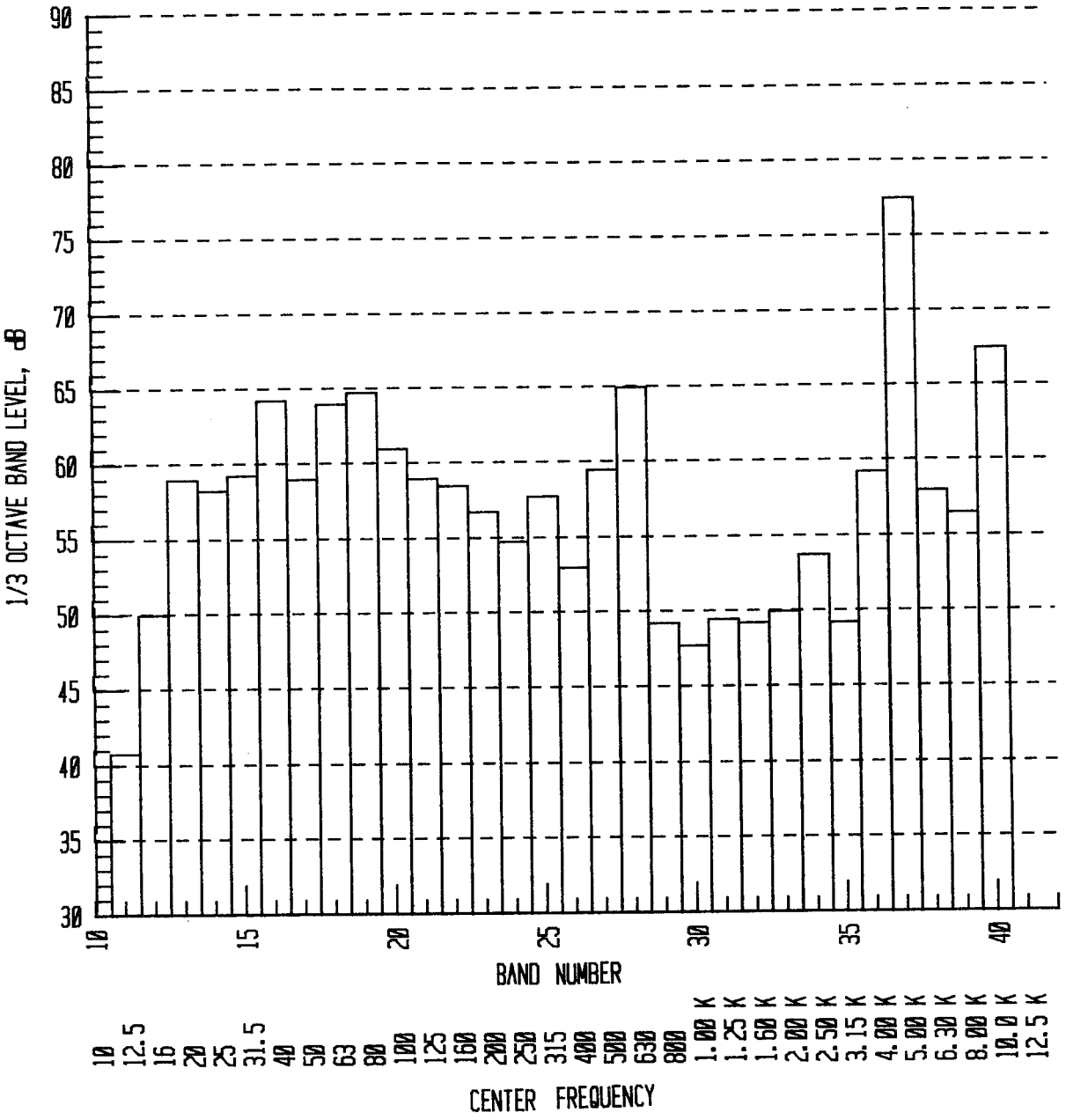

FIGURE 3.48. 1/3 OCTAVE BAND SPECTRUM--CENTER OF LOOP AT 15 MI/H CLOCKWISE WITHOUT RESTRAINING RAIL.

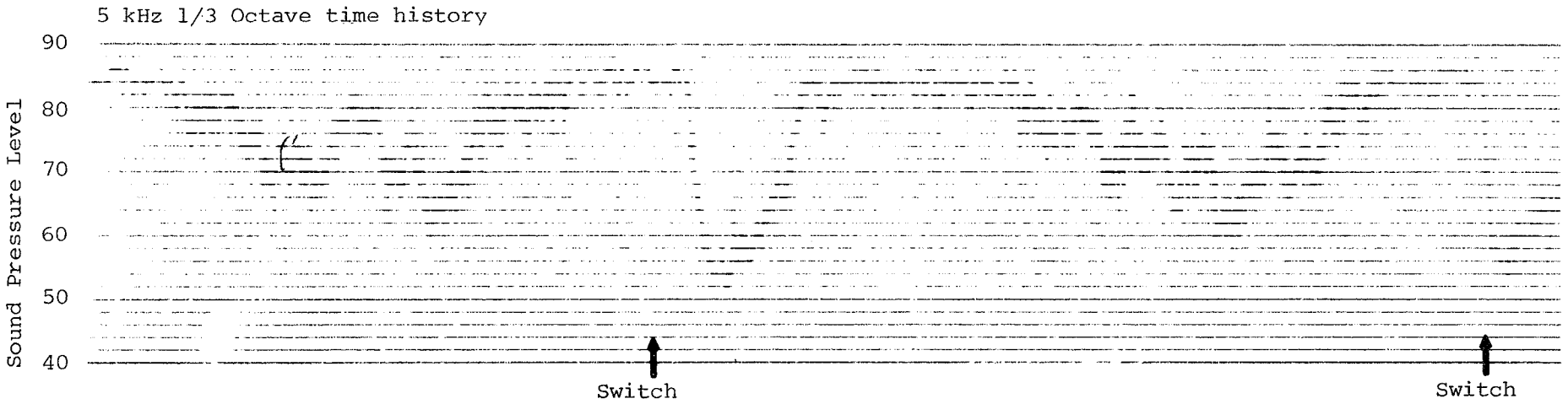

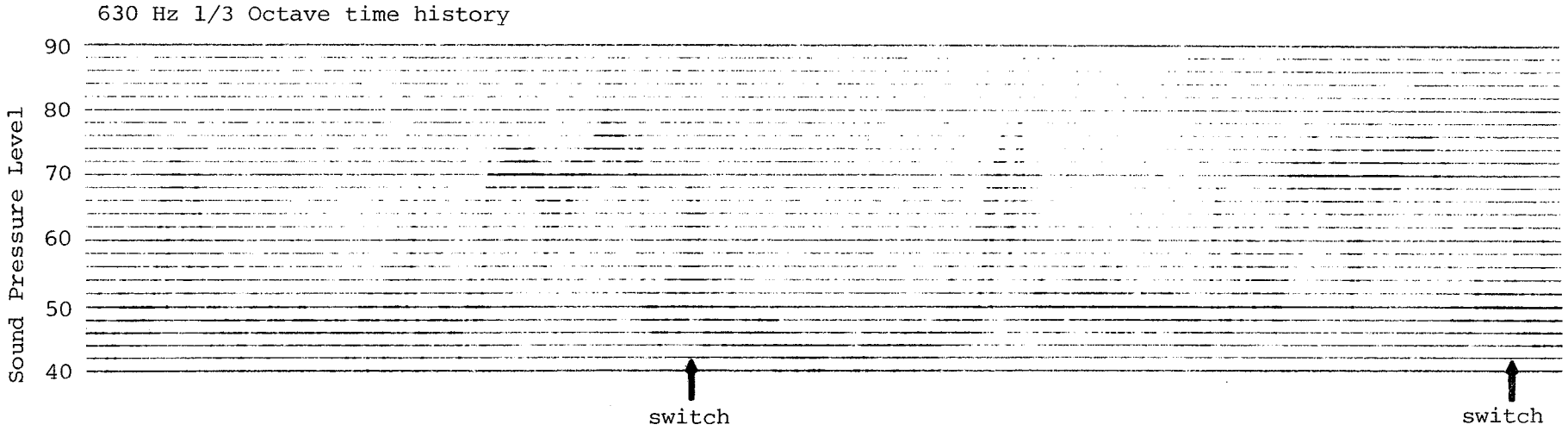

FIGURE 3.49. 5 kHZ and 600 Hz BAND TIME HISTORIES--15 MI/H CLOCKWISE AT CENTER OF LOOP.

the same region. The superelevation peak occurs at 11,850 ft, which is too far removed.

Referring to the LVDT outputs for 15 mi/h run, there is no signal which shows the same variation to such a degree as the 5 kHz 1/3 octave band. The channel showing the most variation with a change of level just past the switch is the rear lateral channel (Ch. 5).

3.8.4 With Restraining Rail

The recording from an on-board clockwise run at 15 mi/h was analyzed into 1/3 octave band levels over a 30 second time interval and is shown in Figure 3.50. This corresponds to the 'without restraining rail' case shown in Figure 3.47. The 'with restraining rail' spectrum shows greater band levels in the 500 and 630 Hz bands and the 2.5 kHz band, but less activity in the 5 kHz and 10 kHz band. The wayside data (center of track) as shown in Figure 3.51 shows similar characteristics but with a high level in the 6.3 kHz band.

The time history of the 6.3 kHz band and 630 Hz band is shown in Figure 3.52. It has a different signature than the corresponding without restraining rail case although levels are high at the strain gaged section. Again there is very high variation of band level (40 dB) and the signatures exhibit the same repeatability.

The pass-by data with microphone located 10 ft from the track exhibits interesting characteristics. Very high band levels in the 20 kHz band are evident, reaching a maximum of 110 dB for a counterclockwise run for the trailing truck (see Figure 3.53). The clockwise also shown in the figure did not produce such high level, being 30 dB down. Curiously the 6.3 kHz band level shows the reverse characteristics with the clockwise level being greater.

3.8.5 Discussion

The acoustic tests did not meet the objectives of relating sound pressure level to any other parameters measured in the tests in a decisive way. However, a significant finding was the fact that the sound pressure level in a given 1/3 octave band exhibited remarkable repeatability for consecutive runs around the loop, although the signatures between bands did not exhibit the same characteristics.

Very large variations in 1/3 octave band level are evident in the recordings with a subjective loudness level variation of the order of 1/16th. This variation occurs even for apparently small changes in track condition or even the minor change of reversing

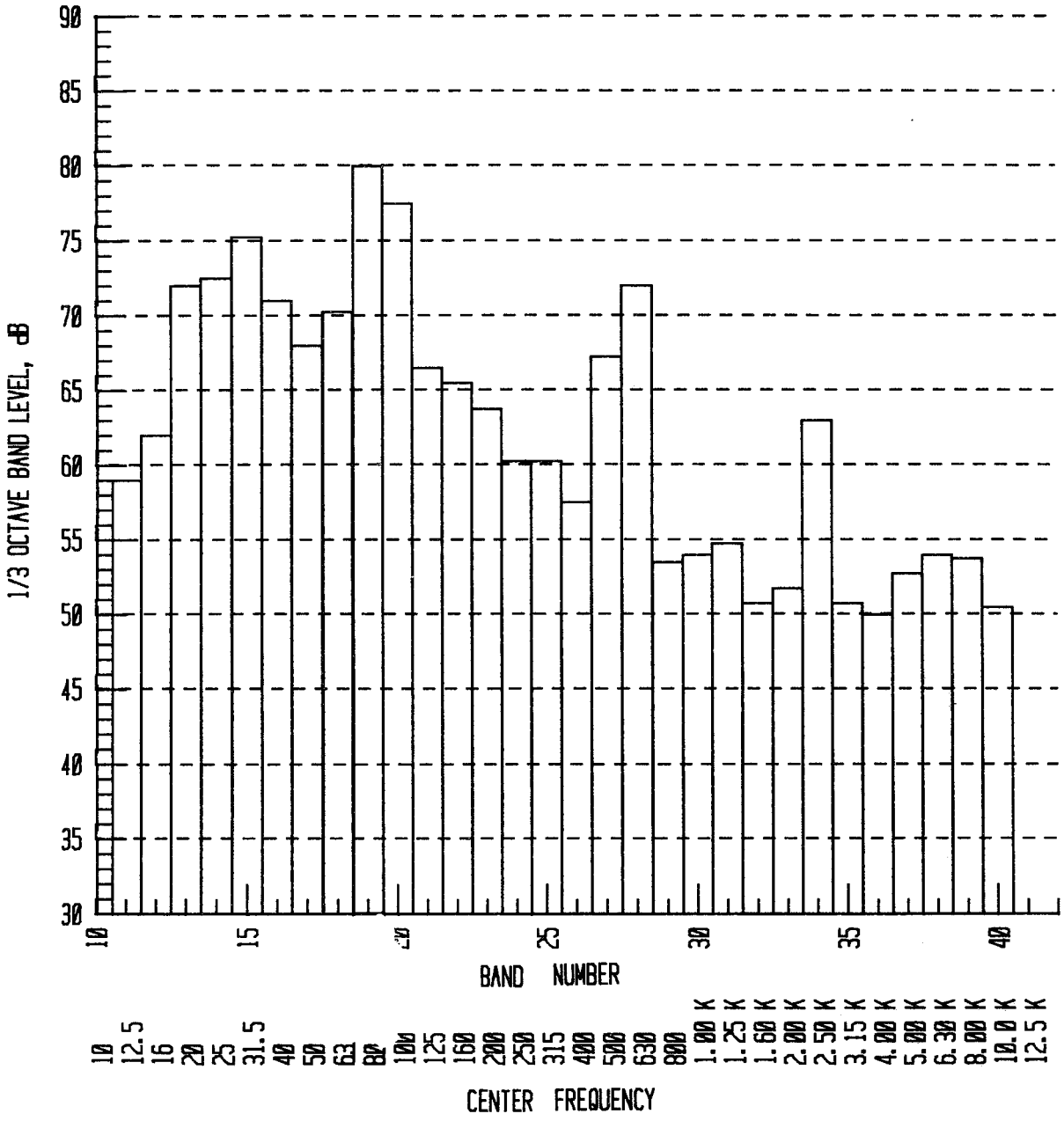

FIGURE 3.50. 1/3 OCTAVE BAND SPECTRUM--ON-BOARD AT 15 MI/H CLOCKWISE WITH RESTRAINING RAIL.

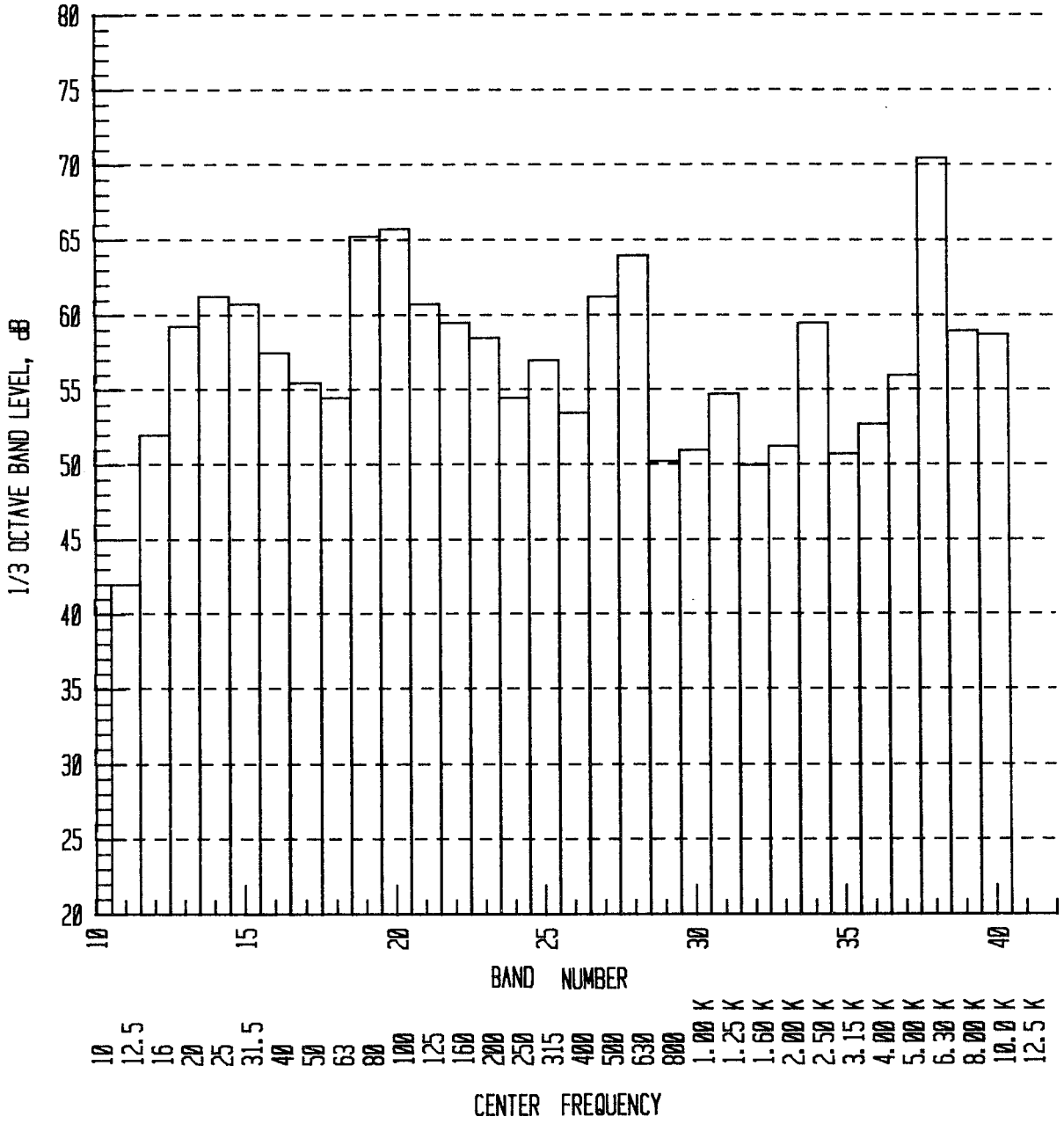

FIGURE 3.51. 1/3 OCTAVE BAND SPECTRUM--CENTER OF LOOP AT 15 MI/H CLOCKWISE WITH RESTRAINING RAIL.

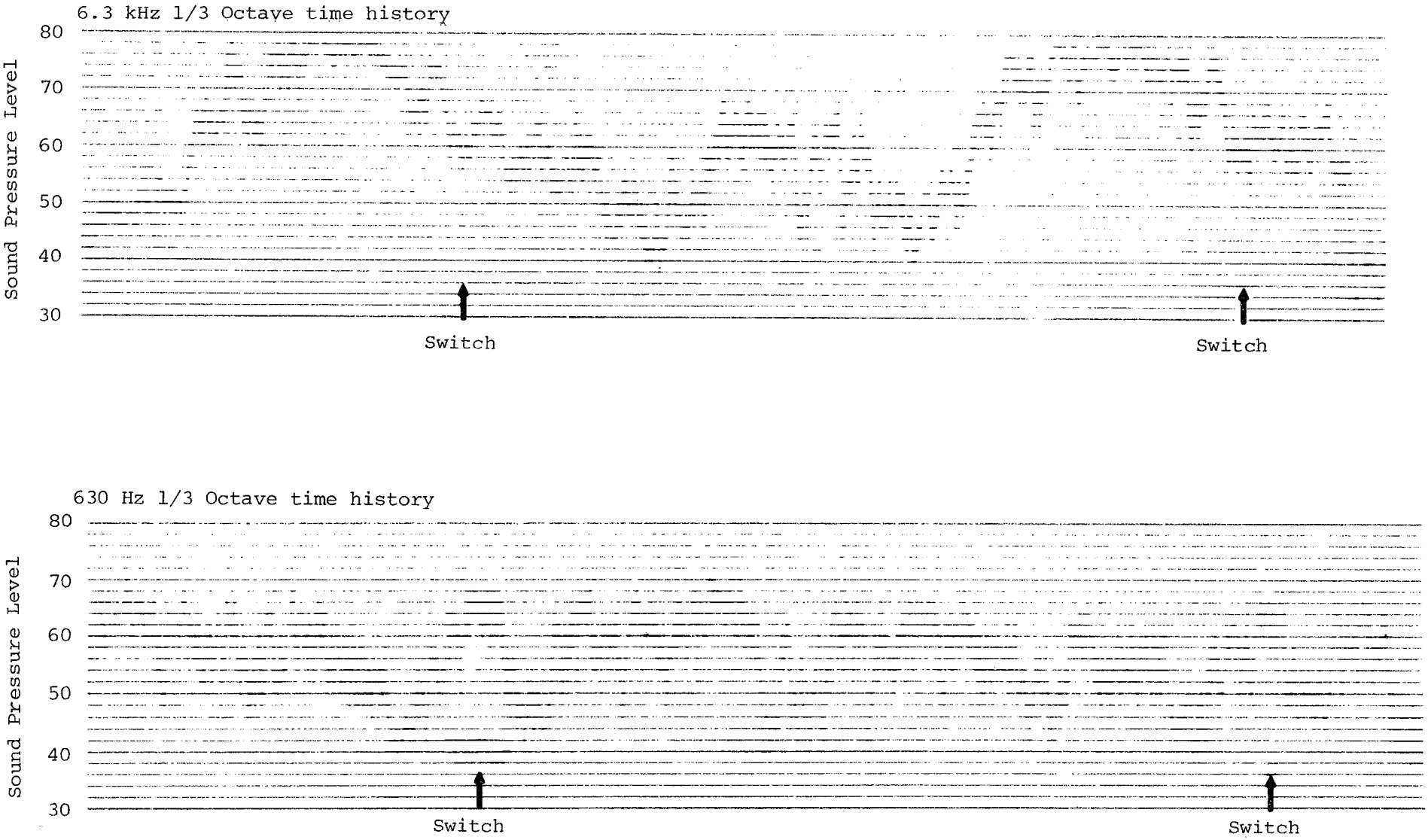

FIGURE 3.52. 20 kHz AND 6.3 kHz BAND TIME HISTORIES--10 FT FROM TRACK WITH RESTRAINING RAIL.

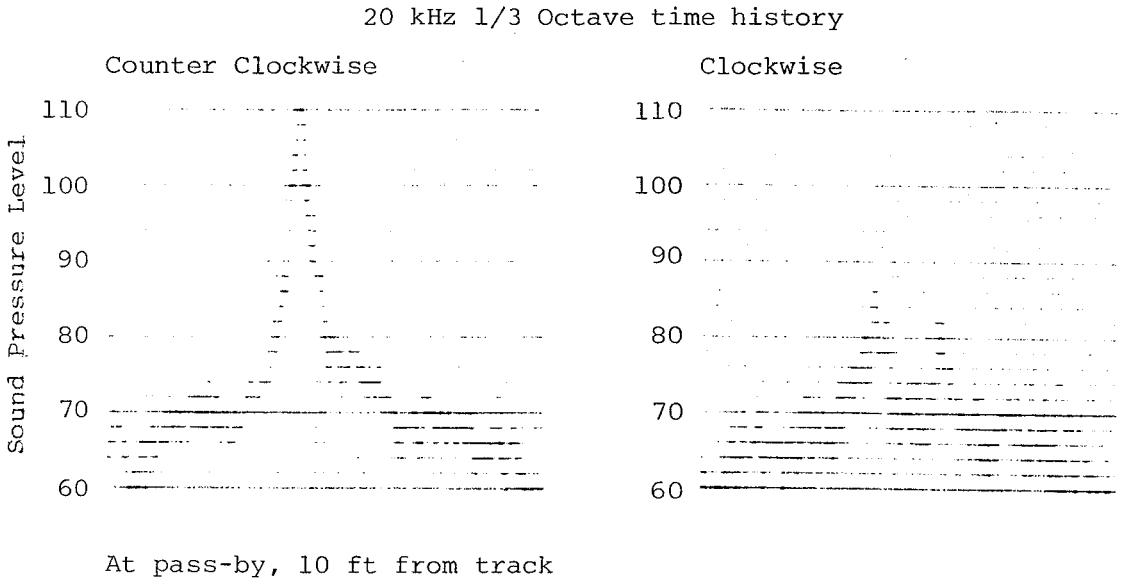

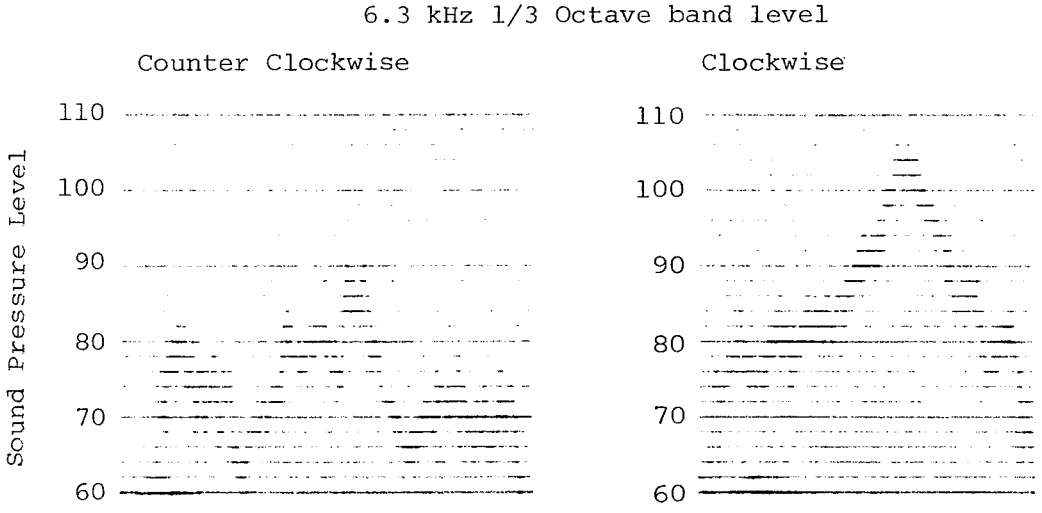

FIGURE 3.53. 20 Hz and 6.3 kHz BAND TIME HISTORIES--PASS-BY DATA 10 FT FROM TRACK.

vehicle direction. It is concluded that very significant reduction of squeal could be made for small adjustments of track condition or truck condition.

Analysis of the data was made more difficult because of variations of superelevation, gage, etc. Control of these parameters could simplify the relationship between band level and track location.

Future work must include syncronization between the 'cue' track on the Nagra IV-SJ and the other parameters being measured by on-board and wayside instrumentation.

Microphones placed directly at the wheels could identify which wheel is radiating. Care would need to be taken not to exceed the maximum level of the microphones. Pass-by at 10 ft from the track is too far away to pick up these differences.

4.0 COMPARISON OF CURVING PERFORMANCE WITH MATHEMATICAL MODEL PREDICTIONS

4.1 MATHEMATICAL MODEL

The mathematical model that is used in this work is a development of the linear curving theory developed by both Boocock[4] and Newland[5]. In their analyses, the wheel/rail geometry was represented by linear functions and contact with the flange was considered to be a limiting case. In addition, the relationship between creepage and creep force was assumed to be linear, and Kalker's simple linear relationships were used. The limit of this assumption was established by determining a slip boundary beyond which slippage would occur.

The curving models were later refined to include the effect of gravitational stiffness and spin creep, which were shown to be significant with worn or profiled wheels, particularly when contact occurred close to the flange root. The analyses that were conducted using the linear theory considered flange contact as a condition to be avoided and, therefore, at the limit of the analysis. However, the limitation occurred for almost all vehicles on curves having a radius of smaller than 2000 ft (3°), and for most vehicles on much larger radius curves, whereas the major problems of rail wear and track damage were occurring on smaller radius curves.

In Britain, the desire to have wheel profiles which would retain their initial shape throughout the period between reprofiling, led to the development of wheels initially machined to a worn profile. These profiles were found to give only a single point of contact with the rail for most of the rail profiles, new or worn, found in practice. In order to evaluate the performance of these profiled wheels, detailed analytical models of the wheel/rail interaction were developed. These models made use of Kalker's nonlinear creep theory,[6] which had become available at about this time. As a result, the nonlinearities arising from both the single point contact wheel/rail geometries and the creep force/creepage relationships, inherent in Kalker's theory, were modeled. These developments are described in the work of Gilchrist and Brickel,[7] Elkins and Gostling[1] and Elkins and Eickhoff.[8] Experimental results for wheel/rail lateral forces and yaw moments were obtained from both model and full scale experiments, which were shown to be in good agreement with the predicted results.

Recently, a test program was carried out at the Washington Metropolitan Area Transit Authority (WMATA). As part of this test program, the effects on curving behavior of changes in wheel profile and primary suspension stiffness were examined. A comparison of the measured curving forces with predictions from the single point contact curving model was performed. This comparison showed that the theoretical predictions were unable to account for the changes in wheel/rail forces that were occurring with different wheel profiles.

The new wheel and rail profile combinations that are used in the United States and many other parts of the world have two points of contact between a single wheel and rail when the wheel is in flange contact. This is typical of the situation that occurs with the lead axle wheel in contact with the high rail on tight curves.

The typical contact geometry in this situation is shown in an end elevation of the wheel and rail (Figure 4.1). Important parameters, which are required to calculate the creepages and resulting forces are the heights of the two points of contact below the axis of rotation of the wheelset and the angles of the planes of contact. In addition, when the wheelset is yawed, the points of contact move from vertically below the axis of rotation of the wheelset as shown in Figure 4.2. This was dicussed by Elkins and Eickhoff.[8] The longitudinal movement is much more pronounced for the flange contact point because of the larger angle of contact.

Predictions using the two point contact curving model were found to be in much better agreement with the measured results from the WMATA test program.[3]

When a restraining rail is used on a curve, a two point contact situation also occurs. In this case the second point of contact is between the back face of the flange and the guard face of the restraining rail (Figure 4.3). The contact geometry resulting from this situation is of special importance. The two dimensional rail/wheel contact geometry, that is normally used when contact is on the tread and flange front, is not adequate in this circumstance and a three dimensional model is required. In particular, yaw of the wheelset results in a large longitudinal movement of the point of contact from vertically below the wheelset axis of rotation (Figure 4.4). This movement is a nonlinear function of the wheelset angle of attack and is dependent on the rail and flange back relative geometry. Also dependent upon this geometry, and established in the model, is the height of the point of contact of the flange back with the restraining rail, relative to the wheel tread contact with the running rail. The angle of the contact plane to the horiztonal is very large, typically in the range of 80° - 90°.

After the geometry of the flange back contact is established, the two point contact model may be used for predicting the curving behavior in this circumstance. The equations of motion are the same whether contact is on the front or the back face of the flange.

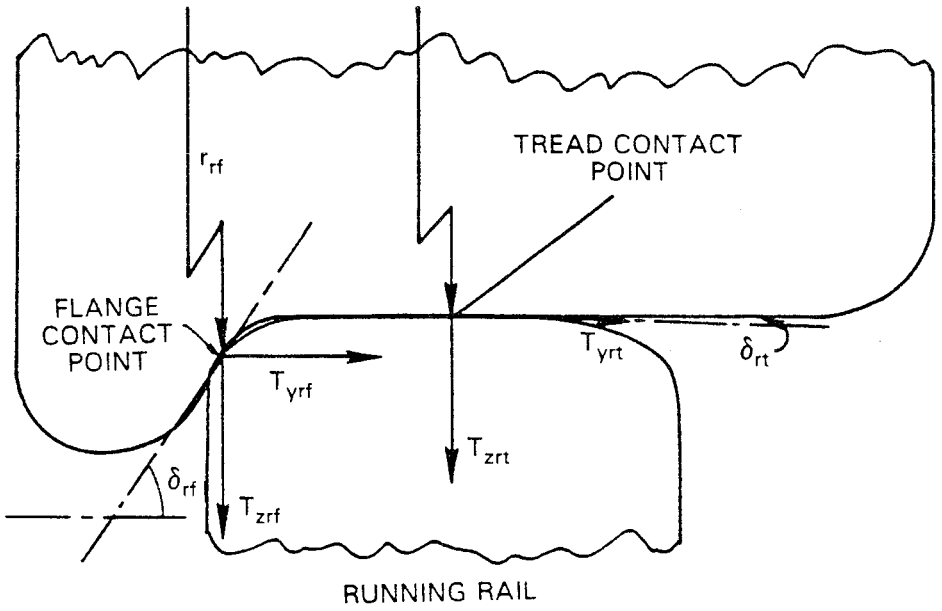

FIGURE 4.1. END VIEW OF WHEEL AND RAIL WITH SECOND CONTACT POINT ON FLANGE FRONT.

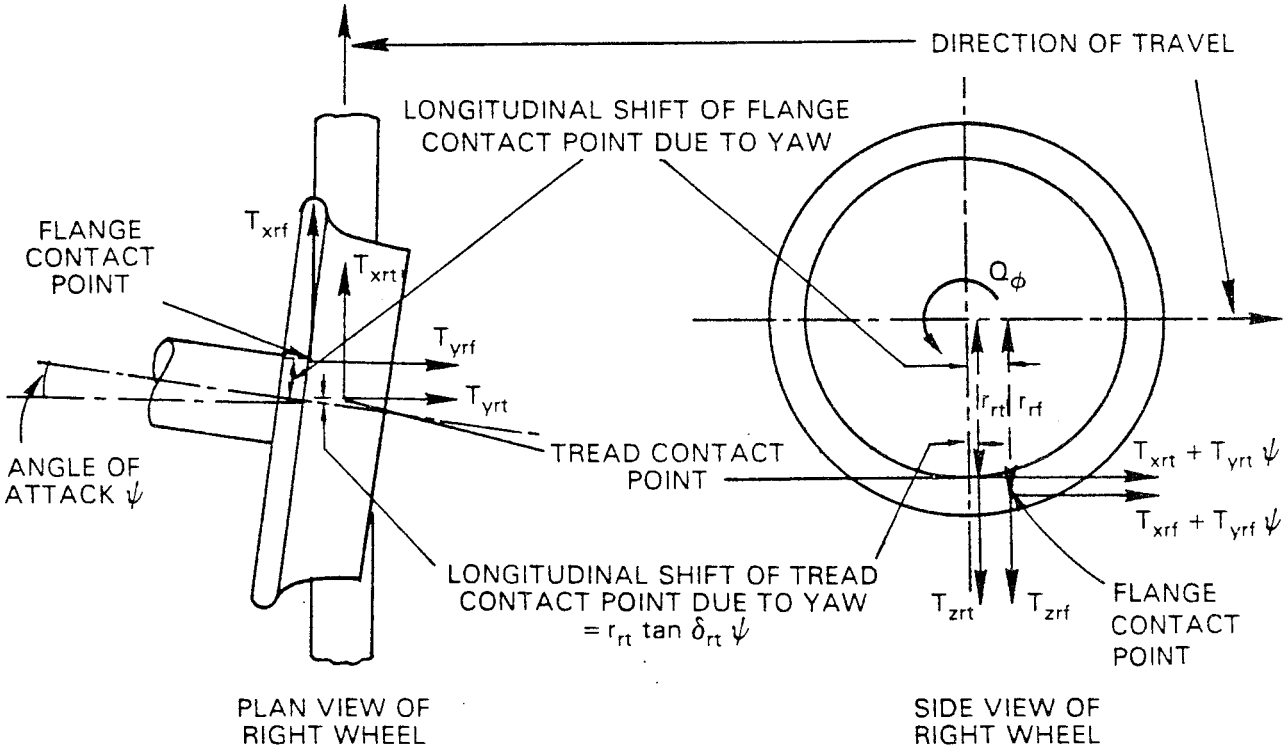

FIGURE 4.2. FORCES AND TORQUES ACTING ABOUT WHEELSET BEARING AXIS WITH SECOND POINT OF CONTACT ON FLANGE FRONT (ONLY FORCES ON RIGHT WHEEL ARE SHOWN).

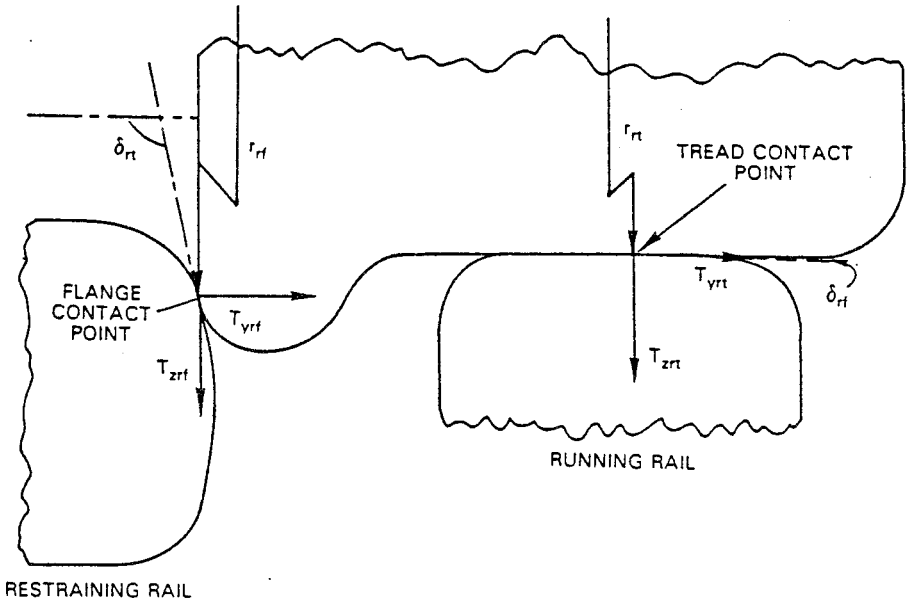

FIGURE 4.3. END VIEW OF WHEEL AND RAIL WITH SECOND CONTACT POINT ON FLANGE BACK.

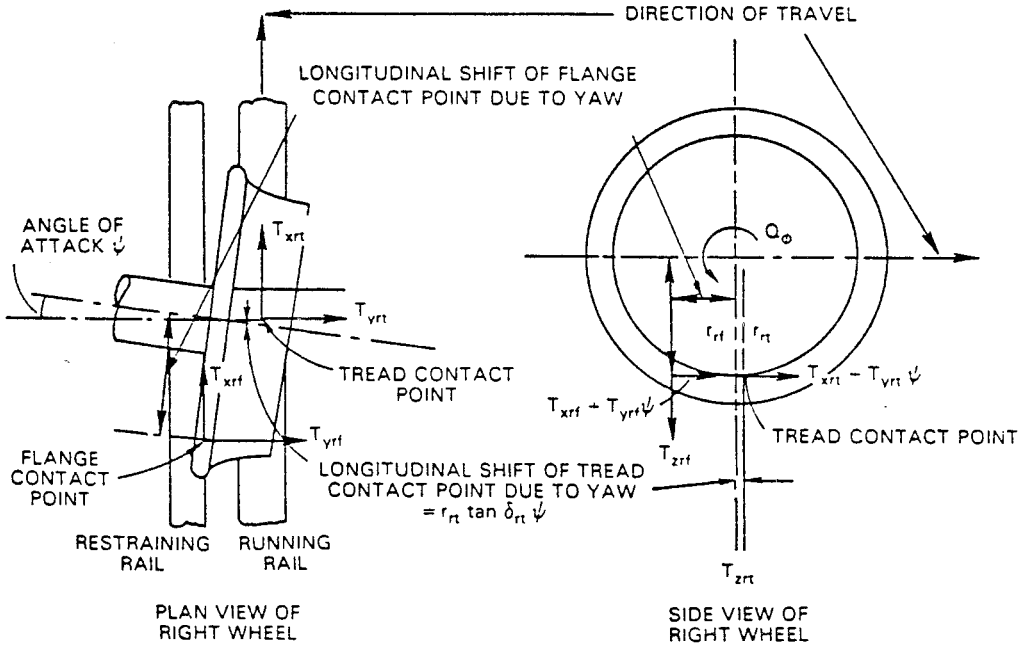

FIGURE 4.4. FORCES AND TORQUES ACTING ABOUT WHEELSET BEARING AXIS WITH SECOND CONTACT POINT ON FLANGE BACK (ONLY FORCES ON RIGHT WHEEL ARE SHOWN).

4.2 VEHICLE AND TRACK PARAMETERS USED IN THE CURVING MODEL

4.2.1 General

In order to make accurate predictions of curving behavior, it is necessary to know the actual values of a number of the vehicle and track parameters. Previous experience[2] has shown that design values supplied by the manufacturer are often considerably different from the actual measured values. Accordingly, many of the vehicle and track parameters were measured directly.

4.2.2 Vehicle Parameters

The various laboratory experiments that were performed to measure truck parameters are described in Section 3. The measured axle misalignments were relatively small compared to the angles-of-attack that were predicted for lead and trail axles on the Tight Turn Loop. As a result, the measured axle misalignments were not used in the predictions. In addition to these parameters, a number of geometrical parameters were determined from engineering drawings of the car and truck.

The vehicle was weighed to determine the axle loadings. During the track tests, the vertical wheel loads were measured using strain gaged rails. Large differences were found among the individual wheels on a truck at the balance speed for the curve, and a definite pattern of load variations was noted in which the lead outside wheel and trailing inside wheel experienced higher than average loads and the remaining two wheels correspondingly lower than average loads. The average vertical loads that were determined are shown in Table 4.1.

TABLE 4.1. AVERAGE VERTICAL WHEEL LOADS AT BALANCE SPEED.

Wheel	Load (kips)
Lead Axle High Rail	13.8
Lead Axle Low Rail	10.6
Trail Axle High Rail	10.6
Trail Axle Low Rail	13.8

The reason for this uneven load distribution has not been determined, although some possible reasons are discussed in Section 3.4.5. Wheel lift due to flange climbing has been largely discounted as a primary cause because of the relatively low vertical stiffness of the suspension. The reason for this load distribution

should be determined as it has a significant effect on the vehicle's curving behavior and propensity for derailment.

Variation of the vertical load distribution with speed was used to determine an effective height for the vehicle center of gravity. All of the parameters that were used in the vehicle model are illustrated in Table 4.2.

TABLE 4.2. VEHICLE PARAMETERS USED IN CURVING MODEL.

Mass Parameters	Values
Truck Frame and ½ Car	108.3 lb-sec^2/in
Axle Mass	9.3 lb-sec^2/in
Stiffness Parameters	
Primary Longitudinal Stiffness (per wheel)	154,000 lb/in
Primary Yaw Stiffness (per axle)	158.10^6 lb-in/rad
Primary Lateral Stiffness (per wheel)	28,750 lb/in
Primary Vertical Stiffness (per wheel)	14,500 lb/in
Primary Roll Stiffness (per axle)	14.9 10^6 lb-in/rad
Geometrical Parameters	
Truck Semi-Wheelbase	45 in
Lateral Semi-Spacing of Primary Suspension	22.63 in
Lateral Semi-Spacing of Wheel/Rail Contact Patches	29.9 in
Mean Wheel Radius	15 in
Effective Height of Vehicle C G Above Rail	60.25 in
Other Parameters	
Axle Load	24,500 lbs

4.2.3 Track Geometry

The track was surveyed in detail and the results of this survey are described in Section 3.1. These data were used to determine mean values of various track parameters in the region of the test zone. The values that were used are listed in Table 4.3.

TABLE 4.3. MEAN TRACK PARAMETERS.

Parameter	
Curve Radius	150 ft
Superelevation	1.5 in
Gage	57.0 in
Restraining Rail Clearance	2.0 in
Restraining Rail Height	0.53 in

4.3 TEST RESULTS WITHOUT RESTRAINING RAIL AND COMPARISON WITH THEORETICAL PREDICTIONS

Tests were conducted over a speed range from 2-18 mi/h. The average superelevation in the region of the test zone was 1.5 inches. As a result, the relationship between cant deficiency and speed is as shown in Figure 4.5. A speed of 2 mi/h is equivalent to 1.4 degrees of cant excess and 18 mi/h is equivalent to 6.75 degrees of cant deficiency.

Figure 4.6 shows the predicted lead axle high and low rail lateral forces compared with the test results. Predictions are made for wheel/rail friction coefficients of 0.4, 0.5, and 0.6. The lateral forces on the two wheels are in the opposite direction and tend to spread the gage of the track. Increasing the coefficient of friction increases the magnitude of both forces. There is a tendency for the high rail force to increase in magnitude with speed, whereas the low rail force decreases. The high rail wheel is in flange contact and the lateral force is approximately 9.5 kips at balance speed.

The unequal vertical wheel loads, which were discussed previously, make the vehicle less prone to derailment. This is so because the lateral force on the low rail wheel, which provides most of the lateral force tending to derail the high rail wheel, is reduced because of its reduced vertical load. At the same time, the increased vertical load on the high rail wheel acts to reduce the L/V ratio on that wheel and, therefore, the propensity to derailment. The L/V ratio on the lead axle high rail wheel is approximately 0.68, for a coefficient of friction of 0.5, throughout the speed range.

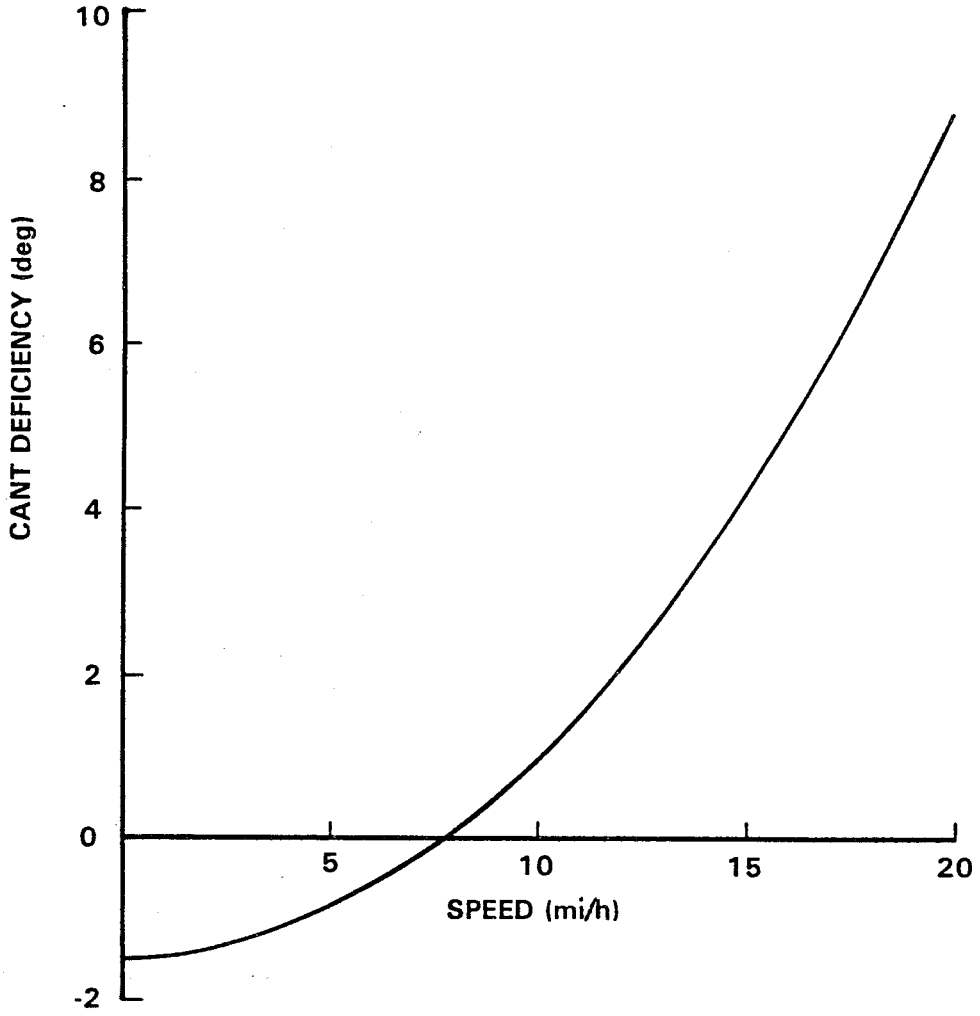

FIGURE 4.5. CANT DEFICIENCY ~ SPEED (1.5 INCH SUPERELEVATION).

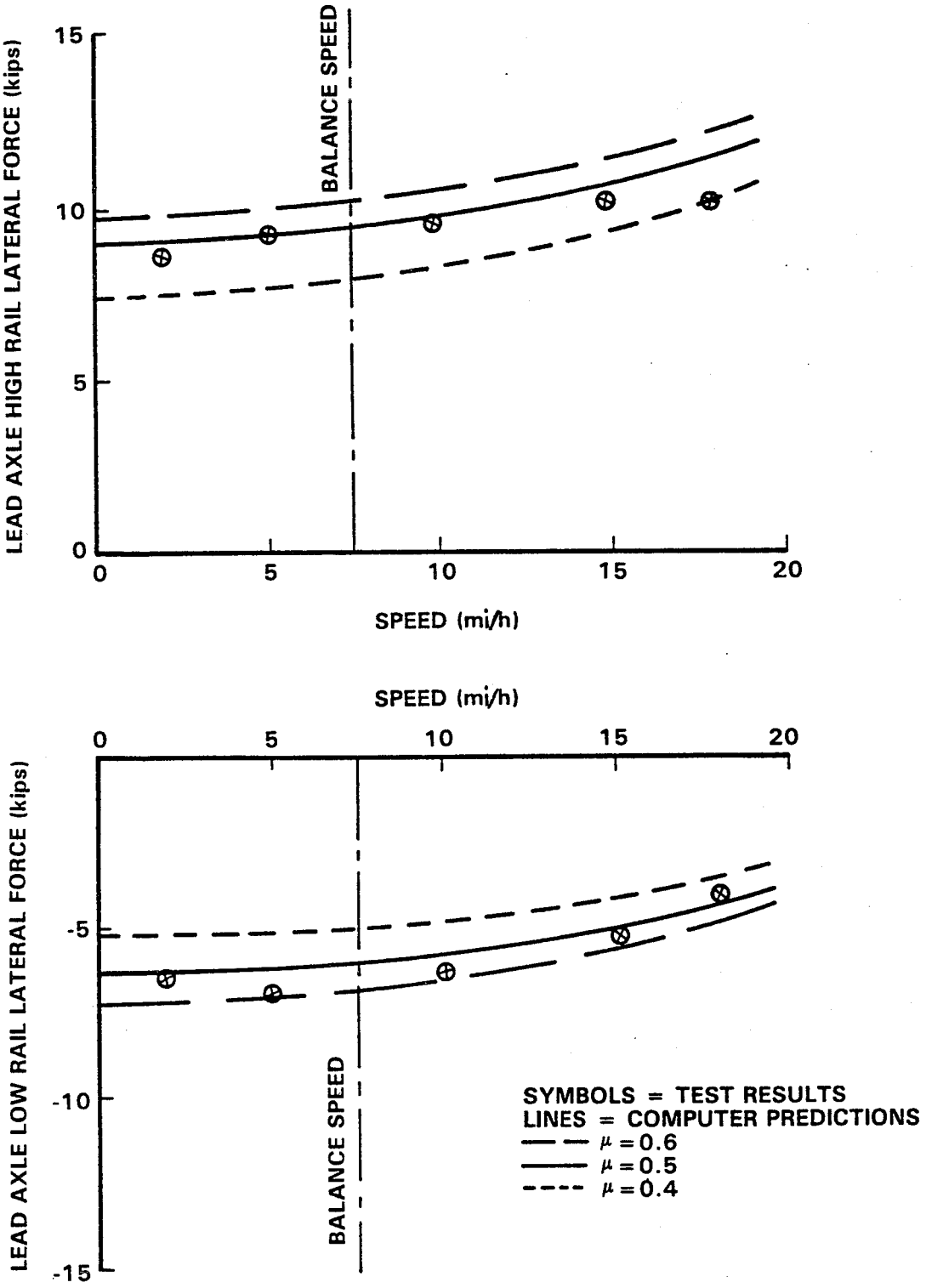

FIGURE 4.6. LEAD AXLE HIGH AND LOW RAIL LATERAL FORCE ~ SPEED (WITHOUT RESTRAINING RAIL).

The lateral forces on the trailing axle wheels are shown in Figure 4.7. The forces are lower than on the lead axle and do not vary much with changing coefficient of friction. In this case, it is the low rail wheel that is in flange contact with a lateral force of approximately 5 kips at balance speed.

The predictions are in good agreement with the measured lateral forces, particularly for a wheel/rail friction coefficient of 0.5.

In Figure 4.8 the lead and trail axle yaw moments are presented. In general, there is a fairly small yaw moment on the lead axle, which is dominated by lateral forces due to the large angle of attack. The trail axle, however, has a large yaw moment and the predominant wheel rail forces are in the longitudinal direction contributing to this moment. The trail axle yaw moment increases with increasing friction coefficient.

The predictions are not in particularly good agreement with the test results. The lead axle measurements are larger in magnitude than the predictions. The trail axle measurements are of similar magnitude to the predictions but appear to show a trend with speed which is in the opposite direction. The predictions show a yaw moment which increases with speed whereas the measurements show the yaw decreasing with speed.

The yaw moments were determined by measuring primary longitudinal displacements and converting these to forces using the measured stiffness. Problems were encountered in this process, which were related to the determination of the absolute datums for the displacement measurements. These problems are described in Section 4. As a result, there must be some doubt concerning the accuracy of the yaw moment measurements and, for any future test program, an improved measurement procedure will be required.

Lead and trail axle angle-of-attack are presented in Figure 4.9. The angles-of-attack are large because of the small radius of the test curve. Changing the coefficient of friction has little effect on the predicted angle-of-attack values. This is because the truck curving attitude is controlled predominantly by the degree of track curvature and the flangeway clearance. The truck is in a regime which is known as restrained curving where both the lead axle high rail wheel and the trail axle low rail wheel are in flange contact. Lead axle angle of attack is typically -40 mrads and the trail axle angle of attack is about 8 mrads.

In Figure 4.10 results for the tractive resistance of the truck are presented. This is the additional tractive resistance that is present due to the creep forces generated during negotiation of the curve. The measured value is obtained from a mean value of the vehicle resistance in the curve at 10 mi/h from a number of tests. The mean value of the vehicle resistance on tangent track was subtracted from this in order to arrive at the

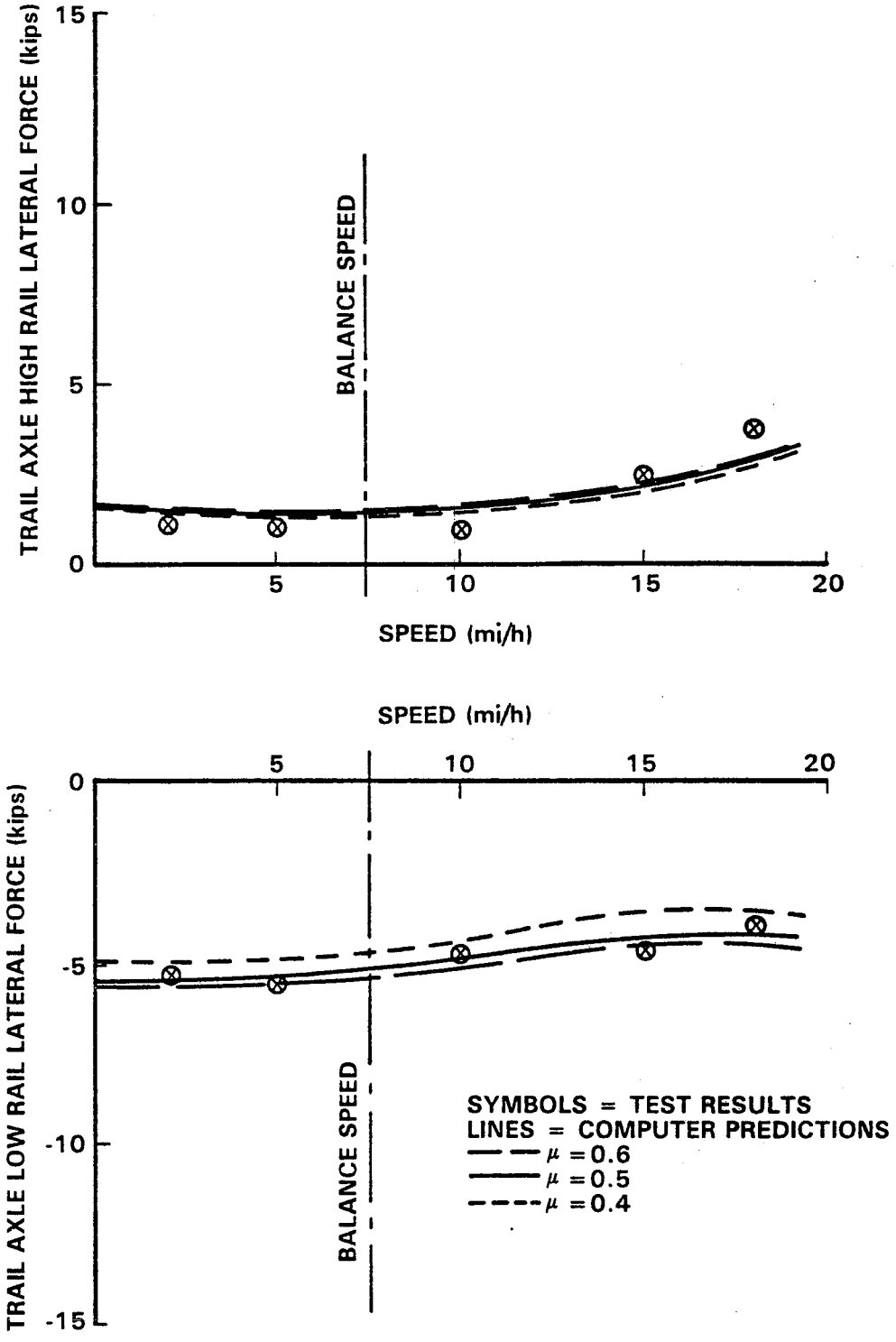

FIGURE 4.7. TRAIL AXLE HIGH AND LOW RAIL LATERAL FORCE ~ SPEED (WITHOUT RESTRAINING RAIL).

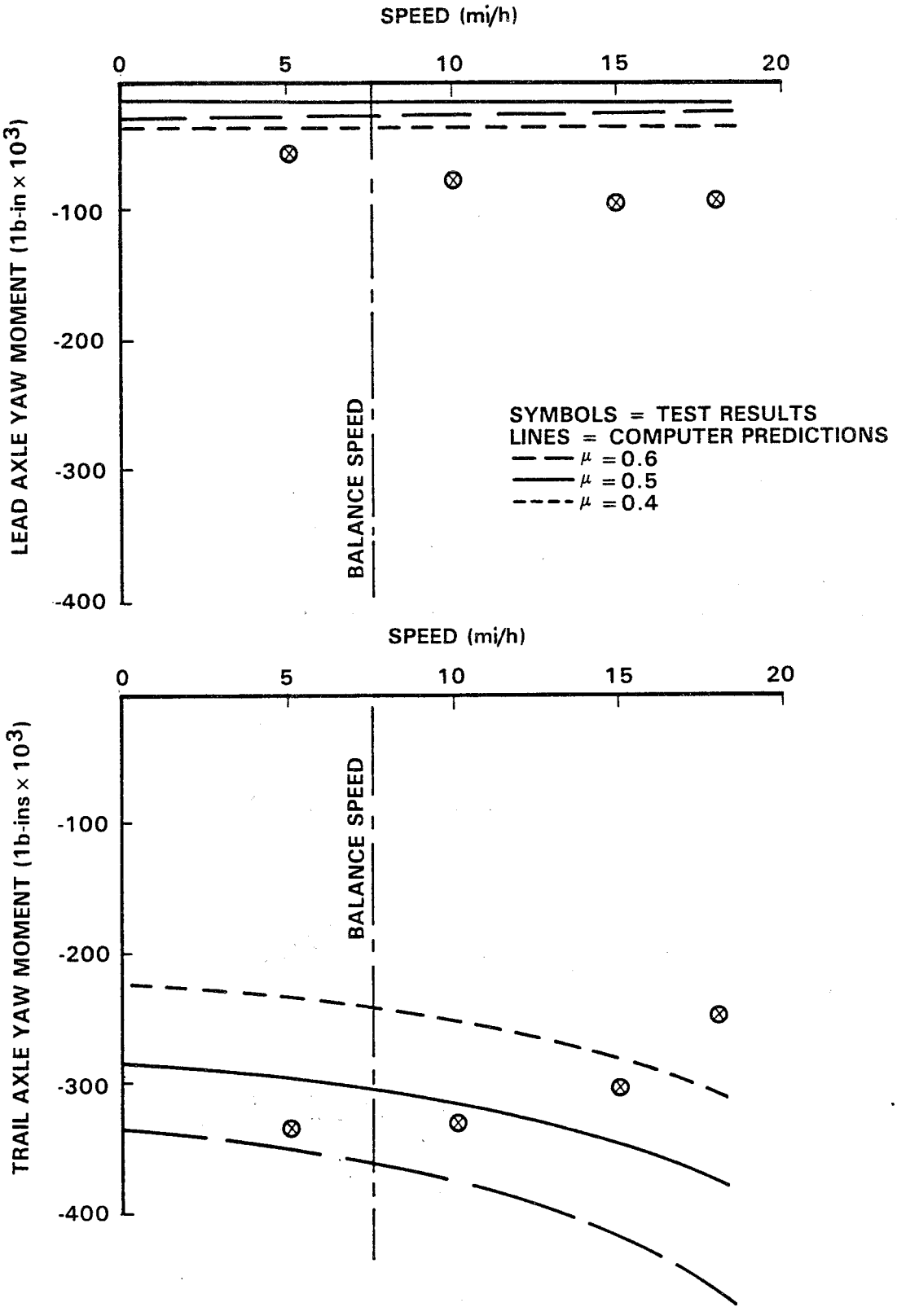

FIGURE 4.8. LEAD AND TRAIL AXLE YAW MOMENT ~ SPEED (WITHOUT RESTRAINING RAIL).

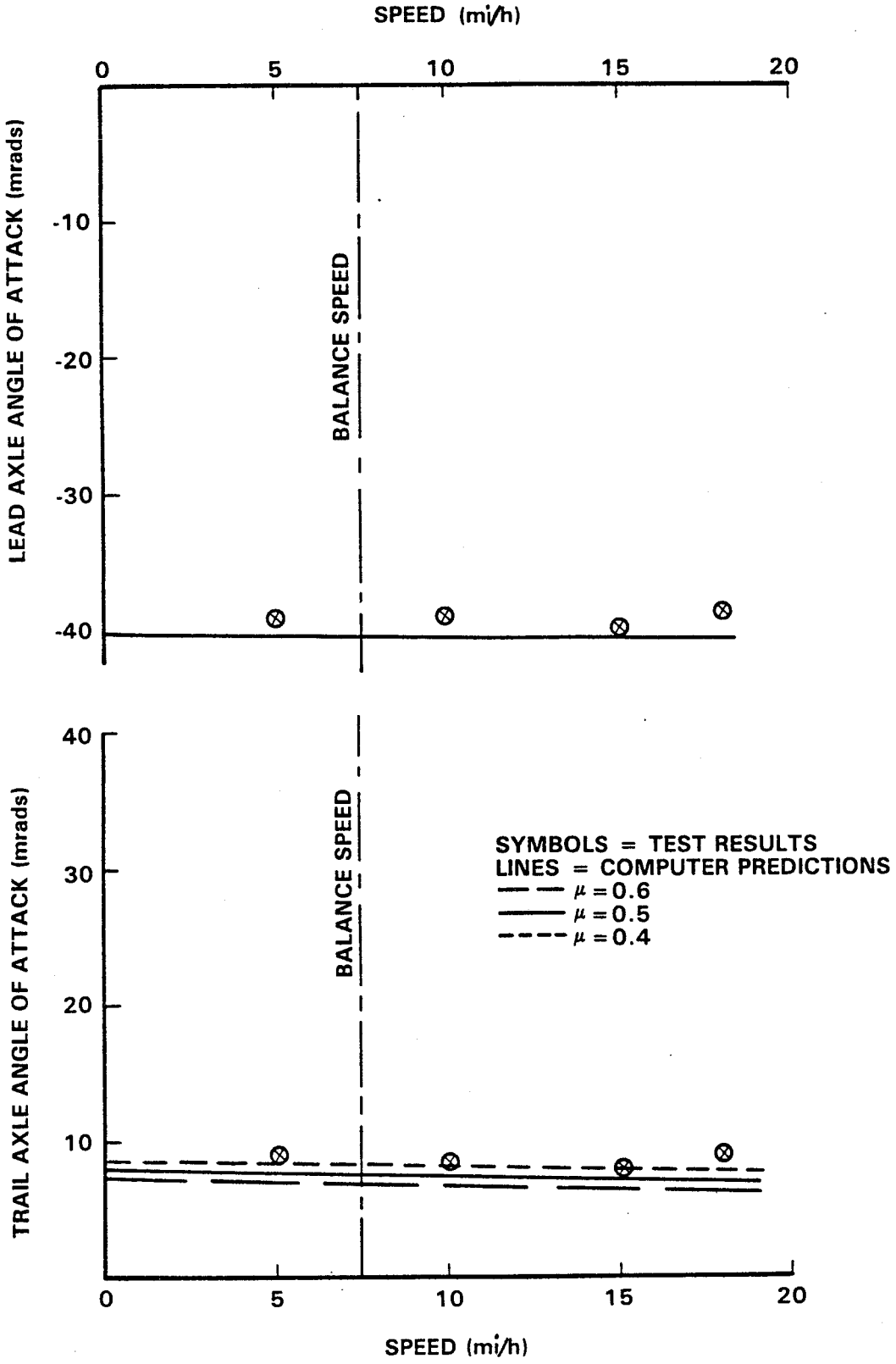

FIGURE 4.9. LEAD AND TRAIL AXLE ANGLE-OF-ATTACK ~ SPEED (WITHOUT RESTRAINING RAIL).

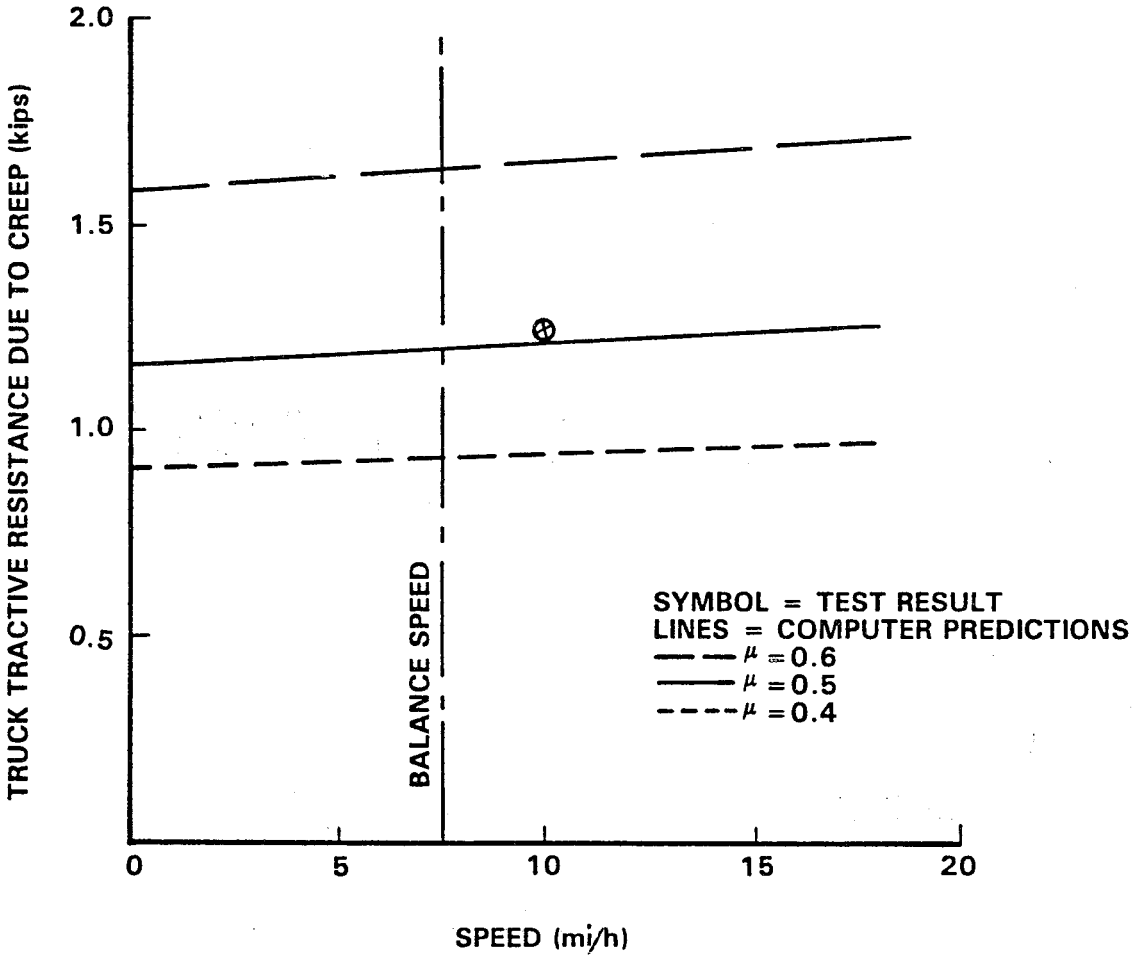

FIGURE 4.10. TRUCK TRACTIVE RESISTANCE DUE TO CREEP FORCES ~ SPEED (WITHOUT RESTRAINING RAIL).

tractive resistance due to the curve alone. Predictions are presented for wheel/rail friction coefficients of 0.4, 0.5, and 0.6. These show the resistance increasing with both friction coefficient and speed. With a friction coefficient of 0.5, the prediction gives 1.21 kips resistance at 10 mi/h compared with 1.25 kips measured. The theoretical resistance is calculated from the total work done due to creep forces at each of the contact points and the method is presented in detail by Elkins and Eickhoff.[8]

4.4 TEST RESULTS WITH RESTRAINING RAIL AND COMPARISON WITH THEORETICAL PREDICTION

With the restraining rail installed, tests were conducted over the same speed range as before, 2-18 mi/h. The same unequal vertical wheel load distribution at balance speed that had been observed during the tests without the restraining rail was obtained during this test series.

Results from the test series that had been conducted without the restraining rail seem to indicate that the friction coefficient between wheel and rail is approximately 0.5. Therefore, the predictions for the case with the restraining rail have assumed a friction coefficient of 0.5 for all wheel/rail contact points on the running rails. However, μ_{RR}, the friction coefficient at the restraining rail contact point, is varied during the analysis.

The vertical forces on the lead axle low rail wheel are shown in Figure 4.11. This is the wheel that is in flange back contact with the restraining rail and tread contact with the low rail. At the restraining rail contact there is a large lateral creepage in the plane of contact, which produces a large lateral force. Because the plane of contact is inclined at approximately 82° to the horizontal and, therefore, almost vertical. This lateral force in the plane of contact has a large vertical component. Through this mechanism, the restraining rail supports a significant proportion of the vertical load on the wheel. Figure 4.11 shows that the load supported by the restraining rail increases as the restraining rail friction coefficient is increased. In addition, the load increases moderately with increasing speed. At the same time the total vertical load on the low rail wheel is decreasing with speed due to cant deficiency. As a result, the load between the tread of the wheel and the low rail decreases with speed. The prediction suggests, that for a restraining rail friction coefficient of 0.5, this load will reach zero at approximately 16 mi/h. With a friction coefficient of 0.3 the load reaches zero at approximately 20 mi/h.

When the load between the tread of the wheel and the low rail reaches zero, the vehicle is at the point of impending flange climb. This is so because the angle of the contact plane of the restraining rail will decrease once the flange back starts to climb

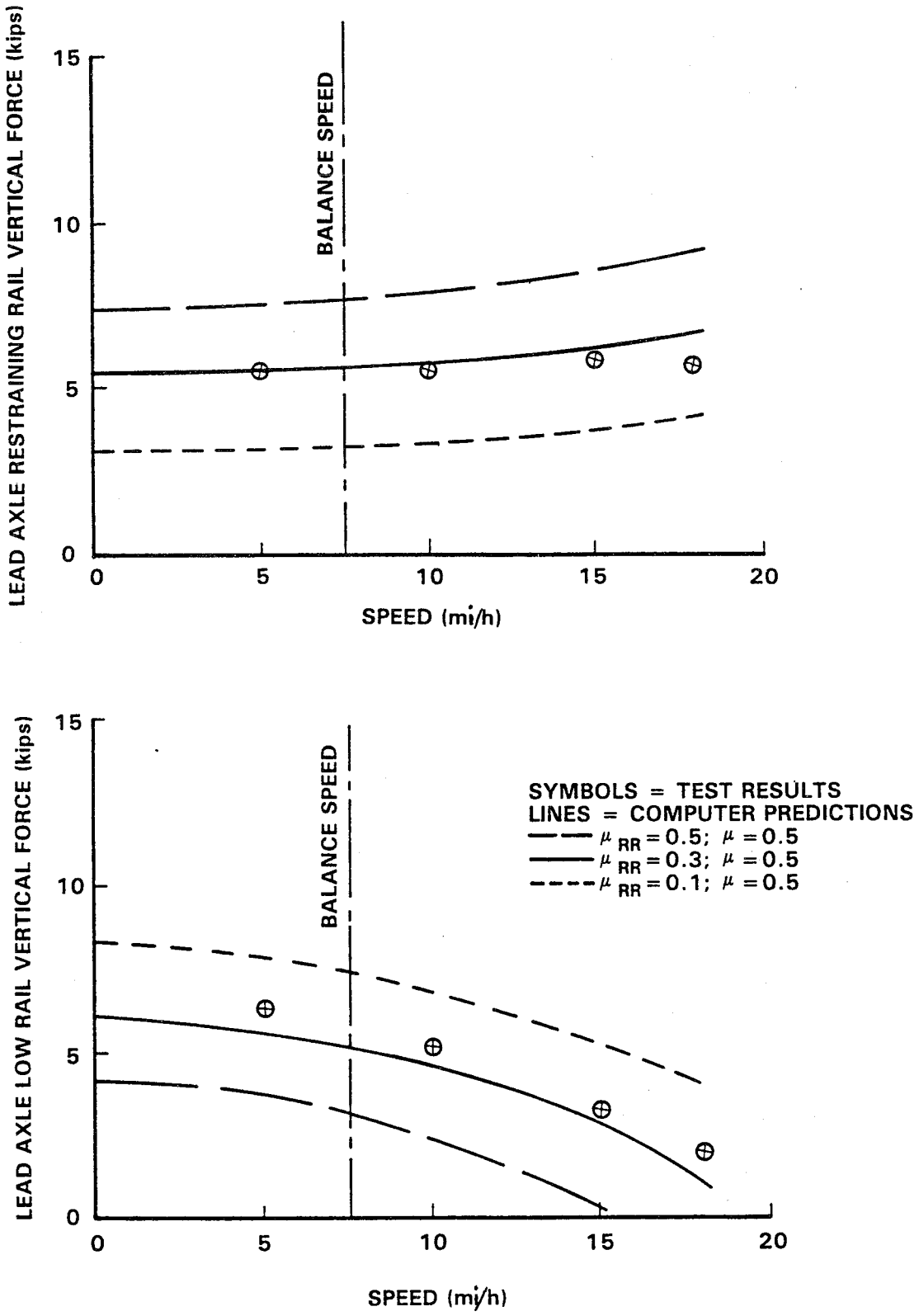

FIGURE 4.11. LEAD AXLE LOW RAIL AND RESTRAINING RAIL VERTICAL FORCE ~ SPEED (WITH RESTRAINING RAIL).

up. These flange climb speeds are surprisingly low but are confirmed by the measurements. The SOAC vehicle is particularly prone to flange climb with a restraining rail because of the uneven vertical load distribution that has been discussed previously. This leads to a reduced vertical load on the low rail wheel making it more prone to flange climb.

Lateral forces on the high and low rail are shown in Figure 4.12. The lateral force on the high rail is now in the rail and increases in magnitude with speed. The lead axle high rail is held clear of flange contact by the restraining rail contacting the flange back of the low rail wheel. Therefore, the lateral force on the high rail comes entirely from tread contact and is in a direction which tends to close the gage. The force is also independent of restraining rail friction coefficient.

On the low rail the lateral force is in the same direction as the high rail but decreases rapidly with increasing speed. In addition, the force increases with decreasing friction coefficient on the restraining rail. The lateral force tends to zero at the speed at which the vertical load has been reduced to zero.

The lateral load on the restraining rail is shown in Figure 4.13. This force increases as the restraining rail friction coefficient is decreased and also increases with speed. At balance speed, with a restraining rail friction coefficient of 0.3, the lateral force on the restraining rail is approximately 14 kips.

Trailing axle lateral forces are presented in Figure 4.14. The predictions show that these forces do not change if the restraining rail friction coefficient is varied. The high rail wheel is in tread contact and the lateral force is relatively low. The low rail wheel is in two point contact with tread and flange, and the net lateral force is approximately 6 kips at balance speed.

Figure 4.15 shows the lead and trail axle yaw moments. Variation of restraining rail friction coefficient has little effect on either of them. The results are very similar to those obtained without the restraining rail, with the trail fairly small. The measurements suffer from the same uncertainty that was discussed previously. However, they are of a similar magnitude to the predictions.

The angles-of-attack are illustrated in Figure 4.16. The predictions indicate that the lead and trail axle angles-of-attack should both have changed by approximately 3 mrads as a result of installing the restraining rail. This would give predicted values of approximately -37 mrads and 11 mrads for the lead and trail axle, respectively. This reduction is a direct result of the reduced lateral movement available to the lead axle, due to the presence of the restraining rail, which reduces the angle of truck rotation. The measurements do not seem to confirm this predicted change. It may be that the angle-of-attack measurement is not

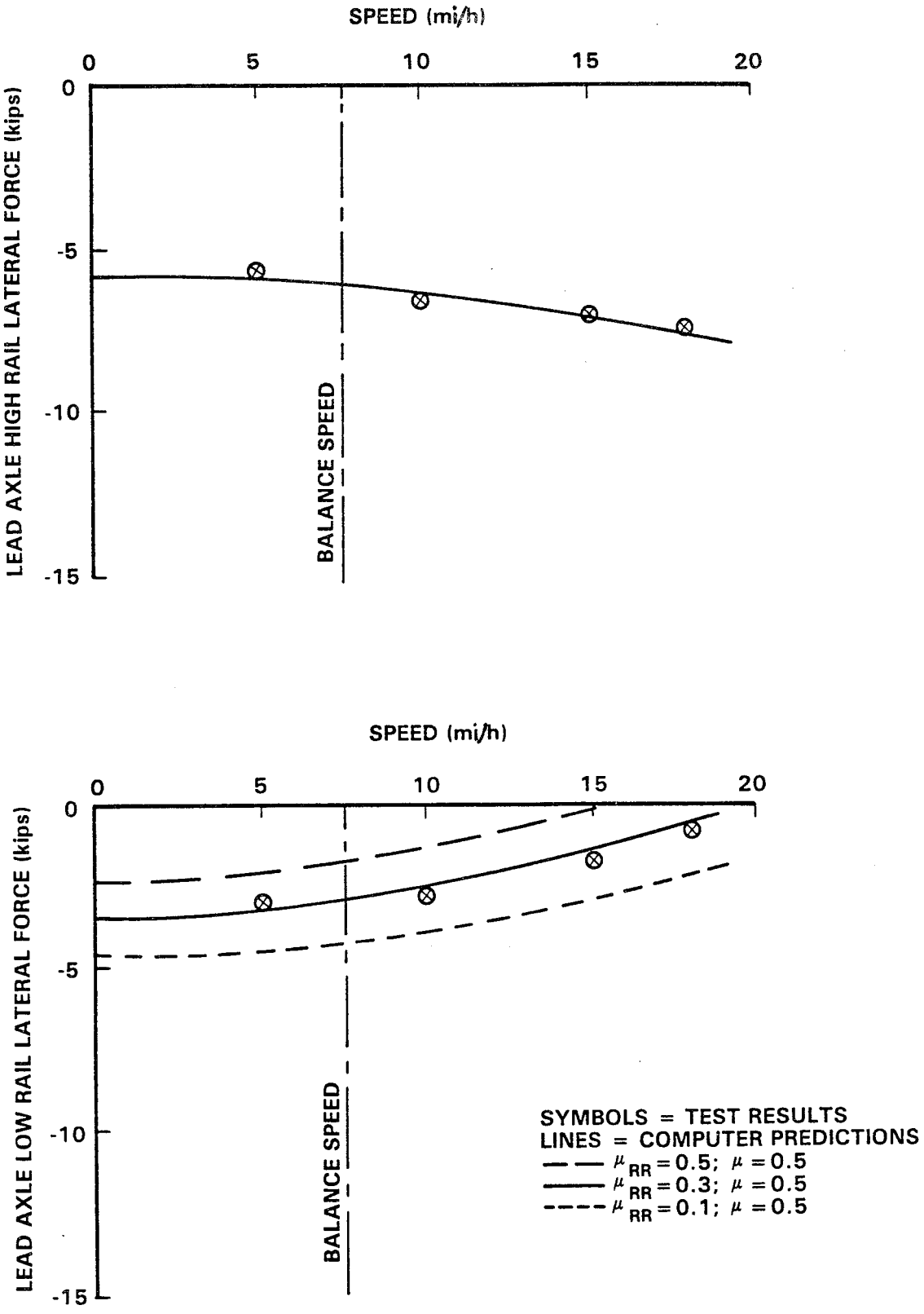

FIGURE 4.12. LEAD AXLE HIGH AND LOW RAIL LATERAL FORCE ~ SPEED (WITH RESTRAINING RAIL).

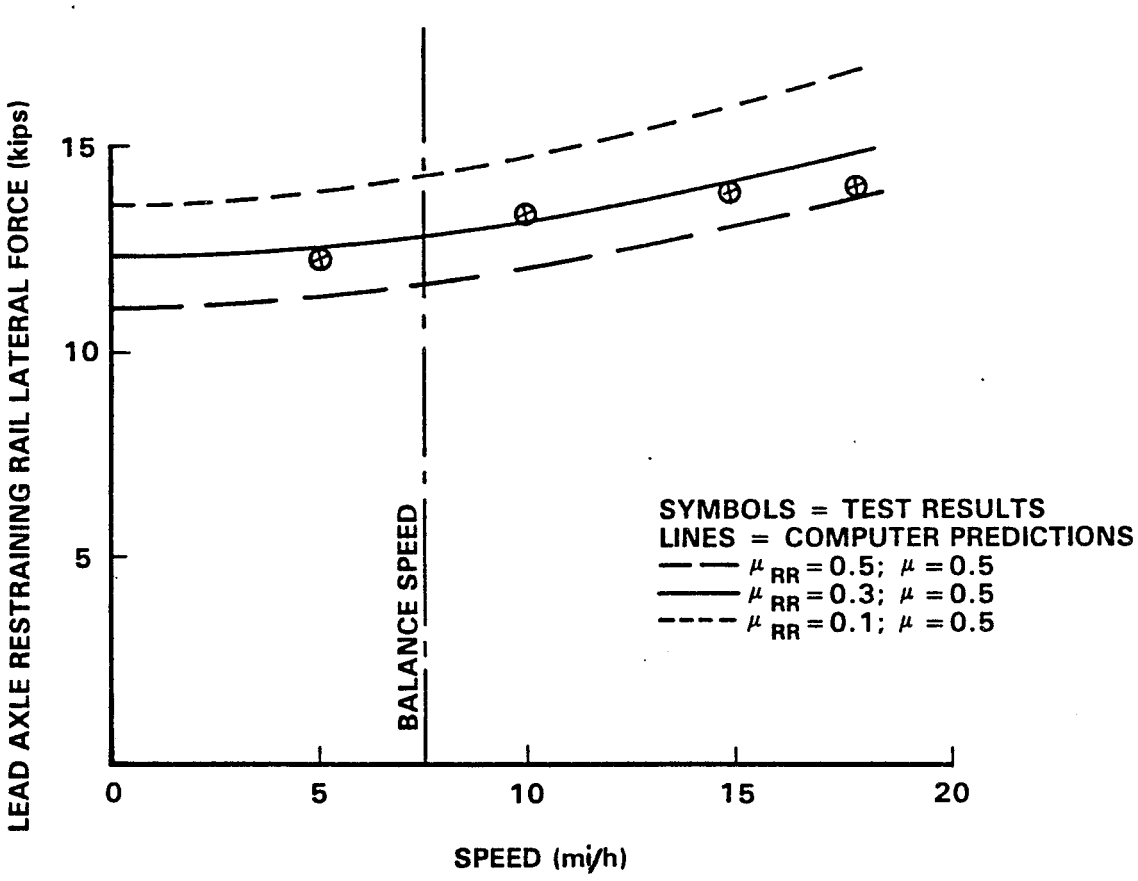

FIGURE 4.13. LEAD AXLE RESTRAINING RAIL LATERAL FORCE ~ SPEED (WITH RESTRAINING RAIL).

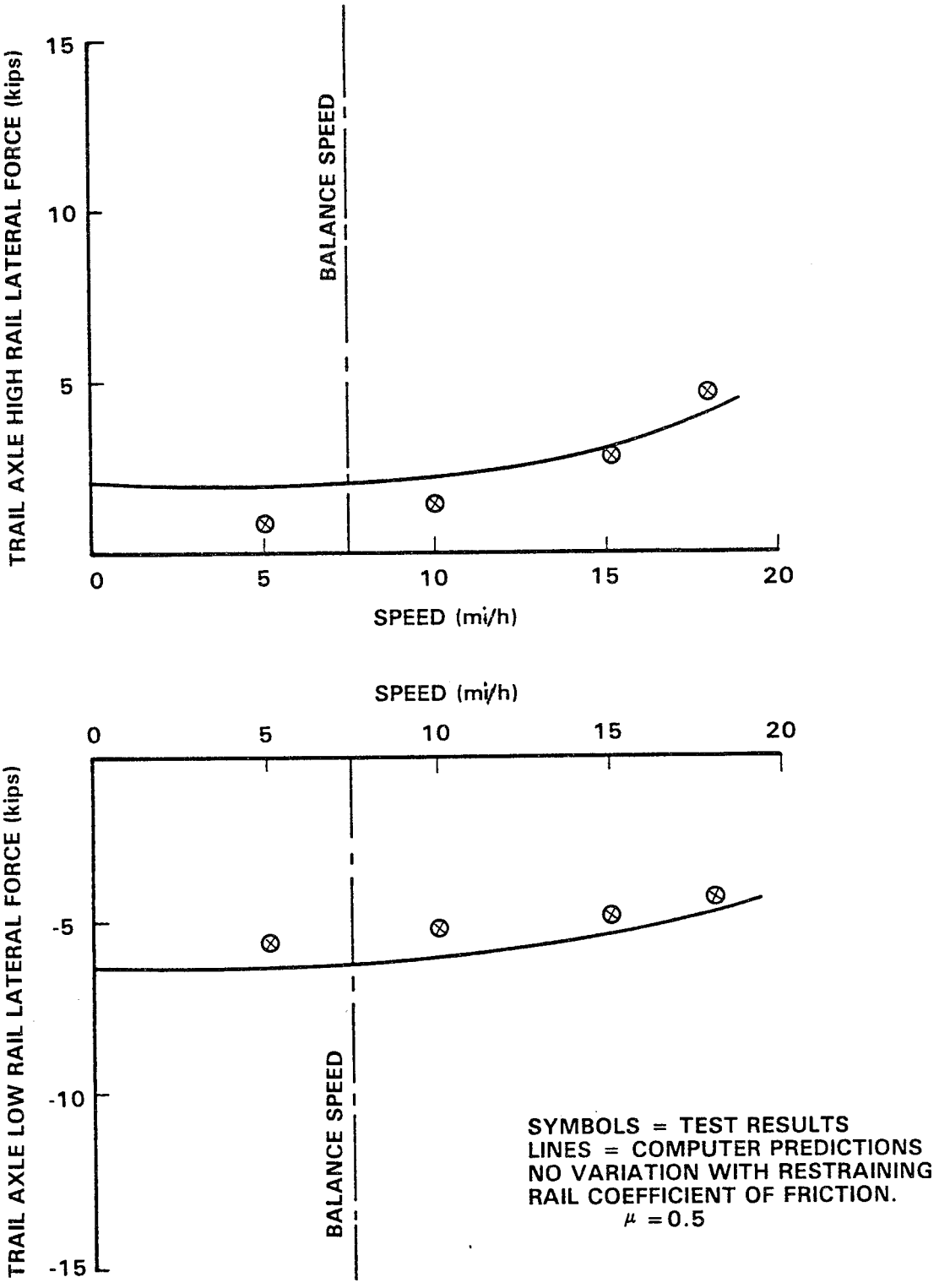

FIGURE 4.14. TRAIL AXLE HIGH AND LOW RAIL LATERAL FORCE ~ SPEED (WITH RESTRAINING RAIL).

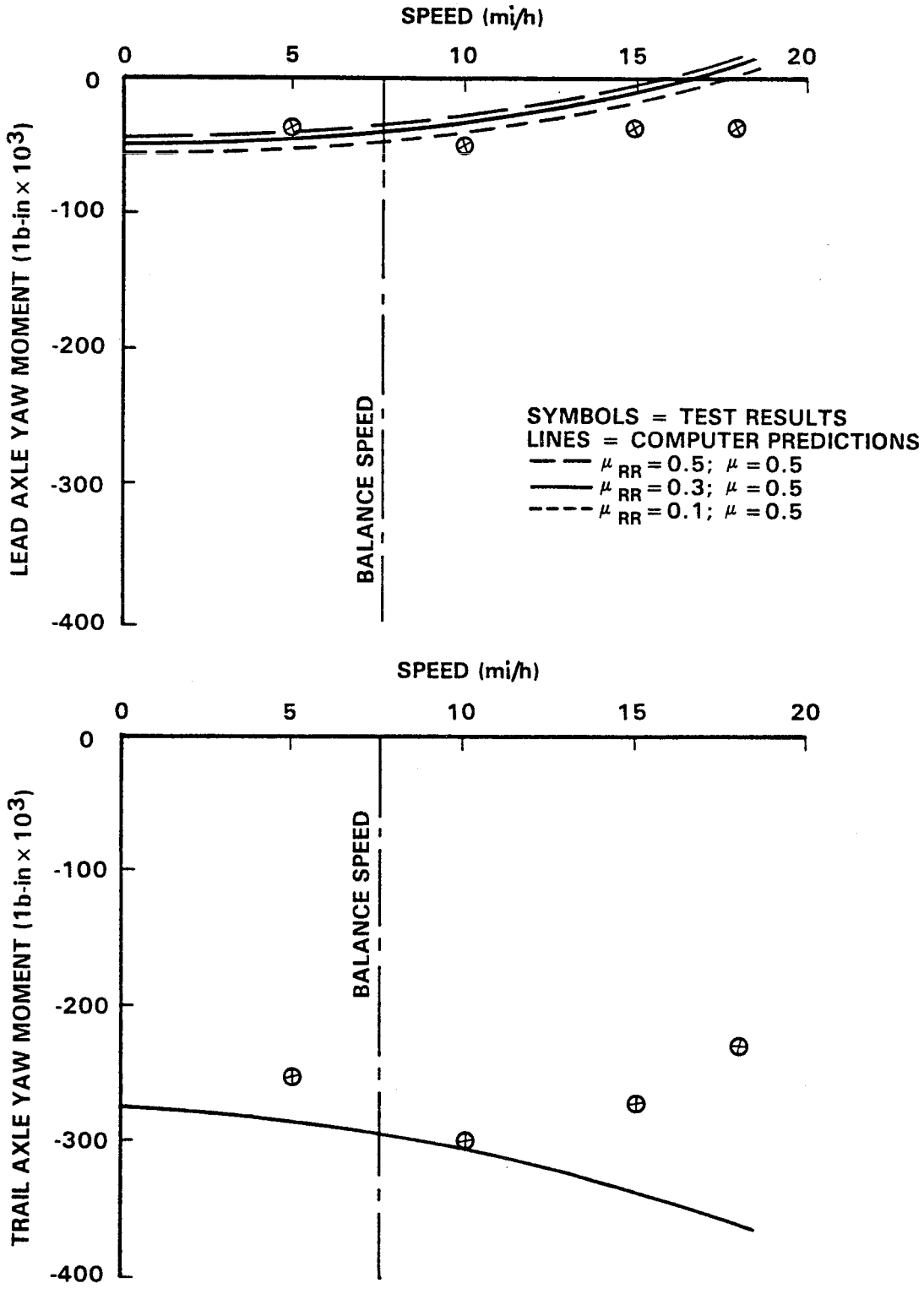

FIGURE 4.15. LEAD AND TRAIL AXLE YAW MOMENT ~ SPEED (WITH RESTRAINING RAIL).

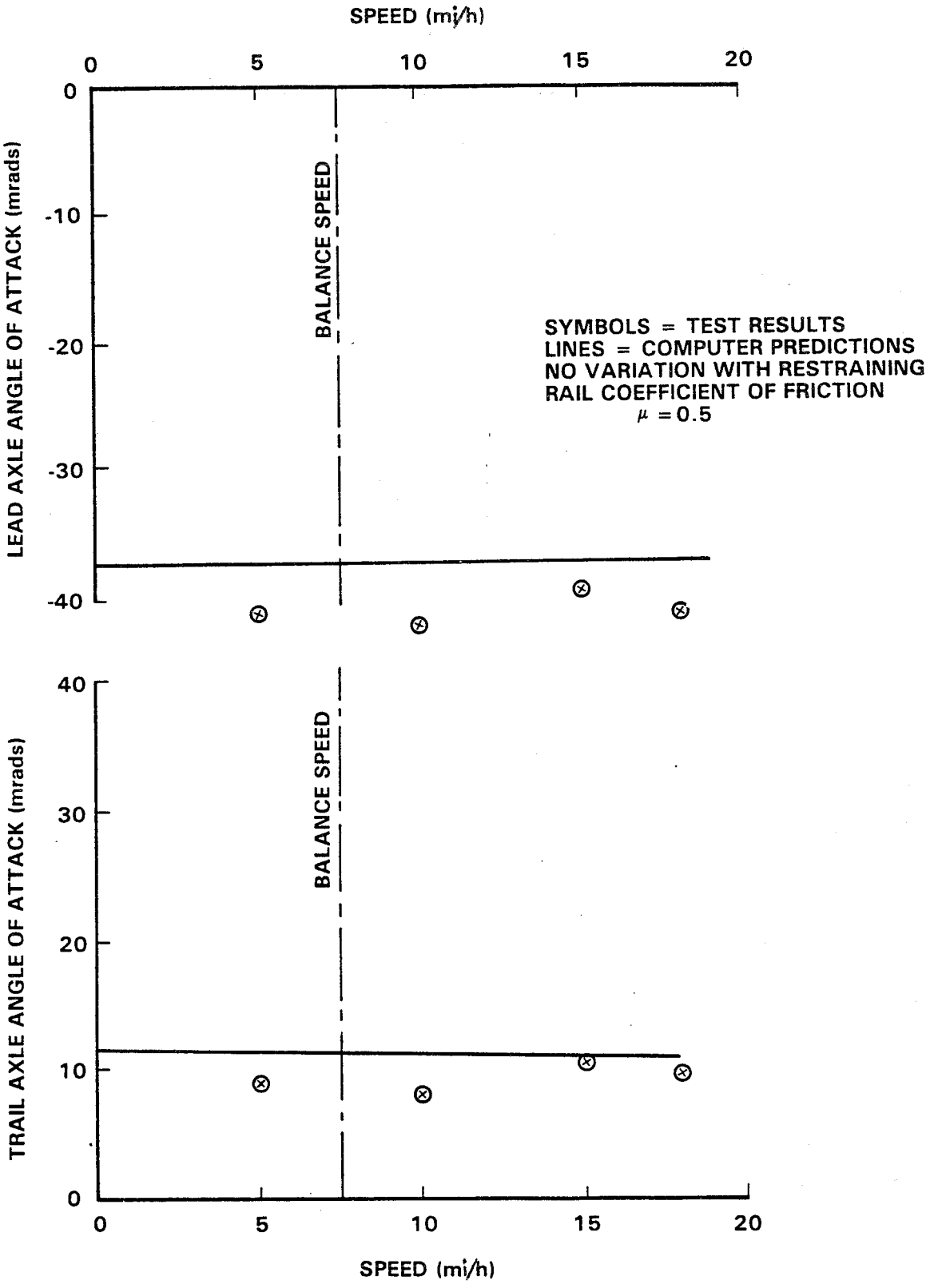

FIGURE 4.16. LEAD AND TRAIL AXLE ANGLE-OF-ATTACK ~ SPEED (WITH RESTRAINING RAIL).

sufficiently accurate to detect the change. Otherwise, one possibility would be that the restraining rail is deflected laterally by a significant amount under the applied lateral load, leading to a larger lateral travel for the lead axle.

Measured tractive resistance due to the curve was obtained in the same manner as described previously. The mean measured value for the curve at 10 mi/h was 1.77 kips. This and predicted values for varying restraining rail friction coefficient are illustrated in Figure 4.17. Increasing the friction coefficient on the restraining rail give an increased resistance. In fact, even with a friction coefficient of 0.1 the resistance is higher than was obtained without the restraining rail.

Almost all of the comparisons between measured and predicted results seem to be consistent in indicating that the friction coefficient between restraining rail and flange back was approximately 0.3, whereas the friction coefficient on the running rails was 0.5. It may be that the restraining rail contact surface was not adequately cleaned at the time the curving performance tests were made. The restraining rail had not been used for a considerable time and was very rusty prior to the tests.

It would be interesting to discover whether, given sufficient running, the restraining rail friction coefficient would increase to a value of 0.5. There does not seem to be any reason why it should not. Monitoring of rail forces during the subsequent wear test might have provided this information. However, owing to the very rapid flange back wear rates, this test was of such short duration that it had been completed before the monitoring could take place.

On the basis that the restraining rail friction coefficient was equal to 0.3, the agreement between the theoretical predictions and the measurements is remarkably good.

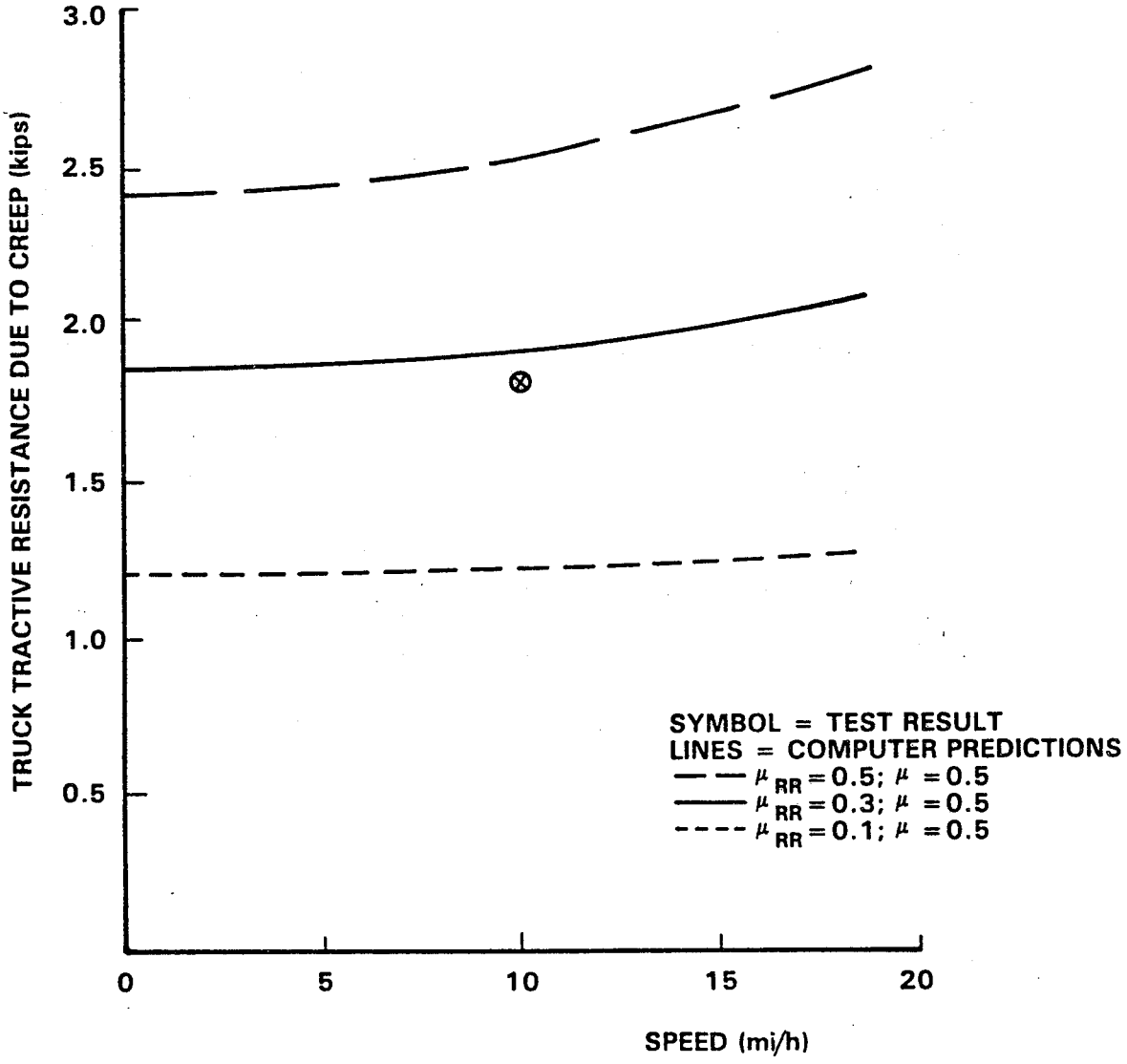

FIGURE 4.17. TRUCK TRACTIVE RESISTANCE DUE TO CREEP FORCES ~ SPEED (WITH RESTRAINING RAIL).

5.0 COMPARISON OF WEAR DATA WITH WEAR INDEX PREDICTIONS FROM MATHEMATICAL MODEL

5.1 BACKGROUND

It would be extremely valuable to be able to relate wheel and rail wear for a given set of wheel and rail metallurgy and environmental conditions to the mechanical parameters associated with the wheel/rail interaction. A number of wear index formulae have been proposed for this purpose by various authors. Some of these have been used as predictions of wheel and/or rail wear but with little full scale data available to establish their validity.

Almost all of these wear indices are dealing only with wheel flange and gage face wear and suggest that this wear is proportional to the flange force multiplied by the angle-of-attack. However, this hypothesis seems to ignore the effects of longitudinal force and creepage.

Elkins and Eickhoff[9] have derived expressions for the work done due to creep forces and showed how this is related to tractive resistance. In addition, they have suggested that the wear rates of wheels and rails may be related to the total work done due to creepages at the wheel/rail interface. It is shown that the work done is a simple addition of multipliers of the individual creep forces and their related creepages. Research is currently in progress to relate the wear of wheels and rails to this proposed wear index.

Bolton, Clayton, and McEwan[9] have described some early results from a series of small scale laboratory experiments. Figure 5.1 is reproduced from their work in the form of wear rate plotted against wear index. Their results seem to indicate two distinct regimes of wear. First, there is a regime in which no significant wear takes place until a certain threshold value of wear index is reached. Beyond this threshold, wear rate appears to increase linearly with further increases in wear index.

5.2 WHEEL WEAR TEST RESULTS AND COMPARISON WITH THEORETICAL WEAR INDEX

These tests were conducted by running in the clockwise direction around the loop at a nominal speed of 15 mi/h in two separate test series. In the first, the restraining rail was removed and in the second the restraining rail was installed. Measurements of wheel and rail wear were made after specified numbers of laps using profilometers available at the TTC. A detailed description of the tests, the measuring techniques, and the results is given in Section 3.2.

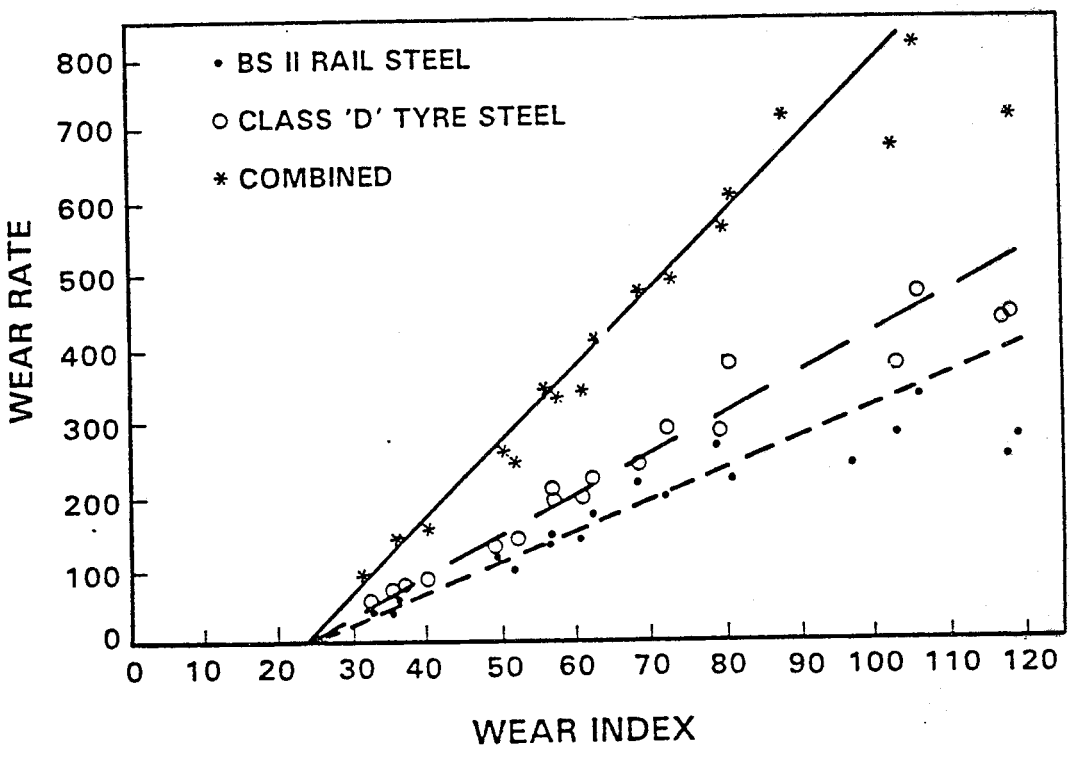

FIGURE 5.1. LABORATORY WEAR RATE/WEAR INDEX RELATIONSHIP.

Wear measurements, in terms of area loss from the profile, were made on all four wheels of the truck. When the restraining rail was present, flange back profile measurements were also made using a specially designed profilometer.

The wheel wear measurements that were made without the restraining rail determined measurable rate of wear at each of the four wheels of the truck. These results are presented in Section 3.1. The wear rates are different for each wheel. In some cases the wear is on the tread of the wheel, and in others it is on the flange. As a result the one test under fixed conditions data was available to generate a range of measured wear rates.

In a similar manner, the test case with the restraining rail should have yielded wear rate data for each wheel plus the flange back in contact with the restraining rail. However, because the wear rate on the flange back was so high, the wear test in this configuration was completed in relatively few laps. As a result, measurable wear data was not obtained for the trail axle wheels in this configuration. Therefore, the two tests, with and without restraining rail, yielded seven measured wear rates, which are tabulated in Table 5.1.

The curving model was then used to generate theoretical wear index values based on the work done at the wheel/rail interface. It was assumed for this purpose that the coefficient of friction between wheel and rail was equal to 0.5 at all the points of contact. The curving tests that were carried out without the restraining rail seemed to indicate that a value of 0.5 was obtained on the running rails. However, the test with the restraining rail present seemed to indicate that although a friction coefficient of 0.5 was present on the running rails, a value of 0.3 was more appropriate for the restraining rail. This lower value was attributed to the contact zone on the restraining rail not being adequately cleaned at the time of the test. However, it must be assumed that at some point in the wear test that followed, adequate cleaning was obtained. In this event, the friction coefficient could be expected to reach 0.5 as well. This possibility cannot be confirmed because wheel/rail forces were not monitored during the short duration of the wear test. However, for the purpose of the theoretical wear index calculation, it is assumed that value of friction coefficient of 0.5 was present on the restraining rail.

The theoretical wear index values for each wheel both with and without restraining rail are presented in Table 5.1 along with the available measured wear rates. The data are also plotted in Figure 5.2 in the form of measured wear rate against wear index. A straight line relationship between the two is assumed and indicated on the graph. This gives a reasonable fit to the data. However, there are two points, lead axle low rail wheel tread without restraining rail and lead axle high rail wheel tread with restraining rail that give measured wear rates which are twice the value indicated by the straight line characteristic. In addition, the wear

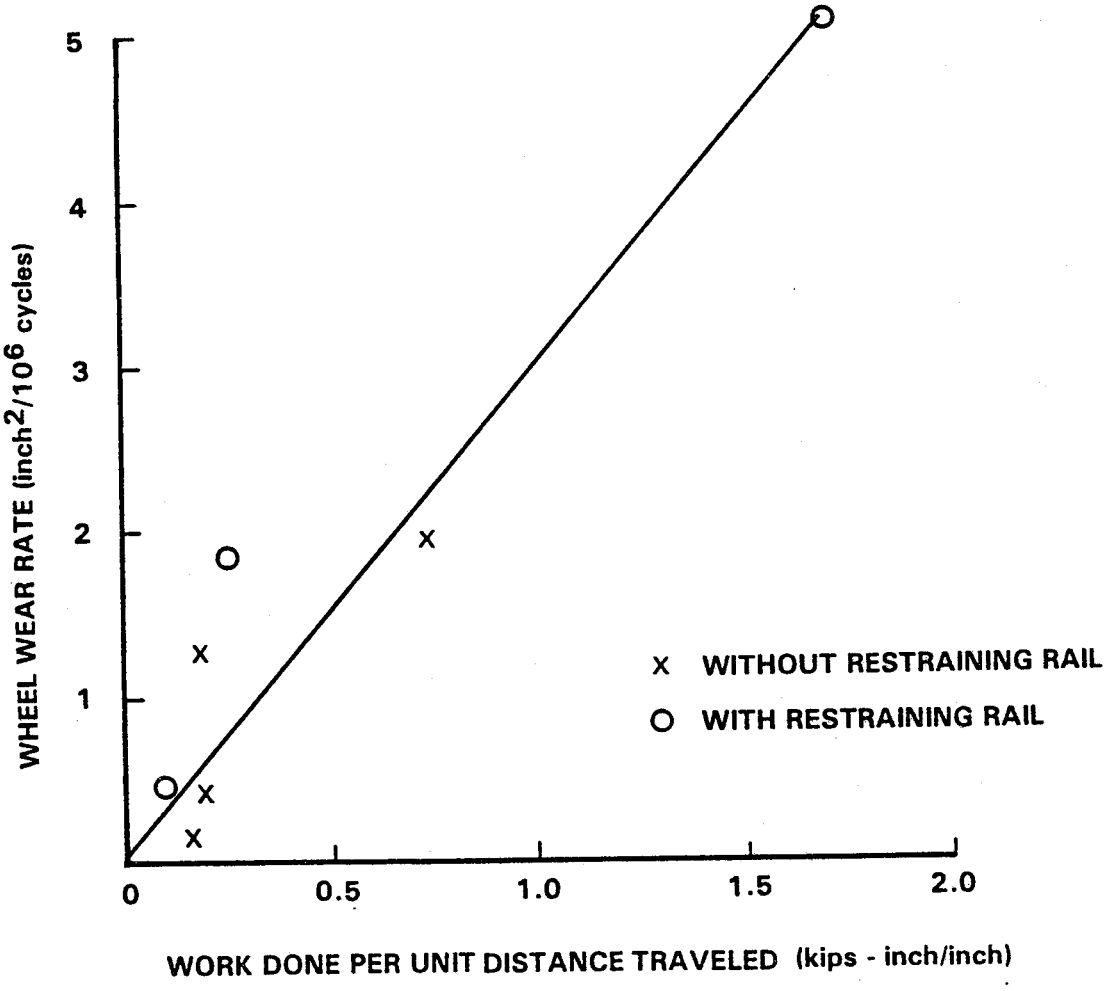

FIGURE 6.2. MEASURED WHEEL WEAR RATE ~ WORK DONE WEAR INDEX.

rate at the trail axle high rail wheel tread is only a third of the straight line value.

TABLE 5.1. THEORETICAL WHEEL WEAR INDEX VALUES.

Wheel Contact Point Point	With or Without Restraining Rail	Theoretical Wear Index (Kip-in/in)	Measured Wear Rate ($in^2/10^6$) Cycles
Lead Axle High Rail Wheel Flange	Without	0.73	1.92
Lead Axle Low Rail Wheel Tread	Without	0.18	1.25
Trail Axle High Rail Wheel Tread	Without	0.16	0.13
Trail Axle Low Rail Wheel Tread	Without	0.19	0.39
Lead Axle High Rail Tread	With	0.25	1.84
Lead Axle Low Rail Tread	With	0.085	1.08
Lead Axle Low Rail Wheel Flange Back	With	1.71	5.08
Trail Axle High Rail Wheel Tread	With	0.17	----
Trail Axle Low Rail Wheel Flange	With	0.23	----

This is the first attempt, as far as the authors are aware, to take full scale wheel wear data from a number of different wheels in a truck, with contacts on flange front, flange back, and tread, and construct a wear rate against wear index characteristic. It was also the first time that the wheel and rail profilometers and the supporting computer software at the TTC had been used to produce measured area losses in an experiment. In view of this, the characteristic, which is shown in Figure 6.2, is a good result from a first attempt to establish such a characteristic.

5.3 RAIL WEAR TEST RESULTS AND COMPARISON WITH THEORETICAL WEAR INDEX

As well as measuring the wear rates that occurred on the wheels, wear of the rails was also monitored. However, the rails are exposed to fewer wear cycles than the wheels. For one lap of the Tight Turn Loop each wheel rotates through approximately 120 revolutions and, therefore, a point on the circumference of a wheel experiences 120 wear cycles per lap. During one lap of the vehicle, a point on the rail experiences 4 wheel passes. However, the gate faces of the high and low rail are only contacted by 2 of these axles as is the restraining rail when it is present. Without the restraining rail, the head of the high rail is only contacted heavily by the trail axle and the head of the low rail by the lead axle. With the restraining rail, the head of the high rail experiences significant wear from both lead and trail axle wheels.

Therefore, in general, a point on the rail experiences 2 wear cycles per lap compared with 120 wear cycles for a point on the wheel. For this reason, given similar metallurgy for wheel and rail steel, one would expect wear rates on the rails that were only 0.107 of the wheel wear rates. During the course of the wear test, total area losses of approximately 0.1 square inches on the flange and 0.05 square inches on the tread were measured. Whereas, for the rail only, 0.01 square inches were measured, and this is of the same order as the likely accuracy of the profilometer and computer software.

Theoretical wear indices for head and gage face of each running rail and the guard face of the restraining rail were calculated from the curving model and are presented in Table 5.2. Also presented are measured rail wear rates.

TABLE 5.2. THEORETICAL WEAR INDICES FOR HEAD AND GAGE FACE.

Rail Contact Point	With or Without Restraining Rail	Theoretical Wear Index (Kip-in/in)	Measured Wear Rate ($in^2/10^6$) Cycles
High Rail Gage Face	Without	0.73	8.1
High Rail Head	Without	0.16	----
Low Rail Gage Face	Without	0.19	----
Low Rail Head	Without	0.18	3.6
High Rail Head	With	0.42	----
Low Rail Gage Face	With	0.23	----
Low Rail Head	With	0.085	----
Restraining Rail Guard Face	With	1.71	----

Measured rail wear data was obtained for the high rail gage face and low head without the restraining rail. With the restraining rail present only a small number of laps was completed because of the high rate of wear on the flange back. As a result, there is rail wear data only for the high rail head. However, this is based on only a single measurement and gives a much higher rate than would be expected. It was not possible to detect a measurable amount of wear on the restraining rail even though this contact point has the highest wear index and would, therefore, be expected to have the highest wear rate.

The two measured results that were obtained for the case without restraining rail are presented, plotted against theoretical wear indices, in Figure 5.3. A nominal straight line characteristic is drawn, which has a much greater slope than for the wheel wear data--approximately four times the slope.

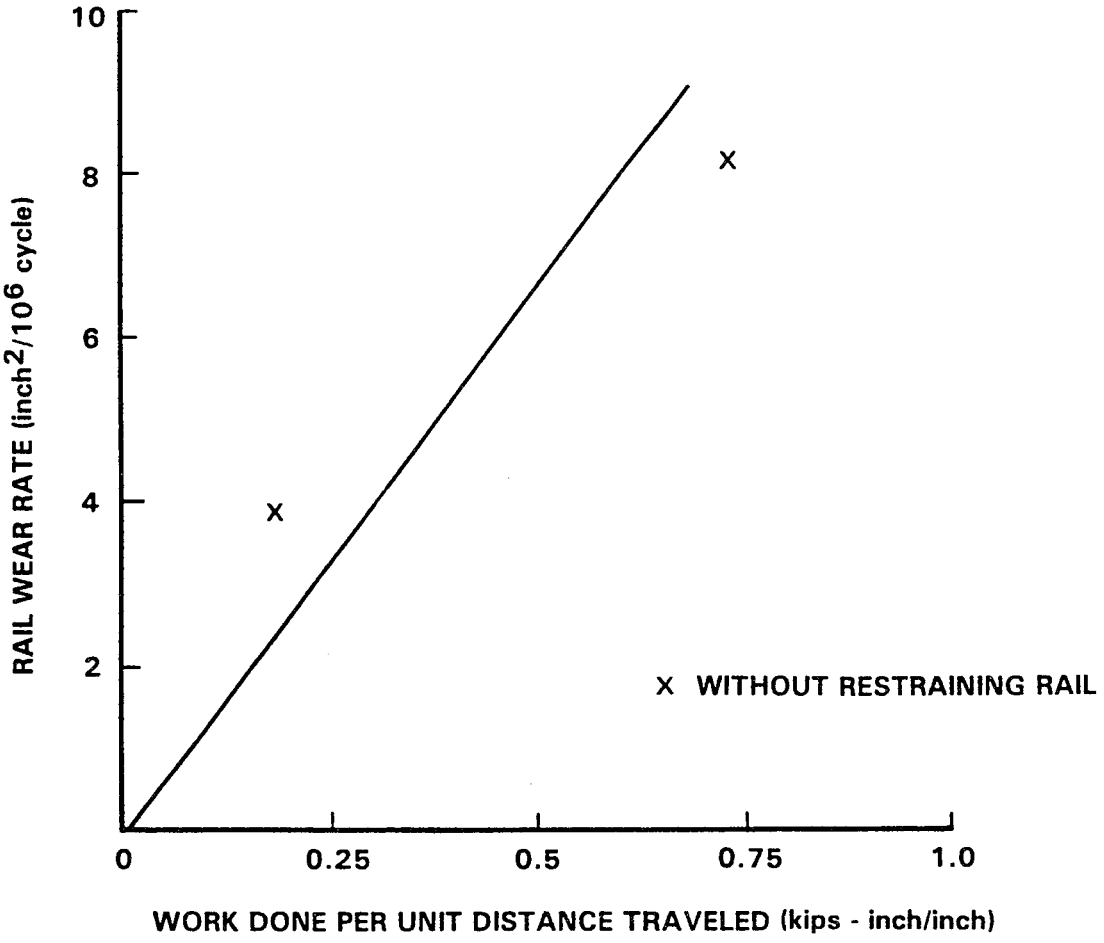

FIGURE 6.3. MEASURED RAIL WEAR RATE ~ WORK DONE WEAR INDEX.

Previous laboratory data for wheel and rail wear rates,[9] as shown in Figure 5.1, indicated wear rates for wheel and rail that were very similar for the particular metallurgies in that experiment. The reason for the much higher rail wear rates in the current experiment is not known at this time.

6.0 CONCLUSIONS

Measurements of the curving behavior of the SOAC vehicle on the Tight Turn Loop have been in good agreement with theoretical predictions from a mathematical curving model, both with and without a restraining rail. Rail force measurements using strain-gaged rails are in particularly good agreement, surprising even the authors by the degree of correlation that is obtained.

The measurements of primary suspension longitudinal displacement, which were used to determine primary suspension yaw moment, were less satisfactory and some means for establishing an accurate datum needs to be determined for future tests.

The SOAC vehicle has a very significant unequal vertical wheel load distribution while negotiating curves even at balance speed. This is seen as a higher load on diagonally opposite wheels in the truck. This has a significant effect upon the vehicle's propensity for derailment. The vehicle being less likely to experience a wheel climb derailment of the lead axle wheel at the high rail but more likely to experience a wheel climb of the lead axle wheel at the low rail, which is in contact with the restraining rail.

The lateral force on the restraining rail is larger than the lateral force on the high rail without the restraining rail. This force is in effect the flange force on the high rail wheel, because the wheel is at the point where virtually zero load is supported by the tread and the contact plane on the flange is at approximately 60° to the horizontal. It is interesting to note that a reduction of the friction coefficient on the restraining rail through lubrication would increase the lateral force on the restraining rail.

The results from this experiment and the predictions from the mathematical model indicate a real risk of the low rail wheel climbing onto the restraining rail above a certain speed. This would not be likely to lead to a derailment because flange contact of the outer wheel with the high rail would prevent further lateral travel of the wheelset. However, this situation is not one that should be allowed to occur in service. It is interesting to note that restraining rails are used in some cases to prevent derailment on tight curves. It would seem, from this experiment, that they may cause a situation where wheel climb of the restraining rail is a real possibility.

The measured wheel wear data has permitted an initial estimate to be made of the relationship between wheel wear rate and a theoretical wear index. This will permit estimates of likely wheel wear rates for other vehicles from a knowledge of their suspension parameters and the track geometry of the route over which they run.

Much lower wear rates were expected and occurred on the rails during this experiment. As a result, rail wear rates have not been established with the same degree of confidence as the wheel wear rates. Because of the lower wear rates that occur on the rail during normal operation on the Tight Turn Loop, it would seem that more accurate techniques for measuring rail wear may be needed in any future tests.

The 1/3 octave band sound pressure levels containing the objectional 'screech' sounds showed remarkable repeatability for subsequent runs round the loop by the SOAC car. The band levels also showed very high variations of band level effected by apparently small variations in track geometry.

The Tight Turn Loop has been found to be an excellent site for this form of testing because it provided a dedicated facility in which important parameters could be controlled. The closed loop enabled a steady-state curving mode to be achieved, and the ability to stop the test at any time to observe and check progress was a key feature in the success of this experiment.

7.0 RECOMMENDATIONS

The recommendations can be divided into two groups, those pertaining to the mathematical model, and those pertaining to improvements of experimental technique and future Tight Turn Loop experiments.

7.1 MATHEMATICAL MODEL

The steady-state curving mathematical model should be used to investigate alternative restraining rail geometry. It seems unlikely that the geometry tested on the Tight Turn Loop is the optimum. This would be a cost effective means of obtaining a theoretically improved system before track testing with modified hardware is begun.

The current model is limited to the three point contact situation with restraining rail of:

a. Restraining rail with low wheel flange back.
b. Low wheel tread with low rail top surface.
c. High wheel tread with high rail top surface.

However, the more general case, which occurs in service, includes the 4th contact which occurs following significant flange back wear:

d. High wheel flange with high rail gage face.

The mathematical model should be expanded to include this situation.

7.2 EXPERIMENTAL TECHNIQUE AND FUTURE TESTING

Any future tests should employ carefully controlled calibration of the rails with particular attention to the exact manner in which they are loaded. This should improve the rail load data over that achieved which had an error of + or - 5%.

A satisfactory method of obtaining a zero level datum for truck deflections, on a daily basis, must be developed. The values obtainable at the end of a coast to a stop, on tangent track look promising.

Future tests should include acoustic testing relating to particular wheels in a truck. Good identification with position of the car on the track and to other recorded parameters is essential.

Isolation of the cause of the dramatic drop of certain 1/3 octave band levels with track position should be found because it may indicate ways of drastically reducing wheel noise by fairly minor modification to wheels or track.

Future tests could establish the relationship between the rail wear index and rail wear. This could be done either by increasing the number of wheels on the loop by the addition of other vehicles, or possibly by an improvement in the measurement and analysis of rail data. The additional parameter of lubricated track could be investigated.

The SOAC car would be a suitable vehicle for future testing because its suspension is representative of many transit vehicles. The test just performed has given valuable understanding of the SOAC on the Tight Turn Loop, providing a good foundation on which to build. However, the SOAC trucks, as they are presently built, do not have the capability of adjusting axle alignment in order to operate at differing angle-of-attack. A truck with this feature would compensate for the fact that the Tight Turn Loop has a constant radius of curvature.

In summary, based on the success and progress of this experiment, it is recommended that this work be continued, justified by the development of a mathematical model which would address one of the fundamental wear problems of the industry.

REFERENCES

1 Elkins, J.A., and R.J. Gostling, "A General Quasi-Static Curving Theory for Railway Vehicles," Proceedings from 5th VSD-2nd IUTAM Symposium, Vienna, September 1977.

2 Elkins, J.A., "Analytical Studies of Curving Forces and Hunting Stability and Related Support for WMATA Phase II Truck Test Project," UMTA Report, June 1982, to be published.

3 Elkins, J.A., and H. Weinstock, "The Effect of Two-Point Contact on the Curving Behavior of Railroad Vehicles," to be presented at the 1982 ASME Winter Annual Meeting, Phoenix, Arizona, November 1982.

4 Boocock, D., "The Steady-State Motion of Railway Vehicles on Curved Track," Journal of Mechanical Engineering Science, Vol. II, No. 6, 1969.

5 Newland, D., "Steering Characteristics of Bogies," The Railway Gazette, London, 1968.

6 Kalker, J.J., "On the Rolling Contact of Two Elastic Bodies in the Presence of Dry Friction," (plus table book), Doctoral thesis, Delft, 1967.

7 Gilchrist, A.O., and B.V. Brickle, "A Re-Examination of the Proneness to Derailment of a Railway Wheelset," Journal of Mechanical Engineering Science, Vol. 18, No. 3, pp. 131-141, 1976.

8 Elkins, J.A. and B.M. Eickhoff, "Advances in Nonlinear Wheel/Rail Force Prediction Methods and their Validation," Journal of Dynamic Systems, Measurements, and Control, Vol. 104, No. 2, June 1982.

9 Bolton, P.J., P. Clayton, and I.J. McEwan, "Wear of Rail and Tyre Steels Under Rolling/Sliding Conditions," presented at the ASME/ASLE Conference in San Francisco, August 1980.

APPENDIX A

TTL TRACK SURVEY

Tight Turn Loop Track Survey Data

The TTL was surveyed for curvature, gage, and crosslevel both pre- and post-test. The curvature was measured on a 20 ft nominal chord (20 ft + 0.25 in actual). Mid-chord offsets are presented for every 10 ft, commencing at 1183 + 10 ft.

Gage and crosslevel (superelevation) measurements were made at the same 10 ft intervals using the standard 'crosslevel'. The superelevation is presented with the outside rail as a positive (+) value, the gage is presented as the deviation from a nominal 56.5" gage.

Track Location		Mid-Chord Offset (20 ft Nom Chord) ins		Superelevation (1/32") Outside Rail High +Ve		Track Gage (1/32") (56.5" Nominal)	
#	Track Stn	Pre-Test	Post-Test	Pre-Test	Post-Test	Pre-Test	Post-Test
0	1183 (00)	-	-	-	-	-	-
1		4.14	4.13	17	15	-	9
2		3.84	3.95	17	17	7	8
3		3.59	3.81	11	9	6	8
4		3.54	3.60	18	15	7	10
5		3.35	3.07	26	26	4	7
6		3.75	3.80	25	26	7	10
7		3.75	3.92	11	12	8	12
8		3.86	3.74	16	16	9	12
9		4.00	4.28	23	22	7	10
10	1184 - 4'	4.12	4.08	24	26	5	8
11		4.26	4.16	19	18	7	10
12		4.00	4.08	27	26	5	9
13		4.05	4.20	25	32	10	9
14		4.05	3.92	24	23	9	11
15		3.92	3.85	19	18	6	9
16		3.95	4.06	19	19	10	12
17	Cal Zone Center	3.96	3.86	23	23	7	8
18		3.95	3.91	20	23	11	13
19		4.05	3.99	27	24	9	11
20		3.80	3.94	42	39	8	11
21	1185 + 4'	4.20	4.15	45	44	15	16
22		3.95	3.88	43	42	11	13

	Track Location	Mid-Chord Offset (20 ft Nom Chord) ins		Superelevation (1/32") Outside Rail High +Ve		Track Gage (1/32") (56.5" Nominal)	
#	Track Stn	Pre-Test	Post-Test	Pre-Test	Post-Test	Pre-Test	Post-Test
23		3.90	3.94	37	34	6	9
24		4.00	3.95	37	35	9	12
25		3.83	3.81	30	32	10	13
26		3.72	3.82	24	30	8	12
27		4.04	4.13	21	24	12	13
28		4.00	3.97	17	17	9	12
29		3.93	3.93	19	17	11	17
30		3.93	3.80	19	19	7	12
31	1186 + 0	3.86	3.99	21	22	10	13
32		3.95	3.84	23	18	10	12
33		4.09	4.09	26	24	10	13
34		3.92	4.11	13	12	5	8
35		4.09	4.00	18	18	8	10
36		4.05	4.00	22	22	10	13
37		3.82	3.93	25	26	5	7
38		4.05	4.19	17	16	6	12
39		3.68	3.72	16	15	3	8
40		3.92	3.84	21	21	9	14
41	1187 - 4'	4.04	4.06	22	22	7	12
42		4.25	4.01	11	16	8	12
43		3.95	4.05	25	24	8	11
44		3.88	3.89	24	24	2	5
45		3.95	3.95	30	29	6	9
46		3.89	3.87	34	35	3	5
47		3.88	3.92	32	33	5	5
48		3.92	4.13	37	37	9	10
49		3.85	3.94	39	39	7	8
50		4.00	3.99	46	46	5	7
51		3.96	3.97	-	50	-	11
52	1188 + 4'	3.75	3.72	50	49	8	11
53		3.92	4.01	54	54	2	5
54		3.76	3.72	56	54	12	15
55		3.82	3.90	53	53	5	9
56		4.12	4.09	55	56	11	13
57		3.86	3.81	47	48	12	12
58		4.00	4.03	46	48	7	10
59		4.09	4.10	42	41	8	11
60		3.92	3.96	39	39	8	11
61		3.97	3.97	52	49	12	13
62	1189	4.15	4.02	53	51	12	15
63		4.15	4.32	46	46	13	14
64		3.96	4.12	45	46	19	19
65		4.18	4.06	47	48	15	15
66		4.15	4.10	55	54	17	17
67		4.02	4.08	53	51	19	19
68		3.75	3.68	62	62	19	21
69		3.75	3.92	70	68	19	19
70		3.68	3.80	67	66	17	17

	Track Location	Mid-Chord Offset (20 ft Nom Chord) ins		Superelevation (1/32") Outside Rail High +Ve		Track Gage (1/32") (56.5" Nominal)	
#	Track Stn	Pre-Test	Post-Test	Pre-Test	Post-Test	Pre-Test	Post-Test
71		3.70	3.70	66	64	13	15
72	1190 - 5'	3.72	3.75	61	61	14	16
73		3.50	3.60	61	61	17	21
74		3.88	3.87	54	53	17	20
75	Between S.G Stns #1 & 2	3.92	3.87	50	50	14	23
76		4.05	4.08	49	48	18	20
77	S.G Stn #4	4.05	4.15	55	55	19	19
78		4.15	4.19	48	47	17	20
79		4.15	4.15	50	52	18	19
80		4.18	4.07	41	43	17	20
81		3.88	4.15	44	44	13	13
82		3.92	4.04	42	43	17	19
83		3.95	3.91	50	50	12	16
84		4.12	3.90	40	41	13	16
85		3.99	4.25	34	35	16	19
86		3.85	3.96	20	20	12	15
87		3.80	3.98	9	19	13	16
88		3.96	3.86	4	6	13	15
89		3.95	4.01	18	20	11	14
90		3.85	3.79	19	23	10	12
91		4.10	3.74	24	27	14	14
92		3.95	3.87	0	4	8	9
93	Frogs &	4.90	4.14	-4	-1	8	8
94	Switches	2.70	4.80	-5	-5	5	4
95		5.70	-	-	7	-	-2
96		3.65	-	-	-	-	-
97		3.85	-	4	-	5	-

APPENDIX B

TTL WHEEL/RAIL MEASUREMENT

TTL WHEEL/RAIL MEASUREMENTS

Track Location	Measurement d_2 (height)	Measurement d_3 (gap distance)
0	4.335"	1.736"
1	3.655	2.061
2	3.686	2.051
3	3.916	2.088
4	3.766	2.130
5	3.730	2.004
6	3.659	2.082
7	3.763	2.041
8	3.909	2.000
9	3.733	1.998
10	3.786	2.017
11	3.645	2.180
12	3.630	2.046
13	3.717	2.091
14	3.646	2.105
15	3.745	2.095
16	3.701	1.995
17	3.863	1.922
18	3.798	2.004
19	3.797	2.020
20	3.746	2.030
21	3.781	2.017
22	3.983	1.997
23	3.763	2.052
24	3.766	2.051
25	3.656	1.982
26	3.802	1.875
27	3.751	2.023
28	3.752	2.044
29	3.836	2.029
30	3.708	2.046
31	3.780	2.017
32	3.756	1.991
33	3.707	2.114
34	3.675	2.010
35	3.731	1.929
36	3.847	1.992
37	3.836	1.922
38	3.861	2.010
39	3.821	2.024
40	3.809	2.054
41	3.743	2.012
42	3.735	2.071
43	3.700	2.057

Track Location		Measurement d_2 (height)	Measurement d_3 (gap distance)
44		3.754	2.050
45		3.728	2.080
46		3.707	2.012
47		3.700	2.029
48		3.735	1.980
49		3.786	2.002
50		3.758	1.982
51		3.703	2.002
52		3.767	1.963
53		3.734	2.092
54		3.826	1.912
55		3.708	1.985
56		3.692	1.958
57		3.695	2.077
58		3.868	2.041
59		3.715	2.032
60		3.775	2.056
61		3.724	2.052
62		3.740	2.039
63		3.778	1.961
64		3.710	1.959
65		3.823	1.842
66		3.719	1.914
67		3.769	1.980
68		3.763	1.984
69		3.693	2.012
70		3.745	1.997
71		3.683	1.980
72		3.734	2.002
73		3.659	2.037
74	Rail Joint	4.037	1.996
75		3.702	2.057
76		3.753	1.969
77		3.751	1.955
78		3.753	1.933
79		3.726	2.008
80	Rail Joint	3.721	1.952
81		3.760	2.040
82		3.844	2.040
83		3.573	2.061
84		3.730	2.042
85		3.681	2.009
86	Rail Joint	3.744	2.022
87		3.747	1.992
88		3.698	2.036
89		3.840	2.030
90		3.728	2.135

APPENDIX C

AXLE BENDING WITH LONGITUDINAL LOAD

BENDING OF AXLE WITH LONGITUDINAL LOAD ON EITHER WHEEL

The difference between the readings of LVDT's and that of dial gages is attributed to the bending of axle with the application of longitudinal forces on either wheel.

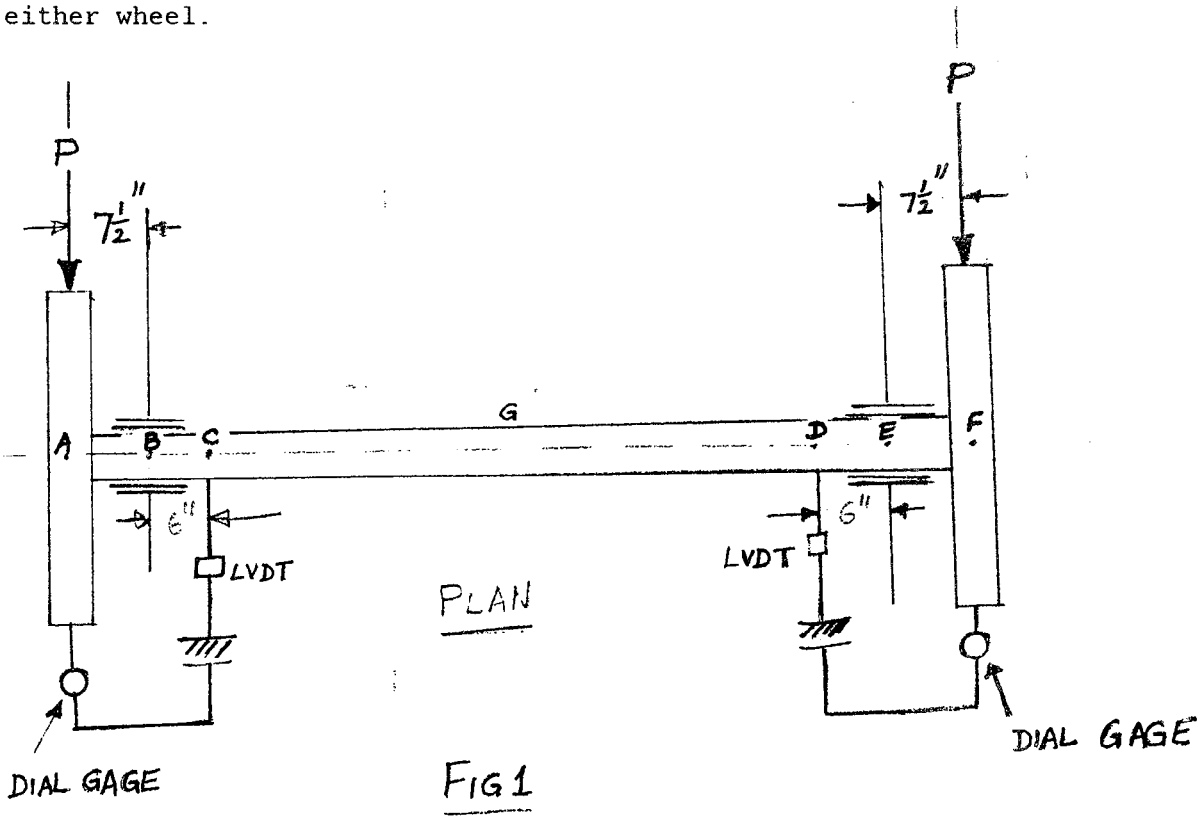

FIG 1

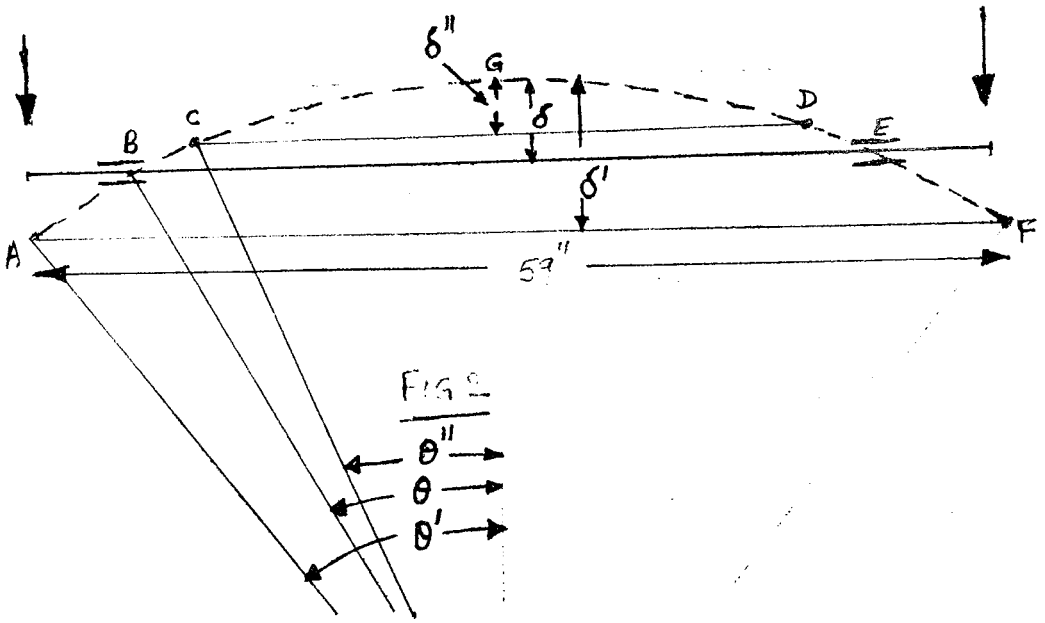

FIG 2

$$\delta'' = \frac{\rho(\theta'')^2}{2} \quad ; \quad \theta'' = \frac{32}{2 \times 25668} = 0.0006233$$

$$\delta'' = \frac{25668}{2} (0.0006233)^2 = 0.004986"$$

$$(\delta' - \delta) = 0.016952 - 0.00943 = 0.00752"$$

$$(\delta - \delta'') = 0.00943 - 0.004986 = 0.00444"$$

$$(\delta' - \delta) + (\delta - \delta'') = (\delta' - \delta'') = 0.00752 + 0.0044 = 0.012"$$

= Difference between the readings of LVDT's and that of dial gages with longitudinal load of 7000 lbs; the above difference agrees with the observed values during Longitudinal Stiffness Tests.

With the variation in longitudinal load (P), the radius of curvature (ρ) of axle varies and the corresponding deflections δ, δ', and δ'' are evaluated and presented in the following table. The agreement of values ($\delta' - \delta''$) with the observed differences between LVDT's and dial gage readings confirm that the axle of wheel set undergoes bending with longitudinal forces applied on either wheel.

Diameter of axle (d) = 5.5"

$$\text{Section Modulus } Z = \frac{\pi d^3}{32}$$

Radius of curvature of circular arc AGF in pure bending is

$$\rho = \frac{EI}{M} = \frac{E\ \pi d^4}{64\ M} \text{ --- (ANNEXURE I)}$$

EXAMPLE:

$$M = P(7.5") = 7000 \times 7.5 \text{ in-lb for } P = 7000 \text{ lbs}$$

$$\rho = \frac{30 \times 10^6 \times \pi \ (5.5)^4}{64 \times 7000 \times 7.5} = 25668 \text{ in}$$

$$\delta = \rho(1 - \cos \theta)$$

$$\theta = \frac{\ell}{2\rho} \quad ; \quad \ell = 59 - 15 = 44"$$

$$\theta = \frac{44}{2 \times 25668} = 0.0008571 \text{ radian}$$

$$\delta = \rho(1 - \cos \theta)$$

For small angles of θ, $\cos \theta = 1 - \theta^2/2$

$$\delta = \rho(1 - 1 + \frac{\theta^2}{2}) = \rho\frac{\theta^2}{2} = \frac{25668}{2} (0.0008571)^2 = 0.00943"$$

$$\delta' = \frac{\rho(\theta')^2}{2} \quad ; \quad \theta' = \frac{59}{2 \times 25668} \text{ radian} \quad (\ell = 59")$$

$$= 0.0011493 \text{ radian}$$

$$\delta' = \frac{25668}{2} (0.0011493)^2 = 0.016952"$$

ANNEXURE - I

To determine the expression for radius of curvature of wheelset axle in pure bending:

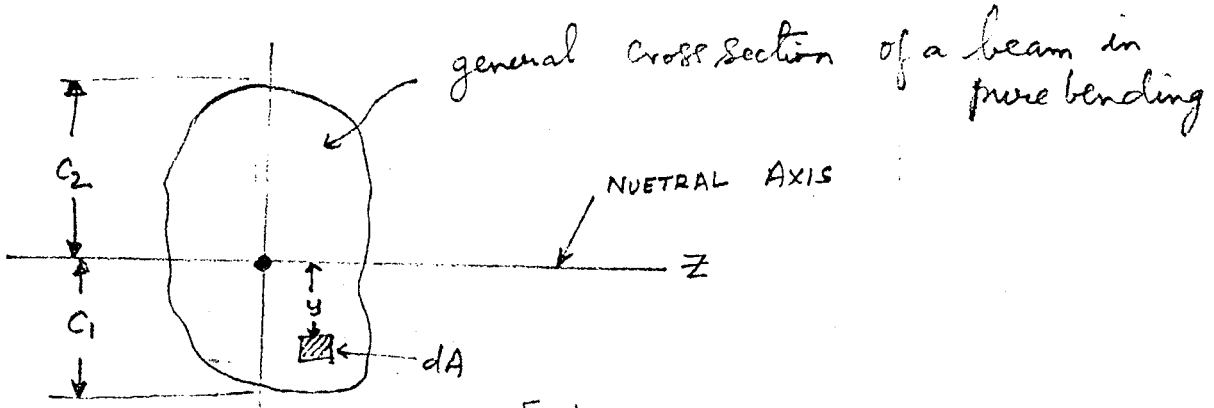

Fig 1

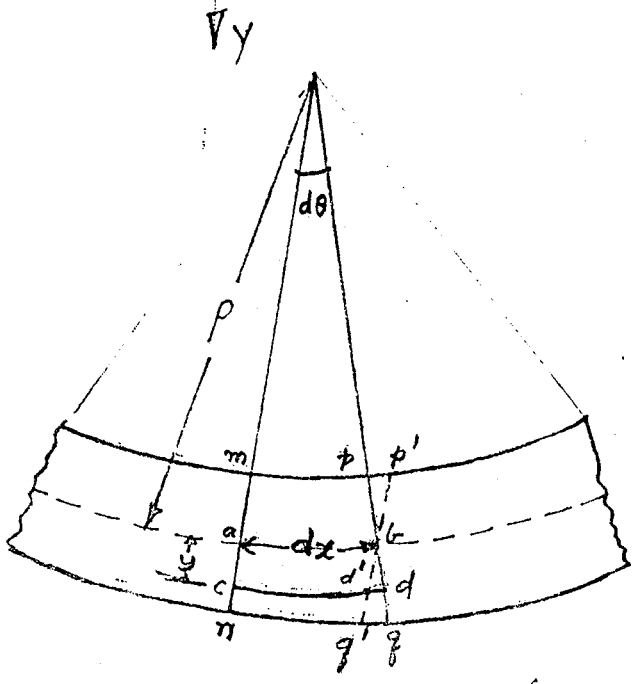

fig 2

In Figure 2, $d\theta = \frac{dx}{\rho}$ where $\frac{1}{\rho}$ is the curvature of neutral axis of beam subjected to pure bending.

In Figure 2, $ab = cd^1 = y\, d\theta\ (= dx)$

$$\text{strain } \varepsilon_x = y \frac{d\theta}{dx} = y/\rho$$

$$\sigma_x = \varepsilon_x \cdot E = \frac{E}{\rho} y$$

In Figure 1, element of force on area dA,

$$\sigma_x\, dA = \frac{E}{\rho} y\, dA$$

$$\int_A \sigma_x\, dA = \int_A \frac{E}{\rho} y\, dA = 0$$

Since $\frac{E}{\rho} \neq 0$; $\int_A y\, dA = 0$

$\int_A y\, dA = A\, y_c = 0$ where y_c = distance from the neutral axis to its centroid

Since $A \neq 0$, $\rightarrow$ $y_c = 0$

Thus the neutral axis of the cross-section passes through its centroid.

The moment of the elemental force $\sigma_x\, dA$ about the neutral axis of the section is $dM = y\, \sigma_x\, dA$. The sum of these elemental moments over the total area of the section must produce the bending moment M on that section.

Thus $M = \int_A y\, \sigma_x\, dA = \frac{E}{\rho} \int_A y^2\, dA$; $I = \int_A y^2\, dA$

$$M = \frac{EI}{\rho} \rightarrow \frac{1}{\rho} = \frac{M}{EI}$$

2. INTRODUCTION

The problem of calculating the forces that guide a railroad axle has been the subject of much study over the last century. There has been particular interest in the prediction of forces that occur during the negotiation of sharp curves because of the large forces that can be generated in this situation. In particular, there is special concern regarding the high rates of wheel and rail wear which sometimes occur and the large expenditures on maintenance and renewal which can result from this situation.

The ability to predict the forces at the wheel/rail interface and the consequent rates of wheel and rail wear is important to the understanding and possible alleviation of these problems. Separate approaches for modeling the wheel/rail interaction have been used by different investigators for predicting the wheel/rail forces that occur during curve negotiation, and for estimating the likely rates of wheel and rail wear. Insufficient experimental data has existed for complete verification of the predictions of these various models. Tests conducted by British Rail, which were reported by Elkins and Gostling in 1977 (Ref. 1), showed excellent agreement with predictions using a single point contact representation of the actual wheel and rail profiles. However, an attempt to apply the same analysis directly to evaluating the influence of wheel profile changes on the curving performance of transit trucks (Ref. 2) failed to yield agreement with the experimental observations.

Accordingly, a review of the modeling approaches in

current use was conducted, to attempt to find the reasons for this discrepancy. This showed that the single point of contact assumption was a gross mathematical approximation for the new wheel and rail profiles in current use on U.S. railroads and transit properties. For these wheel profiles, the curving behavior is dominated by wheel/rail contact at two points on the leading axle wheel at the high rail. This situation has now been modeled by one of the authors and has been shown to give much better agreement with the experimental observations (Ref. 3).

In this work, the two-point contact model is used to examine the curving behavior of a transit vehicle on a very tight curve (150 feet radius). It is common practice on some transit properties to use restraining rails on the sharper curves. The purpose of the restraining rail being to reduce gage face wear on the high rail and to prevent derailment. The use of a restraining rail also results in a two point contact situation on a single wheel. In this case, the second point of contact is on the back face of the flange rather than the front face.

The situation with a restraining rail present is examined. The forces that are generated between wheel and rail at the various points of contact are investigated and compared with those obtained without a restraining rail. The predictions are compared with measurements made during a test program performed by Boeing Services International (BSI) for the Urban Mass Transportation Administration (UMTA) on the Tight Turn Loop at the Transportation Test Center, Pueblo, Colorado.

The creepages that occur between wheel and rail on curves and the resulting forces can cause high rates of wear of both wheels and rails. In particular, wheel flange wear and high rail gage face wear has been a problem that has been experienced by a number of transit properties. This situation tends to be worse on tighter curves. For this reason, some transit properties have used restraining rails on the sharper curves. The purpose of the restraining rail being to prevent the contact between lead axle outer wheel and the gage face of the high rail which causes the wear problem. However, contact occurs instead between the flange back of the lead axle low rail wheel and the restraining rail and high rates of wear may be experienced as a result of this contact.

There are many factors that might affect the rates of wear that could occur in a particular circumstance. Among these factors are the metallurgy of the wheel and rail, the degree of surface contamination and the stresses in the material due to the forces and creepages which occur at the interface.

There has been much work carried out in this field, although most of the literature has resulted from laboratory experiments. Relatively little field work has been carried out, partly because of the high cost associated with this type of testing, but also because of the difficulty of achieving a controlled wear environment. For instance, when studying wheel wear data in service, the results can be very difficult to analyze because of changes in the environmental conditions, varying rail metallurgies and the fact that vehicles in service typically encounter a wide range of track curvatures. Similarly, rail wear data in service is difficult to analyze because of the wide variety of vehicles that might pass over the test site and variations in environmental conditions.

Use of the Tight Turn Loop for wear testing permits the elimination of most of these problems. The vehicle is running continuously on track of nominally constant curvature and, because of the high degree of curvature, measurable wear rates can be determined after relatively short periods of running. Also, because of the relatively dry climate at the test site, it is relatively easy to complete such a test under almost constant environmental conditions. For these reasons, the tight turn loop is an almost ideal site for performing carefully controlled full scale wear tests. A disadvantage might be that the curve is tighter than the majority of service curves and, therefore, it might be difficult to relate the wear data to typical service conditions.

These tests were performed on this curve, with and without the restraining rail in order to provide some basic wear data, which could be compared with a theoretical wear index provided by the mathematical curving model. Given that a relatively simple relationship could be established between the measured wear rates and this wear index, the mathematical model could then be used to predict wear rates for other more typical circumstances.

5. COMPARISON OF CURVING PERFORMANCE WITH MATHEMATICAL MODEL PREDICTIONS

5.1 Mathematical Model

The mathematical model that is used in this work is a development of the linear curving theory developed by both Boocock and Newland (Refs. 4 and 5). In their analyses, the wheel/rail geometry was represented by linear functions and contact with the flange was considered to be a limiting case. In addition, the relationship between creepage and creep force was assumed to be linear and Kalker's simple linear relationships were used. The limit of this assumption was established by determining a slip boundary beyond which slippage would occur.

The curving models were later refined to include the effect of gravitational stiffness and spin creep, which were shown to be significant with worn or profiled wheels, particularly when contact occured close to the flange root. The analyses that were conducted using the linear theory considered flange contact as a condition to be avoided and, therefore, at the limit of the analysis. However, the limitation occured for almost all vehicles on curves having a radius of smaller than 2000 ft (3^{o}), and for most vehicles on much larger radius curves, whereas the major problems of rail wear and track damage were occuring on smaller radius curves.

In Britain, the desire to have wheel profiles which would retain their initial shape throughout the period between reprofiling, led to the development of profiled wheels. These profiles were found to give only a single point of contact with the rail for most of the rail profiles, new or worn, found in practice. In order to evaluate the performance of these profiled wheels, detailed analytical models of the wheel/rail in-

teraction were developed. These models made use of Kalker's nonlinear creep theory (Ref. 6), which had become available at about this time. As a result, the nonlinearities arising from both the single point contact wheel/rail geometries and the creep force/creepage relationships, inherent in Kalker's theory, were modeled. These developments are described in the work of Gilchrist and Brickle (Ref. 7), Elkins and Gostling (Ref. 1) and Elkins and Eickhoff (Ref. 8). Experimental results for wheel/rail lateral forces and yaw moments were obtained from both model and full scale experiments, which were shown to be in good agreement with the predicted results.

Recently, a test program was carried out at the Washington Metropolitan Area Transit Authority (WMATA). As part of this test program, the effects on curving behavior of changes in wheel profile and primary suspension stiffness were examined. A comparison of the measured curving forces with predictions from the single point contact curving model was performed. This comparison showed that the theoretical predictions were unable to account for the changes in wheel/rail forces that were occurring with different wheel profiles.

The new wheel and rail profile combinations that are used in the United States and many other parts of the world have two points of contact between a single wheel and rail when the wheel is in flange contact. This is typical of the situation that occurs with the lead axle wheel in contact with the high rail on tight curves.

The typical contact geometry in this situation is shown in an end elevation of the wheel and rail (Fig. 5-1). Important parameters, which are required to calculate the creepages and resulting forces are the heights of the two points of contact below the axis of rotation of the wheelset and the angles

of the planes of contact. In addition, when the wheelset is yawed, the points of contact move from vertically below the axis of rotation of the wheelset as shown in Fig. 5-2. This was discussed by Elkins and Eickhoff in Ref. 8. The longitudinal movement is much more pronounced for the flange contact point because of the larger angle of contact.

Predictions using the two-point contact curving model were found to be in much better agreement with the measured results from the WMATA test program (Ref. 3).

When a restraining rail is used on a curve, a two point contact situation also occurs. In this case the second point of contact is between the back face of the flange and the guard face of the restraining rail (Fig. 5-3). The contact geometry resulting from this situation is of special importance. The two dimensional rail/wheel contact geometry, that is normally used when contact is on the tread and flange front, is not adequate in this circumstance and a three dimensional model is required. In particular, yaw of the wheelset results in a large longitudinal movement of the point of contact from vertically below the wheelset axis of rotation (Fig. 5-4). This movement is a nonlinear function of the wheelset angle-of-attack and is dependent on the rail and flange back relative geometry. Also dependent upon this geometry, and established in the model, is the height of the point of contact of the flange back with the restraining rail, relative to the wheel tread contact with the running rail. The angle of the contact plane to the horizontal is very large typically in the range 80^{o} - 90^{o}.

Having established the geometry of the flange back contact, the two-point contact model may be used for predicting the curving behavior in this circumstance. The equations

of motion are the same whether contact is on the front or the back face of the flange.

5.2 Vehicle and Track Parameters Used in the Curving Model

5.2.1

In order to make accurate predictions of curving behavior, it is necessary to know the actual values of a number of the vehicle and track parameters. Previous experience (Ref. 2) has shown that design values supplied by the manufacturer are often considerably different from the actual measured values. Accordingly, many of the vehicle and track parameters were measured directly.

5.2.2 Vehicle Parameters

The various laboratory experiments that were performed to measure truck parameters are described in Section 4. The measured axle misalignments were relatively small compared to the angles-of-attack, that were predicted for lead and trail axles on the tight turn loop. As a result, the measured axle misalignments were not used in the predictions. In addition to these parameters, a number of geometrical parameters were determined from engineering drawings of the car and truck.

The vehicle was weighed to determine the axle loadings. During the track tests, the vertical wheel loads were measured using strain gaged rails. These measurements showed that the mean vertical wheel loads were not equal at the balance speed for the curve. The leading axle high rail wheel and the trailing axle low rail wheel had equal loads that were considerably higher than the loads on the other two wheels of the truck. These loads were also equal. The average vertical loads that were determined are shown in Table 5.1

TABLE 5.1

AVERAGE VERTICAL WHEEL LOADS AT BALANCE SPEED

WHEEL	LOAD (Kips)
Lead Axle High Rail	13.8
Lead Axle Low Rail	10.6
Trail Axle High Rail	10.6
Trail Axle Low Rail	13.8

The reason for this uneven load distribution has not been determined. When the vehicle was run in the reverse direction, the load distribution changed, so that the wheels, which were now the lead axle high rail and trail axle low rail became the more heavily loaded. These particular wheels had been the ones that were more lightly loaded in the forward direction. This rules out the possibility that some built in twist in the truck frame is the cause of the unequal loads.

Wheel lift of the leading high rail and trailing low rail wheels due to flange climbing might be a possible cause. However, the primary vertical stiffness is relatively low and, as a result, the roll stiffness between axles is also low. The wheel lift that is obtained is far too small to cause the observed vertical load variation.

The reason for this load distribution should be determined as it has a significant effect on the vehicle's curving behavior and propensity for derailment.

Variation of the vertical load distribution with speed

was used to determine an effective height for the vehicle center of gravity.

All of the parameters that were used in the vehicle model are illustrated in Table 5.2

TABLE 5.2
VEHICLE PARAMETERS USED IN CURVING MODEL

Mass Parameters	Values
Truck Frame and ½ Car	108.3 lb-sec^2/in.
Axle Mass	9.3 lb-sec^2/in.
Stiffness Parameters	
Primary Longitudinal Stiffness (per wheel)	154,000 lb/in.
Primary Yaw Stiffness (per axle)	158.10^6 lb-in/rad
Primary Lateral Stiffness (per wheel)	28,750 lb/in.
Primary Vertical Stiffness (per wheel)	14,500 lb/in.
Primary Roll Stiffness (per axle)	14.9 10^6 lb-in/rad
Geometrical Parameters	
Truck Semi-Wheelbase	45 in.
Lateral Semi-Spacing of Primary Suspension	22.63 in.
Lateral Semi-Spacing of Wheel/Rail Contact Patches	29.9 in.
Mean Wheel Radius	15 in.
Effective Height of Vehicle C G Above Rail	60.25 in.
Other Parameters	
Axle Load	24,500 lbs.

Mass Parameters	Values
Truck Frame and ½ Car	108.3 lb-sec^2/in.
Axle Mass	9.3 lb-sec^2/in.
Stiffness Parameters	
Primary Longitudinal Stiffness (per wheel)	154,000 lb/in.
Primary Yaw Stiffness (per axle)	158.10^6 lb-in/rad
Primary Lateral Stiffness (per wheel)	28,750 lb/in.
Primary Vertical Stiffness (per wheel)	14,500 lb/in.
Primary Roll Stiffness (per axle)	14.9 10^6 lb-in/rad
Geometrical Parameters	
Truck Semi-Wheelbase	45 in.
Lateral Semi-Spacing of Primary Suspension	22.63 in.
Lateral Semi-Spacing of Wheel/Rail Contact Patches	29.9 in.
Mean Wheel Radius	15 in.
Effective Height of Vehicle C G Above Rail	60.25 in.
Other Parameters	
Axle Load	24,500 lbs.

5.2.3 Track Geometry

The track was surveyed in detail and the results of this survey are described in Section 4.1. These data were used to determine mean values of various track parameters in the region of the test zone. The values that were used are listed in Table 5.3.

TABLE 5.3
MEAN TRACK PARAMETERS

PARAMETER	
Curve Radius	150 ft.
Superelevation	1.5 in.
Gage	57.0 in.
Restraining Rail Clearance	2.0 in.
Restraining Rail Height	0.53 in.

5.3 Test Results Without Restraining Rail and Comparison with Theoretical Predictions

Tests were conducted over a speed range from 2-18 mph The average superelevation in the region of the test zone was 1.5 inches. As a result, the relationship between cant defici ency and speed is as shown in Fig. 5.5. A speed of 20 mph is equivalent to 1.4 degrees of cant excess and 18 mph is equivalent to 6.75 degrees of cant deficiency.

Figure 5.6 shows the predicted lead axle high and low rail lateral forces compared with the test results. Predictions are made for wheel/rail friction coefficients of 0.4, 0.5, and 0.6. The lateral forces on the two wheels are in the opposite direction and tending to spread the gage of the track.

Increasing the coefficient of friction increases the magnitude of both forces. There is a tendancy for the high rail force to increase in magnitude with speed, whereas the low rail force decreases. The high rail wheel is in flange contact and the lateral force is approximately 9.5 kips at balance speed.

The unequal vertical wheel loads, which were discussed previously, make the vehicle less prone to derailment. This is so because the lateral force on the low rail wheel, which provides most of the lateral force tending to derail the high rail wheel, is reduced because of its' reduced vertical load. At the same time, the increased vertical load on the high rail wheel acts to reduce the L/V ratio on that wheel and, therefore, the propensity to derailment. The L/V ratio on the lead axle high rail wheel is approximately 0.68, for a coefficient of friction of 0.5, throughout the speed range.

The lateral forces on the trailing axle wheels are shown in Fig. 5.7. The forces are lower than on the lead axle and do not vary much with changing coefficient of friction. In this case, it is the low rail wheel that is in flange contact with a lateral force of approximately 5 kips at balance speed.

The predictions are in good agreement with the measured lateral forces, particularly for a wheel/rail friction coefficient of 0.5.

In Fig. 5.8 the lead and trail axle yaw moments are presented. In general, there is a fairly small yaw moment on the lead axle, which is dominated by lateral forces due to the large angle-of-attack. The trail axle, however, has a large yaw moment and the predominant wheel rail forces are in the longitudinal direction contributing to this moment. The trail

axle yaw moment increases with increasing friction coefficient.

The predictions are not in particularly good agreement with the test results. The lead axle measurements are larger in magnitude than the predictions. The trail axle measurements are of similar magnitude to the predictions but appear to show a trend with speed which is in the opposite direction. The predictions showing a yaw moment which increases with speed whereas the measurements show the yaw moment decreasing with speed.

The yaw moments were determined by measuring primary longitudinal displacements and converting these to forces using the measured stiffness. Problems were encountered in this process, which were related to the determination of the absolute datums for the displacement measurements. These problems are described in Section 4. As a result, there must be some doubt concerning the accuracy of the yaw moment measurements and, for any future test program, an improved measurement procedure will be required.

Lead and trail axle angle-of-attack are presented in Fig. 5.9. The angles of attack are large because of the small radius of the test curve. Changing the coefficient of friction has little effect on the predicted angle of attack values. This is because the truck curving attitude is controlled predominantly by the degree of track curvature and the flangeway clearance. The truck is in a regime which is known as restrained curving where both the lead axle high rail wheel and the trail axle low rail wheel are in flange contact. Lead axle angle-of-attack is typically -40 milliradians and the trail axle angle-of-attack is about 8 milliradians.

In Fig. 5.10, results for the tractive resistance of

the truck are presented. This is the additional tractive resistance that is present due to the creep forces generated during negotiation of the curve. The measured value is obtained from a mean value of the vehicle resistance in the curve at 10 mph from a number of tests. The mean value of the vehicle resistance on tangent track was subtracted from this in order to arrive at the tractive resistance due to the curve alone. Predictions are presented for wheel/rail friction coefficients of 0.4, 0.5, and 0.6. These show the resistance increasing with both friction coefficient and speed. With a friction coefficient of 0.5, the prediction gives 1.21 kips resistance at 10 mph compared with 1.25 kips measured. The theoretical resistance is calculated from the total work done due to creep forces at each of the contact points and the method is presented in detail by Elkins and Eickhoff in Ref. 8.

5.4 Test Results with Restraining Rail and Comparison with Theoretical Prediction

With the restraining rail installed, tests were conducted over the same speed range as before, 2-18 mph. The same unequal vertical wheel load distribution at balance speed, that had been observed during the tests without the restraining rail, was obtained during this test series.

Results from the test series that had been conducted without the restraining rail seem to indicate that the friction coefficient between wheel and rail is approximately 0.5. Therefore, the predictions for the case with the restraining rail have assumed a friction coefficient of 0.5 for all wheel/rail contact points on the running rails. However, μ_{RR}, the friction coefficient at the restraining rail contact point, is varied during the analysis.

The vertical forces on the lead axle low rail wheel are shown in Fig. 5-11. This is the wheel that is in flange back contact with the restraining rail and tread contact with the low rail. At the restraining rail contact there is a large lateral creepage in the plane of contact, which produces a large lateral force. Because the plane of contact is inclined at approximately 82^{o} to the horizontal and, therefore, almost vertical, this lateral force in the plane of contact has a large vertical component. Through this mechanism, the restraining rail supports a significant proportion of the vertical load on the wheel. Figure 5-11 shows that the load supported by the restraining rail increases as the restraining rail friction coefficient is increased. In addition, the load increases moderately with increasing speed. At the same time, the total vertical load on the low rail wheel is decreasing with speed

due to cant deficiency. As a result, the load between the tread of the wheel and the low rail decreases with speed. The prediction suggests, that for a restraining rail friction coefficient of 0.5., this load will reach zero at approximately 16 mph. With a friction coefficient of 0.3 the load reaches zero at approximately 20 mph.

When the load between the tread of the wheel and the low rail reaches zero, the vehicle is at the point of impending flange climb. This is so because the angle of the contact plane on the restraining rail will decrease once the flange back starts to climb up. These flange climb speeds are surprisingly low but are confirmed by the measurements. The SOAC vehicle is particularly prone to flange climb with a restraining rail because of the uneven vertical load distribution that has been discussed previously. This leads to a reduced vertical load on the low rail wheel making it more prone to flange climb.

Lateral forces on the high and low rail are shown in Fig. 5-12. The lateral force on the high rail is now in the opposite direction to that obtained without the restraining rail and increases in magnitude with speed. The lead axle high rail wheel is held clear of flange contact by the restraining rail contacting the flange back of the low rail wheel. Therefore, the lateral force on the high rail comes entirely from tread contact and is in a direction which tends to close the gage. The force is also independent of restraining rail friction coefficient.

On the low rail the lateral force is in the same direction as the high rail but decreases rapidly with increasing speed. In addition, the force increases with decreasing friction coefficient on the restraining rail. The lateral force

tends to zero at the speed at which the vertical load has been reduced to zero.

The lateral load on the restraining rail is shown in Fig. 5-13. This force increases as the restraining rail friction coefficient is decreased and also increases with speed. At balance speed, with a restraining rail friction coefficient of 0.3 the lateral force on the restraining rail is approximately 14 kips.

Trailing axle lateral forces are presented in Fig. 5-14. The predictions show that these forces do not change if the restraining rail friction coefficient is varied. The high rail wheel is in tread contact and the lateral force is relatively low. The low rail wheel is in two-point contact, with tread and flange and the net lateral force is approximately 6 kips at balance speed.

Figure 5.-15 shows the lead and trail axle yaw moments. Variation of restraining rail friction coefficient has little effect on either of them. The results are very similar to those obtained without the restraining rail, with the trail axle generating a large moment and the lead axle moment being fairly small. The measurements suffer from the same uncertainty that was discussed previously. However, they are of a similar magnitude to the predictions.

The angles-of-attack are illustrated in Fig. 5-16. The predictions indicate that the lead and trail axle angles-of-attack should both have changed by approximately 3 milliradians as a result of installing the restraining rail. This would give predicted values of approximately -37 milliradians and 11 milliradians for the lead and trail axle, respectively. This reduction is a direct result of the reduced lateral move-

ment available to the lead axle, due to the presence of the restraining rail, which reduces the angle of truck rotation. The measurements do not seem to confirm this predicted change. It may be that the angle-of-attack measurement is not sufficiently accurate to detect the change. Otherwise, one possibility would be that the restraining rail is deflected laterally by a significant amount under the applied lateral load, leading to a larger lateral travel for the lead axle.

Measured tractive resistance due to the curve was obtained in the same manner as described previously. The mean measured value for the curve at 10 mph was 1.77 kips. This and predicted values for varying restraining rail friction coefficient are illustrated in Fig. 5-17. Increasing the friction coefficient on the restraining rail gives an increased resistance. In fact, even with a friction coefficient of 0.1 the resistance is higher than was obtained without the restraining rail.

Almost all of the comparisons between measured and predicted results seem to be consistent in indicating that the friction coefficient between restraining rail and flange back was approximately 0.3, whereas the friction coefficient on the running rails was 0.5. It may be that the restraining rail contact surface was not adequately cleaned at the time the curving performance tests were made. The restraining rail had not been used for a considerable time and was very rusty prior to the tests.

It would be interesting to discover whether, given sufficient running, the restraining rail friction coefficient would increase to a value of 0.5. There does not seem to be any reason why it should not. Monitoring of rail forces during the subsequent wear test might have provided this information. However, owing to the very rapid flange back wear rates, this test was of such short duration that it had been

completed before the monitoring could take place.

On the basis that the restraining rail friction coefficient was equal to 0.3, the agreement between the theoretical predictions and the measurements is remarkedly good.

6. COMPARISON OF WEAR DATA WITH WEAR INDEX PREDICTIONS FROM MATHEMATICAL MODEL

6.1 Background

It would be extremely valuable to be able to relate wheel and rail wear, for a given set of wheel and rail metallurgy and environmental conditions, to the mechanical parameters associated with the wheel/rail interaction. A number of wear index formulae have been proposed for this purpose by various authors. Some of these have been used as predictions of wheel and/or rail wear rate but with little full scale data available to establish their validity.

Almost all of these wear indices are dealing only with wheel flange and gage face wear and suggest that this wear is proportional to the flange force multiplied by the angle-of-attack. However, this hypothesis seems to ignore the effects of longitudinal force and creepage.

Elkins and Eickhoff in Ref. 9 have derived expressions for the work done due to creep forces and showed how this is related to tractive resistance. In addition, they have suggested that the wear rates of wheels and rails may be related to the total work done due to creepages at the wheel/rail interface. It is shown that the work done is a simple addition of the multipliers of the individual creep forces and their related creepages. Research is currently in progress to relate the wear of wheels and rails to this proposed wear index.

Bolton, Clayton, and McEwan (Ref. 9) have described some early results from a series of small scale laboratory ex-

periments. Figure 6-1 is reproduced from this reference in the form of wear rate plotted against wear index. Their results seem to indicate two distinct regimes of wear. Firstly, there is a regime in which no significant wear takes place until a certain threshold value of wear index is reached. Beyond this threshold, wear rate appears to increase linearly with further increases in wear index.

6.2 Wheel Wear Test Results and Comparison With Theoretical Wear Index

These tests were conducted by running in the clockwise direction around the loop at a nominal speed of 15 mph in two separate test series. In the first, the restraining rail was removed and in the second the restraining rail was installed. Measurements of wheel and rail wear were made after specified numbers of laps using profilometers available at the TTC. A detailed description of the tests, the measuring techniques and the results is given in Section 4.2.

Wear measurements, in terms of area loss from the profile, were made on all four wheels of the truck. When the restraining rail was present, flange back profile measurements were also made using a specially designed profilometer.

The wheel wear measurements, that were made without the restraining rail, determined measurable rates of wear at each of the four wheels of the truck. These results are presented in Section 4.1. The wear rates are different for each wheel and in some cases the wear is on the tread of the wheel and in others it is on the flange. As a result the one test under fixed conditions was able to generate a range of measured wear rates.

In a similar manner, the test case with the restraining rail should have yielded wear rate data for each wheel plus the flange back in contact with the restraining rail. However, because the wear rate on the flange back was so high, the wear test in this configuration was completed in relatively few laps. As a result, measurable wear data was not obtained for the trail axle wheels in this configuration. Therefore, the two tests, with and without restraining rail, yielded seven measured wear rates, which are tabulated in Table 6-1.

The curving model was then used to generate theoretical wear index values based on the work done at the wheel/rail interface. It was assumed for this purpose that the coefficient of friction between wheel and rail was equal to 0.5 at all the points of contact. The curving tests that were carried out without the restraining rail seemed to indicate that a value of 0.5 was obtained on the running rails. However, the test with the restraining rail present seemed to indicate that although a friction coefficient of 0.5 was present on the running rails, a value of 0.3 was more appropriate for the restraining rail. This lower value was attributed to the contact zone on the restraining rail not being adequately cleaned at the time of the test. However, it must be assumed that at some point in the wear test that followed, adequate cleaning was obtained. In this event, the friction coefficient could be expected to reach 0.5 as well. This possibility can not be confirmed because wheel/rail forces were not monitored during the short duration of the wear test. However, for the purpose of the theoretical wear index calculation, it is assumed that a value of friction coefficient of 0.5 was present on the restraining rail.

The theoretical wear index values for each wheel both with and without restraining rail are presented in Table 6.1

TABLE 6.1

THEORETICAL WEAR INDICES AND MEASURED WHEEL WEAR RATES

Wheel Contact Point	With or Without Restraining Rail	Theoretical Wear Index (Kips-in/in)	Measured Wear Rate ($in^2/10^6$ Cycles
Lead Axle High Rail Wheel Flange	Without	0.73	1.92
Lead Axle Low Rail Wheel Tread	Without	0.18	1.25
Trail Axle High Rail Wheel Tread	Without	0.16	0.13
Trail Axle Low Rail Wheel Flange	Without	0.19	0.39
Lead Axle High Rail Wheel Tread	With	0.25	1.84
Lead Axle Low Rail Wheel Tread	With	0.085	1.08
Lead Axle Low Rail Wheel Flange Back	With	1.71	5.08
Trail Axle High Rail Wheel Tread	With	0.17	----
Trail Axle Low Rail Wheel Flange	With	0.23	----

along with the available measured wear rates. The data are also plotted in Fig. 6-2 in the form of measured wear rate against wear index. A straight line relationship between the two is assumed and indicated on the graph. This gives a reasonable fit to the data. However, there are two points, lead axle low rail wheel tread without restraining rail and lead axle high rail wheel tread with restraining rail that give measured wear rates which are twice the value indicated by the straight line characteristic. In addition, the wear rate at the trail axle high rail wheel tread is only a third of the straight line value.

This is the first attempt, as far as the authors are aware, to take full scale wheel wear data from a number of different wheels in a truck, with contacts on flange front, flange back and tread, and construct a wear rate against wear index characteristic. It was also the first time that the wheel and rail profilometers and the supporting computer software at the TTC had been used to produce measured area losses in an experiment. In view of this, the characteristic, which is shown in Fig. 6-2, is a good result from a first attempt to establish such a characteristic.

6.3 Rail Wear Test Results and Comparison with Theoretical Wear Index

As well as measuring the wear rates that occurred on the wheels, wear of the rails was also monitored. However, the rails are exposed to less wear cycles than the wheels. For one lap of the tight turn loop, each wheel rotates through approximately 120 revolutions and therefore, a point on the circumference of a wheel experiences 120 wear cycles per lap. During one lap of the vehicle, a point on the rail experiences 4 wheel passes. However, the gage faces of the high and low rail are only contacted by 2 of these axles as is the restraining rail when it is present. Without the restraining rail, the head of the high rail is only contacted heavily by the trail axle and the head of the low rail by the lead axle. With the restraining rail, the head of the high rail experiences significant wear from both lead and trail axle wheels.

Therefore, in general, a point on the rail experiences 2 wear cycles per lap compared with 120 wear cycles for a point on the wheel. For this reason, given similar metallurgy for wheel and rail steel, one would expect wear rates on the rails that were only 0.017 of the wheel wear rates. During the course of the wear test, total area losses of approximately 0.1 square

inches on the flange and 0.05 square inches on the tread were measured. Whereas, for the rail only 0.01 square inches were measured and this is of the same order as the likely accuracy of the profilometer and computer software.

Theoretical wear indices for head and gage face of each running rail and the guard face of the restraining rail were calculated from the curving model and are presented in Table 6.2. Also presented are measured rail wear rates.

TABLE 6.2
THEORETICAL RAIL WEAR INDICES AND MEASURED RAIL WEAR RATES

Rail Contact Point	With or Without Restraining Rail	Theoretical Wear Index (Kips-in/in)	Measured Wear Rate ($in^2/10^6$ Cycles)
High Rail Gage Face	Without	0.73	8.1
High Rail Head	Without	0.16	----
Low Rail Gage Face	Without	0.19	----
Low Rail Head	Without	0.18	3.6
High Rail Head	With	0.42	----
Low Rail Gage Face	With	0.23	----
Low Rail Head	With	0.085	----
Restraining Rail Guard Face	With	1.71	----

Measured rail wear data was obtained for the high rail gage face and low rail head without the restraining rail. With the restraining rail present, only a small number of laps was completed because of the high rate of wear on the flange back. As a result, there is rail wear data only for the high rail.

head. However, this is based on only a single measurement and gives a much higher rate than would be expected. It was not possible to detect a measurable amount of wear on the restraining rail even though this contact point has the highest wear index and would, therefore, be expected to have the highest wear rate.

The two measured results that were obtained for the case without restraining rail are presented, plotted against theoretical wear index, in Fig. 6-3. A nominal straight line characteristic is drawn, which has a much greater slope than for the wheel wear data; approximately four times the slope.

Previous laboratory data for wheel and rail wear rates (Ref. 9), as shown in Fig. 6-1, indicated wear rates for wheel and rail that were very similar for the particular metallurgies in that experiment. The reason for the much higher rail wear rates in the current experiment is not known at this time.

7. CONCLUSIONS

Measurements of the curving behavior of the SOAC vehicle on the tight turn loop have been in good agreement with theoretical predictions from a mathematical curving model, both with and without a restraining rail. Rail force measurements using strain-gaged rails are in particularly good agreement, surprising even the authors by the degree of correlation that is obtained.

The measurements of primary suspension longitudinal displacement, which were used to determine primary suspension yaw moment were less satisfactory and some means for establishing an accurate datum needs to be determined for future tests.

The SOAC vehicle has a very significant unequal vertical wheel load distribution while negotiating curves even at balance speed. This is seen as a higher load on diagonally opposite wheels in the truck. This has a significant effect upon the vehicle's propensity for derailment. The vehicle being less likely to experience a wheel climb derailment of the lead axle wheel at the high rail but more likely to experience a wheel climb of the lead axle wheel, which is in contact with the restraining rail.

The lateral force on the restraining rail is larger than the lateral force on the high rail without the restraining rail. This force is in effect the flange force on the high rail wheel, because the wheel is at the point where virtually zero load is supported by the tread and the contact plane on the flange is at approximately 60° to the horizontal. It is interesting to note that a reduction of the friction coefficient on the restraining rail through lubrication would increase the lateral force on the restraining rail.

The results from this experiment and the predictions from the mathematical model indicate a real risk of the low rail wheel climbing onto the restraining rail above a certain speed. This would not be likely to lead to a derailment because flange contact of the outer wheel with the high rail would prevent further lateral travel of the wheelset. However, this situation is not one that should be allowed to occur in service. It is interesting to note that restraining rails are used in some cases to prevent derailment on tight curves. It would seem from this experiment, that they may cause a situation where wheel climb of the restraining rail is a real possibility.

The measured wheel wear data has permitted an initial estimate to be made of the relationship between wheel wear rate and a theoretical wear index. This will permit estimates of likely wheel wear rates for other vehicles from a knowledge of their suspension parameters and the track geometry of the route over which they run.

Much lower wear rates were expected and occurred on the rails during this experiment. As a result, rail wear rates have not been established with the same degree of confidence as the wheel wear rates. Because of the lower wear rates that occur on the rail during normal operation on the tight turn loop, it would seem that more accurate techniques for measuring rail wear may be needed in any future tests.

8. RECOMMENDATIONS

- The curving mathematical model should be used to investigate alternative restraining rail geometry as it seems unlikely that the geometry tested on the tight turn loop is the optimum. This would be a cost-effective means of arriving at an improved system before track testing.

- Once a certain amount of material has been removed from the flange back, flange contact of the outer wheel with the gage face of the high rail will occur. In fact, this may be the usual situation found in service. If so, then the computer model should be modified to permit predictions of curving behavior in this situation. This could then be followed by a suitable track test program to determine the validity of the model in this circumstance.

- If more accurate means of measuring rail wear can be established, a future test might help to improve on the quality of rail wear data. This might permit the establishment, with more confidence, of a rail wear - wear index relationship.

REFERENCES

1. Elkins, J.A., and Gostling, R.J., "A General Quasi-Static Curving Theory for Railway Vehicles," Proceedings from 5th VSD-2nd IUTAM Symposium, Vienna, September 1977.

2. Elkins, J.A., "Analytical Studies of Curving Forces and Hunting Stability and Related Support for WMATA Phase II Truck Test Project," UMTA Report, June 1982, to be published.

3. Elkins, J.A. and Weinstock, H., "The Effect of Two-Point Contact on the Curving Behavior of Railroad Vehicles," to be presented at the 1982 ASME Winter Annual Meeting, Phoenix, Arizona, November 1982.

4. Boocock, D., "The Steady-State Motion of Railway Vehicles on Curved Track," Journal of Mechanical Engineering Science, Vol. II, No. 6, 1969.

5. Newland, D., "Steering Characteristics of Bogies," The Railway Gazette, London, 1968.

6. Kalker, J.J., "On the Rolling Contact of Two Elastic Bodies in the Presence of Dry Friction," (plus table book), Doctoral thesis, Delft, 1967.

7. Gilchrist, A.O., and Brickle, B.V., "A Re-Examination of the Proneness to Derailment of a Railway Wheelset," Journal of Mechanical Engineering Science, Vol. 18, No. 3 pp. 131-141, 1976.

8. Elkins, J.A., and Eickhoff, B.M., "Advances in Nonlinear Wheel/Rail Force Prediction Methods and their Validation," Journal of Dynamic Systems, Measurements, and Control, Vol. 104, No. 2, June 1982.

9. Bolton, P.J., Clayton, P., and McEwan,I.J., "Wear of Rail and Tyre Steels Under Rolling/Sliding Conditions," presented at the ASME/ASLE Conference in San Francisco, August 1980.

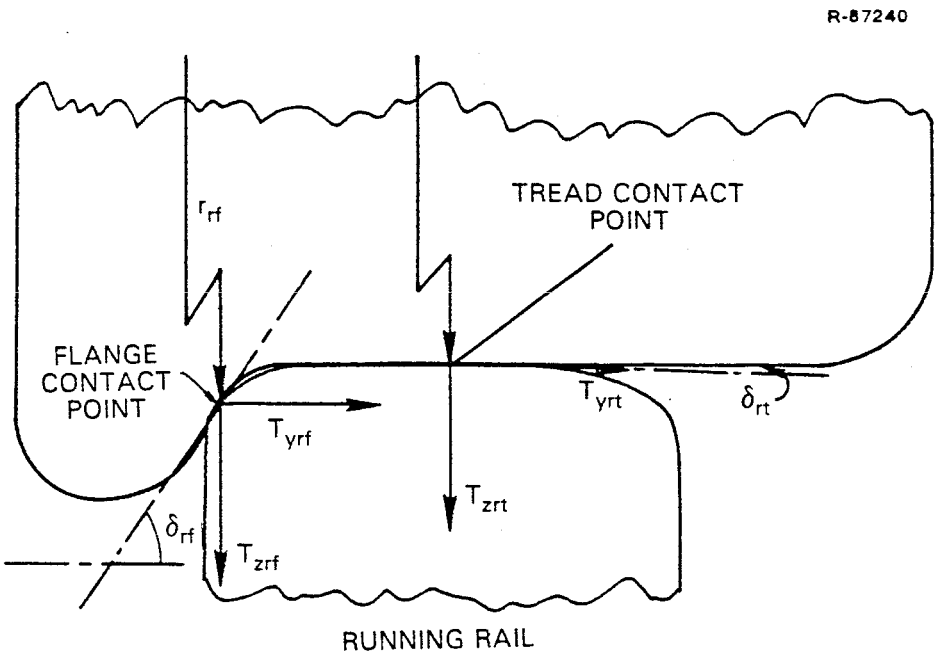

FIG. 5.1 END VIEW OF WHEEL AND RAIL WITH SECOND CONTACT POINT ON FLANGE FRONT

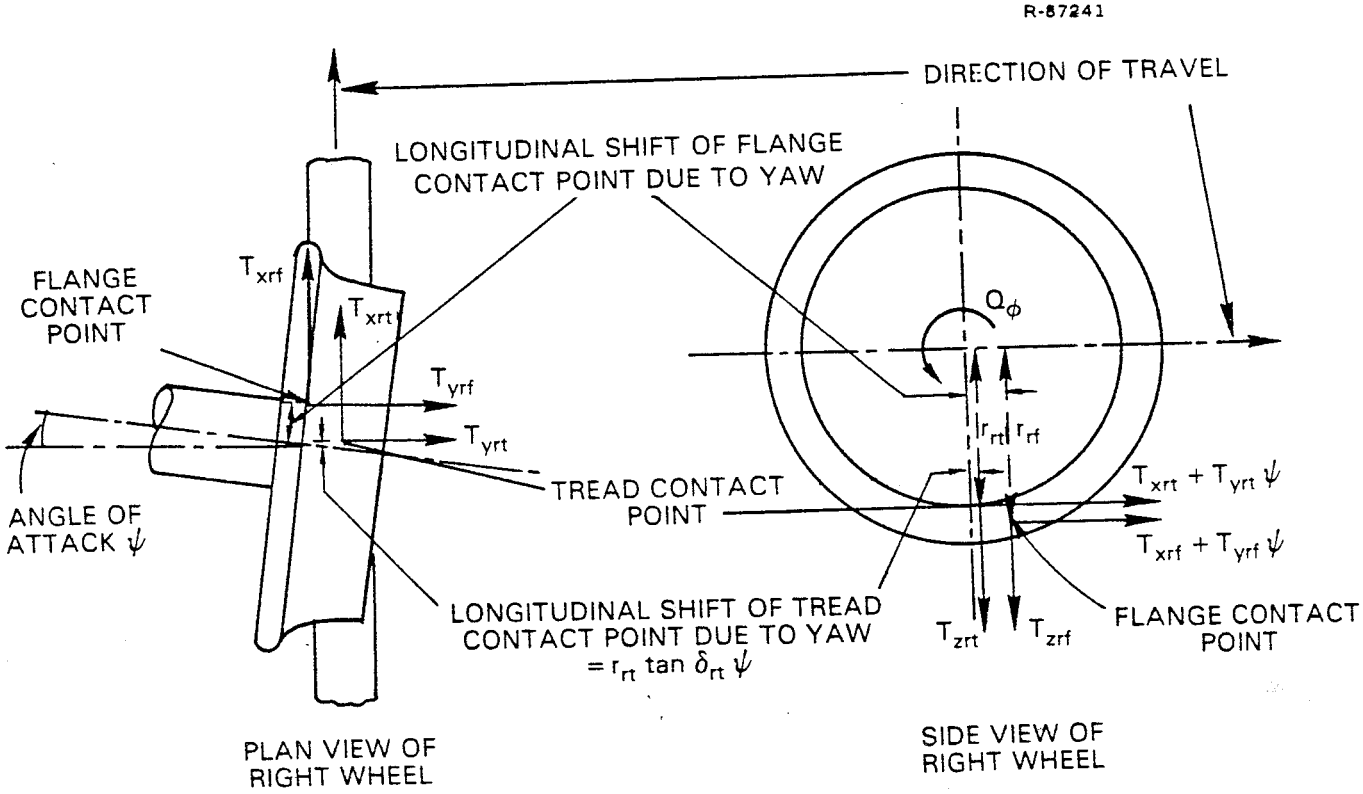

FIG. 5.2 FORCES AND TORQUES ACTING ABOUT WHEELSET BEARING AXIS WITH SECOND POINT OF CONTACT ON FLANGE FRONT (ONLY FORCES ON RIGHT WHEEL ARE SHOWN)

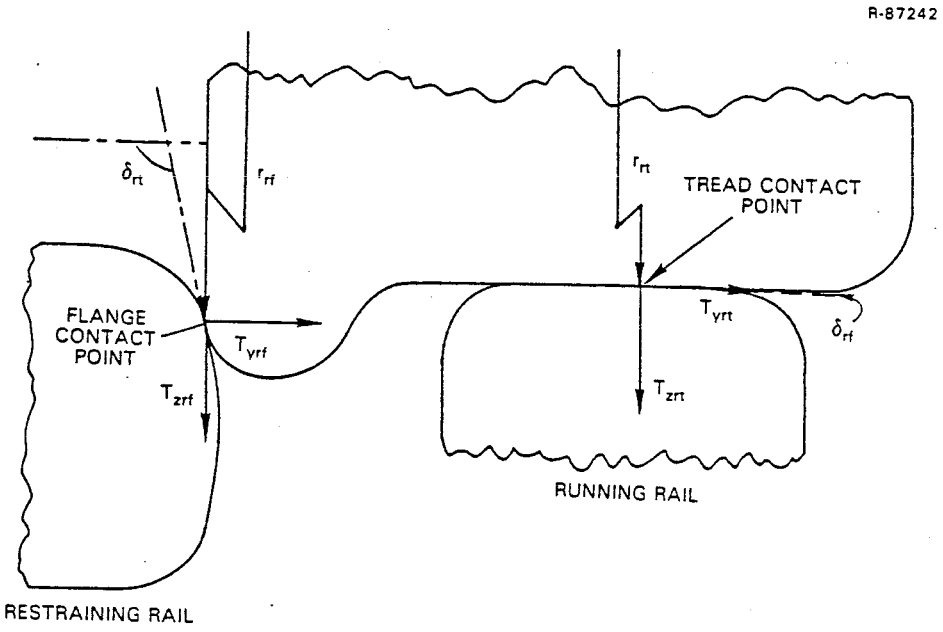

FIG. 5.3 END VIEW OF WHEEL AND RAIL WITH SECOND CONTACT POINT ON FLANGE BACK

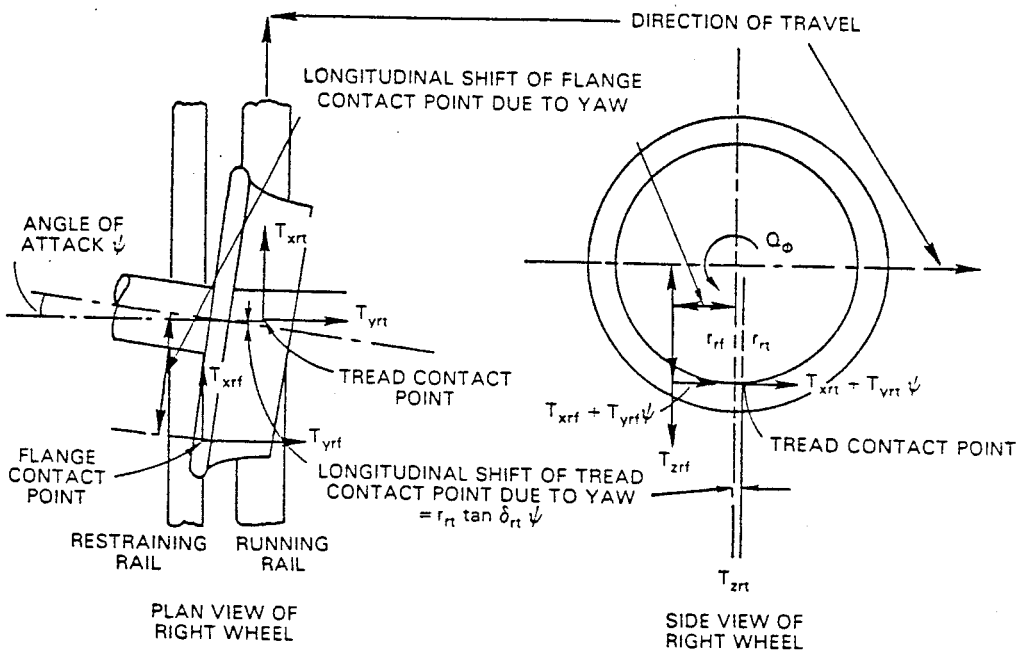

FIG. 5.4 FORCES AND TORQUES ACTING ABOUT WHEELSET BEARING AXIS WITH SECOND CONTACT POINT ON FLANGE BACK (ONLY FORCES ON RIGHT WHEEL ARE SHOWN)

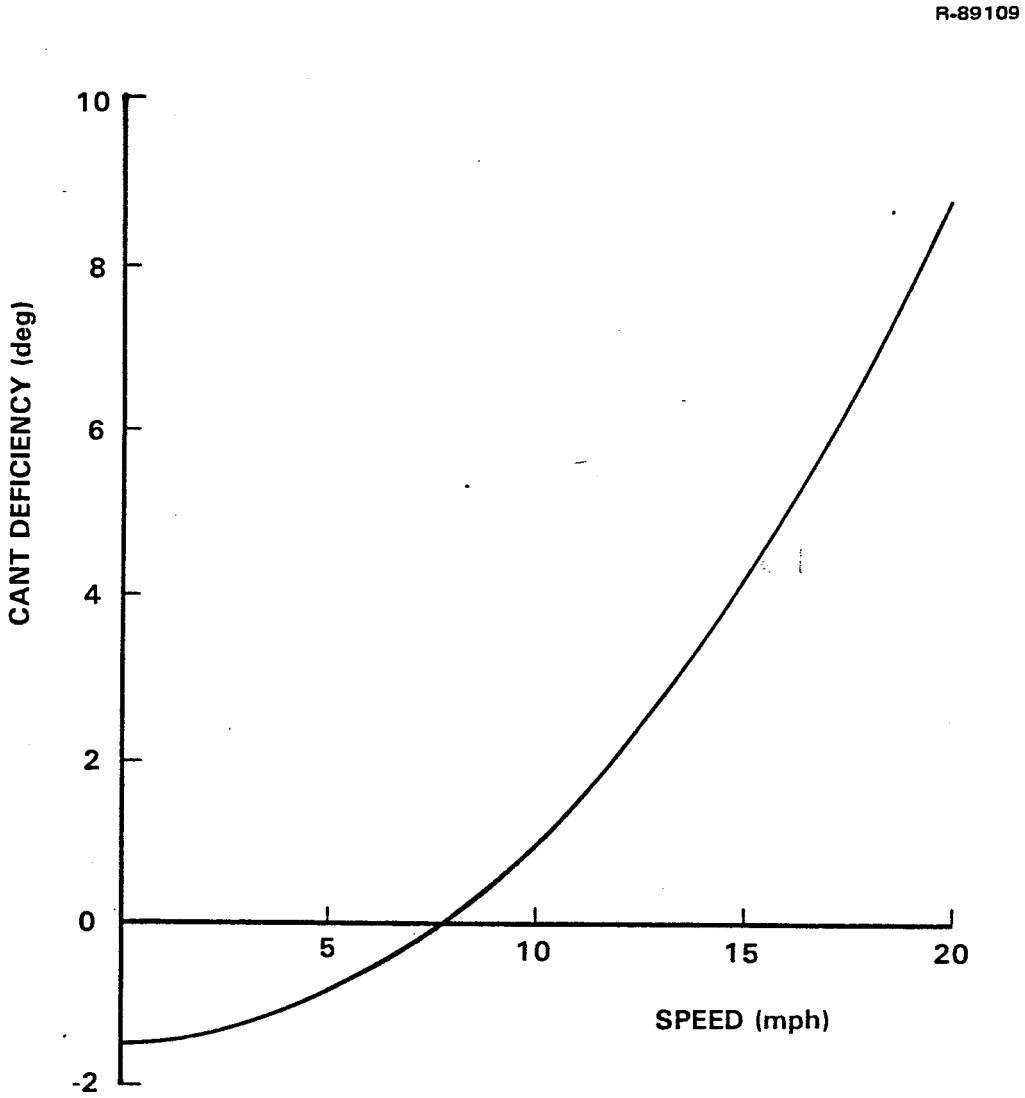

FIG. 5.5 CANT DEFICIENCY ∿ SPEED (1.5 INCH SUPERELEVATION)

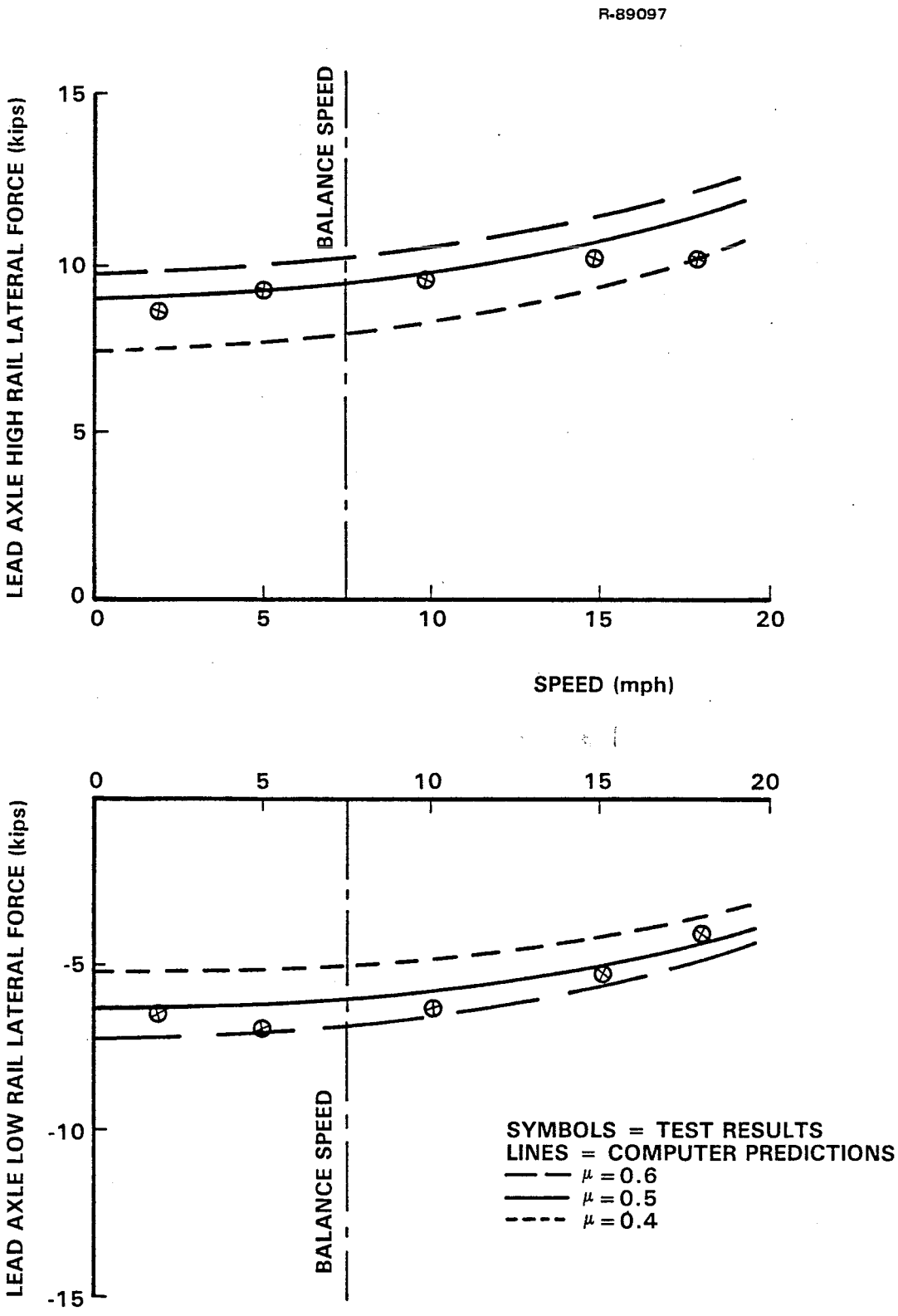

FIG. 5.6 LEAD AXLE HIGH AND LOW RAIL LATERAL FORCE ∿ SPEED (WITHOUT RESTRAINING RAIL)

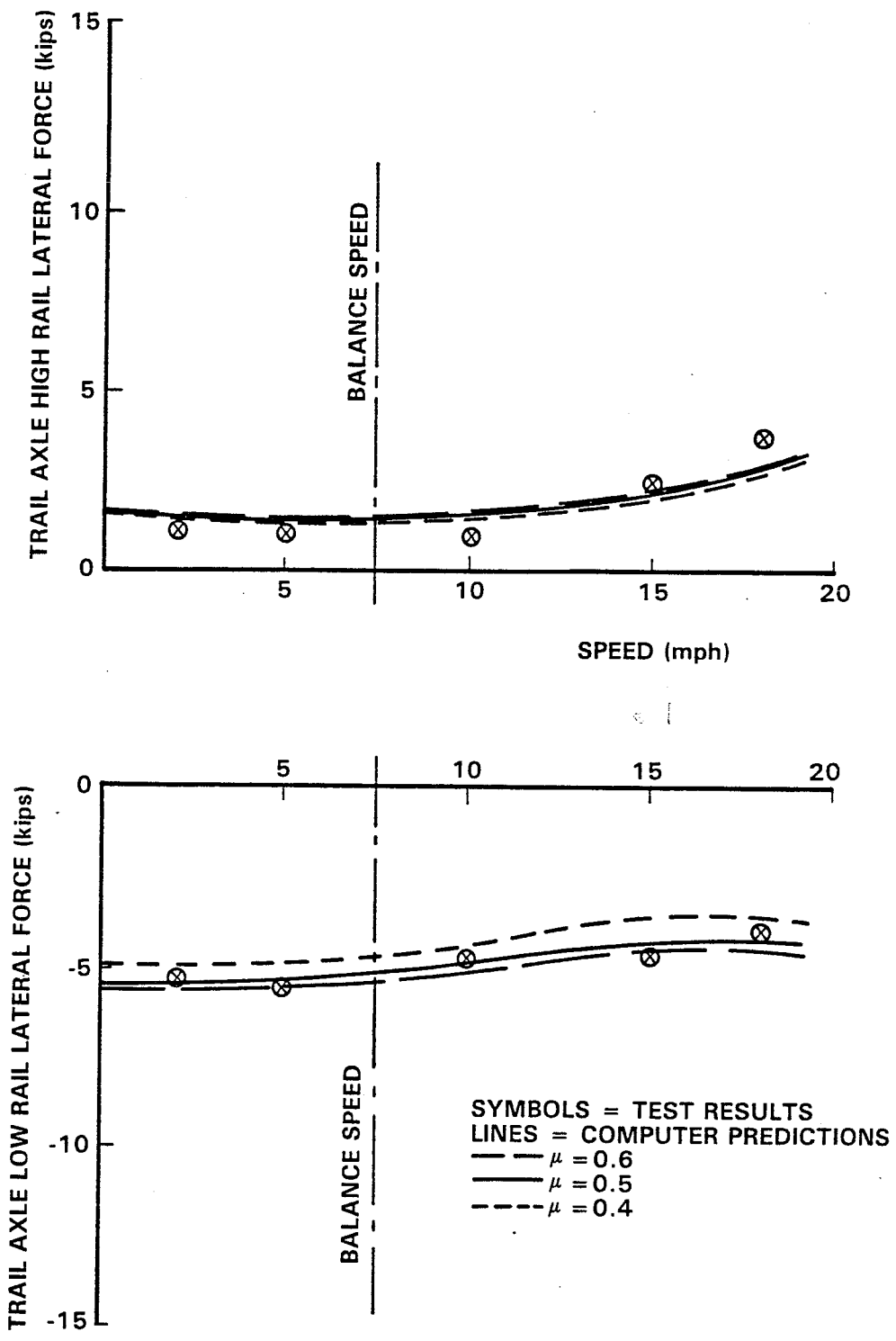

FIG. 5.7 TRAIL AXLE HIGH AND LOW RAIL LATERAL FORCE ~ SPEED (WITHOUT RESTRAINING RAIL)

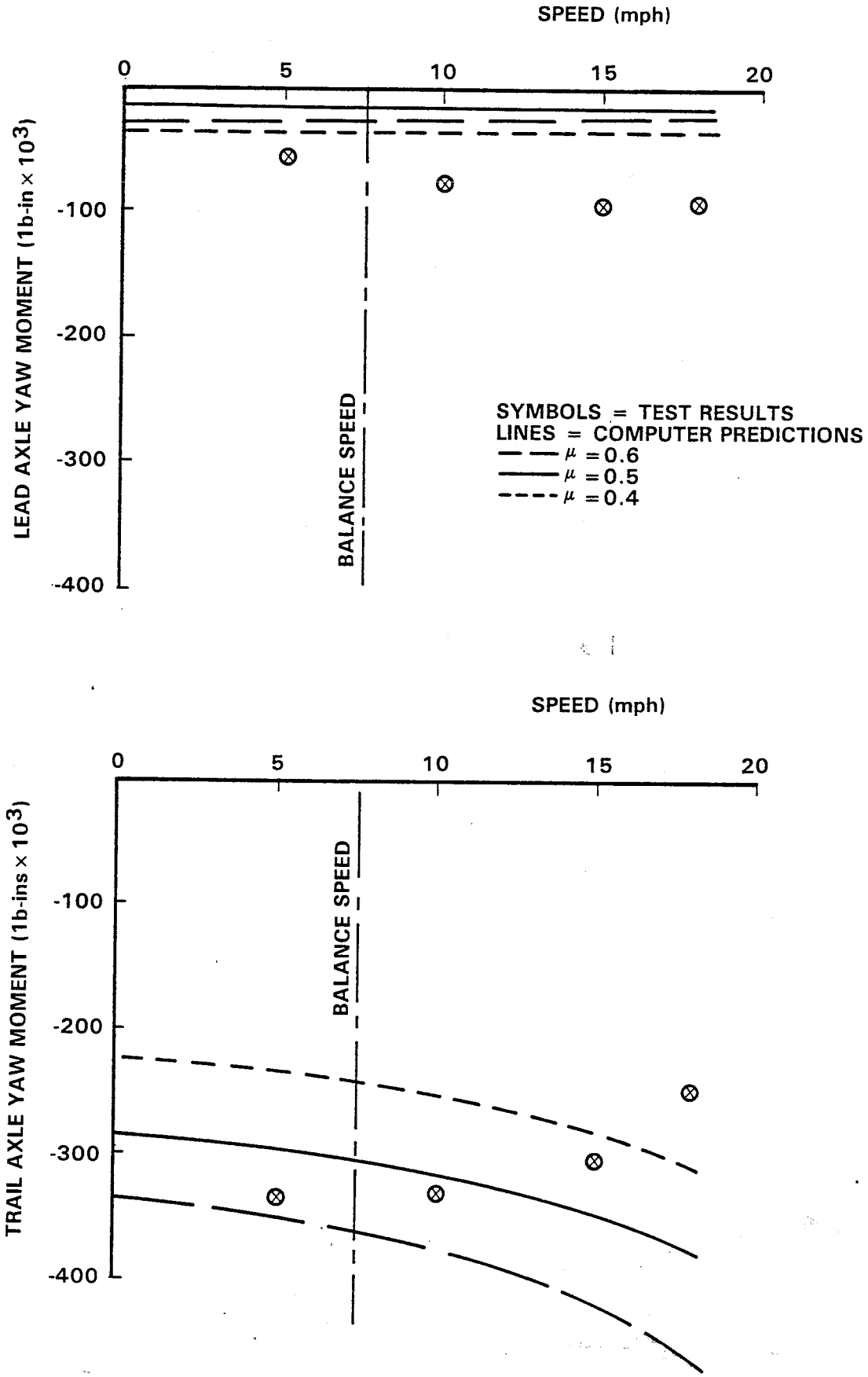

FIG. 5.8 LEAD AND TRAIL AXLE YAW MOMENT ~ SPEED (WITHOUT RESTRAINING RAIL)

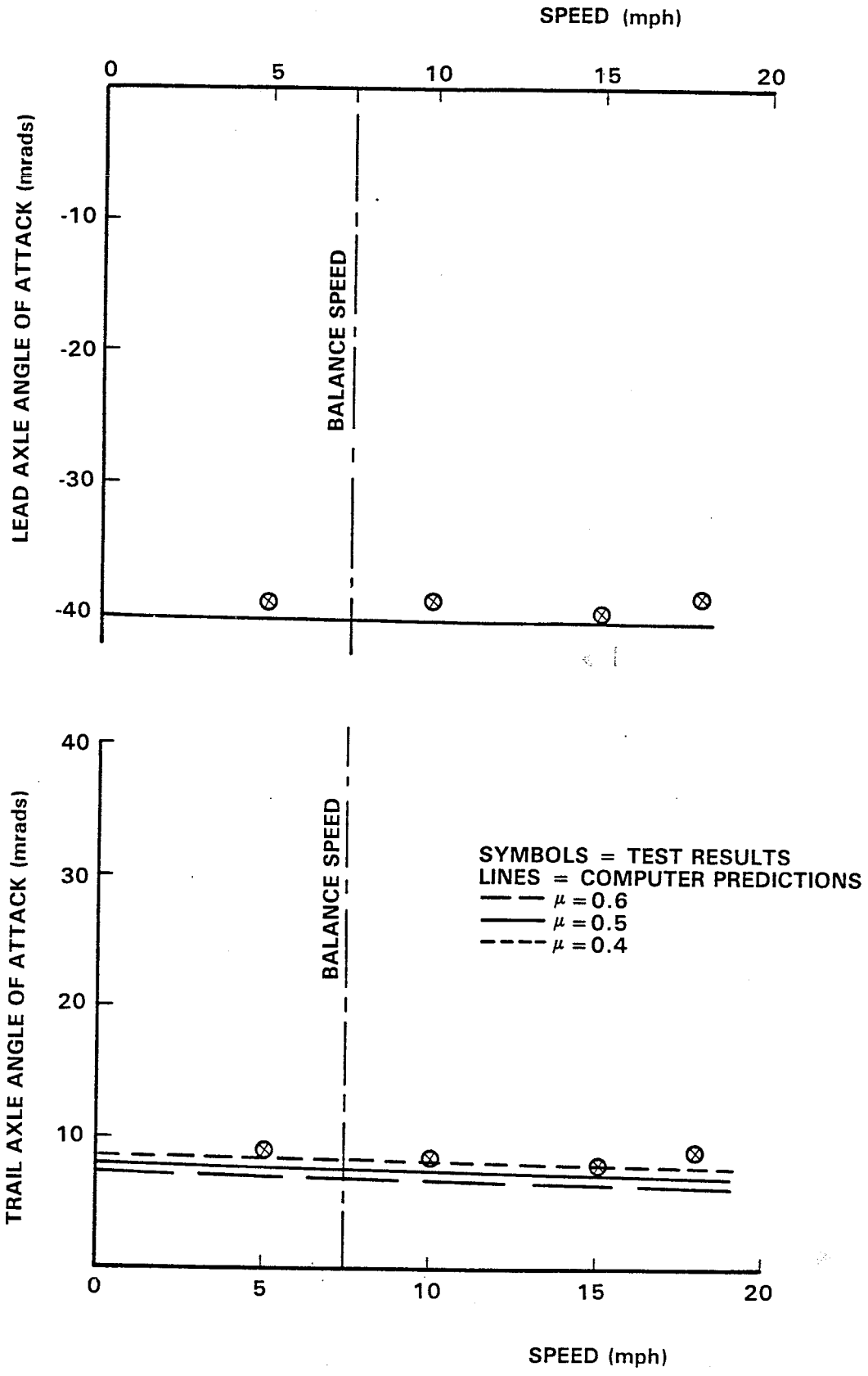

FIG. 5.9 LEAD AND TRAIL AXLE ANGLE-OF-ATTACK ∿ SPEED (WITHOUT RESTRAINING RAIL)

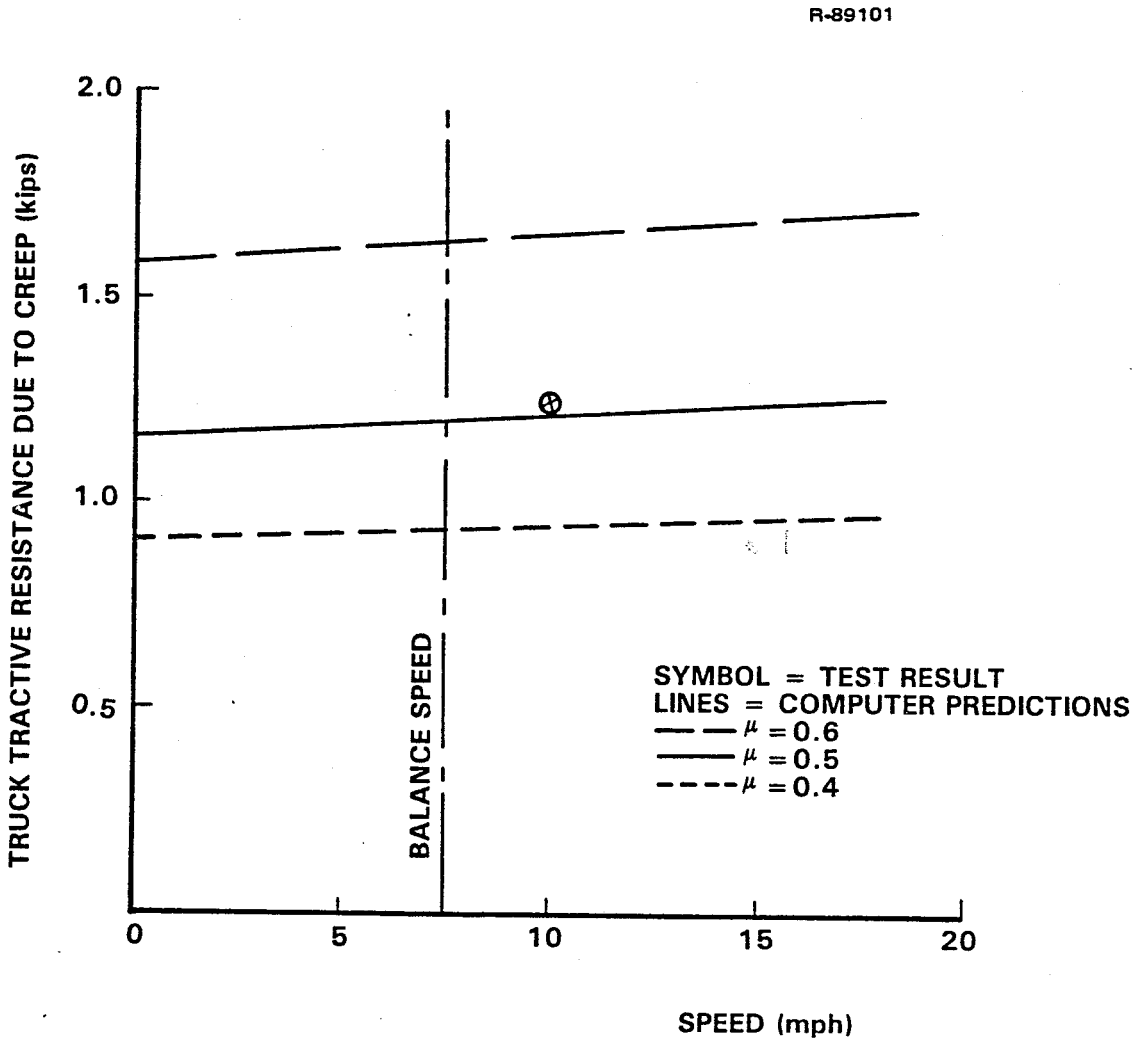

FIG. 5.10 TRUCK TRACTIVE RESISTANCE DUE TO CREEP FORCES ∿ SPEED (WITHOUT RESTRAINING RAIL)

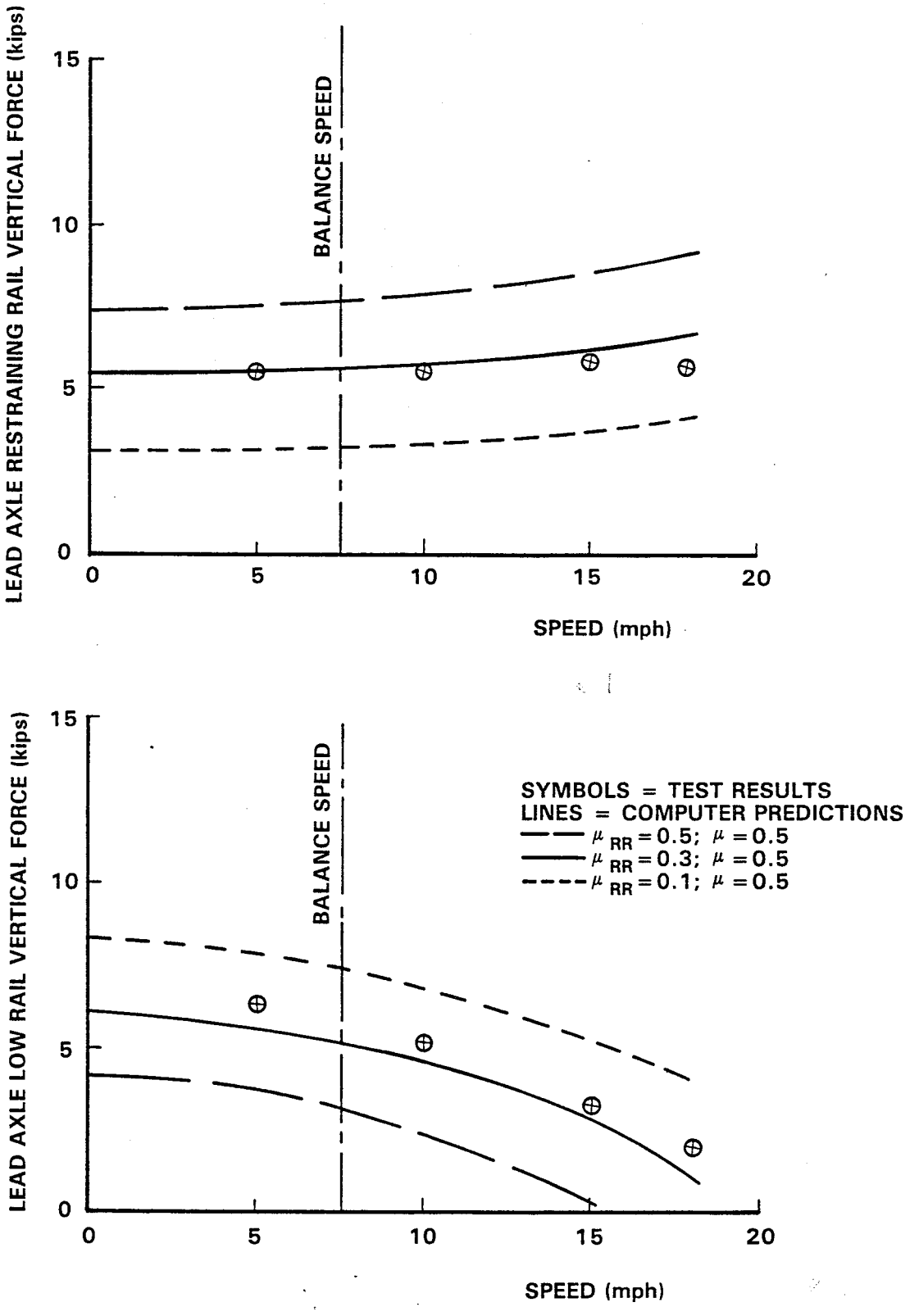

FIG. 5.11 LEAD AXLE LOW RAIL AND RESTRAINING RAIL VERTICAL FORCE ∿ SPEED (WITH RESTRAINING RAIL)

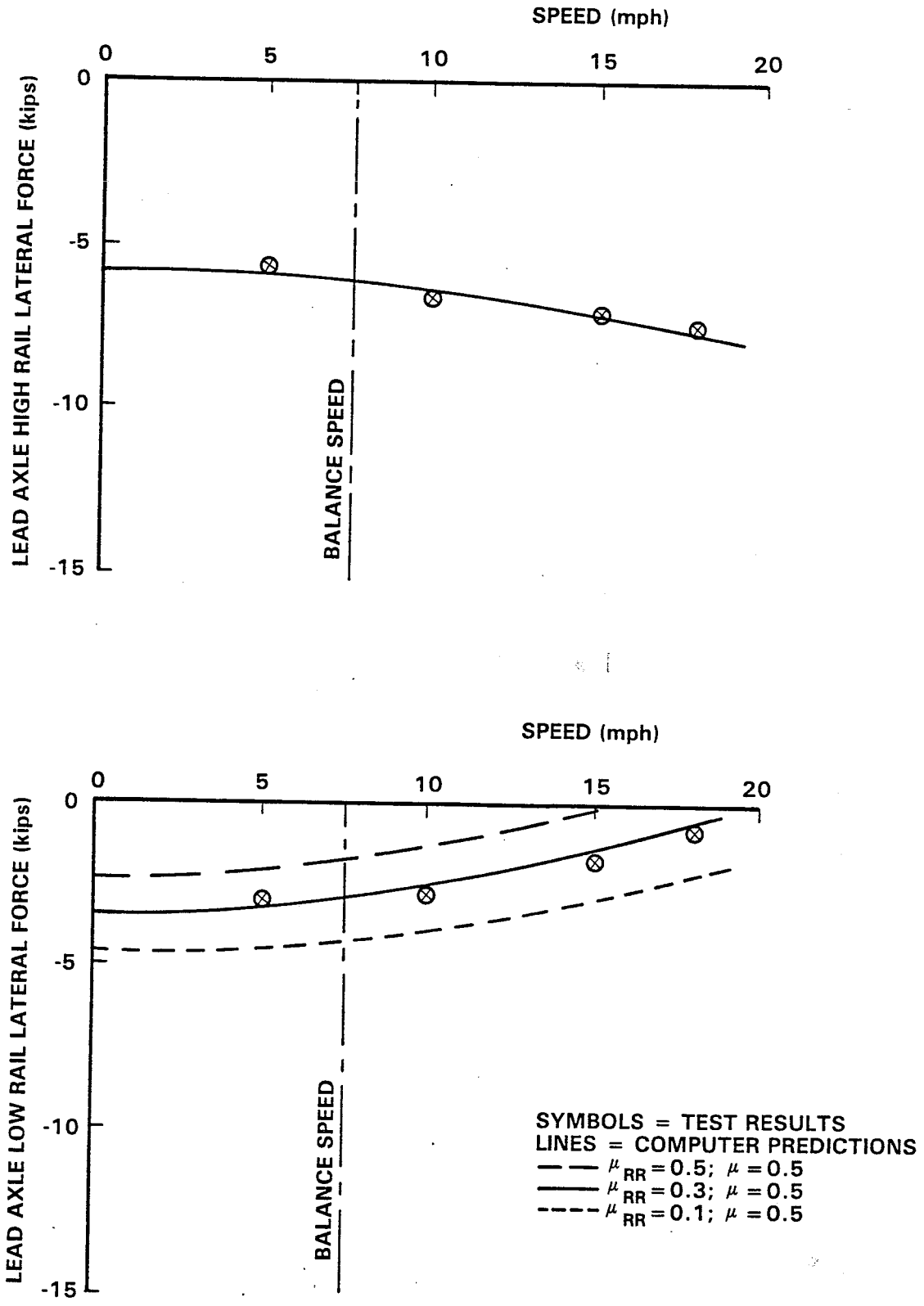

FIG. 5.12 LEAD AXLE HIGH AND LOW RAIL LATERAL FORCE ~ SPEED (WITH RESTRAINING RAIL)

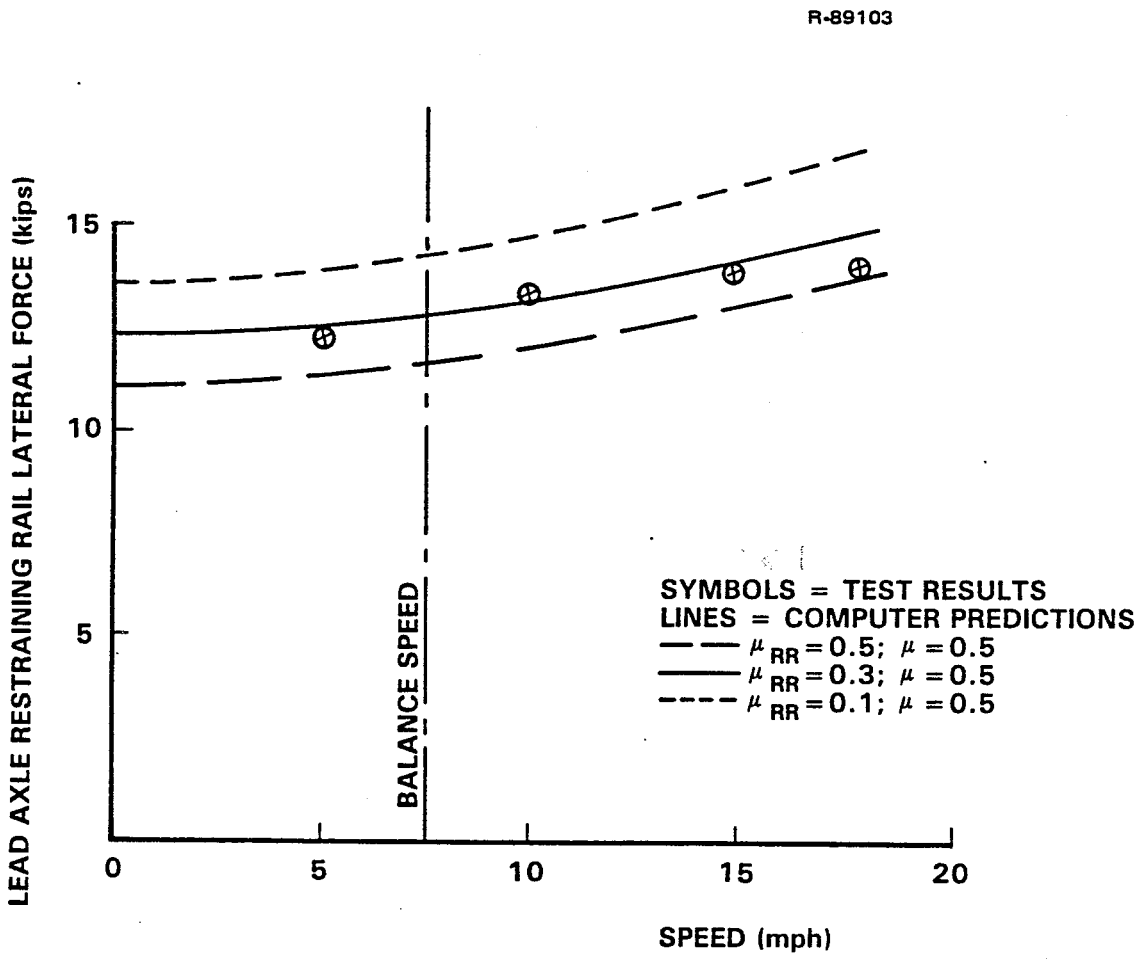

FIG. 5.13 LEAD AXLE RESTRAINING RAIL LATERAL FORCE ∿ SPEED (WITH RESTRAINING RAIL)

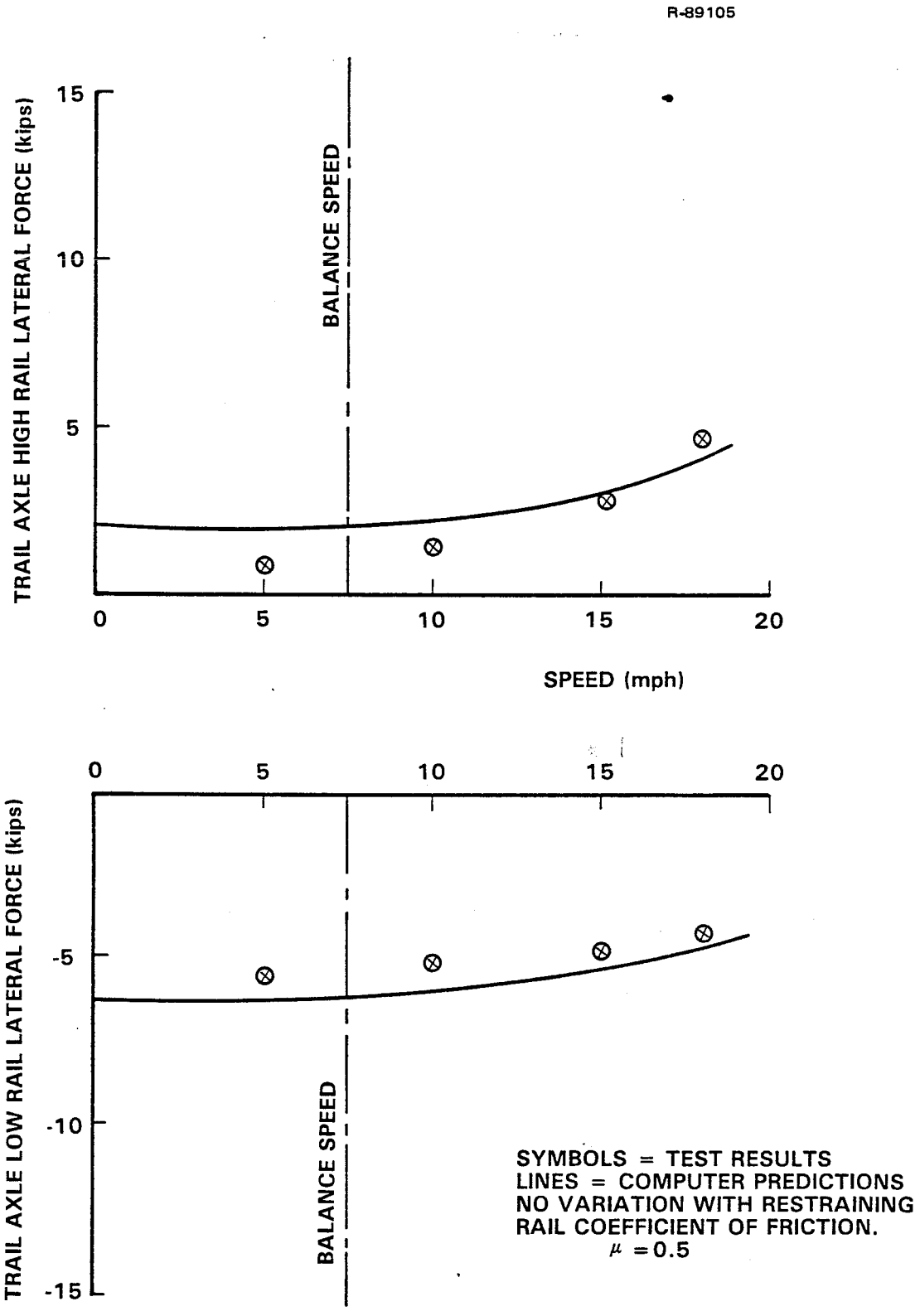

FIG. 5.14 TRAIL AXLE HIGH AND LOW RAIL LATERAL FORCE ∿ SPEED (WITH RESTRAINING RAIL)

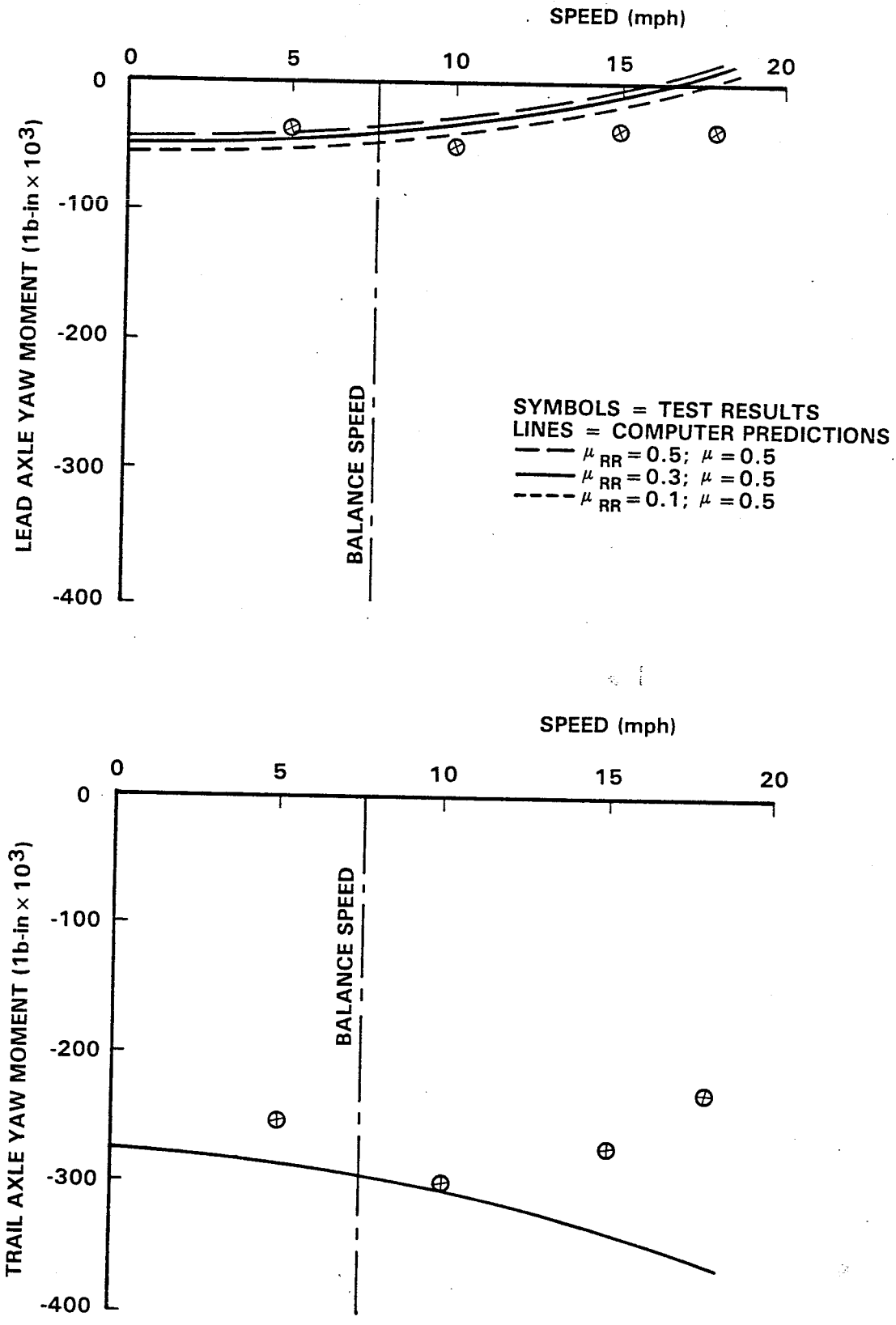

FIG. 5.15 LEAD AND TRAIL AXLE YAW MOMENT ∿ SPEED (WITH RESTRAINING RAIL)

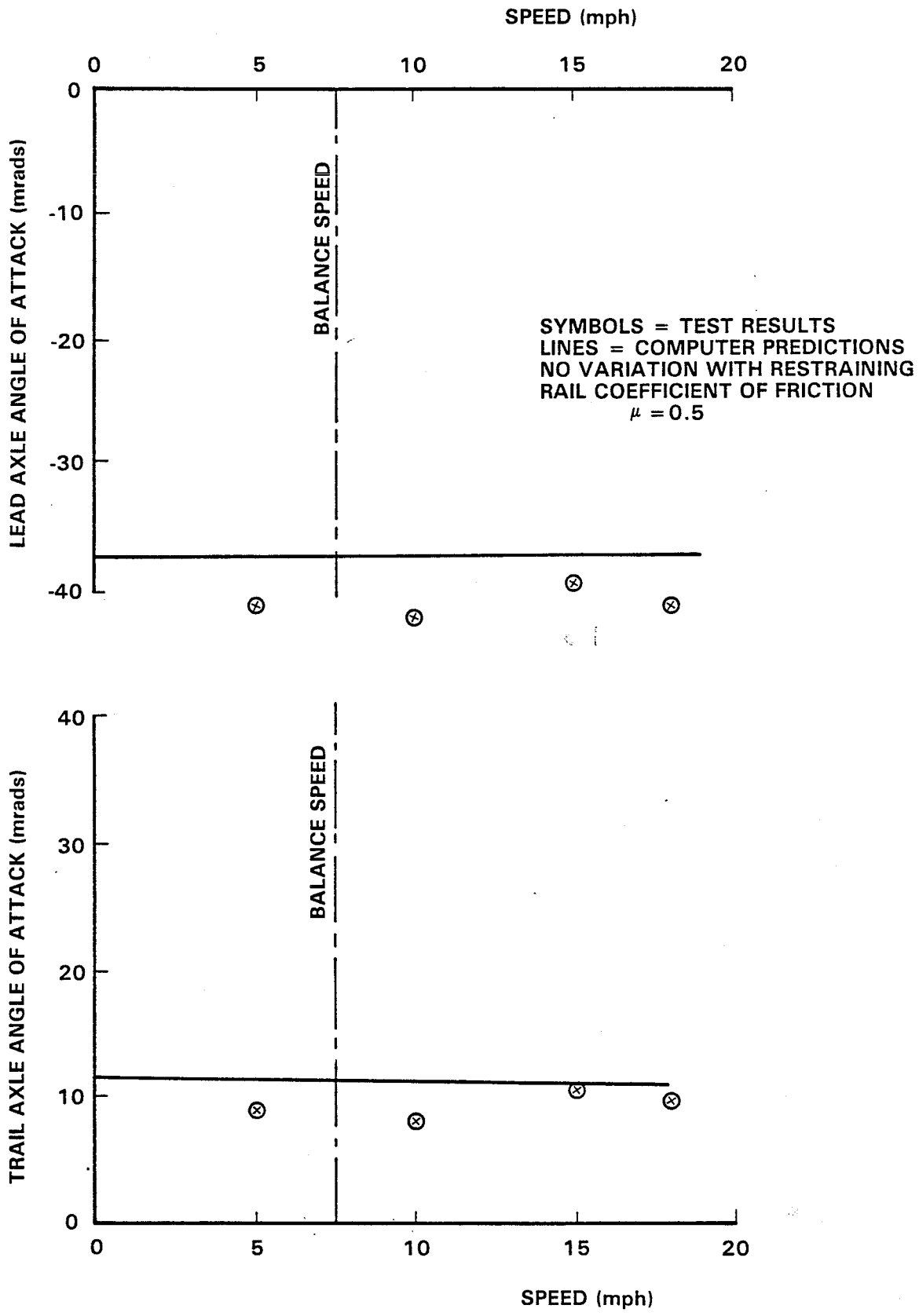

FIG. 5.16 LEAD AND TRAIL AXLE ANGLE-OF-ATTACK ∿ SPEED (WITH RESTRAINING RAIL)

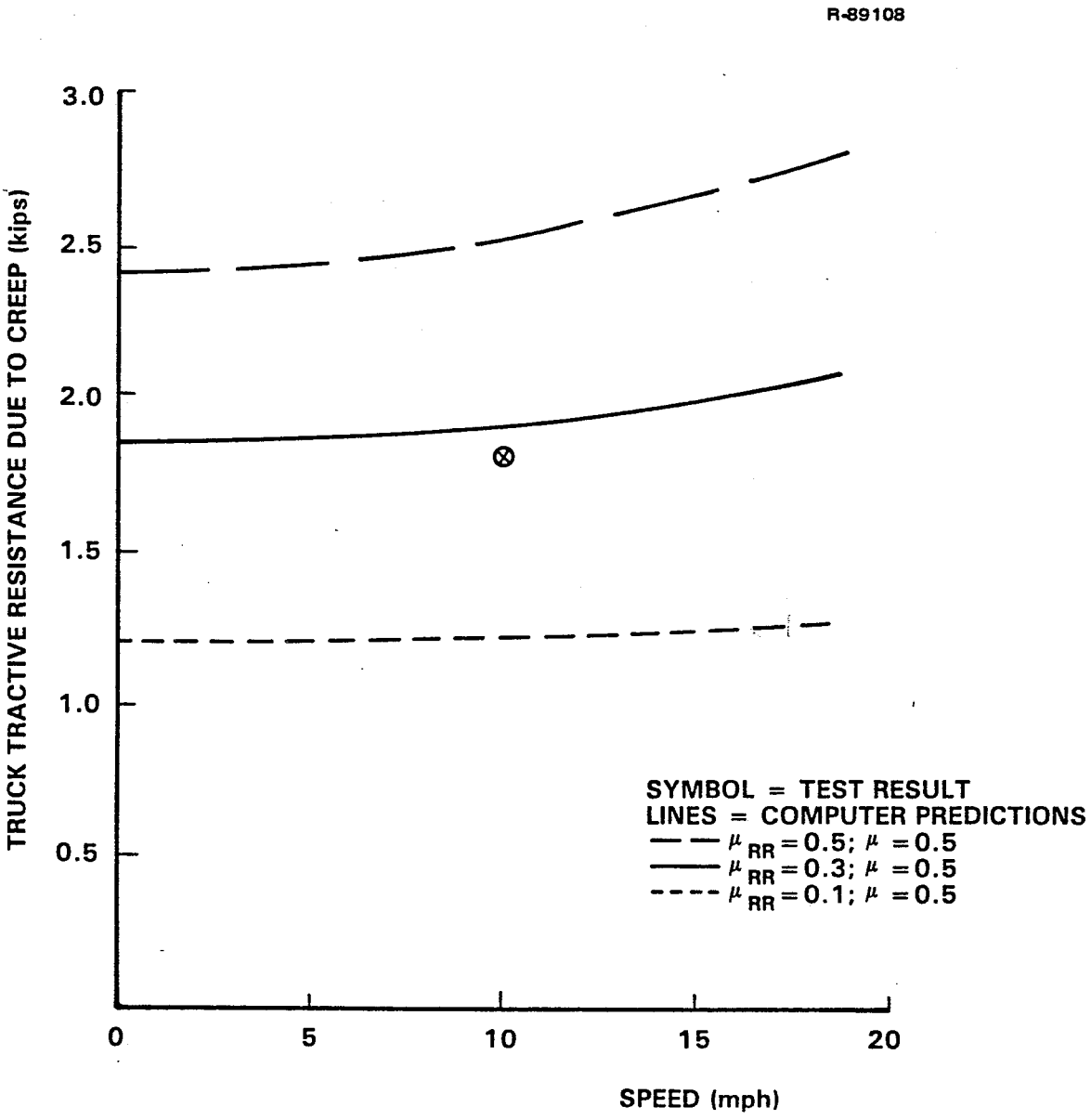

FIG. 5.17 TRUCK TRACTIVE RESISTANCE DUE TO CREEP FORCES ∿ SPEED (WITH RESTRAINING RAIL)

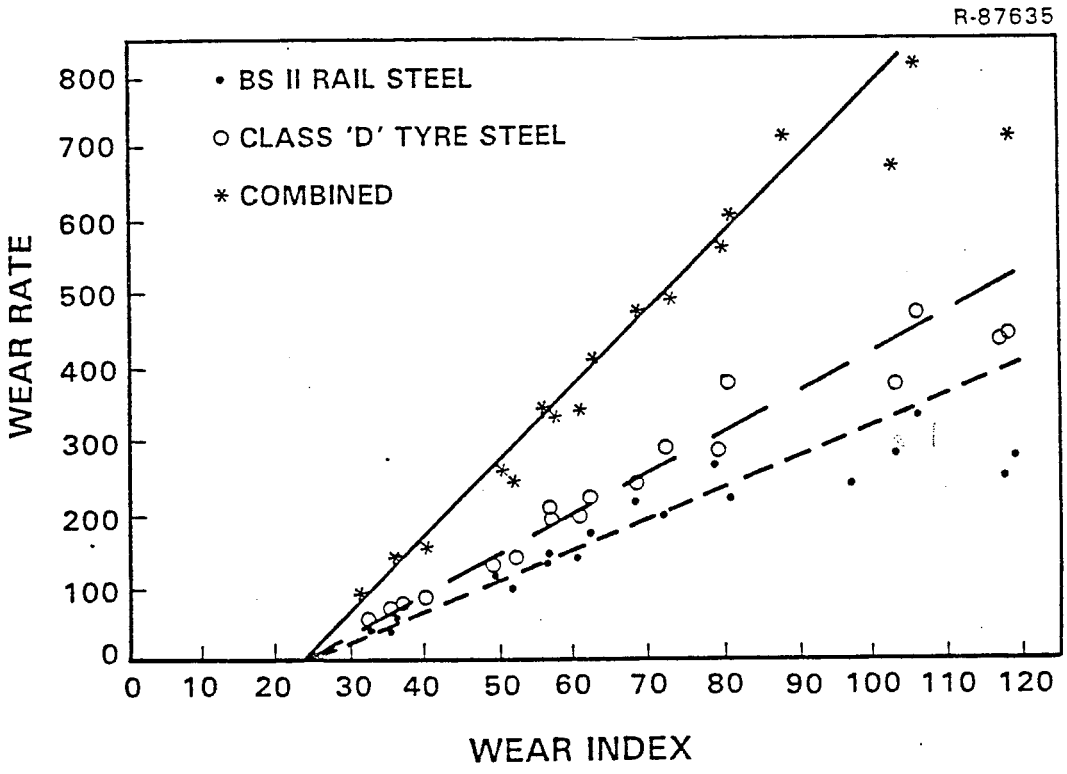

FIG. 6.1 LABORATORY WEAR RATE/WEAR INDEX RELATIONSHIP

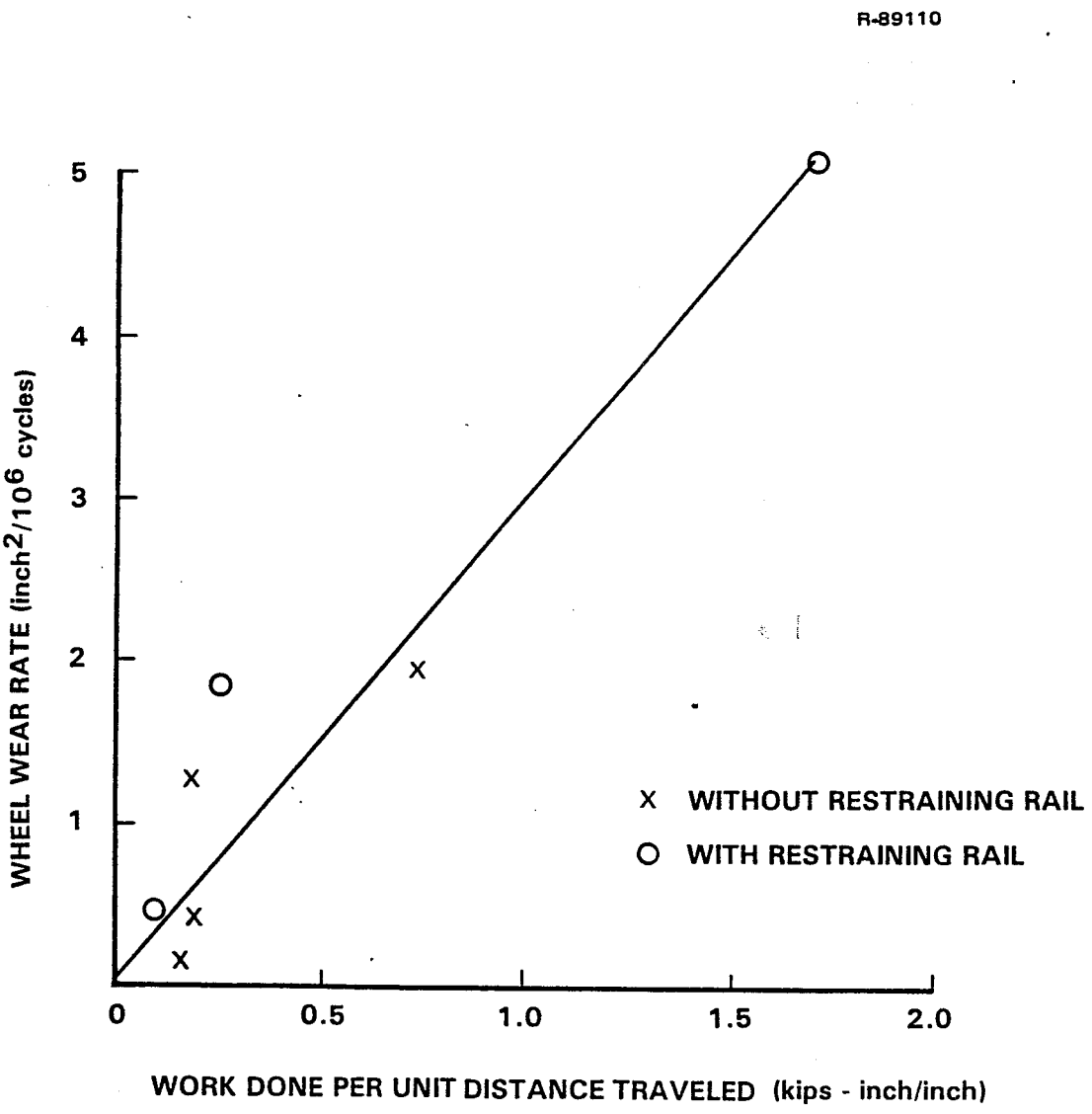

FIG. 6.2 MEASURED WHEEL WEAR RATE ~ WORK DONE WEAR INDEX

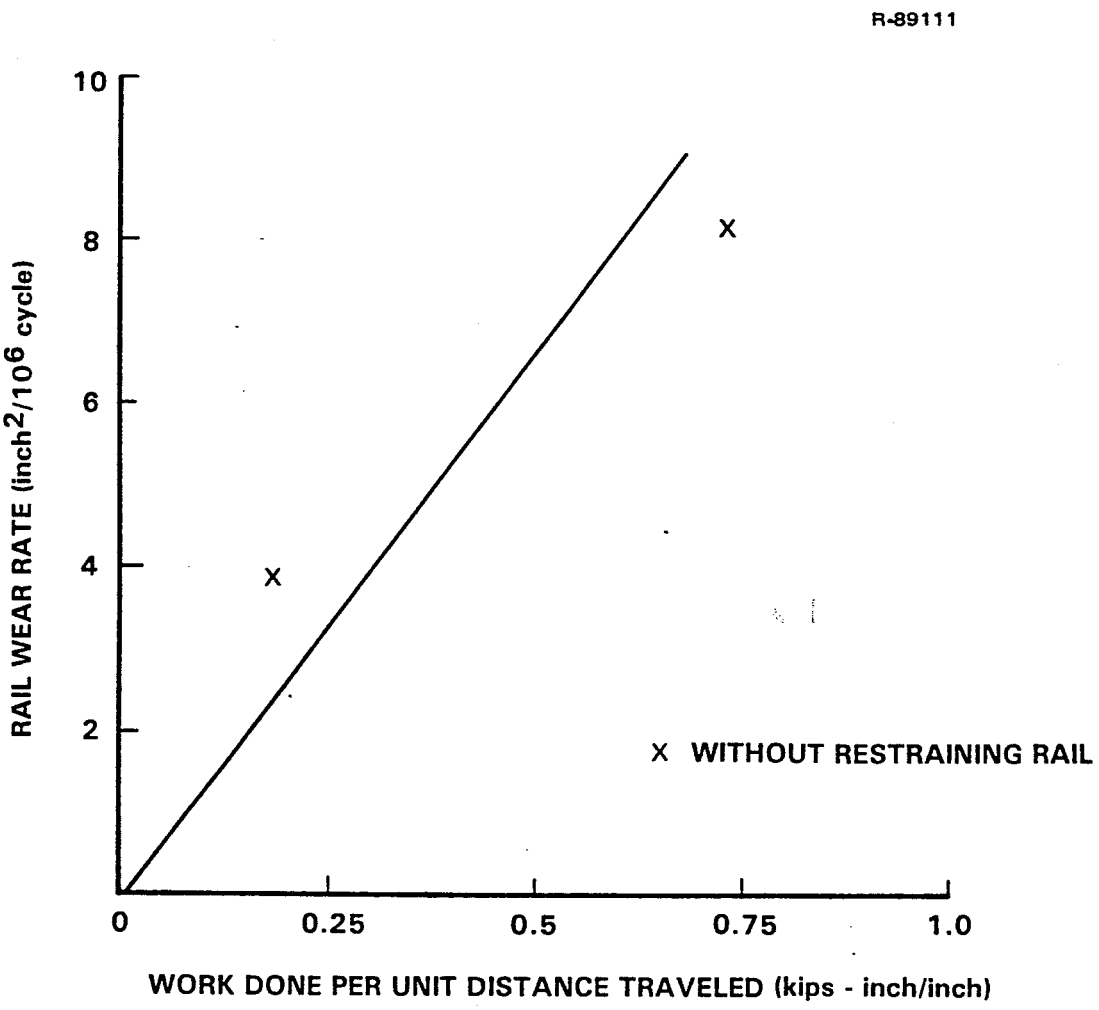

FIG. 6.3 MEASURED RAIL WEAR RATE ∿ WORK DONE WEAR INDEX